University of Alberta

Ediacaran iron formations and carbonates of Uruguay:
palaeoceanographic, palaeoclimatic and palaeobiologic implications

by

Ernesto Pecoits

A thesis submitted to the Faculty of Graduate Studies and Research
in partial fulfillment of the requirements for the degree of

Doctor of Philosophy

Earth and Atmospheric Sciences

©Ernesto Pecoits
Fall, 2010
Edmonton, Alberta

Examining Committee

Kurt O. Konhauser, Earth and Atmospheric Sciences

Murray K. Gingras, Earth and atmospheric Sciences

Robert Creaser, Earth and Atmospheric Sciences

George Pemberton, Earth and Atmospheric Sciences

George Owttrim, Biological Sciences

Carlos A. Rosière, Universidade Federal of Minas Gerais

Dedicada a mi madre *María Luisa Veiga Alegre* por todo su apoyo incondicional

ABSTRACT

The Ediacaran in Uruguay preserves a unique record of deposits generated during the assembly of the palaeocontinent Gondwana and concurrent with major changes in the atmosphere and oceans, and the rise of animal life.

Recent studies have suggested that the deep oceans remained anoxic and highly ferruginous throughout the Ediacaran and possibly into the Cambrian. Unfortunately, acceptance of this idea has been hindered by the virtual absence of iron formations (IF). Detailed studies of Ediacaran IF in Uruguay confirm that ferruginous conditions dominated the pre-Gaskiers (~580 Ma), and interestingly, they also extended well into the upper Ediacaran before complete ocean ventilation occurred. Significantly, a simple two-layer stratified system that argues for an oxygenated surface layer overlying a suboxic zone is proposed.

The association of negative $\delta^{13}C$ excursions in Neoproterozoic carbonates and large-scale glaciations has become a tempting explanation for the short-term perturbation of the global carbon cycle. Not surprisingly, negative $\delta^{13}C$ shifts in Ediacaran-aged carbonates from Uruguay have been interpreted as recording post-Gaskiers glacial events. New high-resolution $\delta^{13}C$-chemostratigraphy of carbonates shows negative fractionations in deep facies with a progressive rise towards shallow-water settings, and suggests a deposition across a stratified ocean. Furthermore, $^{87}Sr/^{86}Sr$ chemostratigraphy coupled with radiometric data allowed a more precise chronostratigraphy, which supports an age of ~600-575 Ma for the unit, and suggests a deposition concurrent with the Gaskiers glaciation. Notwithstanding whether associated $\delta^{13}C$ variations in shallow water facies

were produced by glacially-related conditions or by the dynamic of the basin itself remains unresolved. Although these conclusions are particularly valid for these deposits, they carry important implications for the understanding of other negative $\delta^{13}C$ excursions recorded in the Precambrian.

Finally, bilaterian burrows occur in Gaskiers age glaciomarine rocks in Uruguay implying that these are the oldest definite animal tracks yet reported. Crucially, our new discovery unites the palaeontological and molecular data pertaining to the origin of bilaterians, and brings the origin of animals firmly into the interval of the Neoproterozoic glaciations. It also implies that ancestral bilaterians likely evolved first in relatively shallow seas, and only colonized the deep-sea floor once sufficient bottom water oxygenation had taken place.

ACKNOWLEDGEMENTS

First and foremost I am enormously grateful to my advisors Dr. Kurt O. Konhauser and Dr. Murray K. Gingras for their continuous support and guidance during my Ph.D. program.

I also would like to express my gratitude to the rest of my candidacy and defense committee members: Dr. Robert Creaser, Dr. Larry M. Heaman, Dr. Sally Leys, Dr. George Owttrim, Dr. George Pemberton and Dr. Carlos A. Rosière, who made valuable suggestions and gave constructive advice.

Sincere thanks are extended to Dr. Tom Chacko (Associate Chair) for his support in many respects. My keen appreciation goes to Dr. Sergei Matveev for his valuable assistance with the electron microprobe and to Mark Labbe for making easier all the lab work.

I wish to thank my mates at the 'Geomicrobiology Lab', specially Stefan Lalonde and Larry Amskold, for facilitating my landing in Edmonton and with whom I shared numerous stimulating chats on iron formations, carbonates, etc.

A special thanks goes to my colleague and wife Natalie Aubet for fruitful discussions in the field and her invaluable help during the completion of this thesis.

Finally, I am deeply indebted to many people and friends I have known during my stay in Edmonton: Ali ("el turco"), Alice, Ana ("la gallega"), Andia ("andiecita"), Augusto ("gus"), Carlos ("carlitos"), Claire, Daniel ("el chaman"), Edgar ("el bishop"), Guadalupe ("guada"), Josh, Marcela, Margaret ("margot"), María Paz, Matthew, Mauricio ("tico"), Nelson, Oswald, Saulo ("bebo"), Set ("bebote"), Víctor ("el rodillas"), Virginia ("la otra gallega"), Vivienne and Yi ("el chino").

TABLE OF CONTENTS

CHAPTER 4: C-, O-, AND Sr-ISOTOPE COMPOSITION OF GASKIERS-AGE
CARBONATES FROM THE RÍO DE LA PLATA CRATON;
UNRAVELLING PALAEO-ENVIRONMENTAL CAUSES OF δ^{13}C
NEGATIVE EXCURSIONS   **89**

CHAPTER 5: EDIACARAN IRON FORMATIONS: COMPELLING EVIDENCE FOR
FERRUGINOUS LATE NEOPROTEROZOIC SEAWATER   **137**

CHAPTER 4

CHAPTER 5

CHAPTER 6

APPENDIX I

CHAPTER 1: INTRODUCTION

1.1. RATIONALE

The Ediacaran (635-542 Ma) is a key period in Earth's history for the understanding of the evolution of life and its relationship to global environmental changes (Anbar and Knoll, 2002). During this time, the Earth experienced continental break-up and major changes in the composition of the oceans and atmosphere. Glaciers in the tropics, atypical glacially-related carbonate deposits, the re-emergence of banded iron-formations (BIF) after a billion-year hiatus, deep ocean oxygenation and dramatic shifts in plankton productivity, are some of the features associated with that time (Hoffman and Schrag, 2002). Crucially, these outstanding events preceded the first appearance of animals and suggest a probable link between the rise of animal life and extreme environmental changes (Canfield et al., 2007; Fedonkin et al., 2007).

Despite the importance of this period in Earth's history, studies of the relevant rock successions are comparatively limited to outcrops in Namibia, Australia, China, Russia and Eastern Canada. The recent discovery of Ediacaran rocks in Uruguay is fortuitous because there exists several kilometers of continuous sedimentary sequences, including glacial deposits, the youngest known iron formations and post-glacial carbonates. Significantly, the biosphere at that time is also recorded in these sequences by the occurrence of eukaryotic phytoplankton, the first shelly fauna, stromatolites, and the oldest evidence of animal activity yet reported. Therefore, this assemblage of rocks provides an unparalleled opportunity to examine the conditions surrounding the emergence of complex life.

The Ediacaran to lowermost Cambrian successions of southeastern Uruguay preserve an unusual and significant record of deposits generated during the assembly of the palaeocontinent Gondwana (ca. 620-535 Ma) and concurrent with major changes in the atmosphere and oceans. The geological units within the study area consist of (from base to top) the Maldonado Group (Playa Hermosa, Las Ventanas and San Carlos

formations), the Arroyo del Soldado Group (Yerbal, Polanco Limestones, Barriga Negra and Cerro Espuelitas formations) and the Arroyo de la Pedrera Group (Piedras de Afilar and Cerro Victoria formations). The Maldonado Group is characterized by a glacially influenced volcanogenic-sedimentary sequence with ice-rafted debris and dropstones in the Playa Hermosa and Las Ventanas formations. The Arroyo del Soldado Group is a mixed siliciclastic-carbonate succession, mainly represented by an intercalation of basal pink dolostones, banded siltstones, rhythmites of dolostone-limestone, iron formations, cherts and conglomerates. The Arroyo de la Pedrera Group consists of quartz arenites, and stromatolitic/oolitic dolostones. Preliminary data indicates that the Precambrian-Cambrian boundary might be contained within or at the base of this group. The entire record reaches almost 6000 meters thick wherein a rich fossil assemblage composed by organic-walled microfossils and small shelly fauna, including the index fossil *Cloudina,* has been reported (for a recent review see Pecoits et al., 2008).

Precambrian supracrustal rocks are important for understanding the origin and evolution of the continental crust, its composition, earth's surface processes, sediment provenance, paleoclimate and weathering conditions (Wronkiewicz and Condie, 1989; Taylor and McLennan 1985; Eriksson et al., 2002). Particularly, the study of BIF and carbonates, as well-preserved chemical sediments nearly devoid of detrital input, preserve a history of oceanic elemental abundance by the predictable nature of sorption reactions that occur during the precipitation of carbonate precipitates and hydrous ferric hydroxide (HFO) particles in the water column. This feature has been previously exploited to better understand phosphorus limitations on early biological productivity (Bjerrum and Canfield, 2002, Konhauser et al. 2007) and the availability of other important nutrients, such as enzymatically-required trace elements (Konhauser et al., 2009). In this regard, over the last two years a new research direction that focuses on the rare earth element (REE) and yttrium (Y) data has been developed in order to test, firstly, the compatibility of a marine precipitate origin for BIF and carbonates and, secondly, compatibility with microbial involvement during their precipitation (Konhauser et al., 2009; Pecoits et al., 2009).

1.2. THESIS ORGANIZATION

The main topics to be covered in this study are sedimentology, stratigraphy, palaeontology, petrography, isotope and trace element geochemistry of Ediacaran BIF- and carbonate-bearing successions of Uruguay. Integrating data gathered from rocks, isotope chemostratigraphy, trace-element geochemistry and palaeontology within a geochronological framework will produce consistent results and consequently improve understanding of the sequence of the events, both biotic and environmental during the Ediacaran. This thesis is organized into five chapters. The first chapter provides a detailed sedimentological and stratigraphical framework of the Ediacaran units in Uruguay. The age, geological setting and palaeoenvironmental implications in terms of the observed sedimentological features are considered and related to the palaeobiological complexity during this critical period (Pecoits et al., 2008). Chapter 2 deals with the basal glacigenic Maldonado Group. Structural framework, stratigraphy, glacigenic deposits, relationships with other units, palaeogeography and geochronological constraints are discussed for the less studied Las Ventanas and San Carlos formations (Pecoits et al., 2010a). Chapter 3 focuses on the C-, O-, and Sr-isotope composition of the Polanco Limestone Formation. This chapter aims to: (a) present detailed carbon isotopic profiles from deep-water facies, (b) establish the chemostratigraphic age of the Polanco Limestone Formation by means of Sr– and C-isotope data, and (c) discuss the possible mechanisms that could originate prominent negative excursion in the Polanco carbonates and other Neoproterozoic carbonates elsewhere (Pecoits et al., *Chemical Geology* in review). Chapter 4 describes the sedimentology, stratigraphy and geochemistry of the Yerbal iron formations and associated strata. The resulting palaeoenvironmental and chronostratigraphic framework offers a reliable perspective on the origin and significance of this young iron formation. Finally, these data are used for testing current models for Ediacaran seawater (Pecoits et al., *PNAS* in review). Chapter 5 deals with evidence of early Ediacaran bilaterians. Significantly, these bilaterian burrows occur in glaciomarine sedimentary rocks of the recently defined Tacuarí Formation (ca. 580 Ma) and constitute the oldest evidence of animal life yet reported (Pecoits et al., *Science* in review).

1.3. REFERENCES

Anbar, A., Knoll, A., 2002. Proterozoic ocean chemistry and evolution: A bioinorganic bridge?. Science. 297, 1137-1142.

Bjerrum, C.J., Canfield, D.E., 2002. Ocean productivity before about 1.9 Gyr limited by phosphorous adsorption onto iron oxides. Nature. 417, 159-162.

Canfield, D.E., Poulton, S.W., Narbonne, G., 2007. Late-Neoproterozoic Deep-Ocean Oxygenation and the Rise of Animal Life. Science. 315, 92-95.

Eriksson, P., Altermann, W., Nelson, D., Mueller, W., Catuneanu, O., (Eds) 2002. The Precambrian Earth: Tempos and events, Elsevier, Amsterdam, pp. 941.

Fedonkin, M., Gehling, J., Grey, K., Narbonne, G., Vickers-Rich, P., 2007. The Rise of Animals. John Hopkins Press, Washington, pp. 320.

Hoffman, P.F., Schrag, D.P., 2002. Snowball Earth hypothesis: testing the limits of global change. Terra Nova. 14, 129-155.

Konhauser, K.O., Lalonde, S., Amskold, L., Holland, H.D., 2007. Was there really an Archean phosphate crisis?. Science, 315, 1234.

Konhauser, K.O., Pecoits, E., Lalonde, S.V., Papineau, D., Nisbet, E.G., Barley, M.E., Arndt, N.T., Zahnle, K., Kamber, B.S., 2009. Oceanic Nickel Depletion and a Methanogen Famine Before the Great Oxidation Event. Nature. 459, 750-753.

Pecoits, E., Gingras, M.K., Aubet, N.R., Konhauser, K.O., 2008. Ediacaran in Uruguay; palaeoclimatic and palaeobiologic implications. Sedimentology. 55, 689-719.

Pecoits, E., Gingras, M.K., Barley, M., Kapler, A., Posth, N., Konhauser, K.O., 2009. Petrography and Trace Element Geochemistry of Dales Gorge Banded Iron Formation: Paragenetic Sequence, Source and Implications for the Palaeo-ocean Chemistry. Precambrian Res. 172, 163-187.

Pecoits, E., Gingras, M.K., Konhauser K.O., 2010a. Las Ventanas and San Carlos formations (lower Ediacaran, Uruguay). J. Geol. Soc., London (accepted for publication).

Pecoits, E, Aubet N.R, Gingras, M.K., Muehlenbachs, K., Konhauser, K.O., 2010b. Chemostratigraphy and trace elements of the Ediacaran Polanco Limestone Formation (Uruguay). Chemical Geology (in review).

Pecoits, E., Aubet, N.R., Gingras, M.K., Konhauser, K.O., 2010c. Ediacaran iron formations: compelling evidence for ferruginous late Neoproterozoic seawater. Proc. Natl. Acad. Sci. U.S.A. (in review).

Pecoits, E., Konhauser, K.O., Aubet, N.R., Heaman, L.M., Veroslavsky, G., Gingras, M.K., 2010d. Evidence of early Ediacaran bilaterians. Science (in 2nd review).

Taylor, St.R., McLennan, S.M., 1985. The Continental Crust: Its Composition and Evolution. Blackwell, Oxford, pp. 312.

Wronkiewicz, D.J., Condie, K.C., 1989. Geochemistry and provenance of sediments from the Pongola Supergroup, South Africa: Evidence for a 3.0-Ga-old continental craton. Geochim. Cosmochim. Acta. 53, 1537-1549.

CHAPTER 2: EDIACARAN IN URUGUAY: PALEAOCLIMATIC AND PALAEOBIOLOGICAL IMPLICATIONS

2.1. INTRODUCTION

The Neoproterozoic is characterized by extreme environmental changes. The presence of low-latitude glacial successions, an apparent correlation between banded iron formations (BIF) and glacial events, carbonates deposited during post-glacial sea-level rise ('cap carbonates') and negative carbon-isotope excursions of Neoproterozoic sea water are some of the features associated with that time (Harland, 1964; Kirschvink, 1992; Hoffman et al., 1998a,b; Hoffman and Schrag, 2000, 2002). Correspondingly, the Neoproterozoic marks a time of significant changes in ocean and atmosphere chemistry. Atmospheric oxygen levels may have approached 18% of the present atmospheric levels and, along with the concomitant increase in ocean oxygenation, there would have been an attendant deepening of the oxic–anoxic interface and decreased sulphide levels owing to increased aerobic respiration (Canfield and Teske, 1996). Increased levels of oxygen probably facilitated the emergence of metazoans as early as ca. 600 Ma (Valentine, 2004).

One of the most researched aspects of the Neoproterozoic is the widely distributed glaciogenic deposits, interpreted as resulting from a global glaciation, the so-called 'Snowball Earth' event, in which the world's oceans are hypothesized to have been almost completely covered by continuous sea ice that formed a barrier between the oceans and atmosphere, resulting in severely diminished biological productivity (Hoffman and Schrag, 2002). The insulation of the ocean from the atmosphere led to ocean-water anoxia, resulting in an increase in the concentration of dissolved Fe(II) and Mn(II). Then, as the ice melted and ocean circulation became re-established, the metals became oxidized and accumulated as BIF (Kirschvink, 1992; Klein and Beukes, 1993). Major deposits include the 700 Ma Rapitan Group of the Mackenzie Mountains in Canada and the iron–manganese deposit of the Urucum district in Brazil (Klein and Beukes, 1993; Klein and Ladeira, 2004).

A transient but intense greenhouse climate ensued, leading to enhanced weathering of the glacially eroded landscape, increased alkalinity and carbonate precipitation (Hoffman and Schrag, 2002); this process resulted in the rapid deposition of ^{13}C-depleted, finely laminated dolomicrites (cap carbonates) directly on top of the glacial debris. These atypical carbonates generally are composed of dolostone and sharply overlie the glacial deposits, with no evidence of a hiatus in deposition. An interesting feature of these rocks is the C-isotopic composition which, during the Neoproterozoic, is much more variable than that recorded in the Phanerozoic. Once ice covered the oceans, biological productivity would have collapsed producing a drop in ^{13}C content. The most ^{13}C negative ratios, found in cap carbonates, are equivalent to those of mantle carbon (Hoffman and Schrag, 2002).

What effect global glaciation had on the microbiota is unclear. Certainly, chemotrophic and anaerobically respiring heterotrophic prokaryotes would have survived the polar conditions, but phototrophic bacteria and eukaryotes must have fared worse. In fact, the fossil record suggests that there was a marked decline in palynoflora diversity at the time of the glaciations (Vidal and Knoll, 1982; Vidal and Moczydlowska-Vidal, 1997; Walter et al., 2000), but the existence of extant photosynthetic groups known from pre-glacial times indicates that some found refuge, possibly in pockets of open water in the circum-equatorial ocean or around shallow hot springs associated with volcanic islands (Hyde et al., 2000).

Despite the significant changes that appear to have affected the biosphere during the Neoproterozoic, studies of the rock successions are comparatively limited. Very little work has been conducted in South America, despite the presence of well-exposed sedimentary deposits that bracket the glacial events. In particular, Uruguay possesses several kilometres of continuous Neoproterozoic sequences, but the lack of detailed stratigraphic studies has prevented the correlation of these with other post-glacial carbonates around the world. The aim of this investigation was to provide a detailed lithostratigraphic study of a sedimentary succession that includes pre-glacial and post-glacial events. The age, geological setting and palaeoenvironmental implications in terms of the observed sedimentological features (i.e. BIF, pink dolostones, diamictites and

unique carbonate rhythmites) are considered and related to the palaeobiological complexity during this critical period.

2.2. LITHOSTRATIGRAPHY, SEDIMENTOLOGY AND PALAEONTOLOGY

Three major Ediacaran–lowermost Cambrian lithostratigraphic units were recognized and described in eastern Uruguay: the Maldonado, Arroyo del Soldado and Arroyo de la Pedrera groups. The entire succession has a general NNE-SSW orientation and is ca. 400 km long and more than 80 km wide resting on a diverse assemblage of Proterozoic and Archean rocks belonging to the Piedra Alta, Nico Pérez and Cuchilla Dionisio Terranes (Figure 2.1A-B and 2.2).

2.2.1. Maldonado Group

The Maldonado Group was formally erected by Pecoits et al. (2005a) to include the Playa Hermosa and Las Ventanas formations. The total thickness of the group reaches ca 1600 m comprising acidic and basic volcanic rocks, as well as sedimentary deposits (Figure 2.2), generated in a tectonically active basin. The complete succession shows brittle and ductile deformation as demonstrated by the presence of fractures, strike-slip faults and folds. The unit lies on an angular unconformity above the Mesoproterozoic Lavalleja Group and granitoid rocks of undetermined age. The strata comprising the group originally were described near the towns of Piriápolis and Pan de Azúcar. Subsequent work showed that the sequence continues to the north (Figure 2.1B). Outcrops of the Maldonado Group cover an area of ca. 190 km^2.
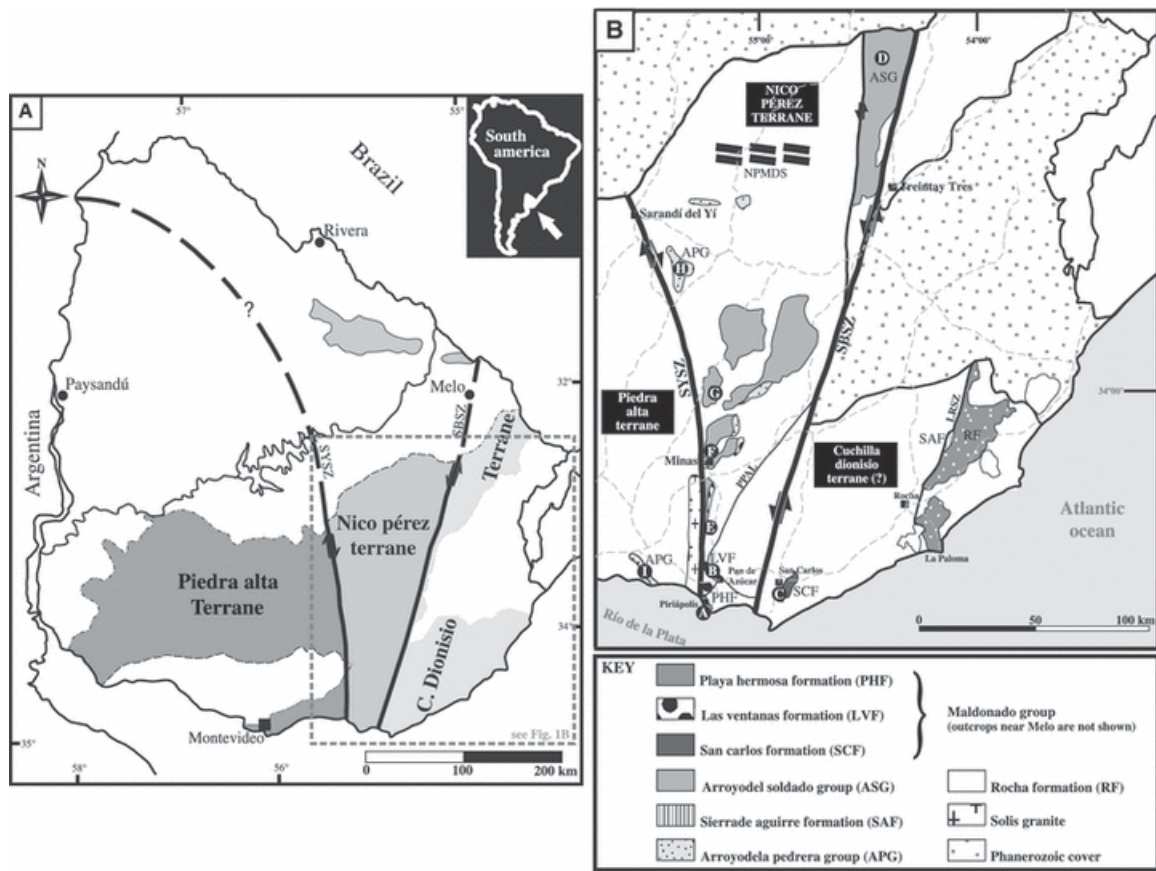
Figure 2.1. (A) Tectonostratigraphic subdivision of the Crystalline Basement of Uruguay according to Bossi (2003). SYSZ, Sarandí del Yí Shear Zone; SBSZ, Sierra Ballena Shear Zone. (B) Distribution of the Neoproterozoic–Cambrian sedimentary and volcanosedimentary sequences and location of the profiles discussed in the text (modified from Pecoits et al., 2005a). NPMDS, Nico Pérez Mafic Dyke Swarm; LRSZ, Laguna de Rocha Shear Zone.
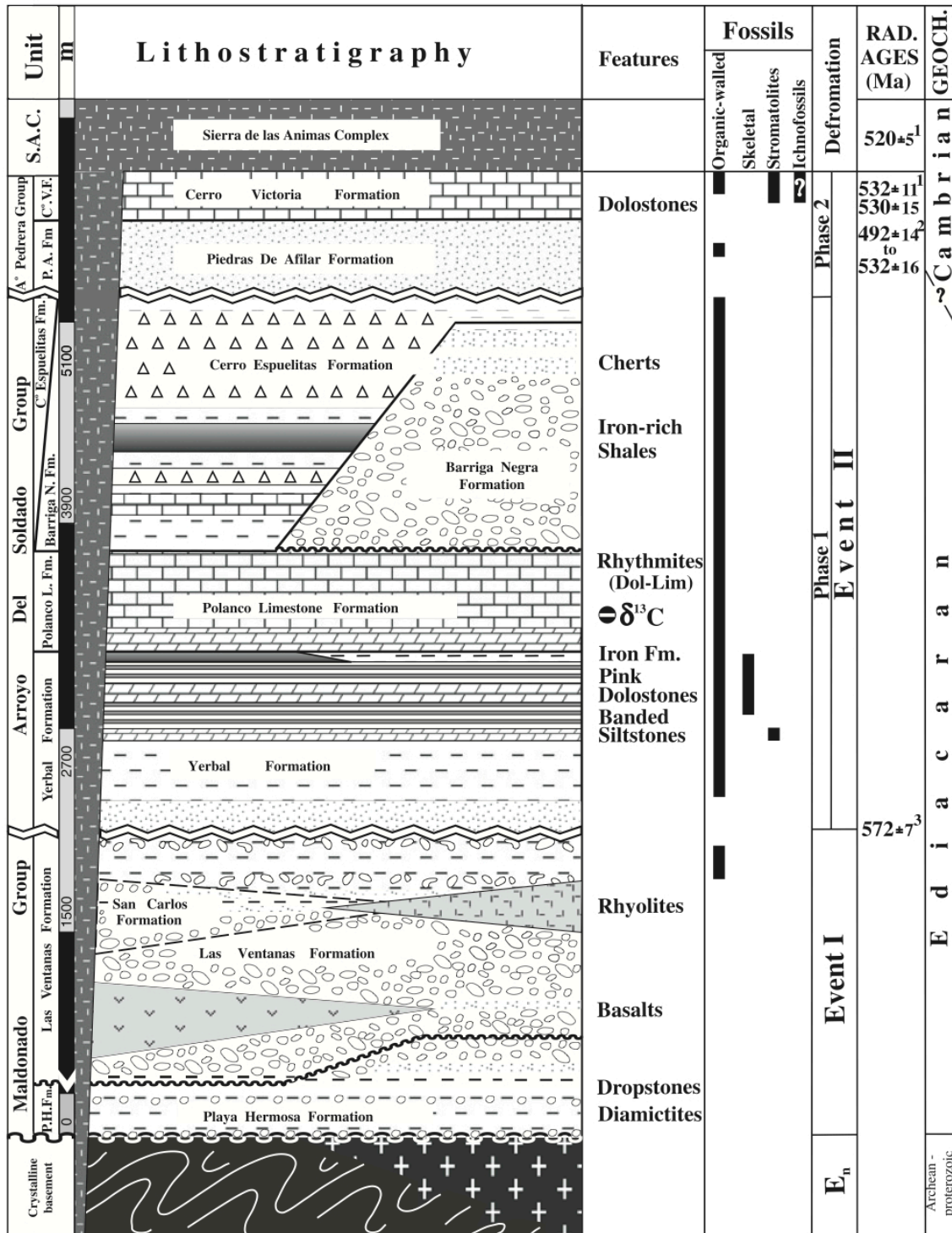
Figure 2.2. Overall lithostratigraphic cross-section showing some key lithological, palaeontological, structural and radiometric age features of Ediacaran-Cambrian units studied in Uruguay (Radiometric ages: 1 intrusive granitoids; 2 recrystallization of clayminerals in shales; 3 synkinematic muscovite in thrust) (see text for explanation).

Lithostratigraphy / Features

- S.A.C. — Sierra de las Animas Complex
- Aº Pedrera Group — Cerro Victoria Formation (C.V.F.) — Dolostones
- P. A. Fm. — Piedras De Afilar Formation
- Cº Espuelitas Fm. — Cerro Espuelitas Formation — Cherts
- Soldado Group — Barriga N. Fm. — Barriga Negra Formation — Iron-rich Shales
- Del Arroyo Group — Polanco L. Fm. — Polanco Limestone Formation — Rhythmites (Dol-Lim), $\delta^{13}C$
- Yerbal Fm. — Yerbal Formation — Iron Fm., Pink Dolostones, Banded Siltstones
- Maldonado Group — Las Ventanas Formation — San Carlos Formation, Las Ventanas Formation — Rhyolites, Basalts
- P.H.Fm. — Playa Hermosa Formation — Dropstones Diamictites
- Crystalline basement

Fossils: Organic-walled, Skeletal, Stromatolites, Ichnofossils

Deformation: Phase 2, Phase 1, Event II, Event I, E_n

RAD. AGES (Ma): 520 ± 5^1; 532 ± 11^1; 530 ± 15; 492 ± 14^2 to 532 ± 16; 572 ± 7^3

GEOCH.: Cambrian, Ediacaran, Archean-proterozoic

m: 0, 1500, 2700, 3900, 5100

2.2.1.1. Playa Hermosa Formation

Masquelin and Sánchez (1993) conducted the first detailed work on the sedimentological and tectonic features of the Playa Hermosa Formation. However, this succession was previously identified by Preciozzi et al. (1989) to include folded and intruded sedimentary rocks cropping out along the south-eastern coast of Uruguay from Playa Verde to Playa Grande (Figure 2.1B). Pazos et al. (2003) described the lower section of this unit and recognized two distinctive facies associations: (i) primarily medium to coarse-grained; and (ii) dominantly fine-grained units. The coarse-grained units consist of interbedded breccias, conglomerates, sandstones and minor mudstones that occur at the base and top of the succession; they were taken to show depositional conditions of slope instability and high rates of sedimentation (interpreted as being proximal to source). The second facies association mainly is composed of diamictites, rhythmites, sandstones and mudstones, which are interpreted to have been deposited in a distal glacially influenced environment. Both facies associations accumulated in a sub-aqueous marine environment and represent a proximal to distal depositional trend. Evidence for the glacial nature of the Playa Hermosa Formation includes dropstones, rhythmites and ice-rafted diamictites. Pazos et al. (2003) contended that this glacial-related succession constituted a record of the Varanger glaciation at the Río de la Plata Craton. The attribution of this unit to the Ediacaran is based on Masquelin and Sánchez (1993) who recognized chilled margins between the sedimentary strata and trachytic dykes. These hypabyssal rocks, which are part of the Sierra de las Animas Complex (Oyhantçabal et al., 1993), have produced Rb/Sr and K/Ar ages between 615 and 500 Ma (Bossi et al., 1993; Sánchez and Linares, 1996). Preliminary palaeomagnetic data obtained from the Playa Hermosa Formation suggest low palaeo-latitudes during the sedimentation (Sánchez and Rapalini, 2002).

The Playa Hermosa Formation unconformably overlies a pink leucocratic granite of unknown age (Fig. 3). The contact is demarcated by a clast-supported conglomerate composed of leucocratic granite (60%), quartzite (25%) and pelitic intraclasts (15%). Up-section, the conglomerates occur as irregular to lenticular bodies within sandstone beds or (more rarely) may grade laterally into sandstone. In the middle and upper part of the section, thin, erosionally based conglomerate beds commonly contain intraclasts.

Conglomerates, similar to those appearing at the base, are present at the top of the Playa Hermosa Formation; these are composed of leucocratic granite (45%), quartzite (40%) and pelitic intraclasts (15%). Matrix-supported conglomerates occur almost exclusively in the middle of the succession although some thin beds are observed up-section. Therein, 5 m thick pebble-diamictite and rare thin-bedded turbidites are present.

The basal conglomerates are interpreted as a product of sediment gravity flows (grain flow and debris flow deposits). The top of the beds are either amalgamated with subsequent flow deposits or grade into overlying turbidites forming a compound debrite–turbidite couplet (Einsele, 2000). The diamictites (located up-section) are dominated by ice-rafted debris. The absence of grain-size segregation and the presence of chatter marks on pebbles strongly reinforce a glacial interpretation (Pazos et al., 2003).

The lower sandstones are both interbedded with the conglomerates, and occur as lenticular beds. These lithologies appear also up-section as lenticular bedding, irregular bodies and massive beds within thicker pelitic beds. The sandstones commonly occur as millimetre to centimetre scale sandstone/siltstone intercalations (Figure 2.3). Coarser-grained beds are thicker. These deposits are interpreted as turbidites. In the middle part of the unit, as much as 10 m of medium to coarse-grained sandstones interbedded with siltstones are observed. Up-section the bedding thickness and grain-size are reduced and climbing ripples become common. The uppermost beds show planar parallel lamination composed of coarse and fine-grained siltstone; this feature represents a thinning and fining-upward trend from more proximal to distal turbidites (Bouma Tb-e–Td-e).
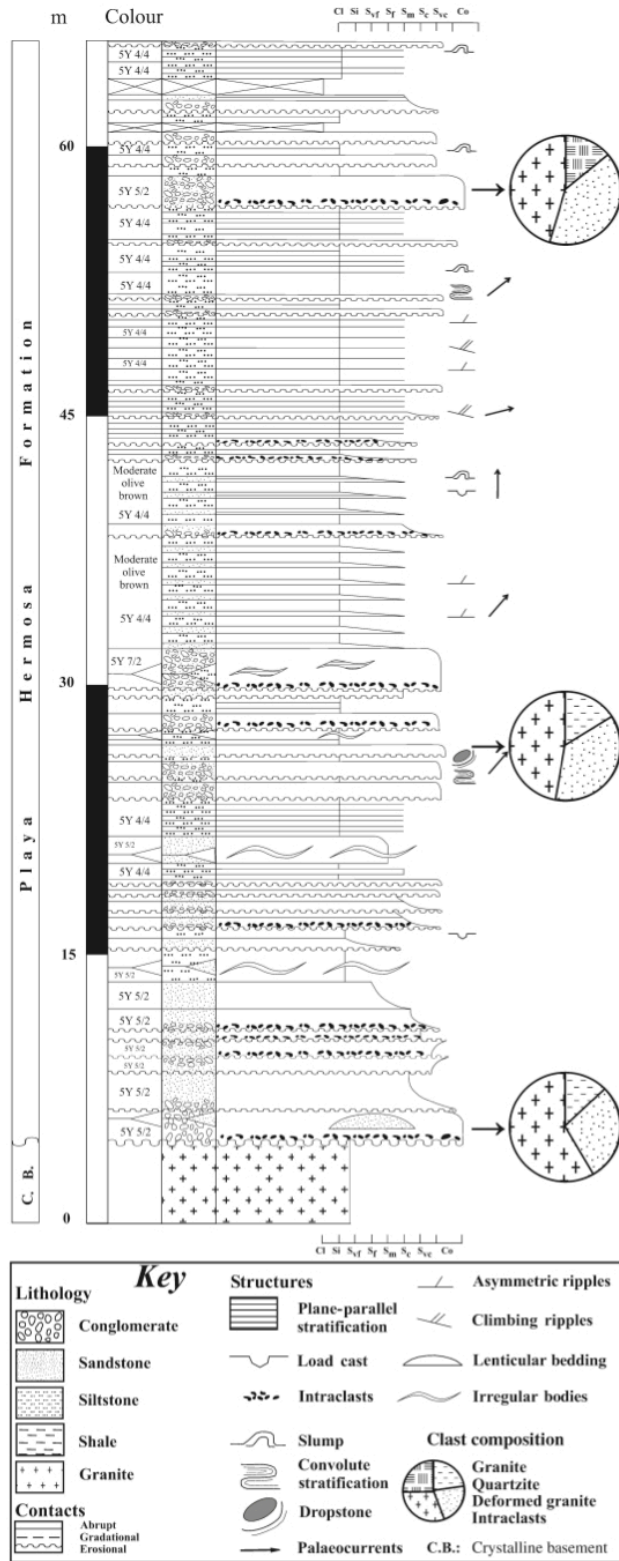
Figure 2.3. Stratigraphic column of the stratotype of the Playa Hermosa Formation (point A, Figure 2.1B; Playa Verde, Piriápolis).

13

The Playa Hermosa Formation records deposition in a tectonically active, extensional basin. Deformational and palaeocurrent structures suggest sediment transport towards N–NNE. Pazos et al. (2003) referred to dropstones, ice-rafted debris, rhythmites and a striated boulder as evidence of a glacial origin for the succession. Given that the rhythmites are interpreted as distal turbidites herein and striated or faceted clasts were not documented, ice-rafted diamictites and dropstones constitute the best evidence of a glaciogenic origin (Figure 2.4A). It is most likely that the described lithofacies represent the record of distal sub-aqueous outwash deposits. Considering the lack of lodgement, ice-contact deposits and proximal outwash deposits, a (maximum) proglacial zone of deposition is suggested (see Edwards, 1986).
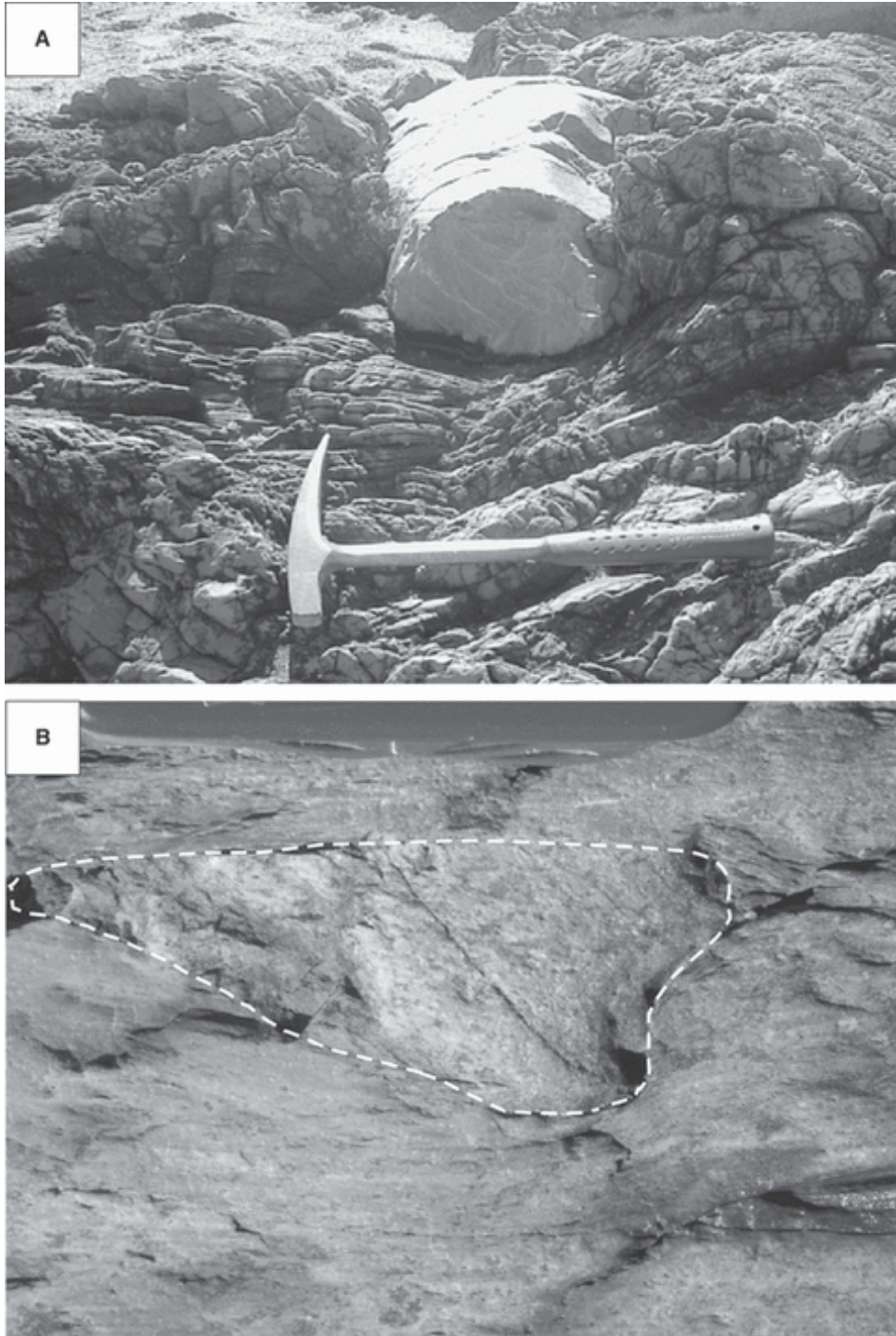
Figure 2.4. (A) Quartzitic dropstone block within the mudstones of the Playa Hermosa Formation (length of hammer: 40 cm). (B) Laminated siltstones facies from the lower Las Ventanas Formation containing dropstones of basaltic composition (knife: 9 cm).

2.2.1.2. Las Ventanas Formation

Midot (1984) erected the Las Ventanas Formation to include conglomerates, sandstones and pelites cropping out at Las Ventanas hill and in the surrounding areas. This unit was considered by Midot (1984) and various other authors as an Ordovician sedimentary sequence (Preciozzi et al., 1988; Bossi and Navarro, 1991; Masquelin and Sánchez, 1993; Bossi et al., 1998; Pazos et al., 2003). This assumption was founded mainly on the supposed development of alluvial fans sourced from the Sierra de las Ánimas Complex (Cambrian), located towards the west.

Recently, mapping and sedimentological and stratigraphical studies of the Las Ventanas Formation carried by Pecoits (2002), led to a redefinition of the unit as a Neoproterozoic volcano-sedimentary sequence. Therein, one proximal and one distal facies association can be recognized (Pecoits, 2002). The first facies association is composed of clast-supported conglomerates, diamictites and massive sandstones. The second facies contains laminated siltstones and sandstone-pelite rhythmites with rare sandstones and conglomerates (Pecoits, 2003a). These deposits were interpreted as a product of sheetflood-dominated fan deltas intercalated with minor marine deposits. Pecoits et al. (2005a) reported evidence of glacial influence in the lower part of the unit, where foliated outsized clasts of volcanic rocks in sedimentary rhythmite layers were documented.

To the south of the mapped area intercalated basalts, acidic volcanoclastic rocks and rhyolites are recognized. This bimodal volcanism was thought to represent part of the Sierra de las Ánimas Complex (see for example Sánchez and Rapalini, 2002 and references therein). However, based on detailed geological mapping of the Las Ventanas Formation it is likely that this unit was influenced by the Puntas del Pan de Azúcar Lineament (Fig. 5). Near this fault, which is located to the east of the study area, the sequence shows intense deformation; this deformation suggests that the deposition of the Las Ventanas Formation occurred before the last reactivation of the lineament, which was dated at 572 ± 7 Ma (K/Ar) (Bossi and Campal, 1992). Furthermore, the late-orogenic Pan de Azúcar Granite, which intrudes the Las Ventanas Formation (Pecoits, 2003b), was

dated at 559 ± 28 Ma (Rb/Sr) (Preciozzi et al., 1993). Also, the trachytes and syenites of the Sierra de Las Ánimas Complex intrude the unit and yield an age of 520 ± 5 Ma (Rb/Sr) (Bossi et al., 1993). Finally, the occurrence of microfossils such as *Bavlinella faveolata* Schepeleva (Vidal, 1976) in shales has been reported by Pecoits (2003a). Although this taxon possesses a long stratigraphic range (Upper Riphean to Ordovician; see, for example Mansuy and Vidal, 1983; Knoll and Sweet, 1985), its acme in the Ediacaran and its occurrence in the Arroyo del Soldado Group has stratigraphic and environmental significance (see Discussion).

The section exposed in the northern part of the type area is designated herein as the stratoype of the Las Ventanas Formation. At this locale 1200 m of Las Ventanas strata are exposed continuously (Figure 2.6). The unit lies unconformably on the Lavalleja Group but the contact is not exposed at this section. The unit begins with a 690 m thick fining-upward and thinning-upward cycle. Conglomerates, sandstones and siltstones dominate the lowermost, medial and uppermost sub-cycles respectively. The conglomerates are typically clast-supported and are composed of granite clasts. Arkosic sandstones are present at the top of each sub-cycle. The following changes occur up-section within the lower cycle: (i) bed thickness progressively decreases, from metre-scale to a few millimetres (laminae); (ii) average grain-size decreases from pebbles to silt; (iii) the proportion of granitic clasts also becomes smaller; and (iv) planar parallel stratification and lamination become a common feature in the siltstones but are absent in the lower and medium part of the cycle.
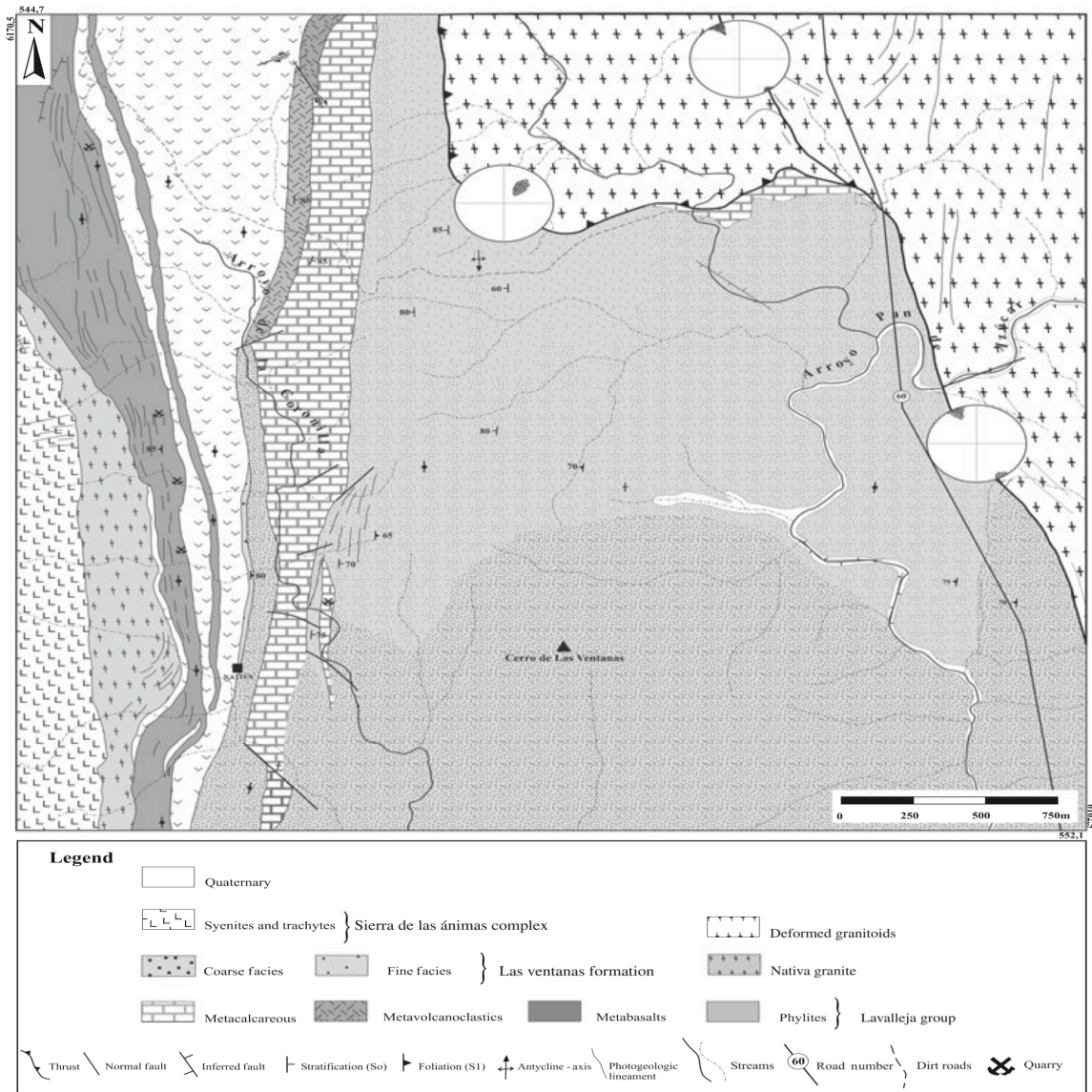
Figure 2.5. Geological map of the type area of the Las Ventanas Formation (modified from Pecoits, 2003a). Note the differences in the stretching lineation measured along the major lineament demonstrating a strike-slip reactivation of an older southwestward thrust, which is associated with folds showing southward vergence.
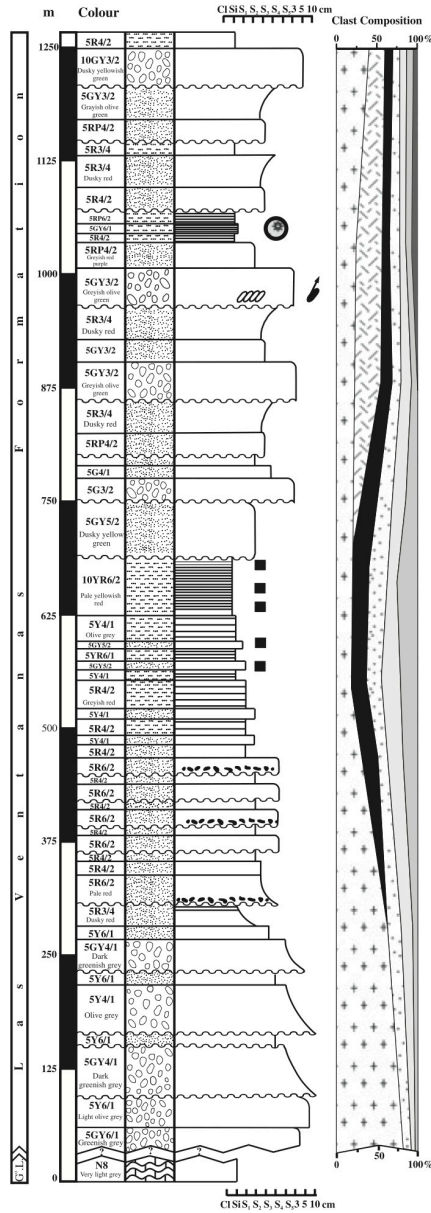
Figure 2.6. Stratigraphic column of the Las Ventanas Formation at its stratotype (point B, Figure 2.1B).

The formation passes up-section into a second cycle almost 560 m thick, which is composed of minor cycles of sandstones and conglomerates (Fig. 6). The sandstones have a tabular geometry, are massive-appearing and possess non-erosive basal contacts. The conglomerates are clast-supported, polymictic and have a modal grain-size of 3 cm. In the uppermost conglomerate bed the clast-size approaches 10 cm. The clast composition is variable (32% rhyolite, 22% granite, 12% quartz, 11% basic volcanic rocks, 10% alkaline feldspar, 8% plagioclase feldspar, 5% schists). Although uncommon, thin interbedded beds of red and grey pelites also occur.

The unconformable contact of the Las Ventanas Formation to the metamorphic basement (Lavalleja Group) is exposed 100 m to the south of the mapped area (close to Nueva Carrara Quarry and Apolonia Mine: Figure 2.7). At this locale, laminated siltstones contain clasts and impact structures that deform the planar-parallel stratification; these are interpreted as dropstones (Pecoits et al., 2005a; Figure 2.4B).
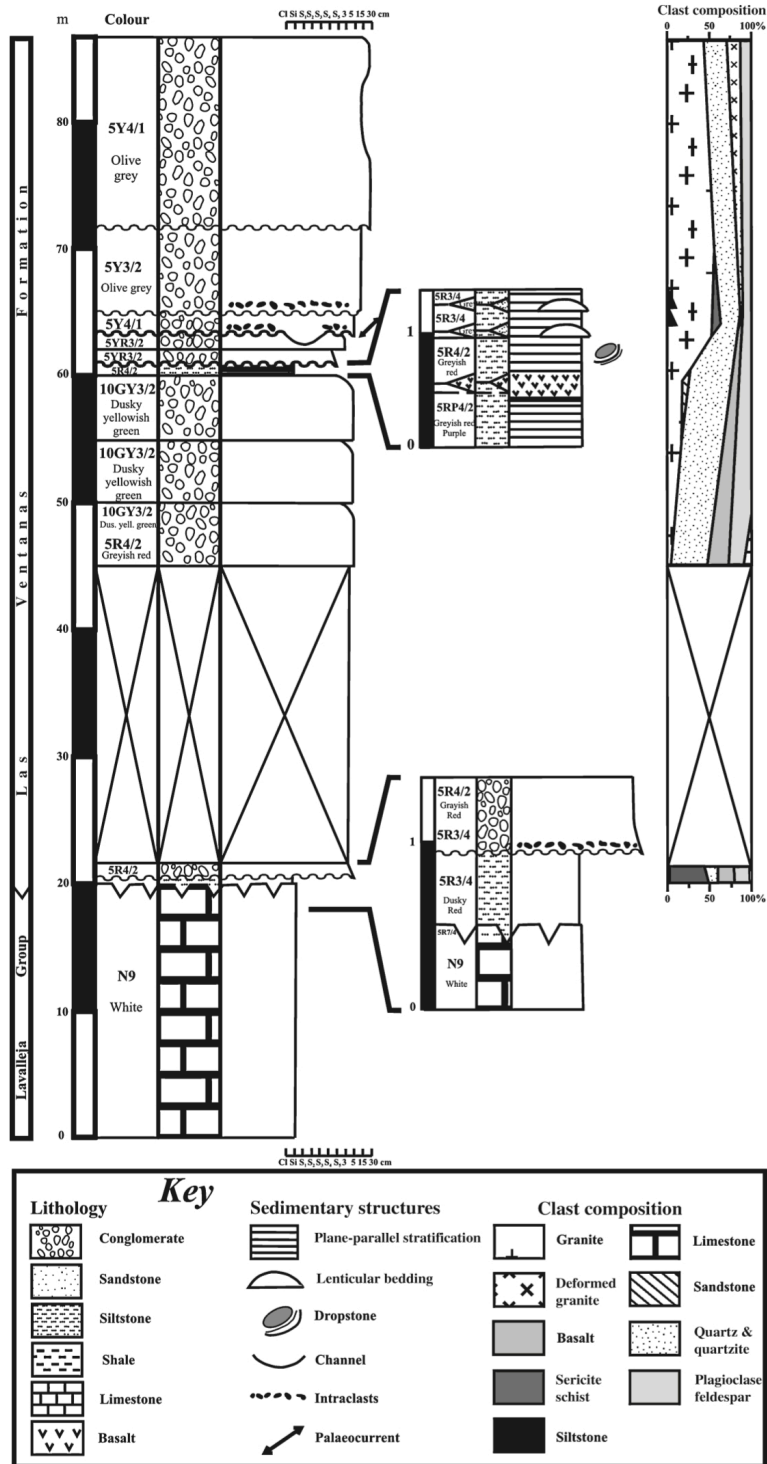
Figure 2.7. Stratigraphic section for the lower Las Ventanas Formation at its parastratotype (8·5 km south of point B, Figure 2.1B).

2.2.1.3. San Carlos Formation

The San Carlos Formation was erected by Masquelin (1990). The unit is well-developed in the Cuchilla Dionisio Terrane near San Carlos (Figure 2.1B). According to previous authors, the unit consists of conglomerates, sandstones and pelites. The San Carlos Formation probably represents a lacustrine or fluvio-lacustrine setting. Sánchez (1998) described trough cross-stratification in sandstone beds indicating palaeocurrents towards the NE and proposed that the San Carlos represents a meandering fluvial depositional system of Ordovician age.

The stratotype of the formation is located 6 km to the south of San Carlos town where 220 m of the formation are exposed (base and top not visible) (Figure 2.8). The succession is composed of interbedded conglomerates, sandstones and pelites, with the latter dominating up-section. The San Carlos Formation is initiated with 120 m clast-supported conglomerates with a maximum clast size of 1·5 cm. Cycles of 0·5 to 0·8 m thick centimetre-scale pelite and sandstone beds comprise the stratum. Up-section, conglomerate clasts reach 30 cm in diameter. The coarser conglomerates persist up-section passing upwards into 70 m of pelite-free conglomerates with minor sandstones.

The sedimentary facies of the San Carlos Formation are similar to those of the middle Las Ventanas Formation (compare Figures 2.6 and 2.8). Preliminary palynological macerations carried out in the pelites (Pecoits et al., 2005a) revealed the occurrence of a microbiota similar to that described for the Las Ventanas Formation (Pecoits, 2003a); mainly present are spheroid vesicles of Bavlinella faveolata Schepeleva (Vidal, 1976).

New fieldwork in the area has revealed interbedded rhyolites within the San Carlos Formation. Neither geochronological nor geochemical data are available from the rhyolites yet. However, it is plausible that these rocks, as in the case of the Las Ventanas Formation, are related to syn-tectonic to late-tectonic granites. The ages obtained for those granites range between 570 and 590 Ma (Umpierre and Halpern, 1971; Preciozzi et al., 1993; Basei et al., 2000).

Figure 2.8. Simplified stratigraphic column of the San Carlos Formation at its stratotype, 6 km SE of San Carlos town (point C, Figure 2.1B).

The above characteristics permit correlation of the San Carlos and Las Ventanas Formations. Further research will be required to determine whether both units were deposited in the same basin and subsequently dismantled by the displacement of the Sierra Ballena Shear Zone. The authors suggest that the San Carlos Formation is a volcano-sedimentary unit of Ediacaran age.

2.2.2. Arroyo del Soldado Group

This lithostratigraphic unit was defined by Gaucher et al. (1996), to include a marine shallowing-upward sequence (ca. 1500 m) comprising (from base to top) the Polanco Limestone (Goñi and Hoffstetter, 1964), Cerro Espuelitas, Cerros San Francisco (Montaña and Sprechmann, 1993) and Cerro Victoria Formations (Montaña and Sprechmann, 1993). Later, Gaucher et al. (1998) included the basal Yerbal Formation and the Barriga Negra Formation (Midot, 1984), totalling more than 5000 m in thickness for the entire group. Gaucher et al. (1996) suggested that the succession was deposited on a stable continental shelf undergoing tectonic quiescence.

The age of the group is constrained by radiochronology and biostratigraphic data (Figure 2. 2). Intrusive syenites and granitoids produced contact metamorphism with ages ranging between 540 and 510 Ma. The characteristics of the organic-walled microfauna and the occurrence of the index late Vendian fossil Cloudina riemkeae (Germs, 1972) have suggested a date for the succession as uppermost Vendian (Valdaian) to lowermost Cambrian.

Due to the distinctive features attributed to the Yerbal and Cerro Espuelitas Formations [i.e. distinctive fossils, pink dolostones and iron formations (IF), among others], the following specifically describes stratigraphic profiles emphasizing those characteristics as they can provide constraints on the palaeoclimatological and palaeoenvironmental conditions.

2.2.2.1. Yerbal Formation

This stratotype is located along the path parallel to the Arroyo Yerbal Chico where the unit reaches 1500 m (location D; Figure 2.1B). There the transition towards the concordantly overlying Polanco Formation is well-exposed; however, the base is exposed only to the south of Rivera (Figure 2.1A), along the Arroyo San Pablo, where the profile has been designated as parastratotype (Gaucher, 2000). According to Gaucher et al. (1998), two different facies associations, shallow-water and deep-water, are present. The shallow-water facies association is the most widely distributed and it consists of basal conglomerates, followed by intercalations of sandstones and pelites in the middle of the succession, grading to banded siltstones at the top. The deep-water facies association comprises an alternation of finely laminated dark shales and arkoses; these represent turbidites. More recently Gaucher et al. (2004) reported the presence of oxide-facies BIF with up to 24% magnetite/hematite. The BIF reaches a thickness of 50 m. It is likely that the Yerbal Formation records the transgression of the Vendian sea displaying a fining and thinning-upward trend. Organic-walled microfossils and a distinct shelly fauna occur at the top of the formation. The fossils include *Cloudina riemkeae* (Germs, 1972), *Titanotheca coimbrae*, *Waltheria marburgensis*, *Soldadotubulus siderophoba* and *Palaeodiscus mendezalzolai* (Gaucher and Sprechmann, 1999).

In the areas of Minas town and La Salvaje farm, the following sedimentary deposits (in order of decreasing abundance) have been observed: (i) pelites; (ii) sandstones; (iii) carbonates; (iv) IF and cherts.

(i) Siltstones represent the most common lithotype of the Yerbal Formation. At La Salvaje farm they occur in the lowermost and middle parts of the section (Figure 2.9). The former consist of dark banded siltstones with rare thin iron-rich bands. Siltstones showing regular microbanding and mesobanding also occur. The rhythmic banding emphasizes the organic-matter content (Figure 2.11A). Near the top, large quantities of vase-shaped skeletal fossils of undetermined affinity have been discovered. Preliminary observations suggest that these minute calcareous cones belong to the metazoan Cloudina. Similar siltstones are present close to Minas town where rhythmically

laminated and banded siltstones are observed in several outcrops (Figures 2.10 and 2.12). Siltstones interbedded with sandstones are common downsection and millimetre to centimetre alternations of iron-rich, carbonate-rich and organic matter-rich dark bands are present in the upper part (Figures 2.12B to 2.12D).

(ii) In the Minas area, resting on granites of unknown age, the unit is composed of alternating sandstones, pelites and carbonates (Figure 2.12A). The basal sandstones are sub-arkosic evolving upwards to orthoquartzites. The sandstones contain ripple cross-stratification and lenticular bedding; near the base they are intercalated with pelites defining fining-upward and thinning-upward cycles. Up-section there is a gradational occurrence of white, laminated carbonates. Sandstones underlying the banded siltstones described above are interbedded with pelites at the base and top of the section (Figure 2.12B). Some of the beds correspond to volcaniclastic sandstones, which constitute the first report of synsedimentary volcanism for the Arroyo del Soldado Group. Underlying the fossiliferous banded siltstones are 80 m of intercalated siltstones and arkoses.

(iii) Limestones and dolostones are described for calcareous units. The former occur near the base of the unit where the limestone reaches 45 m thick and is dominated by parallel bedding and spaced laterally linked hemispheroid stromatolites (Figure 2.11B; Logan et al., 1964). Upwards, pink carbonates are followed by calcisiltites and then typical banded siltstones of the unit (Figure 2.12A). The dolostones observed up-section consist of 50 m thick greyish pink dolostones and 75 m thick pink dolostones, which are finely laminated and resemble cryptalgal laminites. The relationship between the basal stromatolitic carbonates and the overlying pinkish dolostones is not yet resolved, the dolostones are unequivocally interbedded with siltstones and sandstones of the Yerbal Formation. At La Salvaje farm (location E; Figure 2.1B), a 45 m thick interstratified unit of limestones, dolostones and light grey chert is observed near the base (Figure 2.9). Similarly in the overlying Polanco Limestone Formation, fine-grained, grey rhythmic alternations of limestone and primary dolostone with rare chert laminae occur and constitute the most common facies of the mentioned unit (Figure 2.11C).
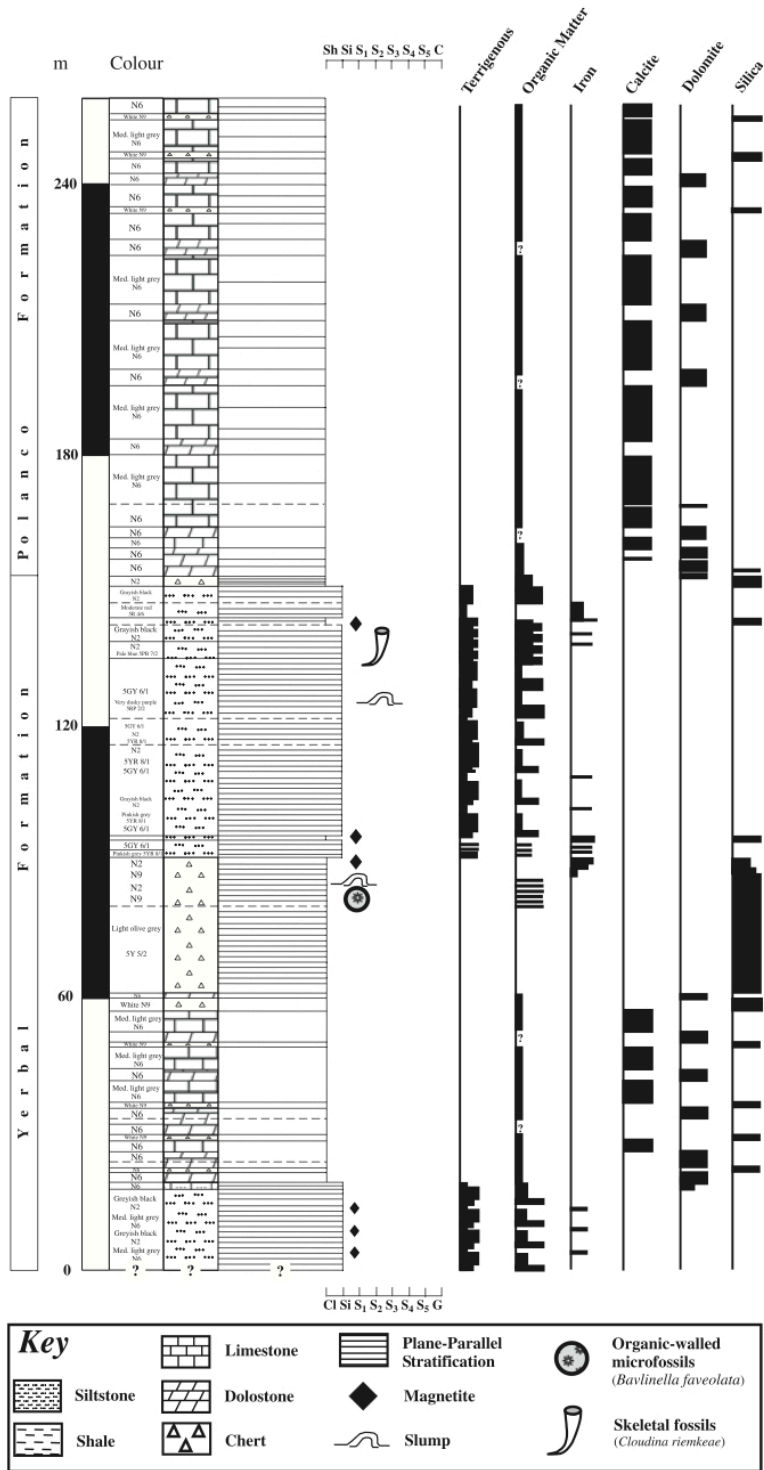
Figure 2.9. Logged section of the upper Yerbal and lower Polanco Formations at La Salvaje farm (point E, Figure 2.1B). Siliciclastic, organic matter, iron, calcite, dolomite and silica content were determined on the basis of hand sample observations and preliminary thin-section analysis.
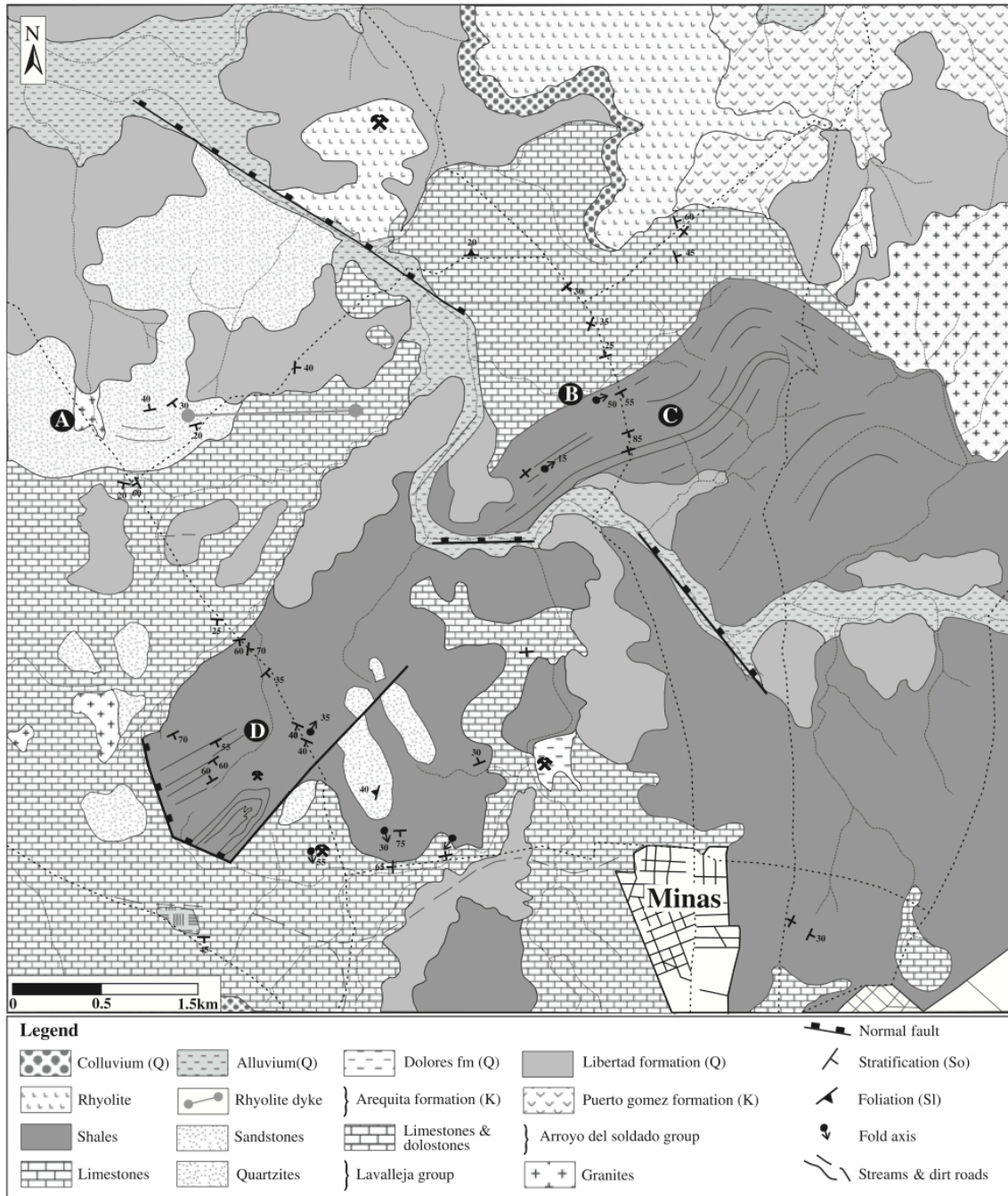
Figure 2.10. Geological map of NE Minas town surrounding area (point F, Figure 2.1B). Only facies belonging to the Yerbal Formation are present in the mapped area. Points A to D indicate location of sections shown in Figure 2.12.
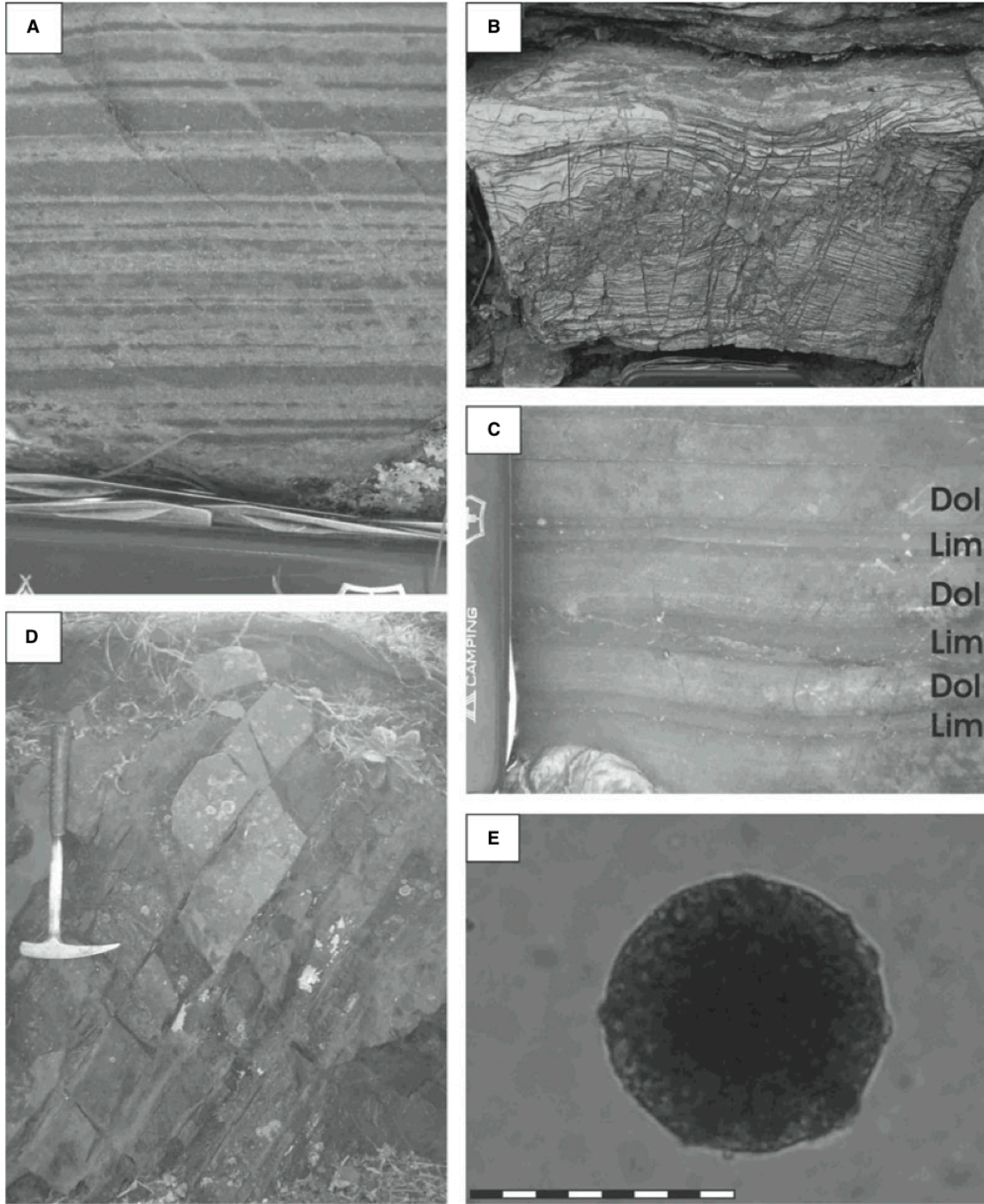
Figure 2.11. (A) Finely laminated siltstones characteristic of the Yerbal Formation (Figure 2.9). (B) Stromatolites in the lower Yerbal Formation (Figure 2.12A). (C) Limestones-dolostones rhythmites. The layers are millimetres to decimetres thick (Polanco Formation; Figure 2.9). (D) Iron formation from the upper Yerbal Formation (Figure 2.12D). (E) *Bavlinella faveolata* Schepeleva (Vidal) occurring in palynological macerations of iron rich shales, Cerro Espuelitas Formation (Figure 2.13). Scale: knife: 9 cm; hammer: 40 cm; bar: 10 μm.
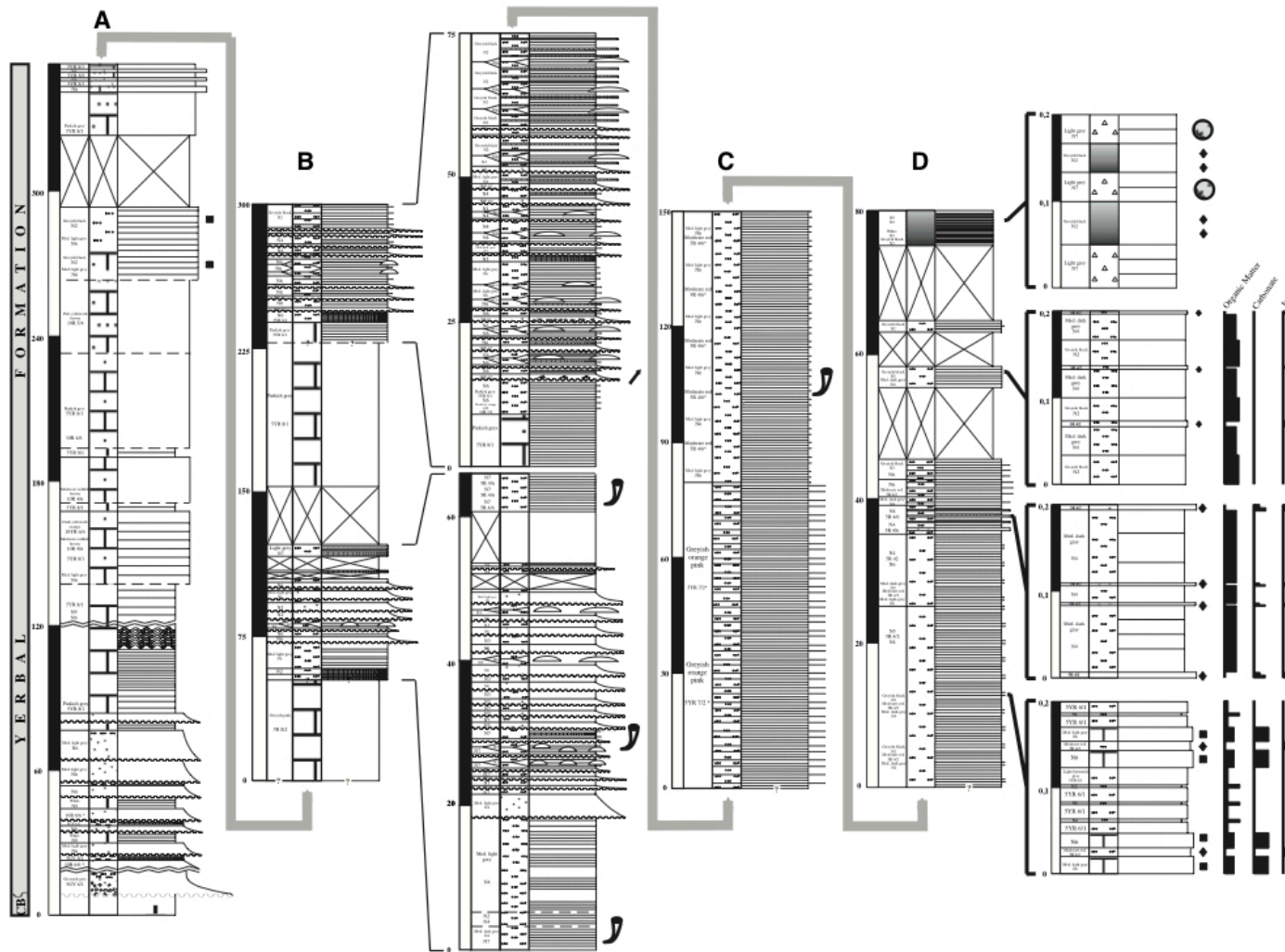
Figure 2.12. Different sections of the Yerbal Formation in the area of NE Minas (see Figure 2.10 for location). Symbols are the same as in Figure 2.9.

(iv) Only two localities are known where these facies occur: La Salvaje farm and east of Minas town. The cherts display different characteristics depending on their stratigraphic position; those interbedded with dolostones and limestones are centimetre-thick greyish white beds (Figure 2.9). Up-section the cherts develop into their maximum thickness (30 m) with bedded greyish green cherts at the base and very finely laminated black and white chert at the top. The latter is rich in organic-walled microfossils. On the uppermost part of the chert beds Fe-enrichment occurs. Elsewhere in the same section (at the base and top of the banded siltstones facies) thin, black, iron-rich chert beds are also present. Banded iron formations are developed at the top of the section located 5 km east of Minas (Figure 2.11D); they can reach 10 m in thickness, and consist of alternating bands of magnetite/hematite and chert. Stratification is variable but always thinner at the base. It is important to note that the BIF is conformable with the overlying thick-banded siltstone succession suggesting a trend of similar palaeoenvironmental conditions of sedimentation (Figure 2.12D).

2.2.2.2. Cerro Espuelitas Formation

The stratotype of the Cerro Espuelitas Formation is located in the Cerro Espuelitas, 40 km north of Minas, where the base of the unit is exposed (location G; Figure 2.1B). The geological map of this area, as well as the stratigraphic column, was established by Gaucher (2000). Later detailed mapping has recognized intense local folding, which is responsible for previous overestimations in the thickness of the succession.

The logged section shows the Cerro Espuelitas Formation concordantly overlying the Polanco Formation; the latter consists of alternating stratified dolostones and laminated cherts, with a thickness of <70 m (Figure 2.13). The top of the unit has not been observed, so the total thickness is unknown. The Cerro Espuelitas Formation is composed of 35 m of pelitic facies with minor cherts at the base; these grade into 110 m of thick-bedded cherts. At the top thickly laminated iron-rich and organic-rich shales are present. A distinctive microflora is present in the shales (Figure 2.11E). The succession

passes up-section into clean cherts, with variable iron and organic-matter content. In the middle part of this facies a 5 m thick fragmented chert bed is present. At the outcrop scale a strong stretching lineation parallel to the So is observed; this lineation suggests a strike-slip displacement along the steep hills formed by cherts. Preliminary analysis of the structures present in the area enables confirmation of the presence of either a progressive strain regime (NE–SW), with rotation of structures, or two discrete deformation regimes with compression phases oriented NE–SW and ENE–WSW. Moreover, fragile deformation produced occasional iron-rich veins and silica-cemented breccias, which had been interpreted as BIF and sedimentary breccias. Therefore, the Cerro Espuelitas Formation is redefined as dominated by shales and cherts. Even though iron-rich rocks are present, BIF and associated breccias were not documented.
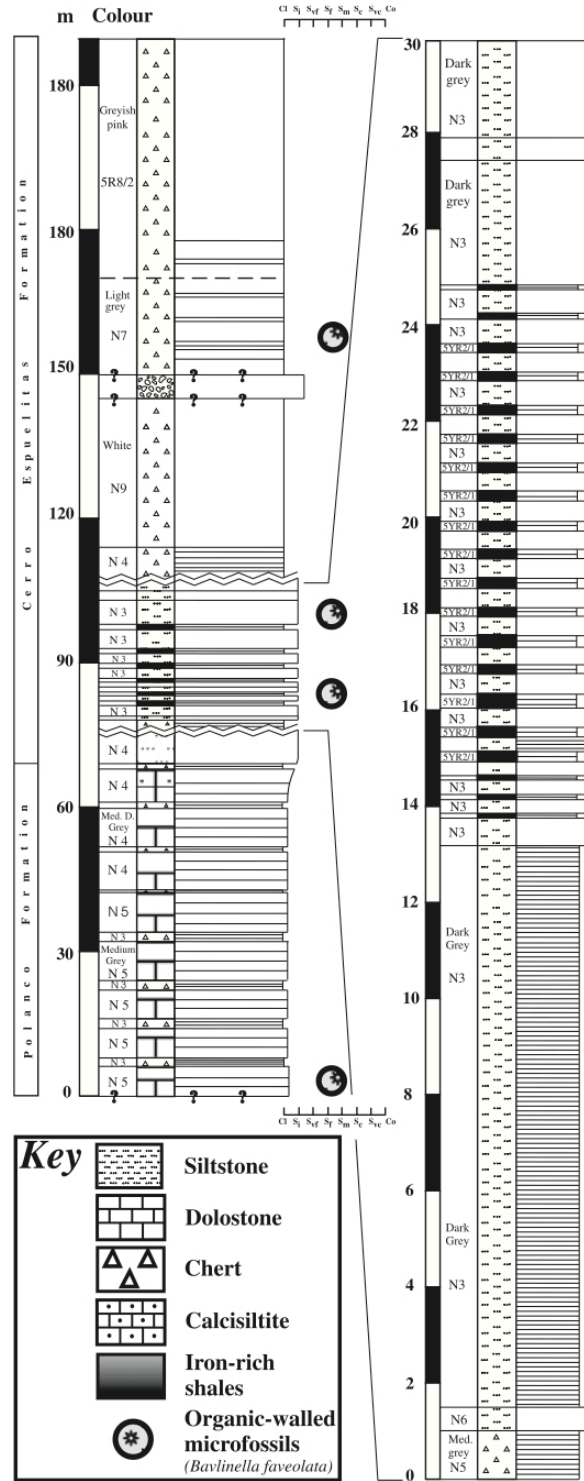
Figure 2.13. Stratigraphic column of the Cerro Espuelitas Formation, showing the stratotype of the unit (point G, Figure 2.1B).

2.2.3. Arroyo de la Pedrera Group

Montaña and Sprechmann (1993) proposed the Arroyo de la Pedrera Formation, which consists of the Cerros San Francisco Member and Cerro Victoria Member. The Cerros San Francisco Member includes sandstones and siltstones, showing well-preserved sedimentary structures, and represents a fining-upward and thinning-upward cycle. According to these authors, the overlying Cerro Victoria Member is characterized by stromatolites and micritic limestones at the base, oolitic calcarenites and micritic limestones in the middle part of the succession and stromatolitic limestones interbedded with micritic limestones and organic-rich chert layers at the top. Even though dolomite has not been recognized previously, almost the whole unit is composed of dolostones ('post-depositional' dolomites). The type area is located to the NW of Illescas, in the Florida Department, where a continuous ~600 m thick succession is exposed (Montaña and Sprechmann, 1993) (location H; Figure 2.1B). Gaucher et al. (1996) promoted both members to formational rank and, due to an apparent stratigraphic continuity, included them in the Arroyo del Soldado Group. Based on previously reported $\delta^{13}C$ values and the stromatolite community, ichnofossil assemblage and ichnofabrics, Sprechmann et al. (2004 and references therein) placed the Cerro Victoria Formation in the lowermost Cambrian (542 to 535 Ma). These authors described a low-diversity stromatolite community and a low-diversity trace fossil association (*Thalassinoides–Gyrolithes–Palaeophycus* assemblage), both of which would confirm a Cambrian age. Sprechmann et al. (2004) concluded that the presence of trace fossils would constitute the best criterion for locating the unit in the lower Cambrian. However, the illustrated structures resemble diagenetic concretions of inorganic origin, and micropalaeontological studies carried out in the underlying Piedras de Afilar Formation reveal microbiota similar to that of the Arroyo del Soldado Group of Ediacaran age (see below). Although information is not yet conclusive, ongoing micropalaeontological research should determine either that the Arroyo de la Pedrera Group is of Cambrian age or that the typical organic-walled microfossils occurring in the Arroyo del Soldado Group (Ediacaran) extend into the Cambrian.

Aubet (2005) presented a detailed sedimentological and stratigraphical study of the Piedras de Afilar Formation, which is correlated with the Cerros San Francisco Formation (see also Aubet et al., 2005). Following recommendations of the International Stratigraphic Guide (Murphy and Salvador, 1999), the Cerros San Francisco name is replaced by the earlier defined Piedras de Afilar Formation (Jones, 1956). The relationship between the Cerro Espuelitas Formation and the Cerros San Francisco Formation (Figure 2.2), originally interpreted as conformable by Gaucher et al. (1996), has not been corroborated in this study. Instead, the later unit rests directly on an angular unconformity to the pre-Ediacaran basement. Therefore, following the original name proposed by Montaña and Sprechmann (1993), the Arroyo de la Pedrera Formation (hosting the Piedras de Afilar and the Cerro Victoria units) is elevated to group status and separated from the Arroyo del Soldado Group (Figure 2.2). Considering new information, a brief description of the Piedras de Afilar Formation is given below. For a recent description of the Cerro Victoria Formation see Sprechmann et al. (2004).

2.2.3.1. Piedras de Afilar Formation

The Piedras de Afilar Formation was formally defined by Jones (1956) as a siliciclastic fining and thinning-upward succession, composed of sandstones, shales and limestones; these rest on the Palaeoproterozoic basement in the south-eastern area of the Piedra Alta Terrane (see Figure 2.1A and 2.1B; location I). Coronel et al. (1982) presented the first detailed geological map of the area. The most recent and comprehensive study by Aubet (2005) described the stratigraphy and facies associations of the unit (Figure 2.14). At the Piedras de Afilar hills, where the basal contact with the underlying Palaeoproterozoic basement and its neostratotype are exposed, the section is up to 600 m thick and consists of two distinct units that are treated herein as lower and upper intervals. The lower part is ~400 m thick and constitutes a sandstone-dominated interval, with subordinate siltstones and thin conglomerates interbedded at the base. Individual sandstone bodies have coarse-grained bases, commonly displaying planar cross-beds; these grade upwards into medium-grained quartz arenites with trough cross-stratification and ripple cross-

lamination indicating waning flow deposits. Interbedded reddish fine-grained sandstone grading to siltstones have been described. Compositionally, the sandstones are sub-arkosic with zircon, sphene and tourmaline present as accessory minerals. The upper 150 to 200 m consists of purple siltstones and minor shales dominated by planar lamination, occasionally interbedded with thin sandstones layers. At the top of this unit, a gradational sedimentary contact with the overlying carbonate unit is observed (Figure 2.14). The authors regard limestone strata above the siliciclastic succession as equivalent to the Cerro Victoria Formation.

On the basis of lithostratigraphy, the Piedras de Afilar Formation was correlated tentatively with the Cerros San Francisco Formation of the Arroyo del Soldado Group (Aubet et al., 2005). New field research permits correlation on the basis of the following characteristics: (i) both rest directly on pre-Ediacaran basement and are overlain by a carbonate unit; (ii) both represent a fining upwards succession; (iii) siltstones are always dominant in the upper interval; (iv) they present similar bimodal palaeocurrent patterns: ~N–S and ~E–W; (v) their facies assemblages and sandstones petrofacies are almost identical; (vi) they have Palaeoproterozoic Nd model ages (~1·9 Ga); and (vii) both units are intruded by the Sierra de las Animas Complex (Cambrian) and other Cambrian granites. Moreover, micropalaeontological studies in the Piedras de Afilar Formation have shown that they contain similar organic-walled microfossils, including the most abundant and widely distributed species of the Arroyo del Soldado Group (*Soldadophycus bossii*). The microbiota recovered from the Piedras de Afilar Formation is characterized by low diversity, with *Bavlinella faveolata*, *Myxococcoides minor*, *Spumosina rubiginosa* and *Soldadophycus bossii* being the most dominant (Figure 2.15).
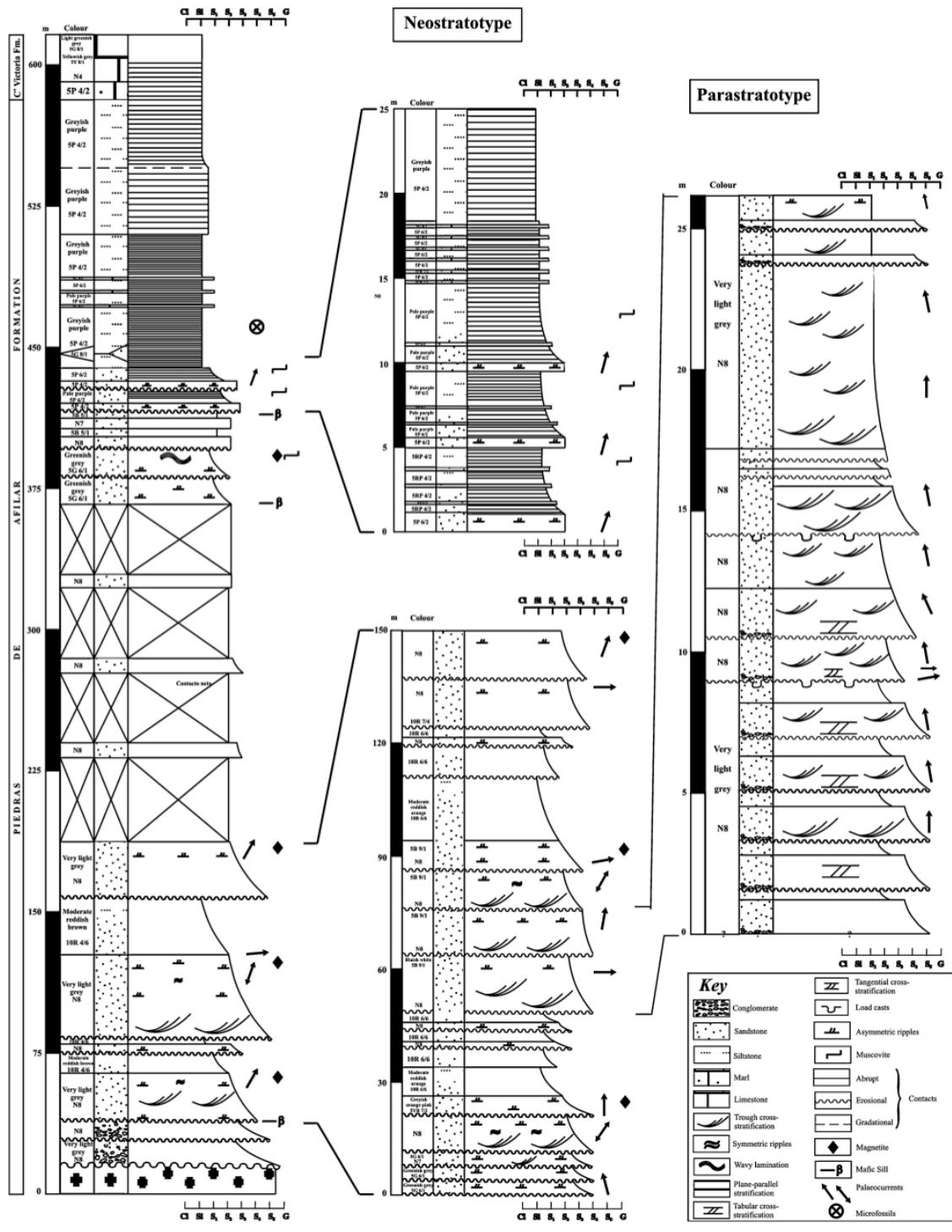
Figure 2.14. Neostratotype and parastratotype of the Piedras de Afilar Formation (point I, Figure 2.1B).
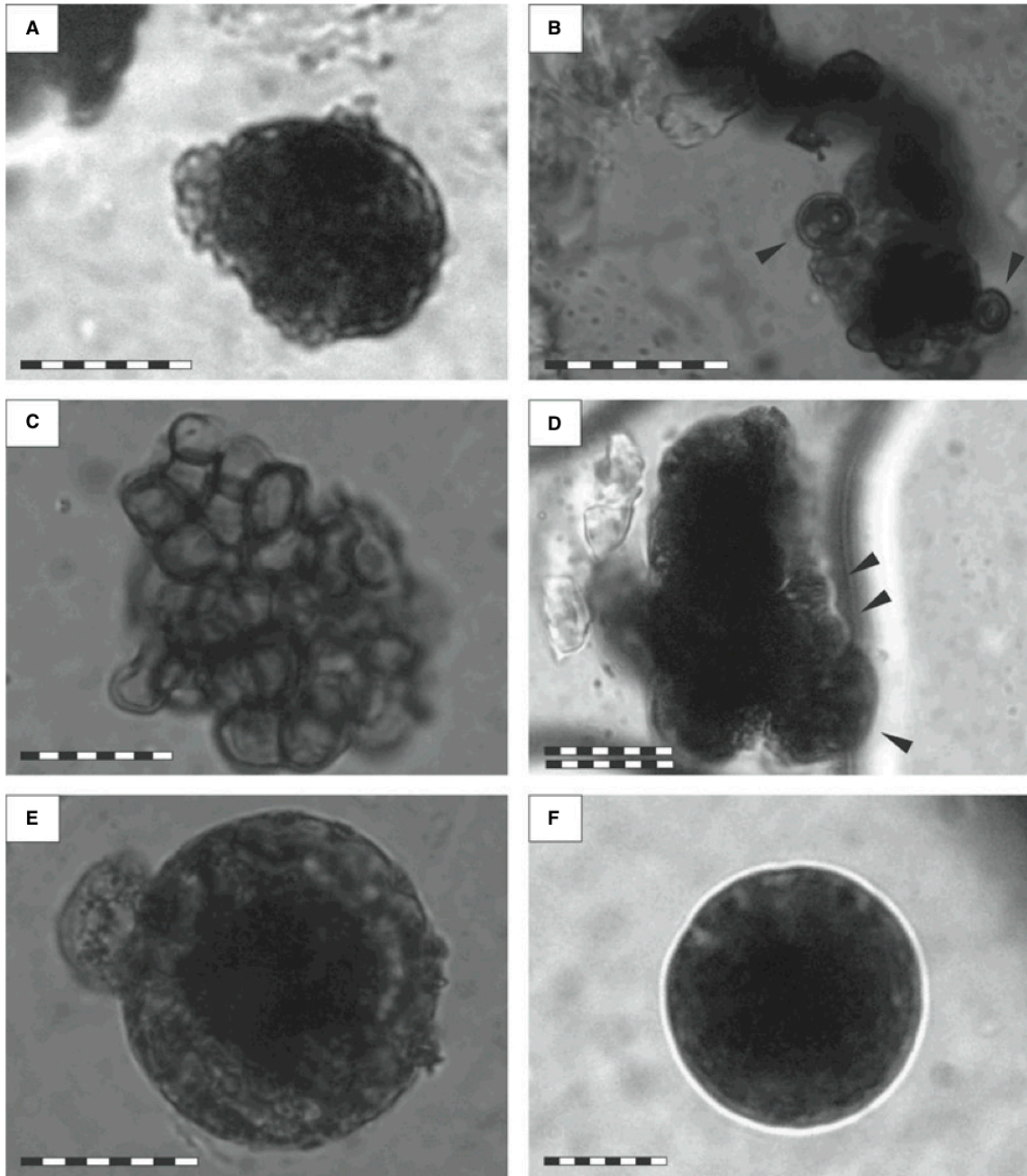
Figure 2.15. Organic-walled microfossils from siltstones of the Piedras de Afilar Formation (Figure 2.14). (A, B) *Bavlinella faveolata* Schepeleva (Vidal, 1976). (C, D) *Soladophycus bosii* Gaucher et al. (1996). (E, F) *Spumosina rubiginosa* Andreeva, emend. Jankauskas and Medvedeva, in Hoffman and Jackson (1996). Simple scale bars represent 10 μm and double 100 μm.

2.3. DISCUSSION

The evidence from Ediacaran to lowermost Cambrian units of Uruguay as a whole, outlined above, suggests significant environmental changes during the deposition of the entire succession, consistent with previously reported data which suggest outstanding events in tectonics, biology, climatology and chemistry of the oceans and atmosphere (Knoll et al., 2006). In the following discussion, stratigraphic, sedimentological, palaeontological and geochronological evidence is examined with the aim of providing a useful insight into existing conditions during sedimentation.

2.3.1. Basin synthesis

2.3.1.1. Age

The available age data constraining each unit described in this study are variable. However, it is reasonable to propose that all the reported strata were deposited during the upper Ediacaran to lowermost Cambrian (ca. 585 to 535 Ma). The relationship between the volcanism present in the Playa Hermosa Formation (Maldonado Group), reported by previous studies, and bimodal magmatism affecting the Las Ventanas Formation in its lower part, is not yet firmly established. Nonetheless the lateral and vertical continuity between sedimentary facies of both units is clear, suggesting a depositional age of ca. 590 to 570 Ma. This observation is supported by the following: (i) the trachytes and syenites of the Sierra de Las Ánimas Complex (520 ± 5 Ma; Bossi et al., 1993) and the Pan de Azúcar Granite (559 ± 28 Ma; Preciozzi et al., 1993) intrude the Las Ventanas Formation; (ii) the Puntas del Pan de Azúcar Lineament affecting the Las Ventanas Formation has a K/Ar age of 572 ± 7 Ma (Bossi and Campal, 1992); (iii) preliminary micropalaeontological study supports an Ediacaran age for this unit (see below); and (iv) Sánchez and Linares (1996) reported radiometric ages of basic rocks occurring at the base of the Las Ventanas Formation between 615 ± 30 and 565 ± 30 Ma (K/Ar).

The age of the San Carlos Formation is less constrained, and the timing of

emplacement of the interbedded rhyolites is unknown. Considering the field relationship between these lithologies and related granites, which yield ages between 570 and 590 Ma, it is reasonable to consider a similar age for this volcanism. The whole unit is deformed by the Sierra Ballena Shear Zone, wherein the last displacement is believed to have occurred at around 525 Ma (Bossi et al., 1993).

Based on 87Sr/86Sr ratios Gaucher et al. (2004) proposed an age of 580 Ma for the base of the Polanco Limestones Formation (Arroyo del Soldado Group). However, it is well-known that the mineralized metazoan *Cloudina* occurs characteristically between ca. 550 and 540 Ma (Grotzinger et al., 1995; Saylor et al., 1998; Martin et al., 2000; Knoll et al., 2004; Hua et al., 2005). Given the fact that only the upper Yerbal Formation would contain that fossil (see page 119 for further discussion), the maximum age for the overlying Polanco Limestones Formation is ca. 550 Ma. These data are in accordance with reinterpreted C-isotopic determinations (see below). Likewise, the assemblage of palynomorphs of the lower-middle Arroyo del Soldado Group supports the later date. On the other hand, absolute minimum age data are provided by intruding granites of 535 to 525 Ma.

Amthor et al. (2003) reported the extinction of Cloudina in Oman coincident with a negative excursion in the carbon isotope composition of the seawater in the Precambrian–Cambrian boundary. Conclusive information is needed to discard the possible presence of this boundary in the Polanco Formation. Nevertheless, the microbiota occurring in the Yerbal, Polanco, Barriga Negra and Cerro Espuelitas Formations can be assigned to the terminal Ediacaran (Vidal and Moczydlowska-Vidal, 1997; Gaucher et al., 2003).

Based mainly on trace fossils and C-isotopic data a lowermost Cambrian age has been proposed for the Cerro Victoria Formation (Arroyo de la Pedrera Group) (Sprechmann et al., 2004). The occurrence of such large ichnofossils in carbonate sediments during the lowermost Cambrian is unusual (Crimes, 1992). Hence, the evidence is not conclusive and more research is needed to determine whether or not these structures are in fact organic. The Cerro Victoria Formation has been considered largely

as composed of limestones (Montaña and Sprechmann, 1993; Sprechmann et al., 2004); however, 'post-depositional' dolostones are the dominant lithologies and limestones are scarce. $\delta^{13}C$ values of limestones therefore are not considered here. Cambrian volcanism and granitogenesis (ca. 530 Ma) provide an upper constraint on the age of deposition of the Arroyo de la Pedrera Group. Consequently, if the maximum age of deposition is constrained by the upper Ediacaran Arroyo del Soldado Group, the Precambrian–Cambrian boundary could be present within Arroyo del la Pedrera, but this is not yet established. Considering that an unconformity separates both groups, the Precambrian–Cambrian boundary can otherwise be located at the base of the Arroyo de la Pedrera Group, which represents a marine transgression and could be correlated with the worldwide transgression in the lowermost Cambrian (Vail et al., 1977).

2.3.1.2. Basin evolution

In Uruguay, an important extensional and synkinematic magmatic event took place during the Neoproterozoic, as represented by the Sierra de Ríos and Cerros de Aguirre Formations. The Sierra de Ríos Formation, located in the northern part of the Sierra Ballena Shear Zone, consists of ignimbrites, and rhyolitic flows and dykes, which are dated at 575 ± 14 Ma (Bossi et al., 1993). Associated with the Laguna de Rocha Shear Zone (Cuchilla Dionisio Terrane; see Figure 2.1B) and deposited on a pull-apart basin type, the Cerros de Aguirre Formation is composed of pyroclastic and rhyolitic rocks yielding an age of 571 ± 8 Ma (Hartmann et al., 2002). Moreover, the Maldonado Group contains a syn-sedimentary bimodal volcanism, which presents similar ages (Pecoits, 2003b; Pecoits et al., 2004a, 2005b). Likewise, extensional basic magmatism represented by a mafic dyke swarm was emplaced at ca. 620 Ma (Rivalenti et al., 1995), indicating an extensional regime in the Nico Pérez Terrane as well (Figure 2.1B).

In close association with the regional magmatism, tectonic activity constituted a primary controlling element on the subsequent basin development. The Sierra Ballena Shear Zone is a high-strain transcurrent structure (Figure 2.1A), operative between ca.

600 and 580 Ma, which contributed significantly to the basin-fill architecture of the Uruguayan units described above. The Sarandí del Yí Shear Zone played a secondary role in this regard (see Figure 2.1B). Other related features allow the authors to constrain the tecto-sedimentary analysis. For example, the Solís de Mataojo pluton is associated with the southern extreme of the shear sone. Structural studies carried out by Oyhantçabal et al. (2001) indicate that this synkinematic granitic body was intruded during the sinistral reactivation of the mega-fault due to the activity of the Sierra Ballena Shear Zone. The age of crystallization of the rock obtained is 584 ± 13 Ma (U/Pb; Oyhantçabal, 2005). Also, synkinematic granitic bodies related to the activity of the Sierra Ballena Shear Zone yield ages between 570 and 590 Ma. Collectively, these features suggest an important tectono-magmatic activity during deposition of the Nico Pérez Terrane and the Cuchilla Dionisio Terrane.

In contrast, Gaucher et al. (2004), contend that the Arroyo del Soldado Group was deposited on a stable, Atlantic-type continental shelf during the Ediacaran–lowermost Cambrian; however, the available data do not support this model. All the aforementioned arguments, and the establishment of lithological, palaeontological and age similarities between the San Carlos Formation (Cuchilla Dionisio Terrane) and the Maldonado Group, located in the Nico Perez Terrane, favour the argument that both were joined by the Ediacaran period. Furthermore, the recent discovery of volcaniclastic rocks in the basal Yerbal Formation, and the apparent continuity between the Maldonado and Arroyo del Soldado Groups, make it unlikely that both sequences formed far apart and joined in a short span of time (ca. 10 Ma) (Pecoits et al., 2005a,b). Rather, the present study suggests an extensional basin (strike-slip and late-orogenic extensional collapse basins) for the Maldonado Group and the San Carlos Formation. Following continental collision, the basin evolved into a foreland basin (Arroyo del Soldado and Arroyo de la Pedrera Groups) (see also Pecoits and Oyhantçabal, 2004).

2.3.2. Palaeoclimatology

Recent radiometric ages have constrained better the timing of the Neoproterozoic glaciations (Allen et al., 2002; Bowring et al., 2003; Hoffmann et al., 2004). Independent evidence supports at least three glacial epochs: Sturtian, Marinoan (or older Varanger) and Gaskiers (Moelv or younger Varanger) (Hoffman and Schrag, 2002; Knoll et al., 2004, 2006; Xiao et al., 2004; Condon et al., 2005; Halverson et al., 2005). Unlike the Marinoan and Sturtian glacial deposits, the Gaskiers episode lacks a well-developed cap carbonate unit, possibly suggesting that this glaciation was diachronous and not a global event. However, the presence of glacially related deposits and $\delta^{13}C$ anomalies above the Marinoan-aged diamictite is consistent with the occurrence of a third Neoproterozoic glaciation (Wonoka anomaly; see Halverson et al., 2005). Correlative deposits of the Gaskiers glaciation have been reported from Australia, Canada, USA, Norway, Scotland, China and western Africa (Xiao et al., 2004; Halverson et al., 2005). Even though this event was dated between 595 ± 2 and 570 Ma (Thompson and Bowring, 2000) and $<601 \pm 4$ Ma (Dempster et al., 2002), the age obtained by Bowring et al. (2003) for the Gaskiers in Newfoundland, ca. 580 Ma, constitutes the best available datum.

As stated above, the glacial deposits are characterized by diamictites, and extremely negative $\delta^{13}C$ values can be observed in the related carbonates (Burns and Matter, 1993; Calver, 2000; Jiang et al., 2002; Wang et al., 2002; Corsetti and Kaufman, 2003). Furthermore, the glaciations pre-date the appearance of macroscopic Ediacaran animals (Narbonne, 2005), the fossil metazoan embryos and algae of the Doushantuo Formation (Xiao et al., 1998), and post-date the Doushantuo-type acritarch assemblage (Zhou et al., 2002). Condon et al. (2005) recognized two $\delta^{13}C$ negative excursions between 580 and 551 Ma. The former is linked to the glacial event, whereas the latter is not related to any known glaciation and constitutes one of the larger carbon isotopic excursions recognized (see also Saylor et al., 1998). Halverson et al. (2005) correlated this anomaly with the Gaskier-related event. Likewise, a recent study carried out by Le Guerrouéet al. (2006), in the well-preserved Huqf Supergroup in Oman, shows the longest-lived and highest amplitude carbon isotopic record documented at around 600 Ma. Even though no glacial deposits occur in the succession, it is likely that this anomaly is correlated with the Gaskiers event. Moreover, no imprint of the anomaly

registered by Condon et al. (2005) and Saylor et al. (1998) ca. 551 Ma is recognizable.

Diverse models have been proposed to explain the carbon isotopic composition and origin of cap dolostones and post-glacial limestones. In the case of the cap dolostones four (deglaciation-related) models have been proposed: (i) overturn of an anoxic deep ocean; (ii) catastrophically accelerated rates of chemical weathering because of super-greenhouse conditions following global glaciation (Snowball Earth Hypothesis); (iii) massive release of carbonate alkalinity from destabilized methane clathrates; and (iv) physical separation of the surface and deep ocean reservoirs, with cap dolostones formed primarily by microbially mediated precipitation of carbonate during algal blooms within a low salinity 'plumeworld' (see Shields, 2005 for review).

In Uruguay the first evidence of glacial influence on Neoproterozoic sequences was documented by Pazos et al. (1998) in the Playa Hermosa Formation. Pecoits (2002) proposed an arid climate for the Las Ventanas Formation and mentioned the existence of possible glacially related sedimentary features. Later Pecoits et al. (2005a) strengthened that hypothesis in reporting outsized clasts, in finely laminated siltstones, interpreted as dropstones. Previous proposals considered a Marinoan-aged glacial deposition for the lower and upper parts of the group (Pazos et al., 2003; Pecoits et al., 2005a). At present, taking into account the geochronological constraints, new field research and reinterpretation of previously presented information, the authors propose that the Maldonado Group records the Gaskiers Glaciation (Halverson et al., 2005); this observation also explains the apparent lack of 'cap carbonates' immediately overlying these deposits (see Figure 2.16). The palaeomagnetic data available for Neoproterozoic rocks of Uruguay are still preliminary (Sánchez and Rapalini, 2002). This research was carried out on igneous and sedimentary rocks of the Sierra de las Ánimas Complex and Playa Hermosa Formation, respectively. The study from the Playa Hermosa Formation, in particular, suggests that it may constitute another case of low latitude glaciation (12·7°+9·5°/−8·1°). No geochemical analyses of the Maldonado Group have been performed.
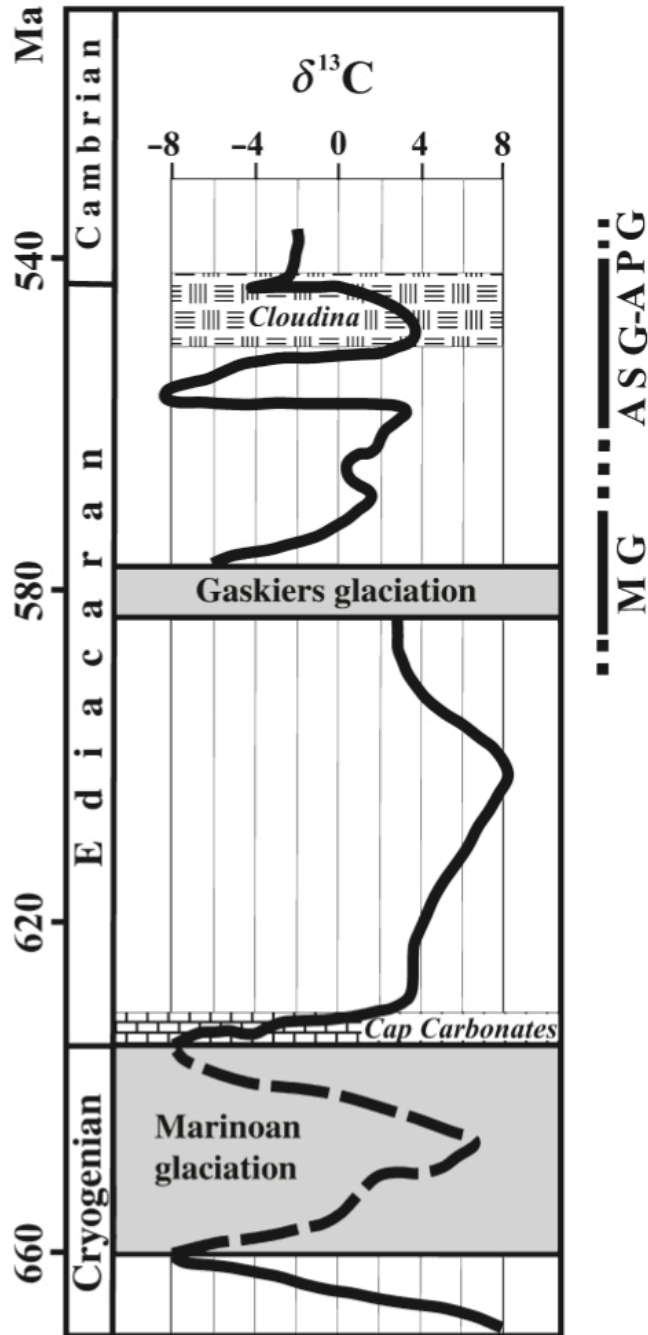
Figure 2.16. Schematic diagram comparing biochron of index fossil Cloudina, cap carbonates location, globally correlated $\delta^{13}C$ excursions spanning the inferred Marinoan and Gaskiers glaciations, and proposed age of deposition of the Maldonado (MG), Arroyo del Soldado (ASG) and Arroyo de la Pedrera (APG) Groups. See text for discussion. (data from Knoll et al., 2004, 2006; Condon et al., 2005; Halverson et al., 2005).

In the lower Arroyo del Soldado Group, only four C-isotopic measurements of pink dolostones from the upper Yerbal Formation have been obtained (Gaucher et al., 2003). The dolomite yielded $\delta^{13}C$ values between +1·17 and +2·15‰PeeDeeBelemnite (PDB), increasing up-section. Likewise, Boggiani (1998) and Gaucher et al. (2004) reported carbon isotope studies from the Polanco Limestones Formation. The strongest negative peak reported (−3·3‰ PDB) occurred in the middle of the unit with an underlying positive peak (+5·3‰ PDB). Considering the stratigraphic location of Cloudina and its range (see above), these peaks can be correlated with the slightly negative (−1·5‰ PDB) and positive (+6‰ PDB) excursions reported by Saylor et al. (1998) for the Kuibis Subgroup (Namibia) at ~548 and ~549 Ma, respectively. According to the same authors, similar trends present in Oman would indicate ages of ~550 and ~551·5 respectively. Recently, Condon et al. (2005), integrating isotope and radiometric data from Oman, China, Namibia and Russia, suggested a global negative $\delta^{13}C$ anomaly at ca. 551 Ma unrelated to obvious glacial episodes (Figure 2.16). No glacial features have been observed in the Arroyo del Soldado Group.

2.3.3. Palaeobiology

Throughout much of the history of the Earth, biology has played a fundamental role in driving low-temperature geochemical reactions (for a recent review see Konhauser, 2006); this is certainly the case during the Neoproterozoic, when significant changes in ocean and atmospheric chemistry were taking place. For example, as the oceans became more oxygenated, through increased cyanobacterial activity, there was an attendant deepening of the oxic–anoxic interface in the oceans. At this stage, $\delta^{34}S$ values between pyrite and sulphates approached 70‰, indicating that wide-scale initiation of the oxidative sulphur cycle, possibly driven by a combination of newly evolved non-photosynthetic sulphide-oxidizing and sulphur-disproportionating bacteria, had taken place (Canfield and Teske, 1996). Increased levels of O_2 could even have facilitated the emergence of metazoans, primitive soft-bodied, multicellular animals, on the shallow sea floor, as early as ca. 600 Ma (Valentine, 2004; Narbonne, 2005). Clearly, the

Neoproterozoic represents a time of significant biological innovation and, not surprisingly, it has been proposed that a causal link exists between environmental change and the diversification of life (Vidal and Knoll, 1982; Schopf, 1991; Fedonkin, 1992; Knoll, 1994; Seilacher, 1996; Conway-Morris, 2000; Walter et al., 2000; Moczydlowska, 2005). Specifically, the Ediacaran records a proliferation of phytoplankton (acritarchs), metazoa and vendobionta that show an increase in morphological complexity.

The Ediacaran biota was eventually eclipsed near the Precambrian–Cambrian boundary (545 Ma) by more complex animal phyla, many of them skeletal with modern body plans and displaying a higher degree of behavioural sophistication, in what is known as the 'Cambrian radiation' (Knoll and Carroll, 1999). The cause for the decline in Ediacaran fauna remains speculative, but it probably involved a combination of factors, such as a rise in predation, increased competition for nutrients, more active bioturbation, or a mass extinction event prompted by an environmental perturbation. Its disappearance from the rock record may also simply be due to reduced preservation potential relative to organisms that evolved mineralizing capabilities. Indeed, Brennan et al. (2004) suggested that a surge in calcium concentrations during the early Cambrian spurred the onset of calcium carbonate biomineralization, which led to a number of marine biota developing calcium carbonate shells, in addition to the advent of calcifying cyanobacteria.

The Ediacaran and lower Phanerozoic successions of Uruguay offer the possibility to explore different ecological aspects of the ocean environment in which microbial and more complex organisms evolved. Accordingly, the occurrence of a well-exposed mixed siliciclastic-carbonate sequence with the development of other chemical sediments, such as cherts and iron formations, is indicative of significantly variable palaeooceanographic conditions. Furthermore, the geological evidence shows important climatic oscillations from glacially influenced sedimentation at the base towards an arid environment at the top of the sequence.

A remarkable aspect of the Uruguayan succession is a palaeontological record consisting of organic-walled and skeletal fossils that display a clear exploitation of different ecological niches. One such example is the occurrence of the distinctive shelly

fauna, including Cloudina, which is restricted to particular facies of the uppermost Yerbal Formation and abruptly disappears at the boundary with the Polanco Limestones Formation. Thus, while some authors have attributed the advent of biomineralization to important increments of the seawater Ca concentration, the explanation seems to be more complex. Likewise, significant alterations in abundance and assemblages of organic-walled microfossils took place at this boundary. Indeed, preliminary palynological macerations have shown the occurrence of different well-preserved assemblages of organic-walled microfossils depending on the nature of the unit, which reinforces the previous observations of Gaucher (2000), who suggested alternations of two different assemblages. Another interesting observation is that the taxon Bavlinella faveolata, identified as an important component of the phytoplankton assemblage in iron-rich facies of the Cerro Espuelitas and Yerbal Formations, becomes very scarce in the carbonate rhythmites of the Polanco Formation. Perhaps this observation reflects specific palaeoecological conditions (i.e. nutrient availability, oxygen concentration, etc.) that were met during times of Fe deposition (see Gaucher, 2000).

Another important aspect is the understanding of the relationship between biologically mediated processes and unusual deposits such as BIF or primary dolostones. In fact, the possible role of micro-organisms has been considered in many genetic models of BIF. For instance, LaBerge et al. (1987) regarded microbiota as essential participants in the process, whereas Walter and Hofmann (1983) gave a list of fossil organisms identified in BIF but assumed a conservative view about the role in precipitating iron. Recent experimental biological studies highlight the potential magnitude of microbial activity as a mechanism of ferric iron precipitation (Konhauser et al., 2002; Kappler et al., 2005). However, its importance in the deposition of IF remains conjectural.

2.3.4. Rhythmites

Rhythmically bedded carbonates occur in the basal Yerbal Formation; these are intercalated with grey cherts and constitute the predominant facies of the Polanco

Limestones Formation (Goñi and Hoffstetter, 1964; Preciozzi and Fay, 1988; Preciozzi et al., 1988; Díaz et al., 1990; Gaucher, 2000). The beds consist of millimetre to decimetre-scale alternations of limestone and dolostone, typically displaying sharp contacts. The limestone beds show variable grain-size, parallel bedding and cross-stratification, including hummocky, which indicates a marine wave-dominated origin (Bossi and Navarro, 1991; Gaucher, 2000). The dolostone layers are finer-grained, but millimetre-thick parallel laminations and normal grading are common. Authigenic albite has been reported by Gaucher (2000) from both limestone and dolostone, which might be indicative of hypersaline, alkaline and marine-evaporitic conditions. The dolostones also contain organic matter and pyrite, but it is unclear whether this suggests a primary feature (see below).

Present-day low-temperature dolomite occurrences are restricted to marine or hypersaline coastal environments such as coastal sabkhas of Abu Dhabi, tidal flats of Andros Island in the Bahamas, Coorong lakes of South Australia and the coastal lagoon, Lagoa Vermelha in Brazil (Vasconcelos and McKenzie, 1997 and references therein). Low-temperature inorganic synthesis of dolomite is difficult to achieve under laboratory conditions without the presence of micro-organisms, in particular sulphate-reducing bacteria (SRB) (see Vasconcelos and McKenzie, 1997; Warthmann et al., 2000; Vasconcelos et al., 2006). The role of SRB in dolomite formation is two-fold. Firstly, the process of sulphate reduction overcomes the kinetic barrier to dolomite formation by increasing the pH and alkalinity, and by removing sulphate, which is a known inhibitor to dolomite formation. Secondly, the cell surfaces of SRB concentrate Ca^{2+} and Mg^{2+} cations around the cell. Once bound, these cations subsequently serve as favourable adsorption sites for CO ions (van Lith et al., 2003).

In preliminary petrographic observations of the Polanco Limestones Formation rhythmites, the authors have observed that pyrite is relatively scarce; this observation suggests that sulphate reduction is not the main control promoting the dolomite formation. At present, the data from the Polanco Limestones Formation are insufficient to address this question further; however, it seems clear that the 'Polanco event' was controlled by palaeooceanographic parameters.

2.3.5. Iron formations

Bracketing the rhythmites of the Polanco Limestones Formation are iron-rich rocks, interpreted as BIF. These rocks display centimetre alternation of chert and iron-rich layers, yet, they do not show the characteristic microbanding of Archean-Palaeoproterozoic BIF. The significance of BIF in the Neoproterozoic is not completely understood. Along with major deposits at Urucum, Brazil, the Rapitan in north-west Canada, the Braemar and Holowilena Formations in Australia, and the Damara Belt in Namibia, South Africa, these BIF have been considered a special case when compared with the more extensive Palaeoproterozoic deposits. The deposition of BIF has often been linked to the termination of global glaciations, when ocean circulation was restored after the ice sheets melted (Kirschvink, 1992; Klein and Beukes, 1993; Hoffman et al., 1998b). Taking into account the associated glaciogenic deposits and hydrothermal imprint, others have suggested an alternative theory involving glaciation of a Red Sea-type rift environment. This theory helps to explain evidence of rift activity in some BIF, such as significant facies and thickness changes, and association with volcanic rocks (see Young, 2002).

Virtually no BIF from the upper Vendian have been described. Gaucher et al. (2004) suggested that deposition of the BIF took place on a shelf, due to enhanced upwelling of nutrient-rich waters and consequent production of phytoplankton blooms during greenhouse conditions (see Button, 1982, for details about the model). However, as stated above, the depositional geological setting of the group does not correspond to an Atlantic-type continental shelf, in which the model was developed, and the age of the whole Arroyo del Soldado Group is younger than the Gaskiers glacial event which is problematic for that model (see Pecoits et al., 2004b for an alternative model). Thus, in the absence of more evidence, the mechanism that triggered the iron precipitation remains unresolved.

2.4. CONCLUSIONS

Field-based research with preliminary micro-palaeontological and petrographical data, and a re-assessment of previous research, was carried out on late Neoproterozoic (volcano) sedimentary units, in south-eastern Uruguay. The studied units comprise the Maldonado, Arroyo del Soldado and Arroyo de la Pedrera Groups, which together contain dropstones, diamictites, banded iron formations, pink dolostones, limestone-dolostone rhythmites, thick stromatolitic/oolitic dolostones, organic-walled and skeletal fossils. The estimated time of deposition for these successions ranges from ca. 590 to 535 Ma, thereby indicating an upper Ediacaran–lowermost Cambrian age. This work shows a temporal correlation between sedimentation and significant changes in global climate and palaeobiology. Also the formations represent the tectonic re-configuration of depositional basins corresponding to the final stages of the SW-Gondwana assembly.

Based on this work, it is suggested that the basal Maldonado Group, which contains ice-rafted diamictites and dropstones, records the Gaskiers Glaciation (~580 Ma). The Arroyo del Soldado Group is more likely to represent post-glacial conditions and, possibly, changes in ocean chemistry; this is demonstrated by the presence of distinctive siliciclastic and chemical sediments, and variations in biota content. Based on the radiometric and biostratigraphic data a maximum age of 560 Ma is proposed for the base of the whole group (Yerbal Formation). Considering the new information, preliminary carbon-isotopic determinations from the Polanco Limestones Formation compares well with the worldwide negative excursion recorded at ca. 551 Ma, which is thought to be unrelated to glacial events. Although there is no conclusive evidence, the uppermost Arroyo de la Pedrera Group is probably lowermost Cambrian in age. Contrary to previous models, which invoke an Atlantic-type passive margin during the Ediacaran in Uruguay, it is suggested that transtensional basins developed, evolving towards a foreland basin in the later stages of the continental collision.

The study not only permits the establishment of a reasonable stratigraphic framework for Neoproterozoic rock successions in Uruguay, but it helps facilitate a better understanding for the origin and significance of peculiar deposits such as BIF, limestone-

dolostone rhythmites, and thick stromatolitic/oolitic dolostones hosting a diverse fossil assemblage. More detailed studies, however, are necessary to interpret whether these features exist just on a regional scale, or whether they are correlative with worldwide events, such as 'Snowball Earth' glaciations, late-stage BIF deposition and the advent of animal skeletons.

2.5. REFERENCES

Allen, P.A., Bowring, S.A., Leather, J., Brasier, M., Cozzi, A., Grotzinger, J.P., McCarron, G., Amthor, J., 2002. Chronology of Neoproterozoic glaciations: new insights from Oman. In: Int. Sedimentological Congress 16th International Association of Sedimentologists, pp. 7-8, Johannesburg (Abstract Volume).

Amthor, J.E., Grotzinger, J.P., Schröder, S., Bowring, S.A., Ramezani, J., Martin, M.W., Matter, A., 2003. Extinction of Cloudina and Namacalathus at the Precambrian–Cambrian boundary in Oman. Geol. Soc. Am. Bull. 31, 431-434.

Aubet, N., 2005. Sedimentología y consideraciones estratigráficas de la Formación Piedras de Afilar, Canelones. Unpublished BSc (Hns). Thesis. Facultad de Ciencias, Montevideo, pp. 41.

Aubet, N., Pecoits E., Sánchez, B.L., Pazos, P., 2005. Consideraciones estratigráficas de la Formación Piedras de Afilar y su correlación con otras unidades neoproterozoicas del Uurugay. In: XII Congreso Latinoamericano de Geología. Resúmenes extendidos, Actas Cd, Quito.

Basei, M., Siga, O., Jr., Masquelin, H., Harara, O., Reis Neto, J., Preciozzi, F., 2000. The Dom Feliciano Belt of Brazil and Uruguay and its foreland domain, the Río de la Plata Craton. In: Tectonic Evolution of South America (Eds U. Cordani, Milani, E., Thomaz F. A. and Campos, D), 1st edn, pp. 311-334.

Boggiani, P.C., 1998. Análise estratigráfica da Bacia Corumbá (Neoproterozoico) -Mato

Grosso do Sul–. Unpublished PhD Thesis, Universidade de São Paulo, São Paulo.

Bossi, J., 2003. Estratigrafía del Precámbrico de Uruguay: terrenos tectono-estratigráficos y geocronología. Revista de la Sociedad Uruguaya de Geología. In: Estratigrafía del Precámbrico del Uruguay (Ed. E. Pecoits). Rev. Soc. Uruguay. Geol. Spec. Publ. 1, 1-17.

Bossi, J., Campal, N., 1992. Magmatismo y tectónica transcurrente durante el Paleozoico Inferior en Uruguay. In: Paleozoico Inferior de Iberoamérica (Eds J.G. Gutiérrez-Marco, J. Saavedra and I. Rabano), 1st edn, pp. 343-356. Universidad de Extremadura, Mérida.

Bossi, J., Navarro, R., 1991. Geología del Uruguay. Universidad de la República, Montevideo, pp. 970.

Bossi, J., Cingolani, C., Lambias, E., Varela, R., Campal, N., 1993. Características del magmatismo post-orogénico finibrasiliano en el Uruguay: formaciones Sierra de Ríos y Sierra de Ánimas. Rev. Brasil. Geocienc. 23, 282-288.

Bossi, J., Ferrando, L., Montaña, J., Campal, N., Morales, H., Gancio, F., Schipilov, A., Piñeyro, D., Sprechmann, P., 1998. Carta Geológica del Uruguay. Escala 1:500·000. Versión digital. Geoeditores, Montevideo.

Bowring, S., Myrow, P., Landing, E., Ramezani, J., Grotzinger, J., 2003. Geochronological constraints on terminal Neoproterozoic events and the rise of metazoans. Geophys. Res. Abstr. 5, 219.

Brennan S.T., Lowenstein T.K., Horita, J., 2004. Seawater chemistry and the advent of biocalcification. Geology. 32, 473-476.

Burns, S.J.,, Matter, A., 1993. Carbon isotopic record of the latest Proterozoic from Oman. Eclogae. Geol. Helv. 86, 595-607.

Button, A., 1982. Sedimentary iron-deposits, evaporates, and phosphorites. State of the art report. In: Mineral Deposits and the Evolution of the Biosphere (Eds H.D. Holland, M. Schidlowski), 1st edn, Springer, Berlin, pp. 259-273.

Calver, C.R., 2000. Isotope stratigraphy of the Ediacarian (Neoproterozoic III) of the Adelaide Rift Complex, Australia, and the overprint of water column stratification. Precambrian Res., 100, 121-150.

Canfield, D.E., Teske, A., 1996. Late Proterozoic rise in atmospheric oxygen concentration inferred from phylogenies and sulfur-isotope studies. Nature. 382, 127-132.

Condon, D., Zhu, M., Bowring, S. and Wang, W., 2005. U-Pb ages from the Neoproterozoic Doushantuo Formation, China. Science. 308, 95-98.

Conway-Morris, S., 2000. The Cambrian "explosion": slow-fuse or megatonnage?. Proc. Natl Acad. Sci. U.S.A. 99, 4426-4429.

Coronel, N., Oyhantçabal, P., Spoturno, J., 1982. Consideraciones estructurales de la Formación Piedras de Afilar en su área tipo, en los alrededores de la estación de Piedras de Afilar, Depto. de Canelones, Uruguay. In: V Congreso Latinoamericano de Geología, pp. 48-60. Actas, AGA, Vol.1., Buenos Aires.

Corsetti, F.A., Kaufman, A.J., 2003. Stratigraphic investigations of carbon isotope anomalies and Neoproterozoic ice ages in Death Valley, California. Geol. Soc. Am. Bull. 115, 916-932.

Crimes, P.T., 1992. The record of trace fossils across the Proterozoic-Cambrian boundary. In: Origin and Early Evolution of the Metazoa (Eds J.H., Lipps, P.W., Signor), 1st edn, Plenum Press, New York, pp. 177-202.

Díaz, R., Albanell, H., Bossi, J., 1990. Carta geológica del Uruguay, Hoja F-24 Cerro Partido, Escala 1:100·000. Memoria explicativa. DINAMIGE-UdelaR, Montevideo.

Dempster, T.J., Rogers, G., Tanner, P.W.G., Bluck, B.J., Muir, R.J., Redwood, S.D., Ireland, T.R. and Paterson, B.A. (2002) Timing of deposition, orogenesis and glaciation within the Dalradian rocks of Scotland: constraints from U-Pb zircon ages. J. Geol. Soc. London. 159, 83-94.

Edwards, M., 1986. Glacial environments. In: Sedimentary Environments and Facies (Ed. H.G. Reading), 2nd edn, Blackwell Science, Oxford, pp. 445-469.

Einsele, G., 2000. Sedimentary Basins. Evolution, Facies, and Sediment Budget. Springer, Berlin, pp. 792.

Fedonkin, M.A., 1992. Vendian faunas and the early evolution of metazoa. In: Origin and Early Evolution of the Metazoa (Eds. J.H., Lipps, P.W., Signor), 1st edn, Plenum Press, New York, pp. 87-129.

Gaucher, C., 2000. Sedimentology, paleontology and stratigraphy of the Arroyo del Soldado Group (Vendian to Cambrian, Uruguay). Beringeria. 26, 1-120.

Gaucher, C., Sprechmann, P., 1999. Upper Vendian skeletal fauna of the Arroyo del Soldado Group, Uruguay. Beringeria. 23, 55-91.

Gaucher, C., Sprechmann, P., Schipilov, A., 1996. Upper and Middle Proterozoic fossiliferous sedimentary sequences of the Nico Pérez Terrane of Uruguay: Lithostratigraphic units, paleontology, depositional environments and correlations. Neues Jb. Geol. Paläontol. Abh. 199, 339-367.

Gaucher, C., Sprechmann, P., Montaña, J., Martínez, S., 1998. Litoestratigrafía, sedimentología y paleogeografía del Grupo Arroyo del Soldado (Vendiano-Cámbrico, Uruguay). In: Actas II Congreso Uruguayo de Geología (Montevideo), pp. 24-31.

Gaucher, C., Boggiani, P.C., Sprechmann, P., Sial, A.N., Fairchild, T.R., 2003. Integrated correlation of the Vendian to Cambrian Arroyo del Soldado and Corumbá Groups (Uruguay and Brazil): palaeogeographic, palaeoclimatic and palaeobiologic implications. Precambrian Res. 120, 241-278.

Gaucher, C., Sial, A.N., Blanco, G., Sprechmann, P., 2004. Chemostratigraphy of the lower Arroyo del Soldado Group (Vendian, Uruguay) and palaeoclimatic implications. Gondwana Res. 7, 715-730.

Germs, G.J.B., 1972. New shelly fossils from Nama Group, South West Africa. Am. J. Sci. 272, 752-761.

Goñi, J.C., Hoffstetter, R., 1964. Uruguay. In: Lexique stratigraphique international (Ed. R. Hoffstetter), Fascicule 9a, Centre National de la Recherche Scientifique, Paris., pp. 1-202.

Grotzinger, J.P., Bowring, S.A., Saylor, B.Z., Kaufman, A.J., 1995. Biostratigraphic and geochronologic constraints on early animal evolution. Science. 270, 598-604.

Halverson, G.P., Hoffman, P.F., Schrag, D.P., Maloof, A.C., Rice, A.H.N., 2005. Toward a Neoproterozoic composite carbon-isotope record. Geol. Soc. Am. Bull. 117, 1181-1207.

Harland, W.B., 1964. Critical evidence for a great infra-Cambrian glaciation. Geol. Rundsch. 54, 45-61.

Hartmann, L., Santos, O., Bossi, J., Campal, N., Schipilov A., Mc Naughton, N.J., 2002. Zircon and Titanite U-Pb SHRIMP geochronology of Neoproterozoic felsic magmatism on the eastern border of the Rio de la Plata Craton, Uruguay. J. S. Am. Earth Sci. 15, 229-236.

Hoffman, P.F., Schrag, D.P., 2000. Snowball Earth. Sci. Am. 282, 68-75.

Hoffman, P.F., Schrag, D.P., 2002. The Snowball Earth hypothesis: testing the limits of global change. Terra Nova. 14, 129-155.

Hoffman, P.F., Kaufman, A.J., Halverson, G.P., 1998a. Coming and goings of global glaciations on a neoproterozoic carbonate platform in Namibia. Geol. Today. 8, 1-9.

Hoffman, P.F., Kaufman, A.J., Halverson, G.P., Schrag, D.P., 1998b. A Neoproterozoic Snowball Earth. Science. 281, 1342-1346.

Hoffmann, K.H., Condon, D.J., Bowring, S.A., Crowley, J.L., 2004. A U-Pb zircon date

from the Neoproterozoic Ghaub Formation, Namibia: constraints on Marinoan glaciation. Geology. 32, 817-820.

Hoffman, H.J., Jackson, G.D., 1996. Notes on the geology and micropaleontology of the Proterozoic Thule Group, Ellesmere Island, Canada, and north-west Greenland. Geol. Surv. Can. Bull. 495, 1-26.

Hua, H., Chen, Z., Yuan, X., Zhang, L., Xiao, S., 2005. Skeletogenesis and asexual reproduction in the earliest biomineralizing animal Cloudina. Geology. 33, 277-280.

Hyde, W.T., Crowley, T.J., Baum, S.K., Peltier, W.R., 2000. Neoproterozoic "snowball earth" simulations with a coupled climate/ice-sheet model. Nature. 405, 425-429.

Jiang, G., Christie-Blick, N., Kaufman, A.J., Banerjee, D.M., Rai, V., 2002. Sequence stratigraphy of the Neoproterozoic Infra Krol Formation and Krol Group, Lesser Himalaya, India. J. Sed. Res. 72, 524-542.

Jones, G., 1956. Memoria explicativa y mapa geológico de la región oriental del Departamento de Canelones, Boletín no. 34, Instituto Geológico del Uruguay, Montevideo, pp. 193.

Kappler, A., Pasquero, C., Konhauser, K.O., Newman, D.K., 2005. Deposition of banded iron formations by anoxygenic photoprotphic Fe(II)-oxidizing bacteria. Geology. 33, 865-868.

Kirschvink, J.L., 1992. Late Proterozoic low-latitude global glaciation: the Snowball Earth. In: The Proterozoic Biosphere, A Multidisciplinary Study (Eds J.W. Schopf and C. Klein), 1st edn, Cambridge University Press, New York, pp. 51-52.

Klein, C., Beukes, N.J., 1993. Sedimentology and geochemistry of the glaciogenic late Proterozoic Rapitan iron-formation, in Canada. Econ. Geol. 80, 542-565.

Klein, C., Ladeira, E.A., 2004. Geochemistry and mineralogy of Neoproterozoic banded iron-formations and some selected siliceous manganese formations from the Urucum

district, Mato Grosso do Sul, Brazil. Econ. Geol. 99, 1233-1244.

Knoll, A.H., 1994. Proterozoic and Early Cambrian protists: evidence for accelerating evolutionary tempo. Proc. Natl Acad. Sci. U.S.A. 91, 6743-6750.

Knoll, A.H., Carroll, S.B., 1999. Early animal evolution: emerging views from comparative biology and geology. Science. 284, 2129-2137.

Knoll, A.H., Sweet, K., 1985. Micropalaeontology of the Late Proterozoic Veteranen Group, Spitsbergen. Palaeontology. 28, 451-473.

Knoll, A.H. Walter, M.R., Narbonne, G.M., Christie-Blick, N., 2004. A New Period for the geologic time scale. Science. 3005, 621-622.

Knoll, A.H. Walter, M.R., Narbonne, G.M., Christie-Blick, N., 2006. The Ediacaran Period: a new addition to the geologic time scale. Lethaia. 39, 13-30.

Konhauser, K., 2006. Introduction to Geomicrobiology. Springer, Berlin, pp. 425.

Konhauser, K.O., Hamade, T., Raiswell, R., Morris, R.C., Ferris, F.G., Canfield, D.E., 2002. Could bacteria have formed the Precambrian banded iron formations?. Geology. 30, 1079-1082.

LaBerge, G.L., Robbins, E.I., Han, T.M., 1987. A model for the biological precipitation of Precambrian iron-formations – geological evidence. In: Precambrian Iron-Formations (Eds P.W. Appel and G.L. LaBerge), 1st edn, Theophrastus, Athens, pp. 69-96.

Le Guerroué, E., Allen, P.A., Cozzi, A., Etienne, J.L., Fanning, M., 2006. 50 Myr recovery from the largest negative $\delta^{13}C$ excursion in the Ediacaran ocean. Terra Nova. 18, 147-153.

van Lith, Y., Warthmann, R., Vasconcelos, C., McKenzie, J.A., 2003. Sulfate-reducing bacteria induce low temperature Ca-dolomite and high Mg-calcite formation. Geobiology. 1, 71-80.

Logan, B.W., Rezak, R., Ginsburg, R. N., 1964. Classification and environmental significance of algal stromatolites. J. Geol. 72, 68-83.

Mansuy, C., Vidal, G., 1983. Late Proterozoic Brioverian microfossils from France: taxonomic affinity and implications of plankton productivity. Nature. 302, 606-607.

Martin, M.W., Grazhdankin, D.V., Bowring, S.A., Evans, D.A.D., Fedonkin, M.A., Kirschvink, J.L., 2000. Age of Neoproterozoic bilatarian body and trace fossils, White Sea, Russia: implications for metazoan evolution. Science. 288, 841-845.

Masquelin, H., 1990. Análisis estructural de las zonas de cizalla en las migmatitas de Punta del Este – Uruguay. Acta Geol. Leopoldensia. 30, 139-158.

Masquelin, H., Sánchez, L., 1993. Propuesta de evolución tectono-sedimentaria para la fosa tardi-brasiliana en la región de Piriápolis, Uruguay. Rev. Brasil. Geocienc. 23, 313-322.

Midot, D., 1984. Etude geologique et diagnostic metallogénique pour l'exploration du secteur de Minas (Uruguay). Diplome de Docteur de 3e Cycle. Universitè Pierre et Marie Curie, Paris.

Moczydlowska M., 2005. Taxonomic review of some Ediacarian acritarchs from the Siberian Platform. Precambrian Res. 136, 283-307.

Montaña, J., Sprechmann, P., 1993. Calizas estromatolíticas y oolíticas y definición de la Formación Arroyo de la Pedrera (?Vendiano, Uruguay). Rev. Brasil. Geocienc. 23, 306-312.

Murphy, M.A, Salvador, A., 1999. International stratigraphic guide – an abridged version. Episodes. 22, 255-271.

Narbonne, G.M., 2005. The Ediacara biota: Neoproterozoic origin of animals and their ecosystems. Annu. Rev. Earth Planet. Sci. 33, 421-442.

Oyhantçabal P., 2005. The Sierra Ballena Shear zone: kinematics, timing and its significance for the geotectonic evolution of southeast Uruguay. PhD Thesis, Georg-August-Universität Göttingen, Göttingen, pp. 147.

Oyhantçabal, P., Derregibus, M., De Souza, S., 1993. Geología do extremo sul da Formaçao Sierra de Ánimas (Uruguay). In: V Simposio Sul-Brasiliero de Geología, (Curitiba, Brazil). Boletín de Resumos. 1, 4-5.

Oyhantçabal, P. Heimann, A., Miranda, S., 2001. An evaluation of strain in the syntectonic Solis de Mataojo Granitic Complex, Uruguay. J. Struct. Geol. 23, 807-817.

Pazos, P., Sánchez Bettucci, L., Tófalo, R., 1998. Procesos sedimentarios e indicadores paleoclimáticos en la sección inferior de la Formación Playa Hermosa, Cuenca Playa Verde, Piriápolis, Uruguay. In: Actas II Congreso Uruguayo de Geología (Punta del Este, Uruguay), pp. 64-69.

Pazos P., Tófalo, R., Sánchez Bettucci, L., 2003. The record of the Varanger Glaciation at the Rio de la Plata Craton, Vendian-Cambian of Uruguay. Gondw. Res. 6, 65-77.

Pecoits, E., 2002. Análisis faciológico y aspectos geológicos de la Formación Las Ventanas; un nuevo enfoque. In: II Taller Sobre la Estratigrafía del Precámbrico del Uruguay (Eds E. Pecoits and H. Masquelin), Facultad de Ciencias, Montevideo, pp. 34-36.

Pecoits E., 2003a. Sedimentología y consideraciones estratigráficas de la Formación Las Ventanas en su área tipo, departamento de Maldonado, Uruguay. In: Estratigrafía del Precámbrico del Uruguay (Ed. E. Pecoits), Rev. Soc. Uruguay. Geol. Spec. Publ.. 1, 124-140.

Pecoits, E., 2003b. Age and preliminary correlation of the Las Ventanas Formation and Bom Jardim-Cerro do Bugio allogroups (Vendian, Uruguay and Brazil). In: III International Colloquium Vendian-Cambrian of W-Gondwana. (Ed. H.E. Frimmel), Programme and Extended Abstracts, pp. 32-34.

Pecoits, E., Oyhantçabal, P., 2004. Geotectonic evolution of Uruguay during the Neoproterozoic-Cambrian. In: 1st Symposium on Neoproterozoic-Early Paleozoic events in SW-Gondwana. Extended Abstracts, IGCP Project 478, Second Meeting (Brazil), pp. 43-45,

Pecoits, E., Aubet, N., Sánchez Bettucci, L., 2004a. Sedimentología, estratigrafía y paleontología de la Formación Las Ventanas (Vendiano inferior, Uruguay). In: Actas X Reunion Argentina de Sedimentología (San Luis, Argentina), pp. 134-135.

Pecoits, E., Aubet, N., Sánchez Bettucci, L., 2004b. Uruguayan Neoproterozoic banded iron formations (BIF) and its tectonic setting. In: Actas X Reunion Argentina de Sedimentología (San Luis, Argentina), pp. 132-134.

Pecoits, E., Aubet, N., Oyhantçabal, P., Sánchez Bettucci, L., 2005a. Estratigrafía de sucesiones sedimentarias y volcanosedimentarias Neoproterozoicas del Uruguay. Rev. Soc. Uruguay. Geol. 11, 18-27.

Pecoits, E., Aubet, N., Sánchez Bettucci, L., 2005b. Estratigrafía de la Formación Las Ventanas y su correlación con los alogrupos Bom Jardim y Cerro do Bugio (Vendiano, Uruguay y Brasil). In: XII Congreso Latinoamericano de Geología, Resúmenes Extendidos (Quito.)

Preciozzi, F., Fay, A., 1988. Carta geológica del Uruguay, Hoja F-23 Pirarajá, Escala 1:100·000. Memoria explicativa. DINAMIGE-UdelaR, Montevideo, pp. 15.

Preciozzi, F., Spoturno, J., Heinzen, W., Rossi, P., 1988. Carta Geológica del Uruguay a escala 1:500·000. Memoria explicativa. DINAMIGE, Montevideo, pp. 90.

Preciozzi, F., Pena, S., Masquelin, E., Pias, J., Tabo, F., 1989. Memoria explicativa del fotoplano Piriápolis. DI.NA.MI.GE. – Fac. de Agronomía – Fac. de Hum. y Ciencias, Montevideo, pp. 11.

Preciozzi, F., Masquelin, H., Sánchez Bettucci, L., 1993. Geología de la Porción Sur del Cinturón Cuchilla de Dionisio (I Simp. Int. Neoproterozoico – Cámbrico de La Cuenca

del Plata), Guía de Excursiones, La Paloma, pp. 1-39.

Rivalenti, G., Mazzucchelli, M., Molesini, M., Petrini, R., Girardi, V.A.V., Bossi, J., Campal, N., 1995. Petrology of Late Proterozoic mafic dykes in the Nico Perez region, Central Uruguay. Mineral. Petrol. 55, 239-263.

Sánchez, L., 1998. Evolución tectónica del Cinturon Dom Feliciano en la región Minas-Piriápolis, Uruguay. Unpublished PhD Thesis, Univ. de Buenos Aires, Buenos Aires, pp. 344.

Sánchez, L., Linares, E., 1996. Primeras edades en basaltos del Complejo Sierra de las Ánimas, Uruguay. In: Actas I, XIII Congreso Geológico Argentino y III Congreso de Exploración de Hidrocarburos, pp. 399-404.

Sánchez, L., Rapalini, A.E., 2002. Paleomagnetism of the Sierra de Las Animas Complex, southern Uruguay: its implications in the assembly of western Gondwana. Precambrian Res. 118, 243–265.

Saylor, B.Z., Kaufman, A.J., Grotzinger, J.P., Urban, F., 1998. A composite reference section for terminal Proterozoic strata of southern Namibia. J. Sed. Res. 68, 1223-1235.

Schopf, J.W., 1991. Collapse of the Late Proterozoic ecosystem. S. Afr. J. Geol. 94, 33-43.

Seilacher, A., 1996. Explosive evolution in the Precambrian/Cambrian transition. In: Evolución: aspectos interdisciplinarios (Ed. E. Molina), Universidad de Zaragoza, (Zaragoza), Vol. 6. pp. 65-78.

Shields, G.A., 2005. Cap carbonates: a critical appraisal of existing formation models and the Plumeworld hypothesis. Terra Nova. 17, 299-310.

Sprechmann, P., Gaucher, C., Blanco, G., Montaña, J., 2004. Stromatolitic and trace fossils community of the Cerro Victoria Formation, Arroyo del Soldado Group (Lowermost Cambrian, Uruguay). Gondwana Res. 7, 753-766.

Thompson, M.D., Bowring, S.A., 2000. Age of the Squantum 'tillite,' Boston basin, Massachusetts: U-Pb zircon constraints on terminal Neoproterozoic glaciation. Am. J. Sci. 300, 630-655.

Umpierre, M., Halpern, M., 1971. Edades Sr-Rb del Sur de la República Oriental del Uruguay. Rev. Asoc. Geol. Argentina. 26, 133-155.

Vail, P.R., Mitchum, R.M., Thompson, S., 1977. Global cycles of relative changes of sea level. In: Seismic Stratigraphy – Applications to Hydrocarbon Exploration (Ed. C.E., Payton), AAPG Mem. 27, 83-98.

Valentine, J.W., 2004. On the Origin of Phyla. The University of Chicago Press, Chicago, 614 pp.

Vasconcelos, C., McKenzie, J.A., 1997. Microbial mediation of modern dolomite precipitation and diagenesis under anoxic conditions (Lagoa Vermelha, Rio de Janeiro, Brazil). J. Sed. Res.. 67, 378-390.

Vasconcelos, C., Warthmann, R., McKenzie, J.A., Visscher, P.T., Bittermann, A.G., van Lith, Y., 2006. Lithifying microbial mats in Lagoa Vermelha, Brazil: modern Precambrian relics?. Sed. Geol. 185, 175-183.

Vidal, G, 1976. Late Precambrian microfossils from the Visingsö Beds in southern Sweden. Fossils Strata. 9, 1-57.

Vidal, G., Knoll, A.H., 1982. Radiations and extinctions of plankton in the late Proterozoic and early Cambrian. Nature. 297, 57-60.

Vidal, G., Moczydlowska-Vidal, M., 1997. Biodiversity, speciation, and extinction trends of Proterozoic and Cambrian Phytoplankton. Paleobiology. 23, 230-246.

Walter, M.R., Hofmann, H.J., 1983. The paleontology and paleoecology of Precambrian iron-formations. In: Iron-Formation: Facts and Problems (Eds. A.F., Trendall, R.C. Morris), 1st edn, Elsevier, Amsterdam, pp. 373-400.

Walter, M.R., Veevers, J.J., Calver, C.R., Gorjan, P., Hill, A.C., 2000. Dating the 840–544 Ma Neoproterozoic interval by isotopes of Strontium, Carbon, and Sulphur in seawater, and some interpretative models. Precambrian Res. 100, 371-433.

Wang, Z., Yin, C., Gao, L., Liu, Y., 2002. Chemostratigraphic characteristics and correlation of the Sinian stratotype in the eastern Yangtze Gorges area, Yichang, Hubei Province. Geol. Rev. 48, 408-415.

Warthmann, R., van Lith, Y., Vasconcelos, C., McKenzie, J.A., 2000. Bacterially induced dolomite precipitation in anoxic culture experiments. Geology. 28, 1091-1094.

Xiao, S., Zhang, Y., Knoll, A.H., 1998. Three-dimensional preservation of algae and animal embryos in a Neoproterozoic phosphorite. Nature. 391, 553-558.

Xiao, S., Bao, H., Wang, H., Kaufman, A.J., Zhou, Ch., Li, G., Yuan, X., Ling, H., 2004. The Neoproterozoic Quruqtagh Group in eastern Chinese Tianshan: evidence for a post-Marinoan glaciation. Precambrian Res. 130, 1-26.

Young, G.M., 2002. Stratigraphic and tectonic settings of Proterozoic glaciogenic rocks and banded iron-formations: relevance to the Snowball Earth debate. J. Afr. Earth Sci. 35, 451-466.

Zhou, C., Chen, Z., Xue, Y., 2002. New microfossils from the late Neoproterozoic Doushantuo Formation at Chaoyang phosphorite deposit in Jiangxi Province, South China. Acta Palaeontol. Sinica. 41, 178-192.

CHAPTER 3: LAS VENTANAS AND SAN CARLOS FORMATIONS, MALDONADO GROUP, URUGUAY

3.1. INTRODUCTION

The Maldonado Group was formally erected by Pecoits et al. (2005) to include the Playa Hermosa and Las Ventanas formations, which are better exposed near the towns of Piriápolis and Pan de Azúcar (Figures 3.1 and 3.2). The San Carlos Formation was informally included. Subsequent work showed that the succession continues to the SW and NE of Minas and Melo cities (Figure 3.1). The Group reaches a maximum thickness of about 1500 m and covers an area of ca. 200 km^2. It comprises acidic and basic volcanic rocks, pyroclastic and sedimentary strata generated in a tectonically active and glacially-influenced basin (for a recent review see Pecoits et al., 2008).

Midot (1984) originally erected the Las Ventanas Formation to include conglomerate, sandstone and pelite outcropping at De Las Ventanas hill and in the surrounding areas (Figure 3.3). This unit was considered by Midot (1984) and various other authors to be Ordovician in age (e.g. Bossi and Navarro 1991; Masquelin and Sánchez 1993; Pazos et al., 2003). This assumption was mainly founded on the inferred development of alluvial fans sourced from the Cambrian Sierra de las Ánimas Complex, located westward (Figure 3.2). However, detailed mapping and stratigraphic analysis of the Las Ventanas Formation led to its redefinition as a Neoproterozoic volcanic / sedimentary succession (Pecoits 2003a). The sections exposed in the northern and southern parts of the type area were designated as the stratoype and parastratotype of the unit respectively (Pecoits 2003a). The former is located near Paso del Molino, where 1200 m of Las Ventanas strata are continuously exposed. The parastratotype is situated near the Burgueño Quarry and Apolonia Mine, where the unconformable contact between the Las Ventanas Formation and the basement (Lavalleja Group) is exposed (Figure 3.3).

The San Carlos Formation was erected by Masquelin (1990) who documented that the unit consists of conglomerate, sandstone and pelite. The depositional environment was likely lacustrine or fluvio-lacustrine. The stratotype of the formation is located 6 km south of San

Carlos town (Figure 3.2), where 220 m of San Carlos strata are exposed with the base and top of formation not visible (Pecoits et al., 2008). The sedimentary facies and volcanic association of the San Carlos Formation are similar to those of the middle Las Ventanas Formation. Likewise, palynological macerations carried out in the pelites of both units reveal the occurrence of similar
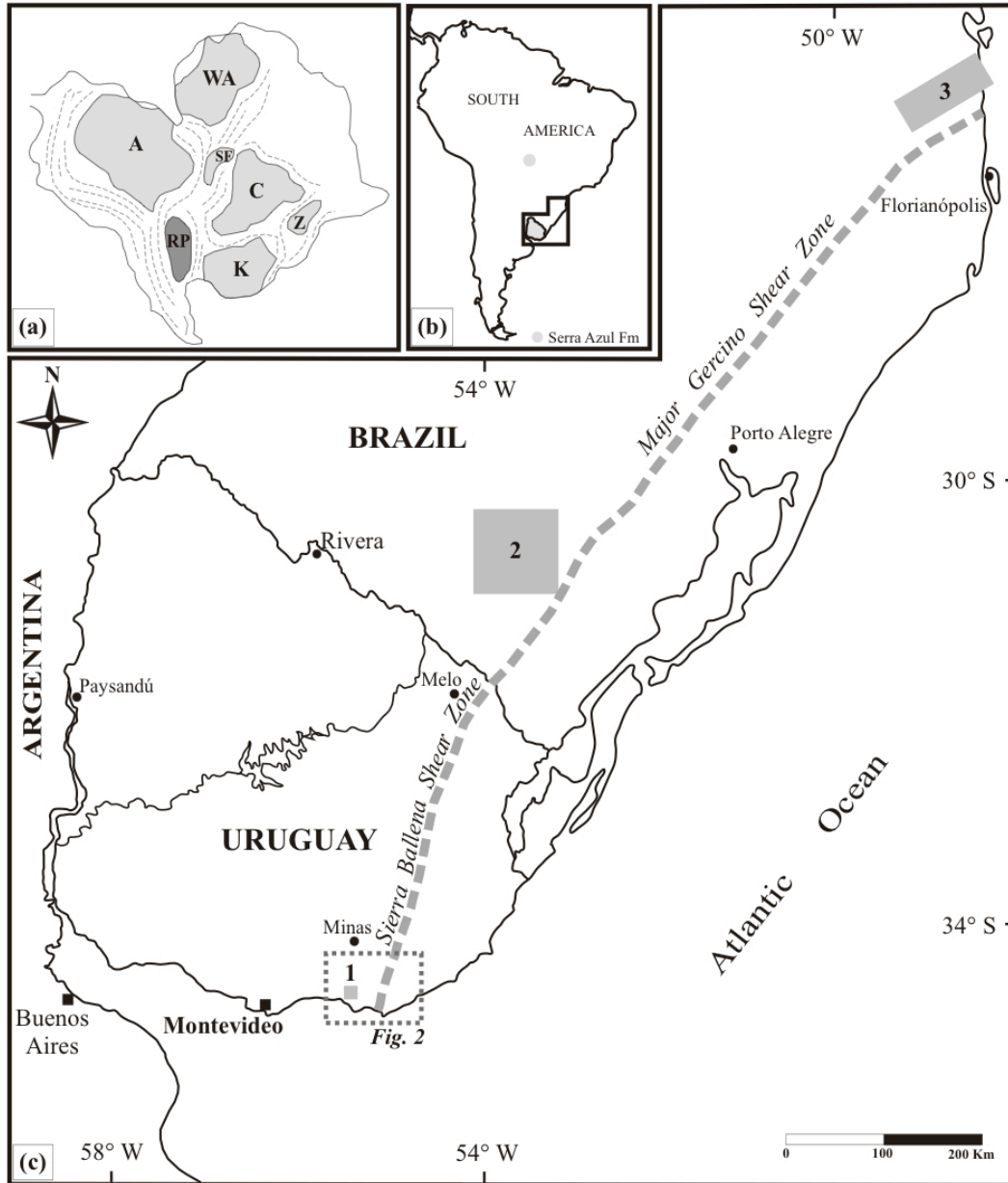
Figure 3.1. (A) Distribution of cratonic blocks of west Gondwana: A: Amazonian; C: Congo: K: Kaoko; SF: São Francisco; RP: Río de la Plata; WA: West African; Z: Zaire. (B) Regional map showing the location of the units discussed in the text (see C for more detail). (C) Distribution of volcano-sedimentary early Ediacaran units of Uruguay and southeastern Brazil: (1) Las Ventanas-San Carlos formations; (2) Camaquã Basin; (3) Itajaí Basin.
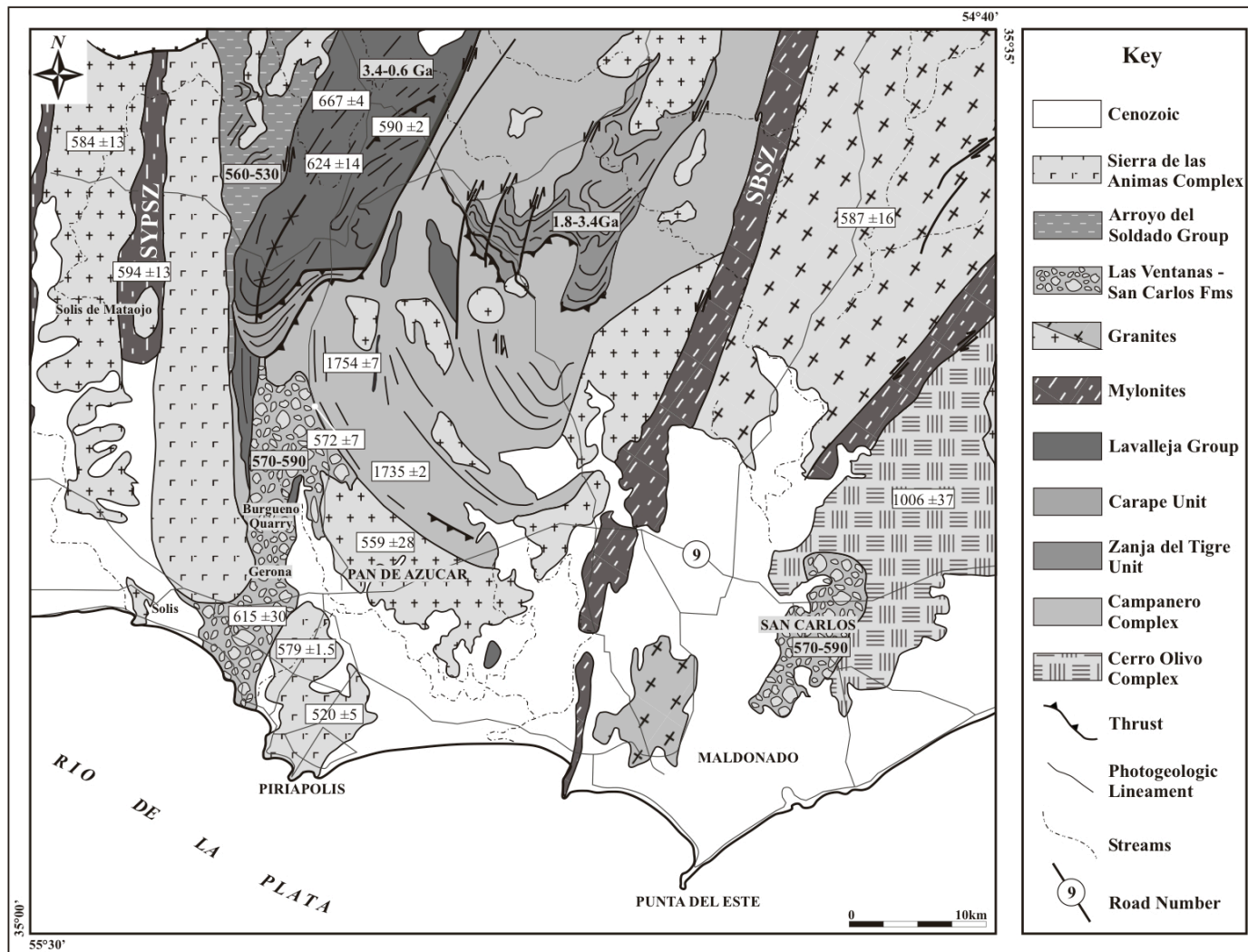
Figure 3.2. Simplified geological map showing the distribution of the Las Ventanas and San Carlos formations (Maldonado Group) and selected age determinations of southeastern Uruguay (see Table 1 and text for explanation) (source of geologic information: Bossi and Navarro 1991; Pecoits et al., 2005; Oyhantçabal 2005 and references therein). SYPSZ: Sarandí del Yí-Piriápolis Shear Zone; SBSZ: Sierra Ballena Shear Zone.
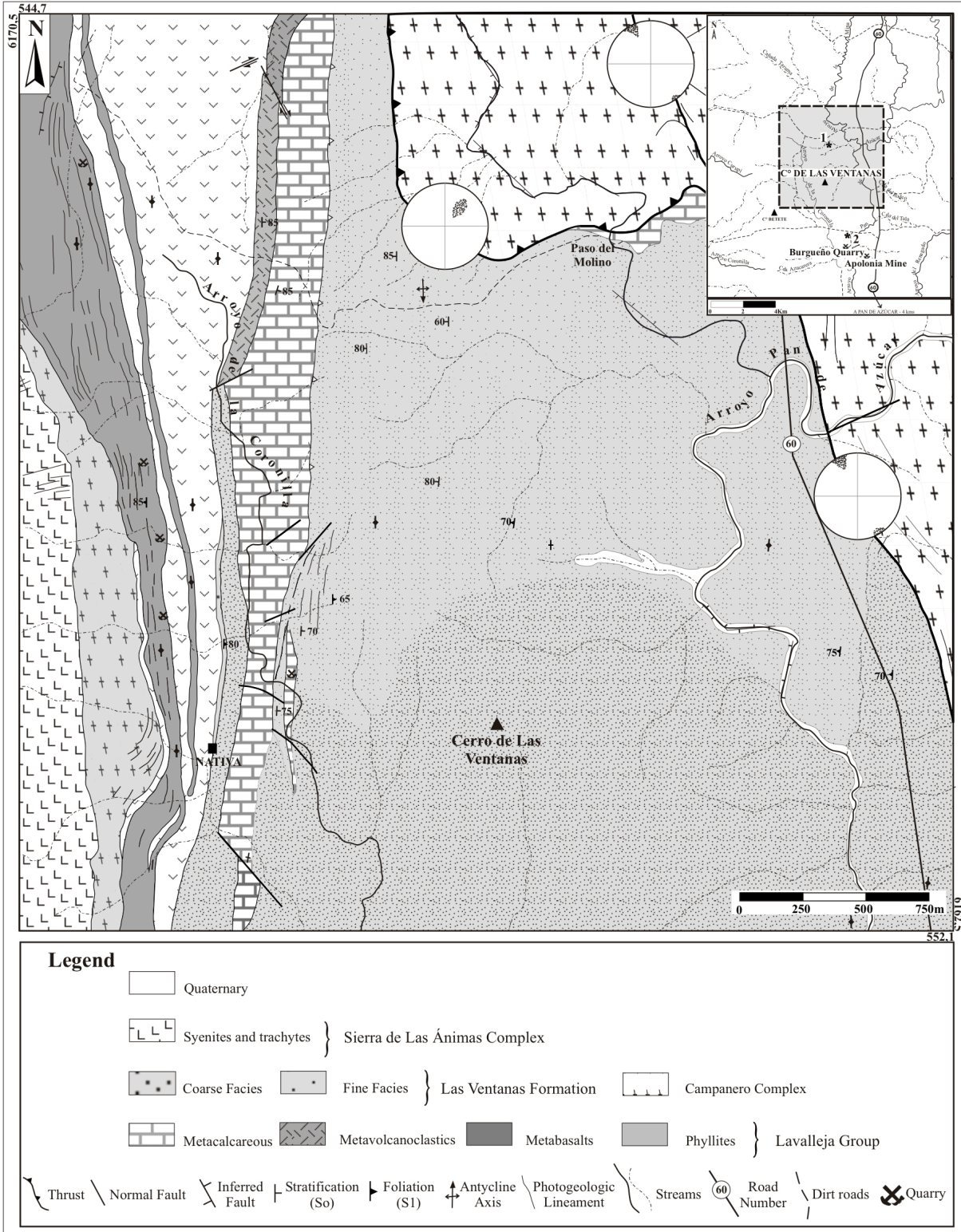
Figure 3.3. Geological map of the type area of the Las Ventanas Formation. The inset shows the location of the stratotype and parastratotype (modified from Pecoits et al., 2008).

microbiota (Pecoits et al., 2005). These observations led Pecoits et al. (2005) to propose a correlation between the San Carlos and Las Ventanas formations. Whether both units were deposited in the same basin, and subsequently dismantled by the displacement of the Sierra Ballena Shear Zone (Figure 3.2), or they were developed within different depocenters remains uncertain.

The first evidence of glacial influence in the Las Ventanas Formation was recorded by Pecoits (2003a), where faceted, outsized clasts in finely laminated rhythmites were interpreted as dropstones. Recently, Gaucher et al. (2008) reported glacial diamictite with associated dropstones occurring in laminated siltstone to the south of Minas (Figure 3.2). Additionally, glacial diamictite and fine-grained rhythmites (varve) containing striated dropstones are well exposed approximately 15 Km northwest (El Perdido area) of this locality (Pecoits et al., 2008). No glacial evidence has yet been recorded in the San Carlos Formation.

3.2. STRUCTURAL FRAMEWORK

In Uruguay, a significant extensional and synkinematic magmatic event corresponding to the final stages of the SW-Gondwana assembly occurred during the Neoproterozoic-lowermost Cambrian (Bossi and Campal 1992; Pecoits 2003*b*; Oyhantçabal 2005). From a structural perspective, the Sierra Ballena Shear Zone (Figures 3.1 and 3.2) constitutes the largest remnant of the Brasilian-Pan African Orogeny (ca. 700-500 Ma). This high-strain transcurrent structure, which was operative primarily between ca. 600-580 Ma, contributed significantly to the basin-fill architecture of the early Ediacaran units (Oyhantçabal 2005). In this regard, Las Ventanas and San Carlos formations were deposited in a strike-slip basin, as indicated by the: (i) diverse depositional facies and their abrupt lateral changes; (ii) apparent migration of the primary depocenter towards the south; (iii) subparallel trend of the basin with respect to its strike-slip margins; and (IV) synchronous timing with regional shearing (Sierra Ballena Shear Zone). Following the development of the widespread transcurrent system, a gravitational orogenic collapse characterized by high angle normal faulting and accompanied by marine transgression occurred during the late Ediacaran-Early Cambrian (Pecoits et al., 2008).

A similar geotectonic evolution is observed in the associated magmatism, which was initiated with highly-fractionated calc-alkaline granite (~584 Ma), followed by mildly alkaline granite and shoshonitic volcanics (~575 Ma), and concluded with peralkaline intrusions and volcanics (~540-520 Ma) (Oyhantçabal et al., 2007). Therefore, the Ediacaran-Early Cambrian in Uruguay is characterized by a transition from a back-arc basin (underlying Lavalleja Group), followed by strike-slip-related basin (Maldonado Group), to a foreland basin (overlying Arroyo del Soldado Group), where strike-slip shear zones of crustal-scale played a major role in the evolution of the orogen.

At the outcrop scale, the Las Ventanas and San Carlos formations show evidence of both brittle and ductile deformation. Small- and large-scale strike-slip faults, westward verging detachment faults, and folds with axis sub-parallel to the strike-slip planes are common features (Figure 3.3). Axial plane slaty and sporadic millimetre-spaced fracture cleavages are present in fine grained facies (pelite). The basic volcanic and pyroclastic rocks show abundant chlorite and epidote as well as pumpellyite and prehnite, demonstrating very low to low-grade metamorphic conditions (Pecoits 2003*a*).

3.3. STRATIGRAPHY

The Las Ventanas and San Carlos formations lie on an angular unconformity above crystalline basement of undetermined age and the Lavalleja Group (Figures 3.4 and 3.**5**). Relatively well dated basement granitoids are represented by the Campanero Complex and the Cerro Olivo Complex, with ages of ~1750 Ma and 1006 ±37 Ma, respectively (Table 1; Oyhantçabal 2005 and references therein). The lithostratigraphy of the Lavalleja Group, although poorly known, is different to that of the Las Ventanas and San Carlos formations. According to Midot (1984) the Lavalleja Group is a volcanosedimentary succession dominated by immature fine grained siliciclastics, marl, basalt and limestone towards the top. This limestone host columnar stromatolites assignable to *Conophyton* (Poiré et al., 2005), and although their occurrence extend from the early Proterozoic to the Ediacaran, preliminary radiometric studies suggest an early Ediacaran age for this unit. SHRIMP U-Pb detrital zircon analyses from the Lavalleja Group

display ages between 3.4-0.6 Ga (Basei et al., 2008). Likewise, interbedded basalt show a crystallization age of 590 ±2 Ma (U-Pb SHRIMP; Mallmann et al., 2007), indicating that the deposition must have occurred ca. 590 million years ago.

The whole succession (i.e. the Las Ventanas and San Carlos formations) can be divided (from base to top) into three informal intervals, namely: (i) volcanic and pyroclastic deposits; (ii) conglomerate-dominated lithofacies; and (iii) pelite-dominated lithofacies. Volcanic and pyroclastic rocks including basalt, mafic hyaloclastic breccias and subaqueous tuff (Las Flores Formation), as well as rhyolite, acidic volcanoclastic and pyroclastic rocks have been recognized as part of the Maldonado Group (Figure 3.4A). This bimodal volcanism has long been thought to represent part of the Sierra de las Ánimas Complex (see for example Sánchez and Rapalini 2002 and references therein). The latter, however, shows geochemical signatures, radiometric ages and structural features indicating anorogenic magmatism, which was extruded after the main deformational phase that affected the Maldonado Group (Oyhantçabal 2005). In fact, the Sierra de las Ánimas Complex systematically displays radiometric ages younger than those of the volcanics assigned to the Maldonado Group (see Geochronology constraints) and it neither displays ductile deformation nor metamorphism. Field relationships show that the Sierra de las Ánimas Complex intrudes the Las Ventanas formation, providing definite evidence of the Las Ventanas' older age.

Conglomerate-dominated lithofacies (proximal facies association of Pecoits 2003a) dominate the basal part of the Las Ventanas Formation, including clast-supported conglomerate and breccia, diamictite, massive sandstone and conglomerate-sandstone couplets. Upwards, pelites are abundant with occasional conglomerate beds (pelites-dominated lithofacies or distal facies association of Pecoits 2003a). This lithofacies includes, laminated siltstone and sandstone-pelite rhythmites, and massive sandstone and conglomerate. Likewise, the San Carlos Formation consists of basal conglomerate- and upper pelite-dominated lithofacies, but the clast size in the lower conglomerate never reaches that of the Las Ventanas Formation. In this sense, two possible explanations can be drawn. First, the San Carlos Formation represents a lateral equivalent to the middle and uppermost part of the Las Ventanas Formation, where coarse-grained conglomerate are rare (see Glacigenic deposits and associated strata). Second, both units, although potentially contemporaneous (see below), were deposited in different basins.

Figure 3.4. (A) Stratigraphic column of the Las Ventanas Formation at its stratotype (point 1, Fig. 3). (B) Stratigraphic section for the lower Las Ventanas Formation at its parastratotype (point 2, Figure 3.3) (modified from Pecoits et al., 2008).
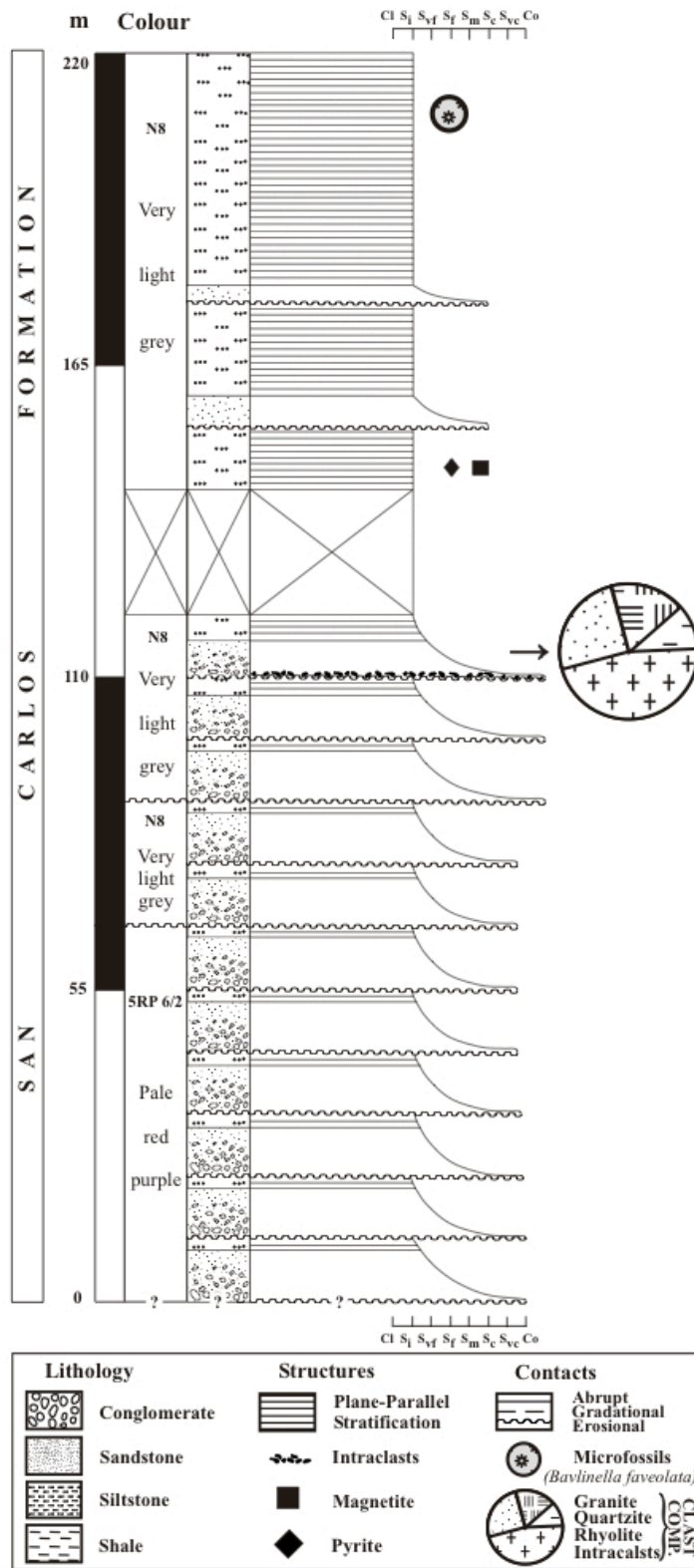
Figure 5. Simplified stratigraphic column of the San Carlos Formation at its stratotype, 6 km SE of San Carlos town (see Figure 3.2) (modified from Pecoits et al., 2008).

Table 3.1. Summary of geochronological data available from southeastern Uruguay (see Figure 3.2). Source: Oyhantçabal 2005 and references therein; Mallmann et al., 2007; Basei et al., 2008; Pecoits et al., 2008. * Volcanic-sedimentary units.

Stratigraphic Unit	Rock type	Method	Age (Ma)
Sierra de las Ánimas Complex	Porphyres	Rb/Sr	520 ±5
	Syenite	Ar/Ar	579 ±1.5
A° del Soldado Group*	Depositional Age: ~560-530 Ma		
El Renegado	Granite	Rb/Sr	559 ±28
Puntas del Pan de Azúcar Lineament	'Mylonite'	K/Ar $_{Musc}$	572 ±7
Aiguá Batholith	Granite	Rb/Sr	587 ±16
Solís de Mataojo	Tonalite	U/Pb	584 ±13
Aguas Blancas	Mylonite	K/Ar $_{Musc}$	594 ±13
Las Ventanas and San Carlos formations*	Depositional Age: ~590-570 Ma		
Las Flores	Trachybasalt	K/Ar	615 ±30
	Quartz-sericite schist	U/Pb $_{(SHRIMP)}$	600-3,400
Lavalleja Group*	Metabasalt	U/Pb $_{(SHRIMP)}$	590 ±2
	Metarhyolite	U/Pb	624 ±14
	Metarhyolite	U/Pb	667 ±4
Cerro Olivo Complex	Orthogneiss	U/Pb	1,006 ±37
Zanja del Tigre Fm*	Meta-sandstone	U/Pb $_{(SHRIMP)}$	1,800–3,400
Campanero Complex	Orthogneiss	U/Pb	1,735 ±2
	Orthogneiss	U/Pb	1,754 ±7

The Las Ventanas is thought to be overlain by the Arroyo del Soldado Group, a thick (3000 m) mixed siliciclastic-carbonate succession, mainly represented by intercalating conglomerate, sandstone, siltstone, thick carbonate, iron-formation, black- and iron-rich shale and chert. It contains a rich fossil assemblage composed of organic-walled microfossils and small shelly fauna, which would include the index fossil *Cloudina riemkeae* (Gaucher et al., 2004; see also page 119). The distinct lithological differences between Las Ventanas and San Carlos formations with the Arroyo del Soldado Group has been explained by different prevailing climatic conditions and tectonic settings. Whereas an evolution towards tropical conditions (Gaucher et al., 2004) and a marine transgression in a foreland setting (Pecoits et al., 2005; Basei et al., 2008) have been proposed for the latter, a glacially-influenced system in a strike-slip setting was suggested for the Las Ventanas and San Carlos formations (Pecoits et al., 2005; 2008). The presence of abundant organic-walled microfossils and shelly fauna in the Arroyo del Soldado Group points to high biological productivity and an elevated nutrient supply possibly related to increased weathering during warmer conditions (Gaucher et al., 2004). Based on available geochronology, chemostratigraphy and biostratigraphy, Pecoits et al. (2008) proposed a maximum depositional age of ca. 560 Ma for the Group.

3.4. GLACIGENIC DEPOSITS AND ASSOCIATED STRATA

Palaeoenvironmental interpretations indicate that the Las Ventanas-San Carlos system records sheet flood-dominated fan delta deposits in a glacially-influenced setting. Direct evidence of ancient glacial activity comes from the basal and uppermost facies of the Las Ventanas Formation, where some deposits have been described and interpreted as ice-rafted diamictite with striated and faceted clasts and rhythmite-hosting dropstones (Pecoits 2003*a*; Pecoits et al., 2008).

Diamictites are mainly coarse-grained and matrix-supported lithofacies with a massive structure displaying normal and occasionally reversed grading. Clasts are rounded to angular and range from granule to boulder size. Compositionally, the diamictite dominantly contains extrabasinal clasts (rhyolite, basalt, granitoid, gabbro, quartzite). Two types of diamictite can be

distinguished: subrounded pebbles and cobbles in a massive muddy matrix, and angular to subrounded cobbles to boulders in a massive to horizontally laminated silty / clayey matrix. These deposits possess a polymodal texture and form relatively thick (2 to 10 m) tabular beds with faceted and occasionally striated clasts.

Although common in the uppermost part of the succession fine grained rhythmites, are also found interbedded with diamictite at the base of the Las Ventanas Formation. The <3 m thick beds are characterized by mm- to cm-intercalation of silty and sandy material with clay and also by the presence of out-sized clasts deforming the layering. Based on the diverse composition of these large clasts (granite, basalt, gabbro, etc), and on the presence of pre-depositional foliation, an interpretation of the clasts as volcanic bombs or other ballistic / pyroclastic material is discarded. These lithofacies (i.e. rhythmites with out-sized clasts and diamictite) were first described at the parastratotype section of the unit (Burgueño Quarry and Apolonia Mine; Figure 3.3), yet later discovery in other localities (e.g. NE Minas and Melo; Figure 3.1) suggest that they are more extensive than originally thought.

The type section of the Las Ventanas Formation is largely dominated by conglomerate, sandstone and finely laminated siltstone. It begins with a 690 m thick fining- and thinning-upward cycle (Figure 3.4A). Conglomerate, sandstone and laminated siltstone dominate the lowermost, medial and uppermost sub-cycles, respectively. The conglomerate is typically granite clast-supported with arkosic sandstone present at the top of each sub-cycle. The following changes occur up-section within the lower major cycle: (i) bed thickness progressively decreases, from meter-scale to a few millimetres (laminae); (ii) average grain-size decreases from pebbles to silt; (iii) the proportion of granitic clasts becomes smaller; and (iv) planar parallel stratification and lamination become a common feature in the siltstone but are absent in the lower and middle part of the cycle. This finely-laminated siltstone shows similar features to those described in the basal part of the unit. Here, the lithofacies is considerably thicker, but the out-sized clasts (dropstones) identified in it are smaller and rarely reach more than 10 cm.

The formation passes up-section into a second major cycle that is nearly 560 m thick, and is composed of minor subcycles of sandstone and fine-grained conglomerate. The sandstone has a tabular geometry, is massive in appearance, and occasionally possesses non-erosive basal

contacts. The conglomerate is clast-supported, polymictic and has a modal grain size of 3-10 cm. The clast composition is variable, and includes rhyolite (32%), granite (2%), quartz (12%), basic volcanic rocks (11%), alkaline feldspar (10%), plagioclase feldspar (8%), and schist (5%). Clasts, either in conglomerate or sandstone, are fresh and show no signs of chemical weathering.

3.5. BOUNDARY RELATIONS WITH OVERLYING AND UNDERLYING NON-GLACIAL UNITS

The Las Ventanas Formation rests unconformably on the Lavalleja Group. (*ca.* 600 Ma) Palaeoproterozoic orthogneiss (Campanero Complex) and Monzogranite (La Nativa) of unknown age (Pecoits et al., 2008). Similarly, a nonconformity separates the San Carlos Formation from Palaeoproterozoic ortho- and paragneiss (Cerro Olivo Complex; Figure 3.2). Particularly important is the relationship with the Lavalleja Group. This unit is largely dominated by basalt and immature fine-grained siliciclastic rocks (Midot 1984). An evolution towards warm climate and stable tectono-magmatic conditions is evidenced by thick stromatolitic limestones developed in the uppermost part of the unit (Poiré et al., 2005), upon which the Las Ventanas Formation uncomfortably lies. However, as discussed below, the hiatus between both units is poorly constrained. Despite this, the transition from the Lavalleja Group to the Las Ventanas Formation is not only indicated by an angular unconformity but also by a strong change in climatic and tectono-magmatic activity.

The relationship and nature of the contact between Las Ventanas and San Carlos formations with the overlying late Ediacaran Arroyo del Soldado Group is not firmly established. The best locality to study such transition is to the north of Minas (Figure 3.2) where both units are closely exposed. A detailed geological mapping of the area indicates stratal juxtaposition due to tectonic shortening in a zone of major thrusting. In other words, both units would be separated by major structural discontinuities (i.e. thrusts oriented SW-NE) and no conformable contacts have been recorded. The contact between both units -although not well exposed- suggests the presence of an angular unconformity separating the uppermost fine-grained rhythmites of the Las

Ventanas Formation and the sandstone of the basal Arroyo del Soldado Group (Yerbal Formation).

3.6. PALAEOLATITUDE AND PALAEOGEOGRAPHY

The location and kinematic history of the blocks involved during the assembly of W-Gondwana in the late Neoproterozoic is poorly known (Rapela et al., 2007). In particular, the palaeogeographic position of the Río de la Plata Craton (Figure 3.1 inset) during the Ediacaran is highly disputed (e.g. Cordani et al., 2000). In this regard, no palaeomagnetic studies have been performed either in the sedimentary rocks of Las Ventanas Formation or in the San Carlos Formation. Preliminary mean geomagnetic poles were only obtained from sedimentary rocks of the Playa Hermosa Formation, volcanics from the Las Ventanas Formation, and volcanics and intrusives from the Sierra de las Ánimas Complex (Sánchez and Rapalini 2002). According to the same authors, the new data supports the Apparent Polar Wander Path (APWP) previously suggested for the entire Gondwana since *ca.* 550 Ma, indicating that the Río de la Plata Craton was indeed at that time part of the supercontinent. Furthermore, it was suggested that a mean geomagnetic pole obtained from the Playa Hermosa Formation (12.7° +9.5°/-8.1°) meant another example of Neoproterozoic low latitude glaciation is evident in Uruguay.

The most reliable palaeomagnetic pole for early Ediacaran units of the Río de la Plata Craton is derived from the Campo Alegre lavas (Sánchez and Rapalini 2002). The Campo Alegre Formation, dated by U-Pb method at 595 ±5 Ma (Citroni et al., 1999) is located in the Itajaí Basin, south-east Brazil (Figure 3.1). Palaeomagnetic reconstructions indicate a moderate palaeolatitude of 33.3 ±9.5°S (D'Agrella and Paca 1988), in marked contrast to the low palaeolatitudes (12.7° +9.5°/-8.1°) proposed for the Playa Hermosa Formation (Sánchez and Rapalini 2002).

In contrast to the scarce database for the early Ediacaran units, the APWP for Gondwana since 550 Ma is better known. Since 550 Ma poles for the Río de la Plata Craton and other Gondwanan continents tend to form a single APWP ranging from ca. 30°S in the late Ediacaran towards lower palaeolatitudes during Lower Cambrian (Meert and Van der Voo 1996).

3.7. GEOCHRONOLOGICAL CONSTRAINTS

Since the definition of both units, the age of the Las Ventanas and San Carlos formations was considered Ordovician (e.g. Midot 1984; Masquelin and Sánchez 1993; Pazos et al., 2003). This assumption was challenged by Pecoits et al., (2008) in reporting cross-cutting relationships with several intrusive Ediacaran bodies and major faults indicating a minimum depositional age of ca. 570 Ma. The age of deposition of the Las Ventanas and San Carlos formations is now relatively well constrained to ca. 590-575 Ma by radiometric data based on K-Ar, Rb-Sr and U-Pb methods on basement rocks, interbedded basalt, intrusive syenite, granitic and trachytic dykes, and cross-cutting faults (Table 3.1).

This inference is supported by the 590 ±2 Ma age (SHRIMP U-Pb) obtained for a metabasalt (Mallmann et al., 2007) and detrital zircons from the Lavalleja Group, basement of the Las Ventanas Formation, that show U-Pb (SHRIMP) ages between 3.4 and 0.6 Ga (Basei et al., 2008), and an intrusive syenite that yield Ar-Ar ages of 579 ±1.5 Ma (Oyhantçabal et al., 2007). Furthermore, the ages are corroborated by the following: (i) basic volcanics interbedded with sedimentary rocks of the Las Ventanas Formation display ages between 615 ±30 and 565 ±30 Ma (K-Ar method; Sánchez and Linares 1996); (ii) Rb-Sr ages from intrusive granite with an age of 559 ±28 Ma (Preciozzi et al., 1993) and trachyte of the Sierra de Las Ánimas Complex –which intrude and overly the Las Ventanas Formation- dated between 520-530 Ma (Bossi et al., 1993; Sánchez and Linares, 1996); (iii) basic dykes cross-cutting the Las Ventanas Formation to the south of Minas yield a K-Ar age of 485 ±12.5 Ma (Poiré et al., 2005); (iv) the last reactivation of the Puntas del Pan de Azúcar Lineament, which cross-cuts the Las Ventanas Formation (Figure 3.3), occurred at 572 ±7 Ma (K-Ar in synkinematic muscovites) (Bossi and Campal 1992), and (v) the San Carlos Formation is intensively deformed by the Sierra Ballena Shear Zone, wherein the third and last deformation phase occurred at around 550-500 Ma (Oyhantçabal 2005). Finally, the transcurrent tectonics that took place during the early Ediacaran, which is closely related to the generation of strike-slip basins recorded for example by the Las Ventanas and San Carlos formations, is also associated with a voluminous synkinematic magmatism (Pecoits 2003*a*; Pecoits et al., 2005). Radiometric studies performed in all this bodies yield ages systematically between 570-590 Ma (Rb-Sr and U-Pb methods) (Bossi et al., 1993; Hartmann et al., 2002; Oyhantçabal 2005).

According to Gaucher et al., (2008) the acritarch assemblage recovered from the Las Ventanas Formation would indicate a depositional age between 635 Ma and 582 Ma, supporting previous data (Pecoits 2003*a*; 2003*b*). This assemblage, however, comprises and is dominated by individuals with no stratigraphic value, such as *Leiosphaeridia*, and other of doubtful origin (e.g. *Soldadophycus*) (Butterfield 2008; *pers. comm.*).

3.8. DISCUSSION AND CONCLUSIONS

The facies associations point to the development of sheet flood-dominated alluvial fans (Blair and McPherson 1994) intercalated with minor lake deposits in a glacially-influenced, transtensional tectonic setting. The proximal facies association comprise massive and horizontally stratified clast-supported conglomerate and rare breccia, massive sandstone, conglomerate-sandstone couplets, and diamictite, while the distal facies include massive and normally graded sandstone, pebbly sandstone, laminated siltstone as well as fine-grained massive and graded conglomerate. The proximal facies association was interpreted by Pecoits (2003*a*) as a subaerial alluvial fan where debris-flow deposits (diamictite) and sheet flood deposits (stratified conglomerate and sandstone) constitute the dominant facies. The subaerial alluvial fan succession is characterized by upward-coarsening and upward-thickening trends resulting from fan progradation. The restricted occurrence of debris flow beds and the comparatively high roundness of the clastic fraction indicate that the preserved succession represents middle and outer regions of the alluvial-fan complex. The distal facies association is thought to represent submarine delta subenvironment with sediment gravity flow deposits occasionally interbedded with turbidites (massive and graded conglomerate and sandstone) and suspension fallout deposits (laminated siltstone). Although some conglomeratic levels are interpreted to represent shoreline deposits along the distal fan, no evidence of wave reworking has been observed (Pecoits 2003*a*).

The proximal facies association offers evidence of sedimentation under arid climatic conditions, as shown by exceptionally fresh well-rounded clasts (e.g. basalt) in conglomerate and sandstone, glacial sedimentary evidence comes from the distal facies association. Therein, outsized clasts within finely laminated siltstone have been recorded and interpreted as

dropstones. This lithofacies has been described at the base and top of the Las Ventanas Formation. In the first case, the laminated strata are "sandwiched" between massive and bedded diamictite, mostly containing extrabasinal clasts. Faceted, striated and bullet-shaped clasts are consistent with glacial transport and suggest glacial influence during the deposition of laminated siltstone and diamictite facies. In contrast, the laminated siltstone described at the top of the unit overlies laminated siltstone and fine-grained sandstone which are interpreted as turbiditic deposits (Pecoits et al., 2008). Here, the glacially influenced laminated siltstone is differentiated from the turbidites by the lack of turbidity current structures, finer grain size and numerous dropstones with impact-induced deformation of underlying laminae.

Despite the lack of evidence for glacially-influenced sedimentation in the San Carlos Formation, the structural and geochronological framework, stratigraphy and fossil-content support the premise that the San Carlos Formation is be correlative with the middle-upper part of the Las Ventanas Formation (compare Figures 3.4A and 3.5). This would explain the absence of the basal and uppermost glacially-influenced facies described for Las Ventanas Formation.

Only one systematic palaeomagnetic study has been performed in glacial Ediacaran units and associated rocks of Uruguay (Sánchez and Rapalini 2002); however, none of the sampled sites correspond to Las Ventanas and San Carlos formations. Unfortunately, all the samples from this work were collected near the border of the Dom Feliciano belt, in an area affected by an intense Neoproterozoic-Cambrian tectono-magmatic activity, and thus probably affected by widespread remagnetization (e.g. Rapalini and Sánchez 2008). The two palaeopoles obtained from volcanic and hypabyssal rocks of the Sierra de las Ánimas Complex are, from the geochronological and structural point of view, poorly constrained. Much of the radiochronology is based on K-Ar method, which usually provides the minimum age, and recent dating on the same lithologies using more precise methods have yielded ages as much as 30 Ma older (Oyhantçabal et al., 2007). Although the early Ediacaran units of Uruguay are extensively deformed, the interbedded basalt sampled for palaeomagnetism were not corrected with respect to the palaeohorizontal. The field relationships have extensively shown that even the youngest rock of the Sierra de las Ánimas Complex (i.e. ~525 million years old), although not folded, are tilted. Therefore the integrity and usability of this palaeomagnetic data is problematic.

Recent palaeogeographic reconstructions locate the Río de la Plata Craton at high palaeolatitudes ca. 580 million years ago (Trinidade and Macouin 2007). Inclination data from deposits slightly older than the Gaskiers equivalent in the Avalon Terrane (Newfoundland) similarly indicate a palaeolatitude of 35°S during the early Ediacaran (ca. 608 Ma; U-Pb zircon age) (Myrow and Kaufman 1999). However, palaeogeographic models between 590 and 560 Ma (i.e. when Gaskiers deposits and their possible Ediacaran correlatives, Squantum, Loch na Cille, and Moelv were formed) are controversial due to the ambiguous results presented by the Laurentian palaeopoles (Trinidade and Macouin 2007 and references therein). For instance, both low and high latitudes for Laurentia at ca. 580 Ma have been proposed. If the latter configuration is confirmed, the glacial strata observed in Laurentia, Baltica, Cadomia, Avalonia and Río de la Plata cratons are compatible with a paleoclimatic scenario similar to the Phanerozoic glaciations rather than that during "snowball" conditions.

Although early proposals promoted a 'Marinoan' age for Las Ventanas and San Carlos formations (Pecoits et al., 2005), an Ediacaran event seems to be a more reasonable alternative (Pecoits et al., 2008) based on the radiometric constraints. Indeed, this would explain the absence of thick 'cap carbonate' facies immediately overlying these deposits as is distinctive for Ediacaran glaciations. Furthermore, the typical facies of the Las Ventanas and San Carlos formations indicates an active participation of the hydrological cycle which is incompatible with the "Snowball Earth" model for Cryogenian glaciations (e.g. Hoffman and Schrag 2002). Alternatively, the absence of cap carbonates might be either due to deposition in a highly active tectonic setting, characterized by high rates of subsidence and high accumulation rates of siliciclastic sediments, or because they were eroded, or simply not found yet.

Recently, a similar glacial succession (Tacuarí Formation) has been described in NE Uruguay (Veroslavsky et al., 2006). These deposits were long-considered a classic example of the Carboniferous-Permian glaciation in Gondwana (e.g. Bossi and Navarro 1991). According to Veroslavsky et al. (2006) and mainly based on a very similar fossil content to that described for the Las Ventanas Formation, this unit was tentatively assigned to the Neoproterozoic. Ongoing research applying radiometric dating on cross-cutting granitic dykes (U-Pb TIMS) and detrital zircons (LA-ICP-MS) has confirmed the Ediacaran age of the succession. The obtained ages constrain the deposition of the unit between 590 and 570 Ma. This is in agreement with the age

proposed for the Las Ventanas Formation (570-590 Ma) and would suggest regional glacial conditions.

Sedimentological, tectonic and magmatic evidence, supported by radiometric ages, show some similarities between the Maldonado Group with other successions in Brazil. In this regard, Las Ventanas and San Carlos formations have been correlated with the Bom Jardim (ca. 592-573 Ma) and Cerro do Bugio (573-559 Ma) allogroups of the Camaquã Basin located in Rio Grande do Sul, southern Brazil (Pecoits 2003*b*; Figure 3.1). The Bom Jardim Allogroup is composed of basic to intermediate volcanic rocks, alluvial conglomerate and turbidites (Paim et al., 2000). SHRIMP age-dating of the volcanics yield an age of ca. 580 Ma (Paim et al., 2000). The Cerro do Bugio Allogroup consists of acidic and basic rocks, alluvial conglomerate, rhythmites (sandstone-pelite) and pelite. Geochronologic studies on acidic rocks yielded a U-Pb age of 573 ±18 Ma (Paim et al., 2000). Both the Bom Jardim and the Cerro do Bugio allogroups were deformed by sinistral transcurrent displacement dated to ca. 570 Ma and were subsequently intruded by granitic bodies dated at 559 ±7 Ma and 565 ±14 - 561 ±6 Ma (Paim et al., 2000 and references therein). Evidence of seasonal glacial influence has been suggested by Eerola (2001; 2006) for the Bom Jardim Allogroup.

Recently, Alvarenga et al*.,* (2007) reported glacial deposits in the Ediacaran Serra Azul Formation in the Paraguay belt, Brazil. The Paraguay belt is located on the south-eastern edge of the Amazon Craton (Figure 3.1), which in conjunction with the Río de la Plata Craton was probably already amalgamated into a single crustal block by the Ediacaran (e.g. Cordani et al., 2000). Unlike the Las Ventanas-San Carlos formations and their Brazilian correlatives Cerro do Bugio-Bom Jardim allogroups, the Serra Azul Formation was deposited on a passive margin (Alvarenga et al., 2007), showing no comparable tectono-magmatic activity but probably similar palaeolatitude (see above). The correlation between Ediacaran (ca. 590-570 Ma) glacially influenced successions of Brazil and Uruguay strengthen the notion of a post Cryogenian glaciation and suggests that these deposits are distributed more extensively than previously recognized in South America. Future efforts focused on the sedimentological constraints of these and other successions (e.g. Itajaí Basin in Brazil) are required to determine the glacial influence on the Brazilian units.

3.9. REFERENCES

Alvarenga, C. J. S de., Figueiredo, M. F., Babinski, M., Pinho, F. E. C., 2007. Glacial diamictites of Serra Azul formation (Ediacaran, Paraguay belt): evidence of the Gaskier event in Brazil. J. S. Am. Earth Sci. 23, 236-241.

Basei, M. A. S., Frimmel, H. E., Nutman, A. P., Preciozzi, F., 2008. West Gondwana amalgamation based on detrital zircon ages from Neoproterozoic Ribeira and Dom Feliciano belts of South America and comparison with coeval sequences from SW Africa. J. Geol. Soc. Lond., Spec. Pub. 294, 239-256.

Blair, T. C., McPherson, J. G., 1994. Alluvial fans processes and forms. In: Geomorphology of desert environments (Eds. A.D., Abrahams, A. J., Parsons), Chapman and Hall, London, 354-402.

Bossi, J., Campal, N., 1992. Magmatismo y tectónica transcurrente durante el Paleozoico Inferior en Uruguay. In: Paleozoico Inferior de Iberoamérica (Eds. J.G., Gutiérrez-Marco, J. Saavedra, I., Rábano), Universidad de Extremadura (Mérida), pp. 343-356.

Bossi, J., Cingolani, C., Lambias, E., Varela, R., Campal, N., 1993. Características del magmatismo post-orogénico finibrasiliano en el Uruguay: formaciones Sierra de Ríos y Sierra de Ánimas. Rev. Brás. Geoc. 23, 282-288.

Bossi, J., Navarro, R., 1991. Geología del Uruguay. Departamento de publicaciones de la Universidad de la República, Montevideo, pp. 970.

Citroni, S. B., Basei, M. A. S., Sato, K., Siga Jr, O., 1999. Petrogenesis of the Campo Alegre Basin magmatism, based on geochemical and isotopic data. In: 2nd South-American symposium on isotope geology. Extended abstracts (Córdoba, Argentina), 1, 174-177

Cordani, U. G., Milani, E. J., Thomaz Filho, A., Campos, D. A., 2000. Proceedings of the 31st International Geological Congress on Tectonic Evolution of South America. Rio de Janeiro, Brazil.

D'Agrella, M. S. F., Pacca, I. G., 1988. Paleomagnetism of the Itajaí, Castro and Bom Jardim Groups from Southern Brazil. Geoph. J. 93, 365-376.

Eerloa, T., 2001. Climate change at the Neoproterozoic-Cambrian transition. In: The ecology of the Cambrian radiation. Perspectives in Paleobiology and Earth History (Eds. A. Y., Zhuravlev, R., Riding), Columbia University Press, pp. 90-106.

Eerola, T., 2006. Myöhäisproterotsooiset ilmastonmuutokset Tutkimuksia Etelä-Brasiliassa. Geology. 58, 164-174.

Gaucher, C., Sial, A. N., Blanco, G., Sprechmann, P., 2004. Chemostratigraphy of the lower Arroyo del Soldado Group (Vendian, Uruguay) and palaeoclimatic implications. Gond. Res. 7, 715-730.

Gaucher, C., Blanco, G., Chiglino, L., Poire, D., Germs, G. J. B., 2008. Acritarchs of the Las Ventanas Formation (Ediacaran, Uruguay): Implications for the timing of coeval rifting and glacial events in western Gondwana. Gond. Res. 13, 488-501.

Hartmann, L., Santos, O., Bossi, J., Campal, N., Schipilov A., Mc Naughton, N. J., 2002. Zircon and Titanite U-Pb SHRIMP geochronology of Neoproterozoic felsic magmatism on the eastern border of the Río de la Plata Craton, Uruguay. J. S. Am. Earth Sci. 15, 229-236.

Hoffman, P. F., Schrag, D. P., 2002. The Snowball Earth hypothesis: testing the limits of global change. Terra Nova. 14, 129–155.

Mallmann, G., Chemale, Jr. F., Ávila, J. N., Kawashita, K., Armstrong, R. A. 2007. Isotope geochemistry and geochronology of the Nico Pérez Terrane, Río de la Plata Craton, Uruguay. Gond. Res. 12, 489-508.

Masquelin, H., 1990. Análisis estructural de las zonas de cizalla en las migmatitas de Punta del Este – Uruguay. Acta Geol. Leopoldensia. 30, 139-158.

Masquelin, H., Sánchez, L., 1993. Propuesta de evolución tectono-sedimentaria para la fosa tardi-brasiliana en la región de Piriápolis, Uruguay. Rev. Bras. Geoc. 23, 313-322.

Meert, J. G., Van der Voo, R., 1996. Paleomagnetic and 40Ar-39Ar study of the Sinyai dolerite,Kenya: implications for Gondwana assembly. J. Geol. 104, 131-142.

Midot, D., 1984. Etude geologique et diagnostic metallogénique pour l'exploration du secteur de Minas (Uruguay). Diplome de Docteur de 3è Cycle. Universitè Pierre et Marie Curie.

Myrow, P. M., Kaufman, A. J., 1999. A newly discovered cap carbonate above Varanger-age glacial deposits in Newfoundland, Canada. J. Sed. Res. 6, 784-793.

Oyhantçabal, P., 2005. The Sierra Ballena Shear Zone: kinematics, timing and its significance fro the geotectonic evolution of southeast Uruguay. Unpublished PhD Thesis. Georg-August-Universität zu Göttingen, pp. 344.

Oyhantçabal, P., Siegesmund, S., Wemmer, K., Frei, R., Layer, P., 2007. Post-collisional transition from calc-alkaline to alkaline magmatism during transcurrent deformation in the southernmost Dom Feliciano Belt (Braziliano–Pan-African, Uruguay). Lithos. 98, 141-159.

Paim, P. S. G., Chemale Jr. F., Lopes, R. da C., 2000. A Bacia do Camaquã. In: A geología do Rio Grande do Sul (Eds. M. Holz, L.F., De Ros), CIGO-Universidade Federal Rio Grande do Sul, Rio Grande do Sul, pp. 231-274.

Pazos, P., Sánchez Bettucci, L., Tófalo, R., 1998. Procesos sedimentarios e indicadores paleoclimáticos en la sección inferior de la Formación Playa Hermosa, Cuenca Playa Verde, Piriápolis, Uruguay. In: Actas 2nd Congreso Uruguayo de Geología, (Montevideo, Uruguay), 64-69.

Pazos, P., Tófalo, R., Sánchez Bettucci, L., 2003. The record of the Varanger Glaciation at the Rio de la Plata Craton, Vendian-Cambian of Uruguay. Gond. Res. 6, 65-77.

Pecoits, E., 2003a. Sedimentología y consideraciones estratigráficas de la Formación Las Ventanas en su área tipo, departamento de Maldonado, Uruguay. Rev. Soc. Uru. Geol. Special Issue. 1, 124-140.

Pecoits, E., 2003b. Age and preliminary correlation of the Las Ventanas Formation and Bom Jardim-Cerro do Bugio allogroups (Vendian, Uruguay and Brazil). In: (Eds. H.E., Frimmel), 3rd International Colloquium Vendian-Cambrian of W-Gondwana. University of Cape Town, Cape Town, South Africa, 32-34.

Pecoits, E., Aubet, N., Oyhantçabal, P., Sánchez Bettucci, L., 2005. Estratigrafía de sucesiones sedimentarias y volcanosedimentarias Neoproterozoicas del Uruguay. Rev. Soc. Uru. Geol. 11, 18-27.

Pecoits, E., Gingras, M., Aubet, N., Konhauser, K., 2008. Ediacaran in Uruguay: palaeoclimatic and palaeobiologic implications. Sedimentology. 55, 689-719.

Poiré, D. G., González, P. D., Canalicchio, J. M. Repetto, F. G., Canessa, N. D., 2005. Estratigrafía del Grupo Mina Verdún, Proterozoico de Minas, Uruguay. Lat. Am. J. Sedimentol. Basin Anal. 12, 125-143.

Preciozzi, F., Masquelin, H., Sánchez Bettucci, L., 1993. Geología de la Porción Sur del Cinturón Cuchilla de Dionisio. In: (Eds. F., Preciozzi, H., Masquelin, H., L., Sánchez Bettucci), 1st Simp. Int. Neoproterozoico – Cámbrico de La Cuenca del Plata, Guía de Excursiones (La Paloma, Uruguay), pp. 3-39.

Rapalini, A. E., Sánchez, L., 2008. Widespread remagnetization of late Proterozoic sedimentary units of Uruguay and the apparent polar wander path for the Rio de La Plata craton. GeophyS. J. Int. 174, 55-74.

Rapela, C. W., Pankhurst, R. J., Casquet, C., Fanning, C. M., Baldo, E. G., González-Casado, J. M., Galindo, C., Dahlquist, J., 2007. The Río de la Plata craton and the assembly of SW Gondwana. Earth Sci. Rev. 83, 49-82.

Sánchez, L., Linares, E., 1996. Primeras edades en basaltos del Complejo Sierra de las Ánimas, Uruguay. In: Actas 13th Congreso Geológico Argentino y 3rd Congreso de Exploración de Hidrocarburos (La Plata, Argentina) I, pp. 399-404.

Sánchez, L., Rapalini, A. E., 2002. Paleomagnetism of the Sierra de Las Animas Complex, southern Uruguay: its implications in the assembly of western Gondwana. Precambrian Res. 118, 243-265.

Trindade, R. I. F., Macouin, M., 2007. Palaeolatitude of glacial deposits and palaeogeography of Neoproterozoic ice ages. Comptes Rendus Geosc. 339, 200–211.

Veroslavsky, G., de Santa Ana, H., Daners, G., 2006. Tacuarí Formation (Nov. Nom.): Lithostratigraphy, facies, environment, age and geological significance (Cerro Largo-Uruguay). Rev. Soc. Uru. Geol. 13, 23-35.

CHAPTER 4: C-, O-, AND SR-ISOTOPE COMPOSITION OF GASKIERS-AGE CARBONATES FROM THE RÍO DE LA PLATA CRATON; UNRAVELLING PALAEO-ENVIRONMENTAL CAUSES OF δ^{13}C NEGATIVE EXCURSIONS.

4.1. INTRODUCTION

The study of carbonate rocks provides important information for characterizing depositional environments, constraining palaeo-oceanographic conditions and providing chemostratigraphic ages, particularly when strata lack recognizable fossils or are radiometrically undatable (e.g., Derry et al., 1989; Knoll and Walter, 1992; Jacobsen and Kaufman, 1999; Halverson et al., 2005; Azmy et al., 2006). Based on the premise that carbonate carbon isotope signatures reflect near-primary marine composition, chemostratigraphy of Neoproterozoic rocks has blossomed and a new paradigm for explaining significant negative anomalies due to cessation of bioproductivity, as a result of glacial events, has emerged (e.g., Knoll et al., 1986; Kaufman and Knoll, 1995; Kaufman et al., 1997; Halverson et al, 2005). However, secular variations in carbon isotope composition of marine carbonates ($\delta^{13}C_{carb}$) may reflect the influence of several factors, including post-depositional alteration and diverse sources of the δ^{13}C-depleted carbon (Hayes et al., 1999).

In Uruguay, previous chemostratigraphic studies on Ediacaran carbonates (Polanco Limestone Formation) have identified a significant δ^{13}C-depleted excursion in shallow-water facies (up to -4.5‰) and a glacial-related event has been suggested as the most likely explanation (Gaucher et al., 2004; Gaucher et al., 2009). According to the same authors, this negative anomaly represents a post-Gaskiers glaciation and is correlated with the Shuram-Wonoka-Johnie anomaly (ca. 551 Ma). Crucially, the apparent synchronicity between this anomaly and glacial conditions carries important implications for the palaeo-oceanographic and palaeo-climatic evolution of the Ediacaran and ultimately, in the rise of animal life (e.g., Canfield et al., 2008). In order to asses the extent of such negative anomaly across the Polanco basin, this study aims to: (a) present

detailed carbon isotopic profiles from deep-water facies, (b) establish the chemostratigraphic age of the Polanco Limestone Formation by means of Sr– and C-isotope data, and (c) discuss the possible mechanisms that could originate this prominent negative excursion.

4.2. GEOLOGIC SETTING AND STRATIGRAPHY

Ediacaran sedimentary and subordinate volcanic rock successions are well exposed on the southeastern and eastern margin of the Río de la Plata craton in Uruguay (South America). These rocks were formed during the final stages of assembly of W-Gondwana as part of the Neoproterozoic Brasiliano-Pan African orogeny when the eastern margin of the Río de la Plata craton collided along the Sierra Ballena Shear Zone with island arcs approaching from the southeast (Oyhantçabal et al., 2007). The Polanco Limestone Formation forms part of a mixed carbonate-siliciclastic succession of marine origin and grouped into the Arroyo del Soldado Group, which is traceable over 300 km along the eastern border of the Río de la Plata craton, covering an area of approximately 2,400 km^2 (Figure 4.1). The group reaches almost 3,000 m in thickness, and has been subdivided into four formations: Yerbal, Polanco Limestone, Cerro Espuelitas and Barriga Negra (Pecoits et al., 2008) that record deep- to shallow-water marine environments developed during a single transgression-regression-transgression cycle with minor superimposed higher-frequency cycles (Figure 4.2).

At the base, the Arroyo del Soldado Group comprises a fining- and thinning-upward succession with a maximum recorded thickness of 900 m. It contains interbedded mudstones and sandstones with minor contributions of carbonates, cherts and iron formations (Yerbal Formation). The overlying Polanco Limestone Formation is a coarsening-upward succession, with minor higher-frequency coarsening-upward cycles. Typical lithologies include pure, dark grey limestones and dolostones rhythmically interbedded (m to mm-scale) and rare chert layers. Bracketed between siliciclastic units, the succession thickens from less than 75 m to a maximum of more than 900 m. The
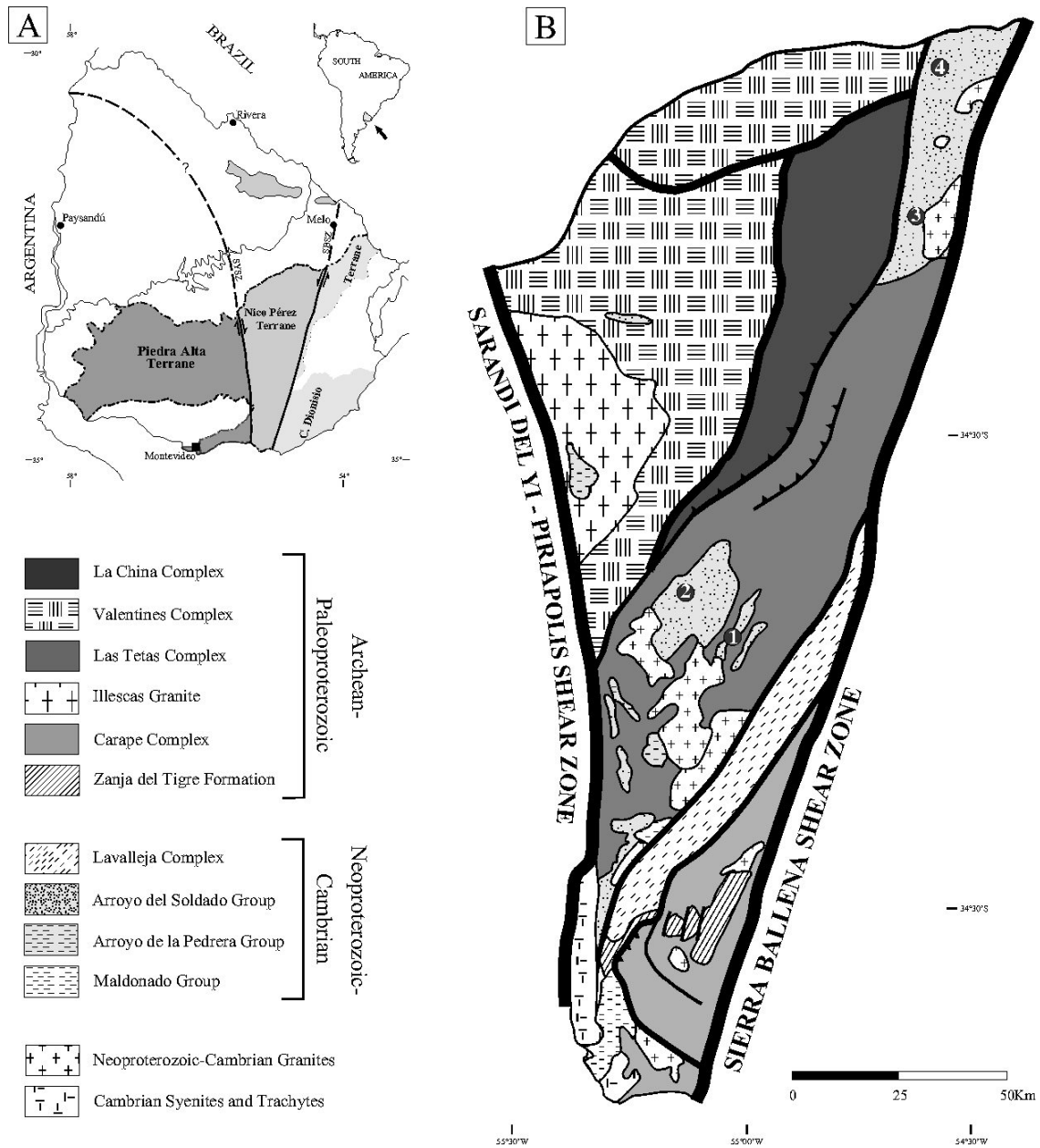
Figure 4.1. (A) Location map of Uruguay and tectonostratigraphic subdivision of the crystalline basement. **(**B) Schematic geological map of part of the Río de la Plata craton (Nico Pérez terrane) showing the distribution of the Arroyo del Soldado Group and location of the sections (1: Los Tapes; 2: Barriga Negra; 3: South Isla Patrulla; 4: Recalde).
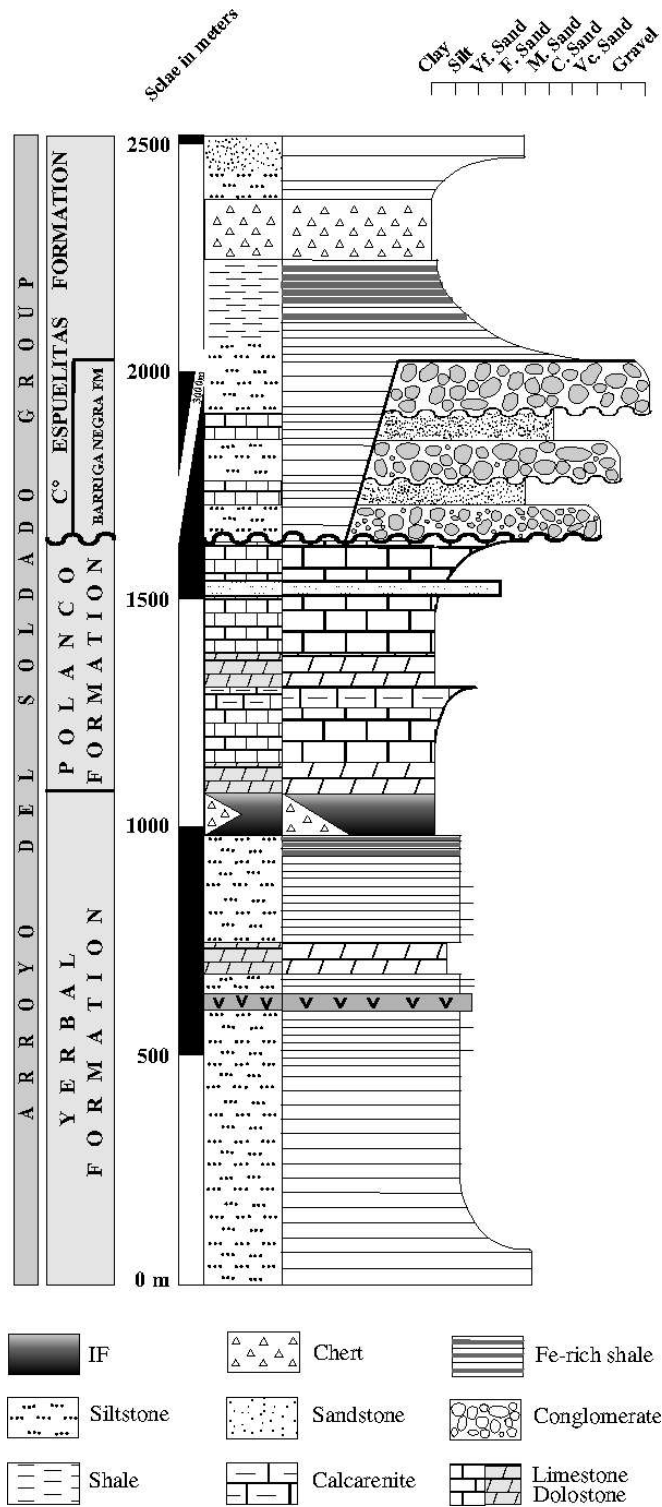
Figure 4.2. Simplified stratigraphic column of the Arroyo del Soldado Group (after Pecoits et al., 2008).

Barriga Negra Formation is restricted to the landward margin where it unconformably overlies the Polanco Limestone Formation as a consequence of the development of alluvial fans. The unit is made up of thick conglomerates, carbonate-breccias, sandstones and mudstones, which gradually pass into the Cerro Espuelitas Formation. The latter consists of an alternation of siltstones, black- and iron-rich shales and cherts, with minor occurrences of sandstones and carbonates. In deeper parts of the basin, it overlies the Polanco Limestone Formation and reaches a thickness of more than 550 m. The age of the Arroyo del Soldado Group is constrained by U-Pb (SHRIMP) ages from basement rocks of the succession (Puntas del Santa Lucía pluton) and Rb-Sr isochron ages of the intrusive Guazunambí granite to between 633±12Ma and 532±11Ma (Hartmann et al., 2002; Kawashita et al., 1999). The occurrence of the index fossil *Cloudina riemkeae* (Germs, 1972)*,* immediately below the Polanco Limestone Formation (Gaucher et al., 2003), would suggest a maximum age of 550-540 Ma for the Polanco carbonates as reported for other *Cloudina* occurrences world-wide (Grotzinger et al., 1995; Saylor et al., 1998; Martin et al., 2000; Knoll et al., 2004; Hua et al., 2005).

4.3. ANALYTICAL METHODS

Rock samples were collected at intervals between 5 to 10 m. Petrographic analyses were performed on sixty-four thin sections, which were stained with Alizarin Red S and potassium ferricyanide to determine calcite, dolomite, and iron content in both mineral phases. Trace element geochemistry was determined using a PerkinElmer Elan6000 Quad-ICPMS (quadrupole inductively coupled plasma mass spectrometer) following Na_2O_2 sintering digestion. Accuracy and precision of the analytical protocol was verified with the use of well-established international whole-rock standards.

Carbonate powders from the Polanco Limestone Formation were obtained by using a dental drill, and were analyzed for carbon and oxygen isotopes in the Stable Isotope Laboratory at the University of Alberta. Carbonates phases were extracted separately, and a total of twenty-nine dolostones and fifty-seven limestones were

analyzed. Carbon and oxygen isotope analyses were obtained by the phosphoric acid method at room temperature (McCrea, 1950). No phosphoric acid fractionation was applied to the dolomite samples. Reproducibility was checked providing an analytical precision of better than ±0.1‰ for $\delta^{13}C$ (1σ) and $\delta^{18}O$ (1σ). From analysis of reference standards, analytical accuracy is estimated to be ± 0.2‰. Approximately 5 grams of sample powder were extracted from the least altered rock specimens (lacking veins, discoloration, weathered rinds, recrystallization features, and silicification). CO_2 gas was extracted from these powdered carbonate samples in a high vacuum line by reacting 20-40 mg of sample with 100% phosphoric acid at 25°C for approximately 24 hours of reaction for limestones or 3 days for dolostones. The released CO_2 gas was analyzed fro O and C isotopes in a multiple collector mass spectrometer (Finnigan MAT 252). All carbon-isotope data are expressed in the δ-notation in parts per thousand (‰) using the Vienna Pee Dee Belemnite (V-PDB) international standard. Replicate analyses (two) using these procedures are within 0.8‰ and 1‰ for $\delta^{13}C$ and $\delta^{18}O$, respectively.

Strontium isotope ratios of seventeen limestones were determined using 20 mg aliquots of sample powder following chemical procedures detailed in Holmden et al. (1996). Strontium isotopes were measured using a NuPlasma MC-ICP-MS instrument at the University of Alberta. Subsequent to ion chromatographic treatment, the Sr-bearing aliquots were diluted in a 2% HNO_3 solution and aspirated into the ICP. Strontium isotope data were acquired in static, multicollection mode using five Faraday collectors for a total of 400 seconds. Prior to the aspiration of a sample, a 30 seconds measurement of the gas (+ acid) blank was conducted, which is critical for the correction of the ^{86}Kr and ^{84}Kr isobaric (plasma-based) interferences. The isobaric interference of ^{87}Rb was also monitored and corrected for using the ^{85}Rb ion signal; however, the latter was negligible for all of the results reported here. Accuracy and reproducibility of the analytical protocol were verified by the repeated analysis of a 100 ppb solution of the NIST SRM 987 Sr isotope standard during the course of this study yielding an average value of 0.710255 ± 0.000020 (1SD; n = 7 analyses) and is indistinguishable compared to the accepted value of 0.710245 (Faure and Mensing, 2005). The typical internal precision ('error') associated with individual Sr isotope analysis ranges from 0.00001 to 0.00003 (2σ level).

4.4. RESULTS

4.4.1. Facies Associations

Three main facies associations were recognized: inner; mid and outer ramp. The lack of gravity induced deposits related to platform margins, the gradual evolution of facies and the absence of barred restricted marine conditions suggest that these facies were deposited in a homoclinal ramp (Read, 1985; Burchette and Wright, 1992).

4.4.1.1. Inner ramp facies

4.4.1.1.1. Description

Inner ramp deposits are documented in the middle and upper Polanco Limestone Formation at the Recalde and Barriga Negra (parastratotype) sections. They are mainly characterized by alternations of medium- to coarse-grained calcarenites, with occasional sandstone beds, wherein three main facies were recognized: (1) alternations of low-angle cross-stratification and asymmetric rippled calcarenites, (2) trough cross-stratified with sporadic swaley cross-stratified calcarenites, and (3) amalgamated hummocky cross-stratified calcarenites. They commonly form coarsening- and thickening-upward regressive cycles. Facies 1 characterizes the top of the upper coarsening-and thickening-upward cycles. It erosively overlies the deposits of facies 2 and consists of grey well sorted, low-angle cross-strata covered by calcarenites with asymmetric ripples with current direction oriented northwestwards although a subordinate, reverse current has also been noted. Trough cross-stratified with sporadic swaley cross-stratified calcarenites of facies 2 commonly appear bracketed between facies 1 and 3. The latter is made of amalgamated hummocky cross-stratified calcarenites, which erosively overlie mid ramp facies (see bellow) and occasionally contains rip-up clasts paving the basal contacts.

4.4.1.1.2. Interpretation

Inner ramp facies association display typical facies of a storm- and wave-dominated shoreface environment. In this regard, facies 1 represent deposition in the upper shoreface setting where well-sorted, low-angle planar-cross-bedded calcarenites are interpreted as being produced in a wave-dominated beachface, by swash and backwash of waves. The underlying trough cross-stratified and swaley cross-stratified calcarenites (facies 2) are characteristic of a storm-dominated middle shoreface environment. Trough cross-bedding is generally directed parallel to the shoreline in response to longshore currents; at deeper depths they are sometimes oriented offshore and most likely reflect offshore movement during storms. Thus, the transition from trough cross-stratified and swaley cross-strata into planar cross-stratification and rippled beds –with occasional sandstone layers- suggests a transition to a shallower, higher energy upper shoreface setting where storm and longshore currents were able to form crescentic megaripples and was sporadically receiving sediments from the land. Hummocky-dominated calcarenites of facies 3, are interpreted as carbonates deposited in the transition between mid-ramp and lower shoreface setting and whose sedimentary structures record frequent storm events in permanent water column above storm-weather wave base.

4.4.1.2. Mid ramp facies

4.4.1.2.1. Description

This facies association, which is a few meters to more than 200 m thick, are the predominant deposits within the lower part of the Recalde section and towards the top interfingers with inner ramp facies 3. It is characterized by alternations of grey, parallel laminated or stratified rhythmites of limestone and dolostone calcisiltites, occasional hummocky cross-stratified calcarenites and thin massive or parallel stratified calcarenite beds. The finer sediments dominate and the thinner the calcisiltite layers are, the thinner the hummocky cross-stratified beds and calcarenite intercalations are between them. Rhythmites are made up of dark-grey organic-rich, medium to coarse calcisiltites

interbedded with fine dolosiltites layers. Individual layers are a few millimetres to a few decimetres thick, have sharp contacts, tabular geometries and are laterally continuous. The thicker calcarenite beds (0.2-2m), in turn, have erosive-based beds, particularly when present hummocky cross-stratification, sometimes showing rip-up clasts at the base of the beds and display upper graded portions.

4.4.1.2.2. Interpretation

The stratigraphic position of this lithofacies in the individual stratigraphic sections at different locations, and the sedimentary features observed, suggest that these high-frequency carbonate rhythmites formed in a mid to proximal outer ramp setting characterized by moderate energy, and subjected episodically to storm events as indicated by the hummocky cross-strata. Likewise, repetitive alternation of fine-grained rhythmites and coarser calcarenite beds reflects alternating storm- and fair-weather deposition in more distal outer ramp areas wherein episodic storms were able to transport coarser sediment into deeper waters. Thus, hummocky cross-stratified and graded sandstones were formed as storm sheets on the mid-ramp above the storm wave-base, whereas finer sediments were deposited from suspension during periods of quiescence after cessation of storms. Palaeocurrent trends from interbedded coarser lithologies (calcarenites), lateral change in facies and thickness, as well as the rare slumps measured, indicate that the ramp deepened gradually to the southeast and the coastline was roughly oriented northeast-southwest.

4.4.1.3. Outer ramp facies

4.4.1.3.1. Description

The outer ramp deposits are volumetrically best represented in Los Tapes section and south Isla Patrulla area. Two main facies can be distinguished: (1) rhythmites limestone-

dolostone, and (2) laminated to bedded dolostones. This facies association thickens seaward and shows typically parallel lamination, marked by subtle changes in grain size, and occasional chert layers and/or nodules with no obvious evidence of storm reworking. Normally, the limestone and dolostone beds are 0.01-1 m thick and grey in colour. The dolostone layers show good grading and display finer grain size than the limestone and tend to be thinner and more even-bedded or laminated. Light grey, fine-grained, thin to medium bedded dolostones with chert nodules only occur at the top of the Polanco Limestone Formation in deep parts of the basin. Petrographic observations of these beds reveal very fine and uniform texture.

4.4.1.3.2. Interpretation

Grain size and sedimentary structures indicate a relatively deep-marine depositional environment characterised by low to moderate energy, in an outer ramp setting, below storm wave base, as suggested by the paucity of graded beds, the presence fine parallel lamination and the lack any evidence of storm or fair weather processes. Indeed, this facies association was deposited at sufficient depth to be unaffected by any of the relative changes in sea-level which so strongly influenced sedimentation in inner and mid ramp facies and thus, the cycles recognized in the two other zones are missing. Because of this partial restriction and as indicated by the dark colour of the laminated rhythmites and dolostones due to the organic matter content, anoxic conditions developed. The poorly oxygenated deep-water masses, however, were most likely non-sulfidic as indicated by the organic rich but pyrite-free nature of the dolostones and limestones.
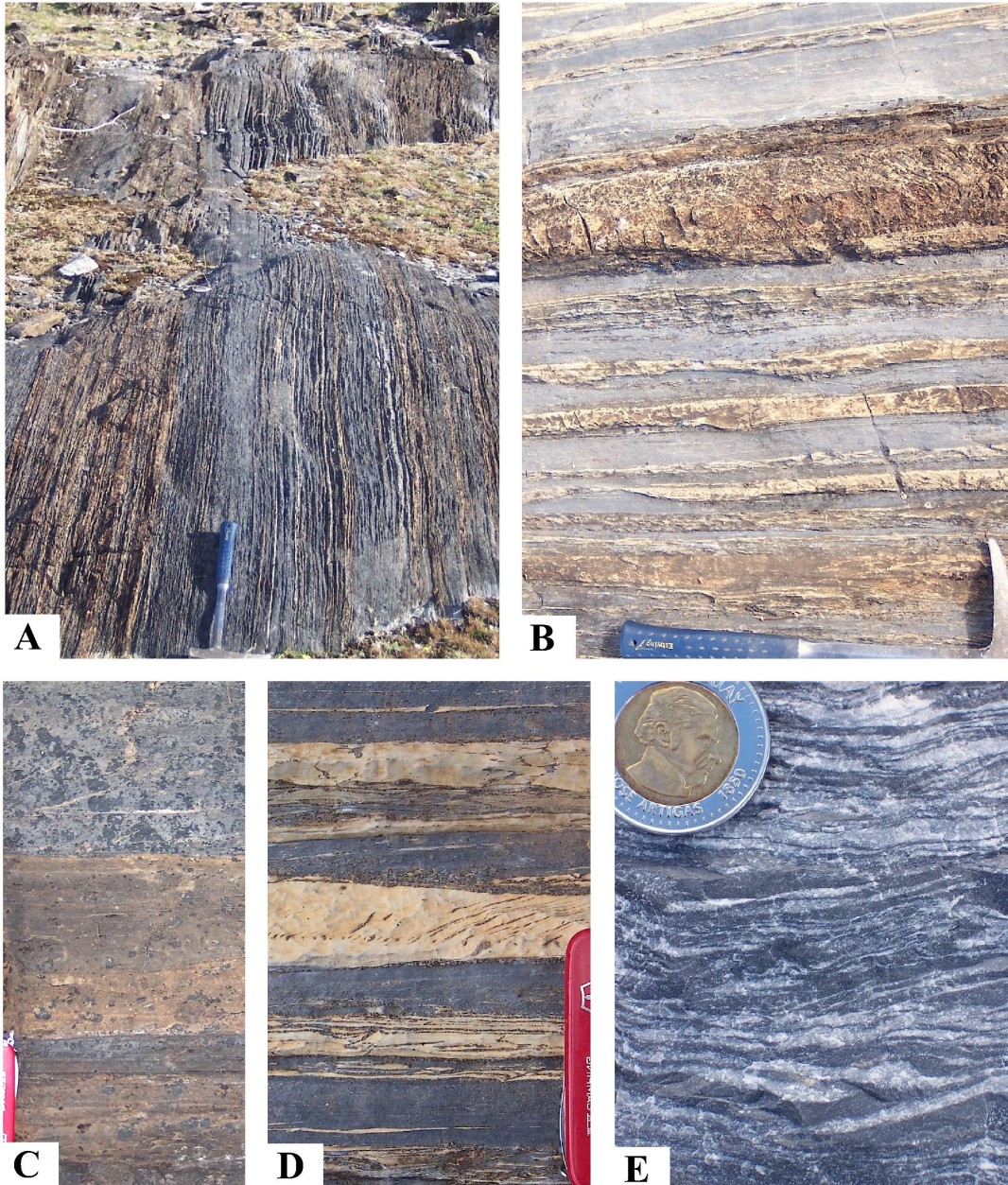
Figure 4.3. Rhythmites from the Polanco Limestone Formation at Los Tapes outcrop. The carbonate rhythmites represent the most common lithotype of the Polanco Limestones Formation. Rhythmites consist of milimetric- to decimetric-alternation of limestone laminae or strata and dolostone beds (A, B). Dolostone predominates over limestone at the base of the section (A). Massive dolostones are usually light beige in colour and make up relatively thick beds -up to 25cm- (C). The contact between dolostone and limestone layers is always sharp, showing no transitions (C, D). Colour of the limestones is typically gray, with darker colours at the base passing into lighter shades towards the top (E). Weathered dolostone beds commonly have light beige color due to the iron content of the dolomite, while limestone beds weather gray (A, B, C, D). Length of hammer = 40cm; length of knife = 10cm.

4.4.2. Petrography

Microscopic observations were conducted in order to identify the diverse carbonate components and evaluate crystal size, percentages of clastic and authigenic minerals, dissolution, recrystallization, and other alteration features. The composition of all studied samples were rather uniform, mostly finely crystalline dolomite (grain size 5-20μm) and calcite (< 50μm), with few samples showing partial recrystallization (Figure 4.4A-D).

The Polanco carbonates at the Los Tapes and South Isla Patrulla sections are characterized by a continuous laminated/bedded structure indicated by the alternation of dolostones and limestones. Petrographically, two main types of dolostones were indentified; massive and laminated. Massive dolostones are composed of a xenotropic mosaic of suheuhedral to anhedral fine-grained dolomite cystals (<20μm) with occasional disseminated euhedral pyrite crystals. Laminated dolostones are mainly an idiotopic mosaic of subeuhedral (planar-s) dolomite crystals with sizes ranging between 5-20 μm (Figure 4.4A-C). Lamination in dolostones is defined by the presence of variable amounts of silt-grain sized clasts of quartz and authigenic chert (Figure 4.4A-B). Alternating laminae/beds of limestones, composed of fine- to medium-grained equigranular calcite (<50μm), define the preserved primary bedding (Figure 4.4C-D). Pressure-dissolution is indicated by micrometric-sized stylolites, which are generally outlined by organic matter. Stylolites are present in areas where dolomite/calcite occur together; carbonate components next to them are usually partially dissolved. When present, matrix intercrystalline porosity is occluded by sparry calcite and dolomite cements (Figure 4.4D), and occasionally by chert. Interestingly, those carbonate cements occur in less that 5% of the rock volume indicating that recrystallization was not extensive. Similarly, fractures are usually small (up to 25mm wide) and always filled. Two types of cement have been recognized, including; (1) subeuhedral blocky spar (> 200μm to < 1cm); and (2) euhedral to subeuhedral saddle dolomite (>300μm to < 500μm) (Figure 4.4E-F).

The near micritic crystal size and retention of the primary fabric might indicate that diagenesis and/or deformation did not greatly alter the original sediment. On the other hand, the presence of blocky spar and fracture filled-generations resemble cements
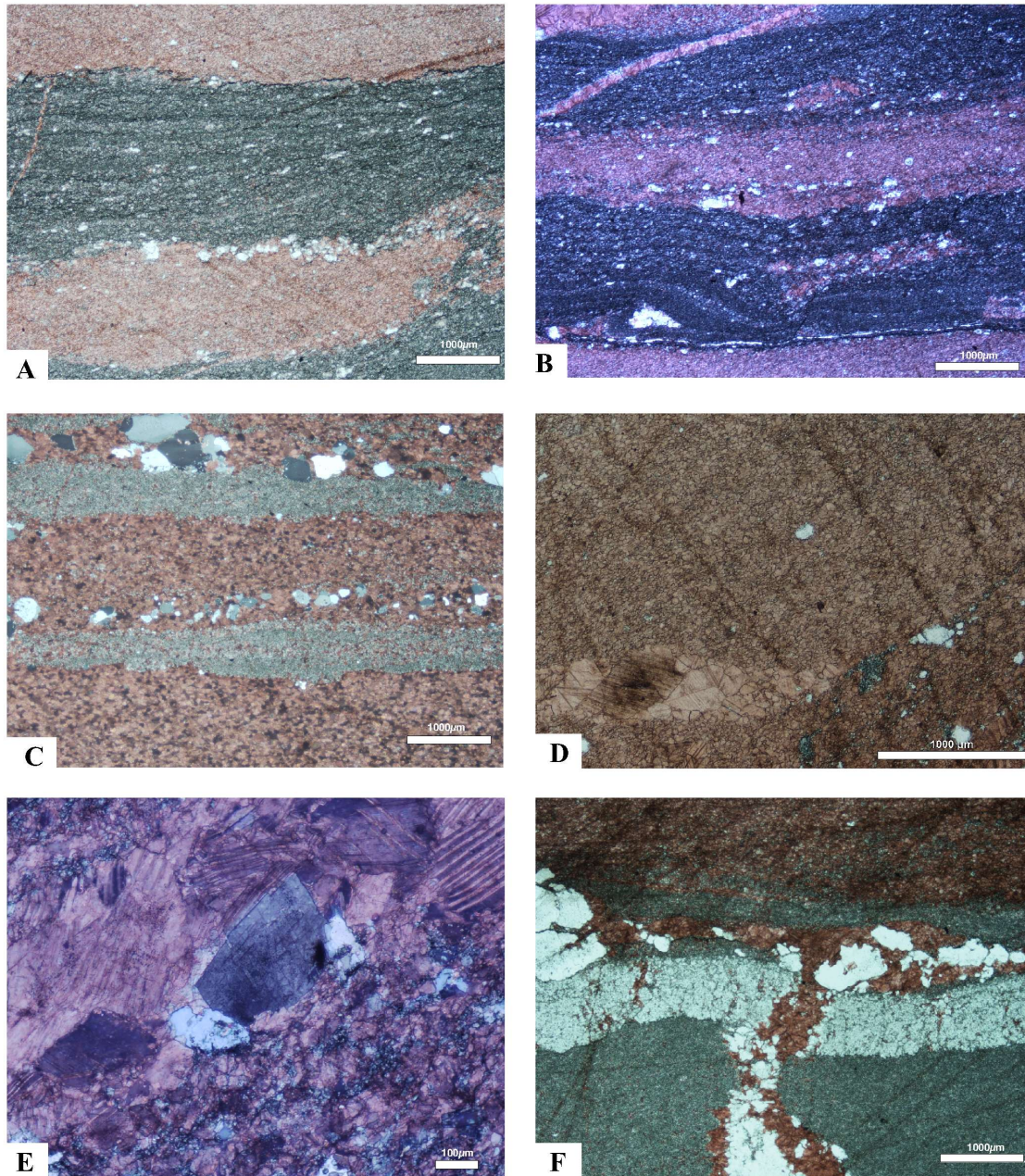
Figure 4.4. Thin section microphotographs for carbonate rocks of the Polanco Limestone Formation. Thinly laminated rythmithes showing the alternation of microspar laminae with finely laminated dolomicrospar **(A, B)**, and massive impure dolostone laminae **(C)**. Terrigenous quartz grains are common but never constitute more than the 5% of the rock **(A, B, C)**. Detail of fenestral fabric in microspar; blocky calcite occluding porosity **(D)**. Saddle dolomite occurs as a late diagenetic phase filling fractures and in intimate association with subeuhedral blocky spar **(E)**. Connection between chert formation and fracturing is possible. Silicification pulses were probably contemporaneous with cementation of fractures since both cements (calcite and chert) are filling-phases **(F)**.

of intermediate to deep burial stages. Therefore, the relative chronology of the diagenetic phases observed in the Polanco Limestone can be summarized as: (1) depositional and/or immediately post-depositional phases (micritic to microspar dolostones and limestones); and (2) burial phases (mechanical compaction-stylolitization-, blocky cementation of microfenestrae cavities, fracturing, and filling-fracture phases).

4.4.3. Carbonate geochemistry

4.4.3.1. Oxygen and carbon isotopes

Results of isotopic analyses on microdrilled carbonates are presented in Table 4.1 and are plotted relative to their stratigraphic position (Figure 4.5). The spread of δ^{13}C-values of dolomite and calcite at Los Tapes section is narrow (standard deviation $s_{dolomite}$ = ±0.8‰, $s_{calcite}$ = ±0.6‰). Carbon isotopic values of dolostones range between -2.7‰ and +0.2‰ (mean = -1.4‰), whereas limestone compositions are between -3.1‰ to -0.4‰ (mean = -1.9‰). The carbon isotope values of both limestones and dolostones show a relatively unimodal distribution, clustered around -1.5‰. At South Isla Patrulla section, δ^{13}C-values range between -1.9‰ and +2.0‰ (mean = +0.2‰; $s_{calcite}$ = ±1.3‰). Most of the δ^{18}O values of the Los Tapes limestones (-7.2 to -13.7‰, with a mean = -11.0 ±1.8‰) overlap the range of the dolostones (-6.2 to -12.3‰), with a mean = -8.6 ±2.2‰). The oxygen isotopes ratios of limestones in the shallow water facies (Recalde) reported by Gaucher et al. (2004) (-6.1 and -10.7‰; mean = -7.9 ±1.5‰) overlap the field of the deep facies limestones of Tapes and those form South Isla Patrulla section, whereas carbon values are much variable (from -3.3 to +5.3‰).

4.4.3.2. Trace elements

Table 4.1 summarizes the concentration and relationship of Mn and Sr in the Polanco Limestone Formation at the Los Tapes, South Isla Patrulla and Recalde sections. The

dolostones and limestones from Los Tapes have relatively low and constant Mn ($Mn_{dolostones}$ = 203 ±41 ppm; $Mn_{limestones}$ = 160 ±49 ppm) and Sr contents ($Sr_{dolostones}$ = 38 ±19 ppm; $Sr_{limestones}$ = 61 ±17 ppm). More variable are the Sr concentrations from the Recalde limestones (1542 ±868 ppm), corresponding to a narrow range of Mn contents ($Mn_{dolostones}$ = 85 ±41 ppm). South Isla Patrulla section show similar Mn (74 and 92 ppm) and Sr (538-619 ppm) values as those found in Recalde.

4.4.3.3. Strontium isotopes

The lowest and highest values in the South Isla Patrulla ($^{87}Sr/^{86}Sr$ = 0.70710 and 0.70728) and Recalde carbonates ($^{87}Sr/^{86}Sr$ = 0.70677 and 0.70791) are separated by an isotope ratio difference of <0.001142. Comparatively, Sr isotopic ratios from the Los Tapes section are significantly more elevated ($^{87}Sr/^{86}Sr$ = 0.72436 to 0.74823) (Table 4.1).
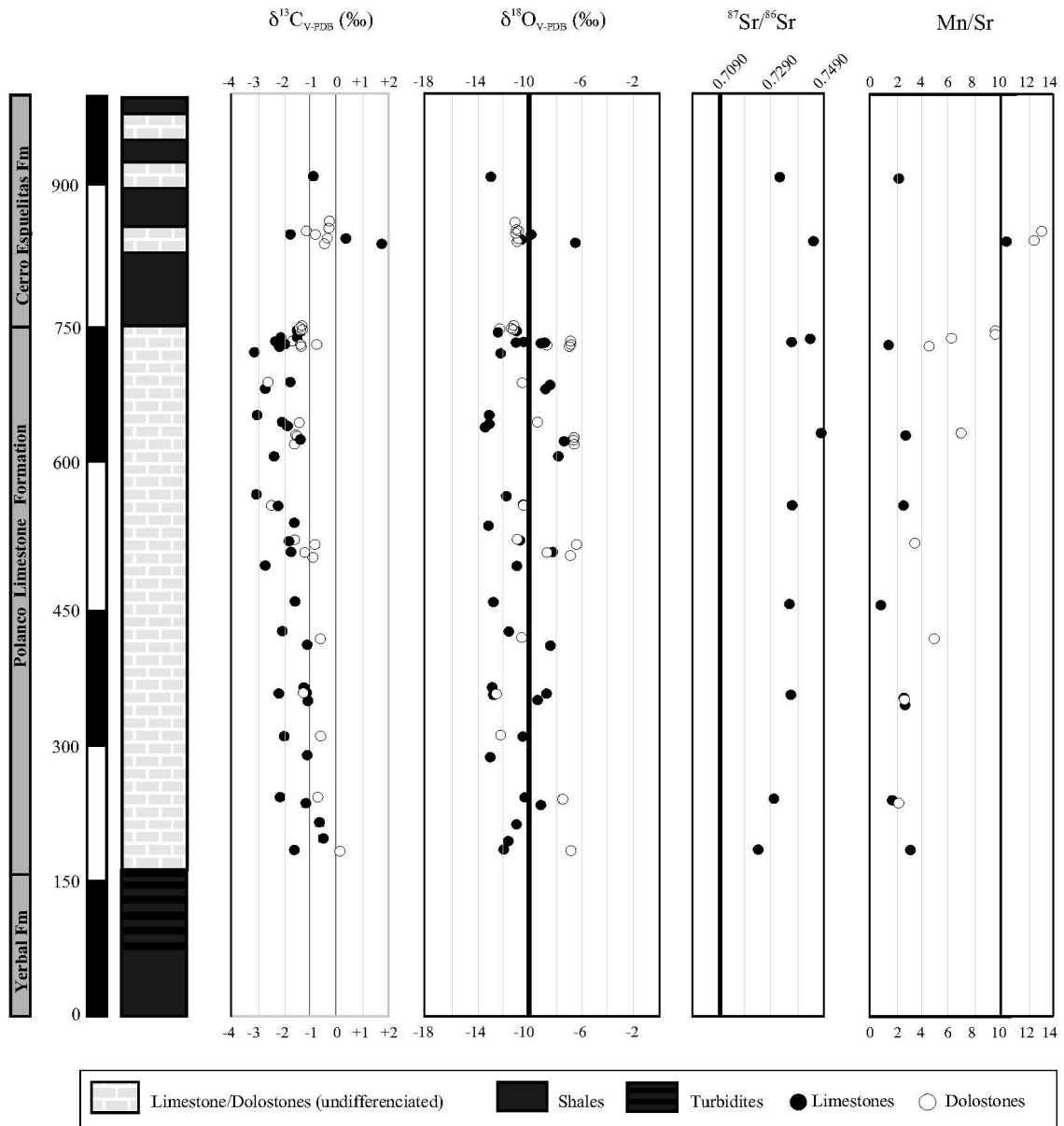
Figure 4.5. Schematic stratigraphic profile of the Polanco Limestones Formation at Los Tapes section and corresponding vertical distribution of δ^{13}C, δ^{18}O, ^{87}Sr/^{86}Sr, and Mn/Sr data.

Table 4.1. Oxygen, C, and Sr isotope ratios as well as trace element concentrations of carbonates from Polanco Limestone and Cerro Espuelitas formations.

Unit	Lithology	Sample	$\delta^{18}O_{PDB}$	$\delta^{13}C_{PBD}$	$\delta^{18}O_{SMOW}$	$^{87}Sr/^{86}Sr$	Mn/Sr	Mn	Sr	Al	K	Rb
Polanco Limestone Fm. (Los Tapes)	Limestone	060524/1	-11.969	-0.488	18.572							
Polanco Limestone Fm. (Los Tapes)	Limestone	060524/1	-12.005	-1.65	18.534	0.72436	3.4	216	63.1	5836	8545	14.6
Polanco Limestone Fm. (Los Tapes)	Limestone	060524/2	-10.93	-0.717	19.642							
Polanco Limestone Fm. (Los Tapes)	Limestone	060524/3	-9.25	-1.289	21.374							
Polanco Limestone Fm. (Los Tapes)	Limestone	060524/3	-10.133	-2.246	20.463	0.73083	1.9	148	79.7	4530	5546	9.08
Polanco Limestone Fm. (Los Tapes)	Limestone	060524/4	-13.512	-1.005	16.98							
Polanco Limestone Fm. (Los Tapes)	Limestone	060524/4	-10.288	-2.058	20.304							
Polanco Limestone Fm. (Los Tapes)	Limestone	060524/5	-12.869	-2.273	17.643							
Polanco Limestone Fm. (Los Tapes)	Limestone	060524/5	-9.795	-1.199	20.182							
Polanco Limestone Fm. (Los Tapes)	Limestone	060524/5	-8.86	-1.27	21.776	0.73701	2.4	139	59.0	6933	5240	14.9
Polanco Limestone Fm. (Los Tapes)	Limestone	060524/5	-12.902	-1.287	17.609		2.4	143	58.5	6909	5243	15.0
Polanco Limestone Fm. (Los Tapes)	Limestone	060524/6	-8.393	-1.283	22.258							
Polanco Limestone Fm. (Los Tapes)	Limestone	060524/6	-11.881	-2.146	18.661							
Polanco Limestone Fm. (Los Tapes)	Limestone	060524/7	-13.161	-1.567	17.342	0.73673	1.2	103	84.3	2239	1893	3.35
Polanco Limestone Fm. (Los Tapes)	Limestone	060524/7	-13.161	-1.567	17.342							
Polanco Limestone Fm. (Los Tapes)	Limestone	060524/8	-8.357	-1.815	22.294							
Polanco Limestone Fm. (Los Tapes)	Limestone	060524/8	-11.351	-2.813	19.208							
Polanco Limestone Fm. (Los Tapes)	Limestone	060524/9	-10.872	-1.908	19.702							
Polanco Limestone Fm. (Los Tapes)	Limestone	060524/10	-13.481	-1.697	17.013							
Polanco Limestone Fm. (Los Tapes)	Limestone	060524/11	-10.328	-2.408	20.263	0.73769	2.5	138	55.5	1494	1741	2.42
Polanco Limestone Fm. (Los Tapes)	Limestone	060524/11	-11.977	-3.079	18.563							
Polanco Limestone Fm. (Los Tapes)	Limestone	060524/12	-7.23	-1.622	23.457							
Polanco Limestone Fm. (Los Tapes)	Limestone	060524/12	-7.999	-2.47	22.664	0.74823						
Polanco Limestone Fm. (Los Tapes)	Limestone	060524/13	-13.079	-3.112	17.427							
Polanco Limestone Fm. (Los Tapes)	Limestone	060524/13	-13.676	-2.002	16.811							
Polanco Limestone Fm. (Los Tapes)	Limestone	060524/13	-13.745	-1.973	16.741							
Polanco Limestone Fm. (Los Tapes)	Limestone	060524/14	-8.299	-1.849	22.354							
Polanco Limestone Fm. (Los Tapes)	Limestone	060524/14	-8.622	-2.942	22.022							
Polanco Limestone Fm. (Los Tapes)	Limestone	060524/15	-12.003	-3.179	18.536							
Polanco Limestone Fm. (Los Tapes)	Limestone	060524/15	-9.58	-2.109	21.034							
Polanco Limestone Fm. (Los Tapes)	Limestone	060524/15	-9.58	-2.109	21.034							
Polanco Limestone Fm. (Los Tapes)	Limestone	060524/15	-9.319	-2.165	21.303							
Polanco Limestone Fm. (Los Tapes)	Limestone	060524/15	-11.099	-2.22	19.468							

Formation	Lithology	Sample										
Polanco Limestone Fm. (Los Tapes)	Limestone	060524/15	-10.105	-2.073	20.493	0.73645	1.6	140	87.0	3238	2682	4.62
Polanco Limestone Fm. (Los Tapes)	Limestone	060524/16				0.74361		256	36.1	15065.8	11735	24.9
Polanco Limestone Fm. (Los Tapes)	Limestone	060524/17	-11.315	-1.53	19.245							
Polanco Limestone Fm. (Los Tapes)	Limestone	060524/17	-12.391	-1.661	18.136							
Cerro Espueltas Formation (Los Tapes)	Limestone	060525/2	-6.405	1.856	24.307	0.74532	10.6	704	66.3	8206	4554	18.6
Cerro Espueltas Formation (Los Tapes)	Limestone	060525/2	-10.227	0.369	20.367							
Cerro Espueltas Formation (Los Tapes)	Limestone	060525/2	-9.999	-1.978	20.602							
Cerro Espueltas Formation (Los Tapes)	Limestone	060525/3	-13.194	-0.944	17.308	0.73100	2.2	249	112	2666	1597	9.60
Polanco Limestone Fm. (Los Tapes)	Dolostone	060524/1	-6.993	0.21	23.701							
Polanco Limestone Fm. (Los Tapes)	Dolostone	060524/3	-7.892	-0.773	22.774		2	161	80.9	4300	5407	8.90
Polanco Limestone Fm. (Los Tapes)	Dolostone	060524/4	-12.312	-0.695	18.217							
Polanco Limestone Fm. (Los Tapes)	Dolostone	060524/5	-12.349	-1.064	18.18		2.3	141	62.5	7476	6141	15.9
Polanco Limestone Fm. (Los Tapes)	Dolostone	060524/6	-10.245	-0.662	20.349		4.9	213	43.6	8204	6871	14.6
Polanco Limestone Fm. (Los Tapes)	Dolostone	060524/8	-7.19	-0.942	23.497							
Polanco Limestone Fm. (Los Tapes)	Dolostone	060524/8	-6.247	-0.915	24.469							
Polanco Limestone Fm. (Los Tapes)	Dolostone	060524/8	-8.59	-1.185	22.055							
Polanco Limestone Fm. (Los Tapes)	Dolostone	060524/9	-11.04	-1.869	19.529		3.2	120	38.1	32448	24590	50.2
Polanco Limestone Fm. (Los Tapes)	Dolostone	060524/11	-10.12	-2.462	20.477							
Polanco Limestone Fm. (Los Tapes)	Dolostone	060524/12	-6.862	-1.591	23.836		6.9	216	31.3	6945	5936	12.6
Polanco Limestone Fm. (Los Tapes)	Dolostone	060524/12	-6.736	-1.613	23.965							
Polanco Limestone Fm. (Los Tapes)	Dolostone	060524/12	-6.674	-1.536	24.03							
Polanco Limestone Fm. (Los Tapes)	Dolostone	060524/13	-9.884	-1.469	20.72							
Polanco Limestone Fm. (Los Tapes)	Dolostone	060524/14	-10.398	-2.715	20.19							
Polanco Limestone Fm. (Los Tapes)	Dolostone	060524/15	-8.411	-1.399	22.239		4.6	249	53.7	6896	5729	8.31
Polanco Limestone Fm. (Los Tapes)	Dolostone	060524/15	-7.246	-1.343	23.44							
Polanco Limestone Fm. (Los Tapes)	Dolostone	060524/15b	-6.638	0.835	24.067							
Polanco Limestone Fm. (Los Tapes)	Dolostone	060524/16	-6.544	-1.776	n		6.2	228	36.6	14049	11199	25.4
Polanco Limestone Fm. (Los Tapes)	Dolostone	060524/17	-11.469	-1.519	19.086		9.6	202	21.1	44653	28517	83.0
Polanco Limestone Fm. (Los Tapes)	Dolostone	060524/17	-12.123	-1.544	18.412		9.7	203	20.9	44647	28892	82.8
Polanco Limestone Fm. (Los Tapes)	Dolostone	060524/17	-11.677	-1.414	18.872							
Polanco Limestone Fm. (Los Tapes)	Dolostone	060524/17	-11.315	-1.53	19.245							
Cerro Espueltas Fm. (Los Tapes)	Dolostone	060525/2	-11.053	-0.489	19.515							
Cerro Espueltas Fm. (Los Tapes)	Dolostone	060525/2	-10.884	-0.247	19.689		12.2	616	50.4	20590	9880	42.9
Cerro Espueltas Fm. (Los Tapes)	Dolostone	060525/2	-11.058	-0.881	19.511							
Cerro Espueltas Fm. (Los Tapes)	Dolostone	060525/2	-10.686	-1.207	19.893							

Formation	Rock type	Sample										
Cerro Espueltas Fm. (Los Tapes)	Dolostone	060525/2	-10.884	-0.247	19.689		13.2	655	49.6	21392	10246	44.8
Cerro Espueltas Fm. (Los Tapes)	Dolostone	060525/2	-10.704	-0.143	19.875							
Cerro Espueltas Fm. (Los Tapes)	Dolostone	060525/3	-9.534	-0.349	21.082							
Polanco Lmestone Fm (South Isla Patrulla)	Limestone	060526/1	-6.92	-1.65	23.78							
Polanco Lmestone Fm (South Isla Patrulla)	Limestone	060526/2	-8.97	-1.71	21.66							
Polanco Lmestone Fm (South Isla Patrulla)	Limestone	060526/3	-7.89	-1.18	22.77							
Polanco Lmestone Fm (South Isla Patrulla)	Limestone	060526/4	-9.12	-1.23	21.51	0.70710	0.17		91.5	538.24	6113	2875	11.22
Polanco Lmestone Fm (South Isla Patrulla)	Limestone	060526/5	-9.9	-0.56	20.71							
Polanco Lmestone Fm (South Isla Patrulla)	Limestone	060526/6	-8.95	-1.86	21.68							
Polanco Lmestone Fm (South Isla Patrulla)	Limestone	060526/7	-11.34	0.2	19.22							
Polanco Lmestone Fm (South Isla Patrulla)	Limestone	060526/8	-8.65	1.98	22							
Polanco Lmestone Fm (South Isla Patrulla)	Limestone	060526/9	-10.06	0.32	20.54							
Polanco Lmestone Fm (South Isla Patrulla)	Limestone	060526/10	-9.9	0.29	20.71							
Polanco Lmestone Fm (South Isla Patrulla)	Limestone	060526/11	-8.18	0.2	18.24							
Polanco Lmestone Fm (South Isla Patrulla)	Limestone	060526/12	-11.14	0.12	19.42							
Polanco Lmestone Fm (South Isla Patrulla)	Limestone	060526/13	-8.83	1.19	21.81							
Polanco Lmestone Fm (South Isla Patrulla)	Limestone	060526/14	-10.51	1.27	20.07	0.70728	0.12		74.3	619.33	5825	4078	7.2
Polanco Lmestone Fm (South Isla Patrulla)	Limestone	060526/15	-9.33	1.4	21.29							
Polanco Lmestone Fm (South Isla Patrulla)	Limestone	060526/16	-7.87	1.68	22.79							
Polanco Lmestone Fm (South Isla Patrulla)	Limestone	060526/17	-7.906	1.89	22.76							
Polanco Limestone Fm. (Recalde)	Limestone	CDC 1A				0.70791	0.04		37.9	933.3	2213	1732	2.26
Polanco Limestone Fm. (Recalde)	Limestone	CDC 1B					0.25		138.0	544.31	6338	4878	13.7
Polanco Limestone Fm. (Recalde)	Limestone	CDC 1C				0.70722	0.01		36.6	2724.3	1631	2480	3.36
Polanco Limestone Fm. (Recalde)	Limestone	CDC 1F				0.70677	0.06		85.8	1541.9	582	1058	1.00
Polanco Limestone Fm. (Recalde)	Limestone	CDC 2B				0.70723	0.06		125.0	2241.3	2195	3841	10.5
Polanco Limestone Fm. (Recalde)	Limestone	CDC 2B (2)					0.06		126.0	2203.5	2217	3848	10.5
Polanco Limestone Fm. (Recalde)	Limestone	CDC 2D				0.70708	0.13		80.5	626.73	6424	2715	9.39

4.5. DISCUSSION

4.5.1. Diagenetic alteration of carbonate carbon, oxygen and strontium isotope composition

A crucial question in any study of carbon isotope chemostratigraphy is whether a primary marine signature is preserved. One traditional screening method for evaluating the effects of diagenesis on primary carbon isotope signatures is a comparison of relative trace element abundances (e.g., Brand and Veizer, 1980). For Proterozoic carbonates, different mean abundance ratios and combinations of trace elements and isotopic data are used but, in any case, the choice of the elemental ratios and their values is empirical and has to be evaluated considering the depositional and diagenetic context (Melezhik et al., 2001). The Mn/Sr ratio has been regarded as a reliable indicator for assessing post-depositional alterations of $\delta^{13}C$. During diagenesis, an enrichment in Mn concentrations is accompanied by a depletion of Sr, which increases the overall Mn/Sr ratio (e.g., Brand and Veizer, 1980; Banner and Hanson, 1990). Carbonates with Mn/Sr ratios lower than 3.0 are considered to be well-preserved (e.g., Derry et al. 1992; Kaufman et al. 1993), as are ratios up to 10.0 (Kaufman and Knoll, 1995), while intermediate values suggest secondary alteration (Kaufman and Knoll, 1995).

Strontium concentrations are uniformly distributed across the entire Los Tapes section (Figure 4.5) and comparatively lower and more homogeneous than those found in South Isla Patrulla and Recalde areas (see Table 4.1). The low Sr values recorded in the Los Tapes section, however, are not accompanied by an increase in the Mn concentration, which suggests that Mn was not severely affected during diagenesis. The Mn/Sr ratios of limestones, although lower, are within the range of those displayed by the dolostones. This difference may be explained by a better fitting of Sr in the crystal lattice of calcite (Veizer, 1983), and does not necessarily imply distinct alteration processes. Limestones exhibiting Mn/Sr values slightly higher than 3.0 might reflect some alteration, however, the consistency shown by $\delta^{13}C$ signatures between closely-spaced samples with variable Mn/Sr values support a near primary signature. Comparatively, Mn/Sr values in the Recalde and South Isla Patrulla areas are <0.25 (see Table 4.1). This variability in Mn/Sr

ratios at different sections may be explained by a better preservation of the primary Sr abundances (i.e., in Recalde and South Isla Patrulla areas). Additionally, the common presence of dolomite in samples from Los Tapes would increase the overall Mn/Sr ratios of the rhythmites because Mn can replace Mg during either precipitation of primary dolomite or dolomitization (Vasconcelos and McKenzie, 1997; Brand and Veizer, 1980; Fairchild et al., 1990). Importantly, the lack of correlation in the Mn/Sr vs. $\delta^{13}C$ (or $\delta^{18}O$) and $\delta^{13}C$ vs. Mn (or Sr) plots suggests that carbon isotopic values from both Los Tapes and Recalde sections were not strongly influenced by post-depositional alteration (Figure 4.6). Therefore, the measured $\delta^{13}C$ ratios most likely reflect contemporaneous ocean water composition.

$\delta^{18}O$ signature is another sensitive marker of diagenetic alteration and indicates the degree of interaction between carbonates and post-depositional fluids (Jacobsen and Kaufman, 1999). Most of the $\delta^{18}O$ values are around -10‰, which suggest diagenetic resetting of the primary signal. Comparatively, $\delta^{18}O$ signatures of the dolostones at Los Tapes section are slightly enriched respect to coexisting limestones (Figure 4.5). In this sense, the smaller grain size and the resulting lower permeability of dolostones might have contributed to a better preservation (Choquette and James, 1988; Pelechaty, 1998). Many of the limestone and dolostone samples display values below the -10‰ cut-off for "least-altered" carbonates (Kaufman and Knoll, 1995) but their $\delta^{13}C$ signatures are similar to those with $\delta^{18}O > -10‰$ (Table 4.1).
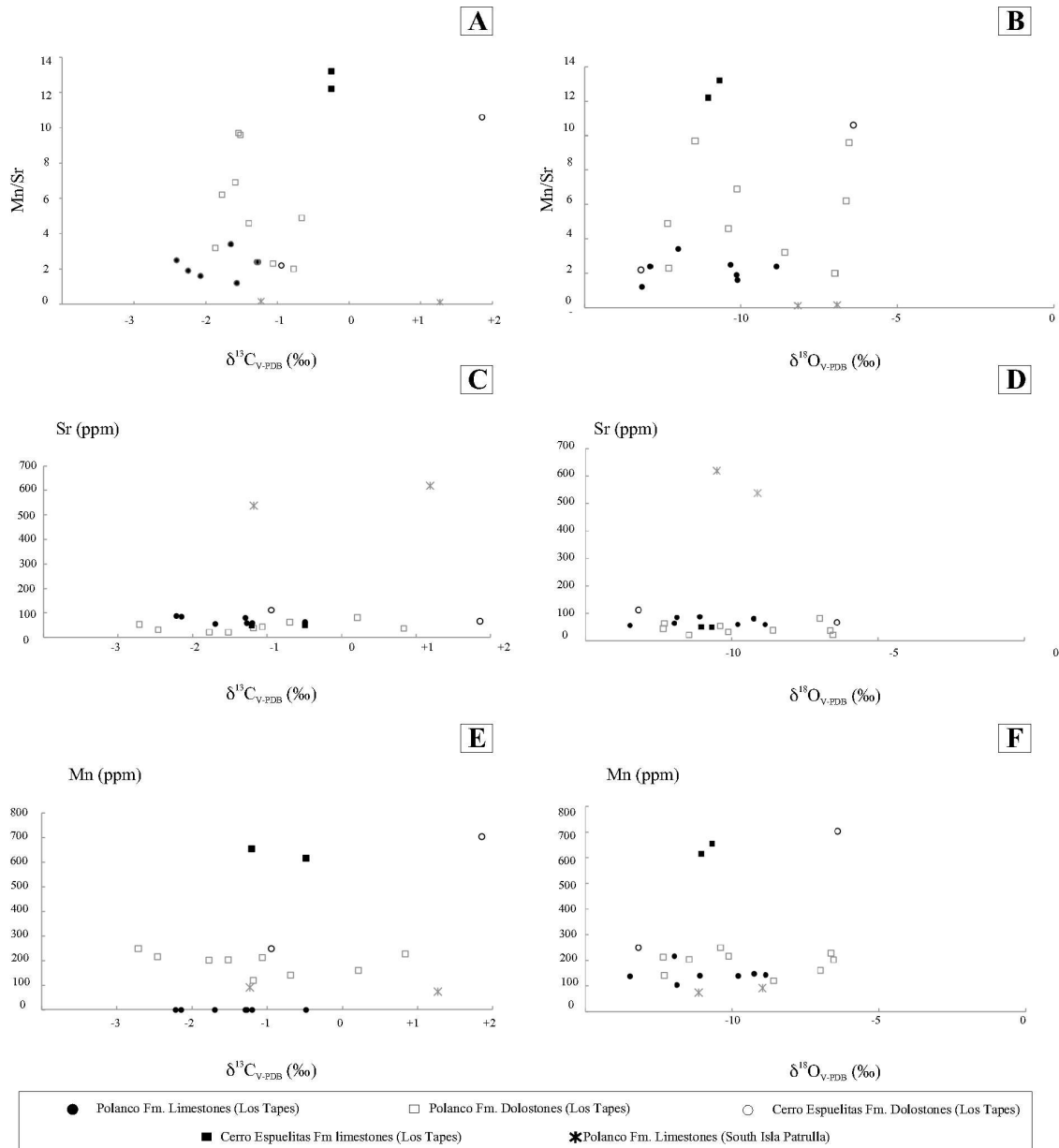
Figure 4.6. Scatter diagrams for the Polanco Limestone Formation and the overlying Cerro Espuelitas Formation at Los Tapes and South Isla Patrulla sections (A) Mn/Sr vs $\delta^{13}C$, (B) Mn/Sr vs $\delta^{18}O$, (C) Sr vs $\delta^{13}C$, (D) Sr vs $\delta^{18}O$, (E) Mn vs $\delta^{13}C$, and (F) Mn/Sr vs $\delta^{18}O$.
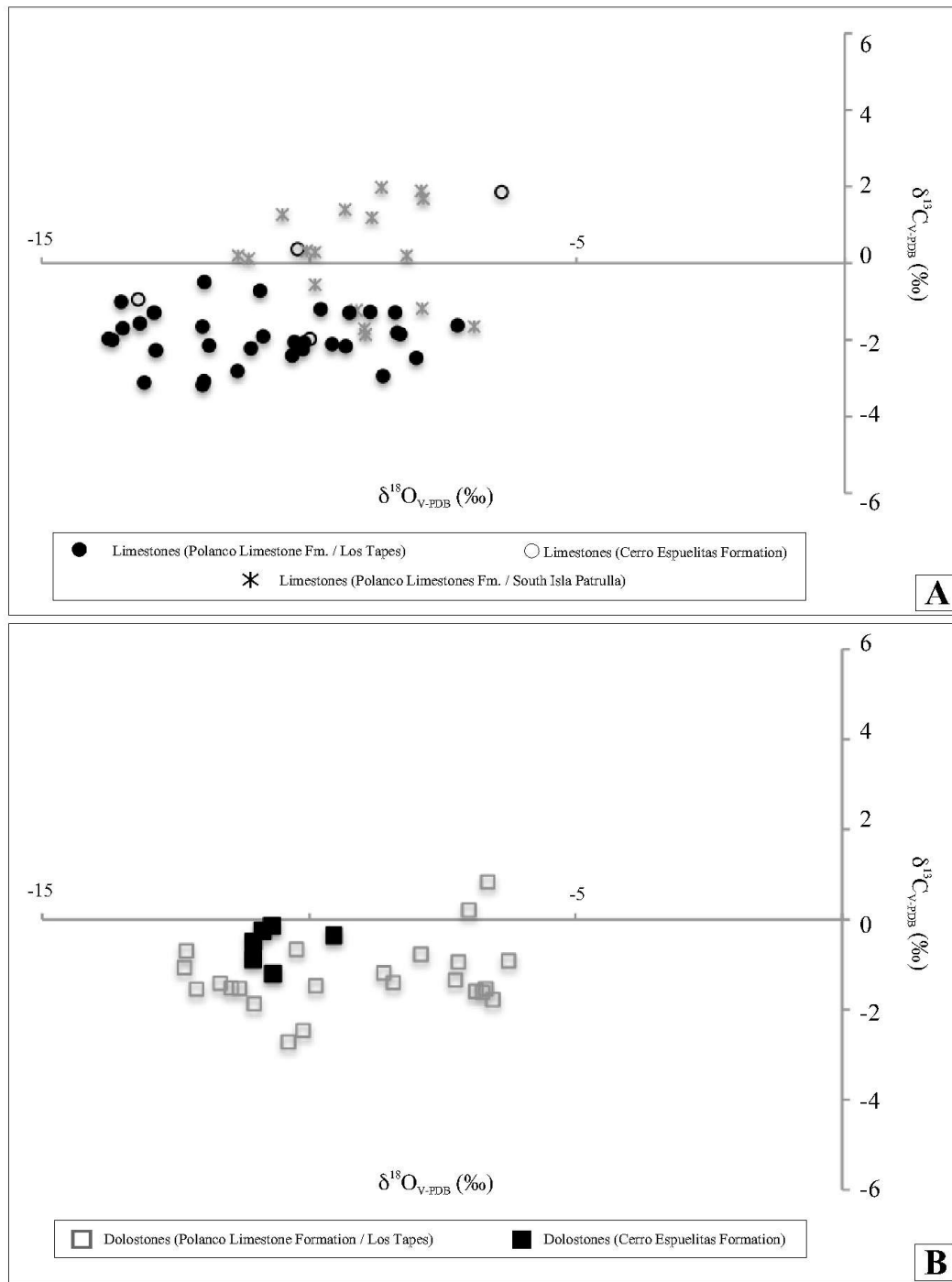
Figure 4.7. $\delta^{18}O$-$\delta^{13}C_{carb}$ cross plot of carbonates from Polanco Limestone Formation, and the overlying Cerro Espuelitas Formation at Los Tapes and South Isla Patrulla profiles. The R^2 coefficient of determination for the $\delta^{18}O$ and $\delta^{13}C_{carb}$ values for the limestones (A) and dolostones (B) are lower than 0.01 indicating no clear correlation between the isotopic dataset.

Furthermore, the lack of correlation between $\delta^{18}O$ and $\delta^{13}C$ supports the idea of an oxygen isotopic exchange without affecting the $\delta^{13}C$ values (Figure 4.7).

Overprinting of primary $^{87}Sr/^{86}Sr$ compositions may result from the addition of external sourced Sr (e.g., Montañez et al., 1996; Sawaki et al., 2008). Indeed, the elevated Sr radiogenic compositions of the limestones at Los Tapes section may be explained in terms of: (1) carbonate precipitation from fluids with elevated $^{87}Sr/^{86}Sr$ ratios, (2) addition of radiogenic Sr after precipitation via siliciclastic input and/or extrabasinal fluids. Average $^{87}Sr/^{86}Sr$ ratios as high as 0.7120 are typical of fluids originated from chemical weathering of the continental crust and its sedimentary cover (Palmer and Edmond, 1989; Peucker-Eherenbrink and Miller, 2006). This value, however, is significantly lower than those found in samples from Los Tapes, ranging from 0.72436 to 0.74823, and does not support a common origin. The slight covariance between $^{87}Sr/^{86}Sr$ values and lithophile elements (e.g., Al, K, Rb) indicates that siliciclastic material contributed to the overall strontium budget (Figure 4.8). However, when samples from Recalde, South Isla Patrulla and Los Tapes are compared, the former shows considerably higher Al values but low $^{87}Sr/^{86}Sr$ ratios. This suggests that siliciclastic material affected the final $^{87}Sr/^{86}Sr$ signatures from Los Tapes but it does not explain the considerably elevated $^{87}Sr/^{86}Sr$ values. Alternatively, highly elevated $^{87}Sr/^{86}Sr$ ratios may indicate injection of fluids from a basin-external source during burial derived from the metasedimentary basement or other siliciclastic Ediacaran strata. Hence, the $^{87}Sr/^{86}Sr$ signature from Los Tapes is not suitable for attempting chemostratigraphic constraints. In turn, the totality of samples from the Recalde area do not evidence correlation of $^{87}Sr/^{86}Sr$ vs. $\delta^{13}C$, Mn/Sr or Sr, which indicate preservation of depositional Sr isotopic values (Figure 4.9).
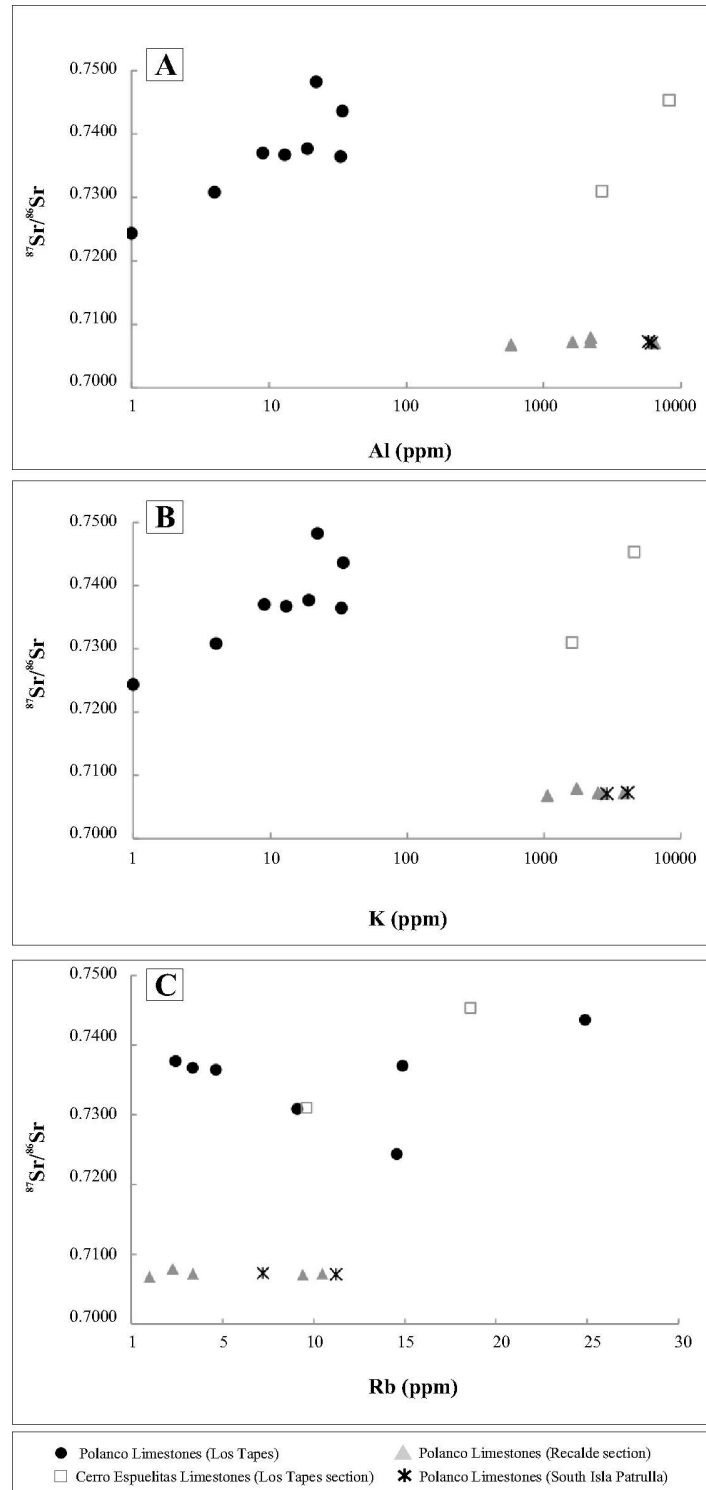
Figure 4.8. Isotopic and elemental cross-plots of $^{87}Sr/^{86}Sr$ ratios and Al, K and Rb contents of limestones at Los Tapes, South Isla Patrulla and Recalde sections. (A) $^{87}Sr/^{86}Sr$ vs. Al (ppm). $R^2_{Tapes} = 0.49$, (B) $^{87}Sr/^{86}Sr$ vs. K (ppm). $R^2_{Tapes} = 0.49$, and (C) $^{87}Sr/^{86}Sr$ vs. Rb (ppm). $R^2_{Tapes} = 0.03$.
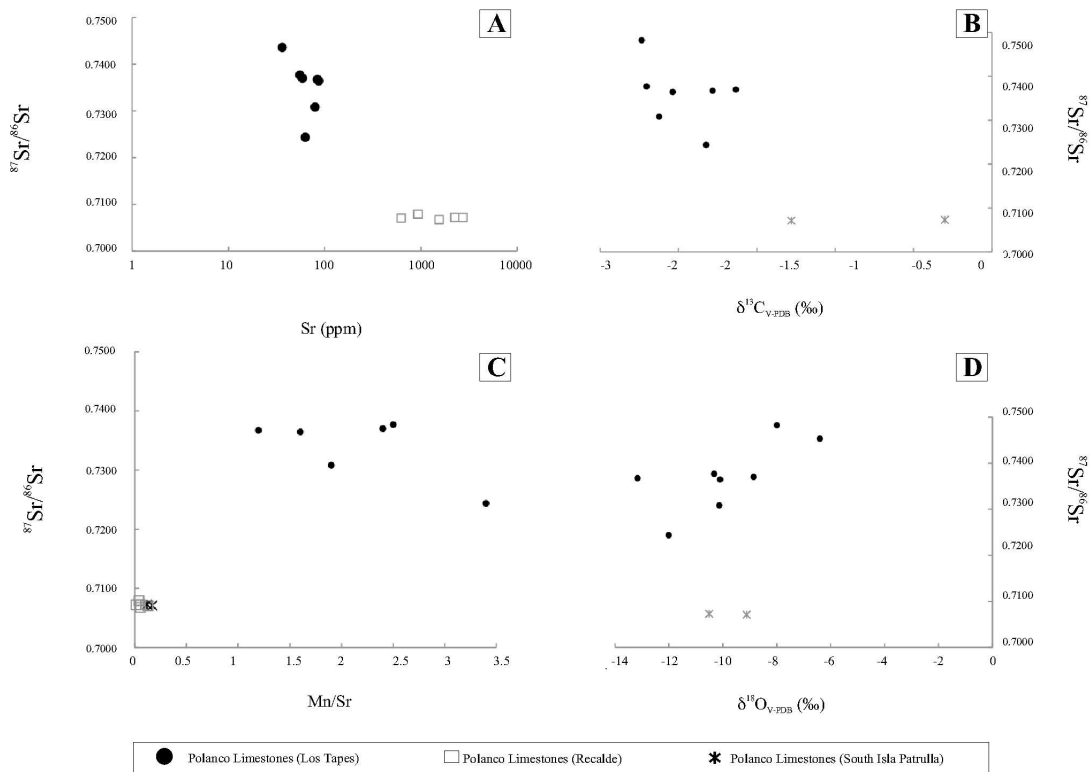
Figure 4.9. Scatter diagrams for limestones from Los Tapes, South Isla Patrulla and Recalde section. (A) $^{87}Sr/^{86}Sr$ vs. Sr (ppm). R^2_{Tapes} = 0.15, (B) $^{87}Sr/^{86}Sr$ vs. $\delta^{13}C$. R^2_{Tapes} = 0.16, (C) $^{87}Sr/^{86}Sr$ vs. Mn/Sr. R^2_{Tapes} = 0.31, and (D) $^{87}Sr/^{86}Sr$ vs. $\delta^{18}O$. R^2_{Tapes} = 0.49.

4.5.2. C- and Sr-isotope chemostratigraphy

Well preserved C- and Sr-isotope data obtained from marine carbonates have provided a detailed record of isotopic variation in seawater through time. Variations in the isotopic composition of carbon ($\delta^{13}C$) in seawater is specifically a useful indicator of biogeochemical changes over geological time, which in turn, is a function of the isotopic composition of carbon inputs to the ocean-atmosphere system, the average fractionation between dissolved inorganic carbon and organic matter, and the proportion of organic matter to carbonate buried in sediments (Kump and Arthur, 1999). By contrast, the $^{87}Sr/^{86}Sr$ of seawater tracks the balance between riverine inputs to the ocean, which result from continental weathering, and contributions from mantle sources through submarine hydrothermal systems (Goldstein and Jacobsen, 1987; Palmer and Edmond, 1989). Hence, the latter is considered a useful approach to trace global-scale changes in tectonics and climate over long timescales.

The dominant features of the carbon and strontium isotopic compositions of the Neoproterozoic-Cambrian seawater have long been recognized and reference curves of secular variations were recently produced by several authors (e.g., Jacobsen and Kaufman, 1999; Walter et al., 2000; Melezhik et al., 2001; Halverson et al., 2005; 2007). Characteristic features include, (i) high average $\delta^{13}C$ values ($\approx$5‰) during the Tonian and Cryogenian, punctuated by three negative $\delta^{13}C$ anomalies (Bitter Spring Stage, Sturtian and Marinoan glaciations), (ii) highly variable and on average low $\delta^{13}C$ values during the Ediacaran Period, including a distinct negative anomaly to values as low as -12‰ (Shuram-Wonoka-Johnie anomaly), and (iii) variable and average $\approx$0‰ values during the Cambrian, after a short-lived negative excursion at the Precambrian-Cambrian boundary (Halverson et al., 2007) (Figure 4.10A). In contrast, as depicted in Figure 4.10B, the general pattern in the $^{87}Sr/^{86}Sr$ record shows a progressive rise through most of the Neoproterozoic (Jacobsen and Kaufman, 1999; Walter et al., 2000; Thomas et al., 2004; Veizer and Shields, 2002; Halverson et al., 2007; Shields, 2007). However, under close scrutiny, some differences arise when comparing different compilations. Whilst some authors suggest a virtually monotonic rise with only minor shifts associated with glaciations (e.g., Halverson et al., 2007), others proposed a discrete "step increment" type

(e.g., Melezhik et al., 2001 and references therein). Overall, low $^{87}Sr/^{86}Sr$ values between 0.7054 and 0.7070 characterize the time span between 900 and 690 Ma, whereas an increase in $^{87}Sr/^{86}Sr$ from 0.7071 to 0.7086 occurs between 670 and 542 Ma, reaching values as high as 0.7095 in the Cambrian (Figure 4.10B).

As a whole, the carbon isotopic composition of the limestones and dolostones of the Polanco Limestone Formation is fairly uniform throughout Los Tapes section. With only one exception, all the values are systematically <0 and the trend reveals a gradual down shift from +0.2‰, at the base, up to -3‰ in the upper part of the section. Following the transitional values found at the South Isla Patrulla section (from -1.9‰ to +2‰), the Recalde area displays positive $\delta^{13}C$ values ranging from +2.5‰ to +5.3‰ occur in the lower part of the stratigraphic profile (Figure 4.11). These values progressively shift to -3.3‰, defining a negative excursion, and return to positive values where they fluctuate between 0.7‰ and 2.8‰ and no obvious excursions are discernible. The high $^{87}Sr/^{86}Sr$ ratios (> 0.72436) of the limestones in Los Tapes section are consistent with them being altered to varying degrees during diagenesis. Limestones with the highest $^{87}Sr/^{86}Sr$ ratios also have much lower Sr contents and would reflect the Sr reservoir of the diagenetic fluid that appears to have affected the carbonates at this location. Accordingly, they cannot be used for Sr chemostratigraphy. In addition to the previously reported $^{87}Sr/^{86}Sr$ values, new calcite $^{87}Sr/^{86}Sr$ data for five limestones from the Recalde area and two from South Isla Patrulla are used to constrain the depositional age. The lowest measured $^{87}Sr/^{86}Sr$ ratio (0.70677) occurs below the main tempestitic interval and is from a limestone having 1541 ppm Sr, which is among the highest concentrations - but with the lowest content of lithophile elements (Figure 4.8). Furthermore, petrographic preservation is best, implying that $\delta^{13}C$ values, which are ca. +4‰ are probably closest to original.
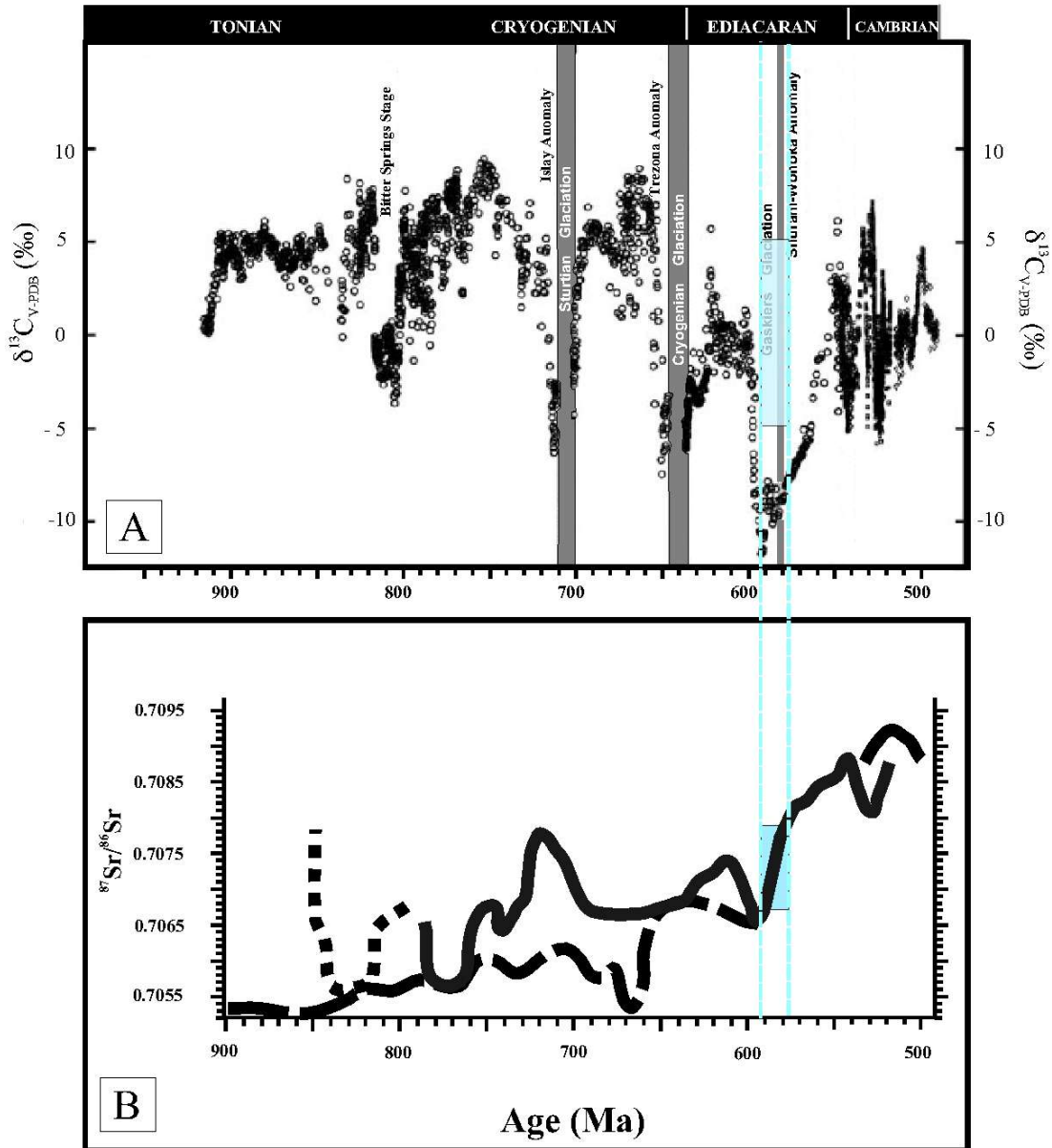
Figure 4.10. Temporal $\delta^{13}C_{carb}$ and $^{87}Sr/^{86}Sr$ evolution curves for the Neoproterozoic seawater according to Halverson et al. (2005) and Melezhik et al. (2001). Blue area in (B) corresponds to the range of $^{87}Sr/^{86}Sr$ values obtained in this work from Polanco Limestones at Recalde section, and the possible age for the Polanco Limestone Formation (see text for further discussion).

Figure 4.11. Comparison of carbon isotope profiles from deep to shallow water sections (database from Barriga Negra (parastratotye) and Recalde sections from Gaucher et al. 2004).

Following the schemes of Melezhik et al. (2001) and Halverson et al. (2007), the least altered radiogenic Sr isotopic value (0.70677), in combination with the range defined by the best preserved and the most positive $\delta^{13}C$ (~+4‰ to +5.3‰) reported by Gaucher et al. (2004), support and age of ca. 590-580 Ma for the middle Polanco Limestone Formation. This age is consistent with reported K/Ar age of ca. 580-600 Ma on diagenetic illite of the uppermost Yerbal Formation (Pecoits et al., *in press*). Additionally, the age of the Polanco Limestone Formation can be constrained by the youngest detrital zircon ages (U-Pb) reported from the underlying Yerbal Formation (~664 Ma) and the overlying Barriga Negra Formation (~566 Ma) (Blanco et al., 2009). Further constraints are provided by the basement of the Arroyo del Soldado Group, which yield an age of 633 ±12 Ma (U-Pb SHRIMP) (Hartmann et al., 2002) and the intrusive Guazuambí granite dated at 532 ±11 Ma (Rb-Sr isochron age; Ro=0.70624) (Kawashita et al., 1999). The age assigned here to the Polanco Limestone Formation, however, is not coincident with the age proposed by previous workers (see below).

Based on palaeontological and chemostratigraphic data, Gaucher et al. (2009) assigned an age of ca. 570-535 Ma for the whole Arroyo del Soldado Group. Significantly, the occurrence of the mineralized metazoan *Cloudina* in the uppermost Yerbal Formation, which occurs characteristically between ca. 550 and 540 Ma (Grotzinger et al., 1995; Saylor et al., 1998; Martin et al., 2000; Knoll et al., 2004; Hua et al., 2005), would allow to constrain the maximum age of Polanco Limestone Formation to 550 Ma. In this regard, Gaucher et al. (2009) correlated the most negative C-isotope shift of this unit with those reported in Oman (Shurman Formation) and Australia (Wonoka Formation) at ca. 551 Ma, which are unrelated to glacial episodes (Condon et al., 2005 and references therein). A glacially related interpretation of the $\delta^{13}C$ drop in the Polanco Limestone Formation was suggested by the same authors when, in reality (see below), no glacial conditions has been associated with the Shuram-Wonoka-Johnie anomaly elsewhere (e.g. Cozzi et al., 2004). The new stable isotope data and radiometric ages presented herein, however, do not support the age originally suggested and most likely indicate an age of ca. 600-590 for the lower Polanco Limestone Formation. Hence, the occurrence of *Cloudina* in Uruguay is either the oldest reported worldwide (ca. 600

Ma), which seems highly improbable given a difference of ca. 50 Ma with the oldest recovered *Cloudina* (Hua et al., 2005), or its occurrence is questionable. In this sense, repeated in situ sampling of the *Cloudina* hosting lithologies did not yield any well preserved and unambiguous specimen. The same few specimens repeatedly illustrated by Gaucher (2000) and Gaucher et al. (2003; 2004; 2009) are poorly preserved and even the original carbonate shell was apparently dissolved and substituted by iron-oxides or silica. In the absence of further discoveries that confirm the presence of this specimen in the Yerbal and Polanco Limestone formations its occurrence must be regarded as equivocal. Finally, the new age proposed for the Polanco Limestone Formation carries important implications because the deposition of this unit would be concurrent with a major climatic event, known as Gaskiers glaciation, that took place at ca. 580 Ma (Bowring et al., 2003). Despite no glacial deposits have been recorded in the Arroyo del Soldado Group, the effects of the palaeo-oceanographic changes and their impact on the biosphere might be recorded in the Polanco Limestone Formation.

4.5.3. Palaeo-oceanographic significance of the C- and Sr-isotope record

As stated above, the long-term secular variation in the carbon isotope composition of marine carbonates ($\delta^{13}C_{carb}$) reflects the influence of several factors. Under steady-state conditions, however, positive excursion are likely driven by nutrient influx to the surface ocean or an increase in the burial efficiency of organic matter, whereas negative excursions result from either a loss of primary productivity or lower burial efficiency in sediments which ultimately result in decreased burial of organic matter (Halverson et al., 2009). Rapid carbon isotope excursions, typically negative, may occur under non-steady-state conditions and are most likely as a result of oxidation and input of massive volumes of ^{13}C-depleted from reduced reservoirs, such as sedimentary methane clathrates, labile organic matter, or dissolved organic carbon (Rothman et al., 2003).

Gaucher et al. (2004; 2009) proposed that the $\delta^{13}C$ negative excursion that occurs in the middle Polanco Limestone Formation was the results of a severe but non-global

glacial event and suggested that the following changes occurred concomitantly to the drop in $\delta^{13}C$: (1) sea-level drop of >50 m due to continental glaciation, (2) low $^{87}Sr/^{86}Sr$ values due to diminished chemical weathering and continental run-off, and (3) lower organic matter contents and diversity of organic-walled microfossils due to decreased plankton bioproductivity, reduction in the amount of organic matter exported to the sediments, and environmental stress leading to lower acritarch diversity. Although the overall model proposed by the authors may constitute one possible explanation, the suggestion of a glacial event coincident with the Shuram-Wonoka-Johnie anomaly, the primary nature of which is still disputed (e.g., Bristow and Kennedy, 2008; Derry, 2010), is problematic because no glacial deposits or glacially-influenced successions concurrent with this anomaly have been yet described (e.g., Cozzi et al., 2004). Furthermore, the three points of evidence supporting the model itself contains inconsistencies, as discussed below:

(1) A sea-level fall up to 100 m, as a consequence of glacial conditions, was proposed to explain the transition to the main tempestitic interval concurrent with the most negative $\delta^{13}C$ (Gaucher et al., 2004). This palaeo-bathymetric estimation is purely based on sedimentary structures (e.g., hummocky cross-stratification) and, although this approach is partially valid, do not consider other important aspects such as the slope-gradient of the ramp. Normally, the slope-gradient of ramps are smaller than 1°, although in some cases they can reach up to 2°, and have no slope break (Read, 1985; Burchette and Wright, 1992). This indicates that a sea-level fall of about only 10 m would expose ca. 20 to 50 km of the inner- and mid-ramp section. A major sea-level fall of 50 m (taken as the most conservative value) means that the whole ramp becomes exposed. Such conditions may be developed during lowstand system tracts and produce a regional subaerial unconformity due to the erosion of the ramp such as that described at the top of the unit by Pecoits et al. (*in press*), which represent the sequence boundary. Neither a subaerial unconformity nor low-stand conditions have been recorded in the Polanco Limestone Formation. Instead, highstand and falling stage system tracts, bounded below by a maximum flooding surface and above by a sequence boundary, characterized the ramp during this interval (Pecoits et al., *in press*).

(2) Gaucher and Poiré (2009; pp. 127-section 4.5.5.1) report $^{87}Sr/^{86}Sr$ ratios between 0.7073 and 0.7077 throughout the negative $\delta^{13}C$ excursion, as compared to $^{87}Sr/^{86}Sr$ ratios for underlying carbonates of 0.7080 to 0.7085. However, detailed resolution of the chemostratigraphy shows that the model is too simplistic. At the Recalde section, the lowermost Polanco Limestone Formation is characterized by values ranging from 0.7073 to 0.7085. However, up-section, in the lower part of the main tempestitic interval, a clear shift towards higher ratios is observed, wherein values as high as those recorded in the lowermost interval (0.7085) are found. The upper part of the main tempestitic interval is characterized by constant $^{87}Sr/^{86}Sr$ ratios between 0.7074 and 0.7077. Throughout the upper part of the section, values also remain relatively constant, between 0.7073 and 0.7083. Therefore, the claimed lowering of $^{87}Sr/^{86}Sr$ values due to diminished chemical weathering and continental run-off concurrent with the $\delta^{13}C$ drop is questionable. Furthermore, it seems unlikely that $^{87}Sr/^{86}Sr$ ratios should decline, due to the shutdown of the hydrologic cycle, during a non-global glacial event if, as stated by Gaucher et al. (2004), the Polanco Ramp was located at tropical latitudes at that time.

(3) Gaucher et al. (2004; 2009) hypothesized that glacial conditions would have produced an environmental stress leading to a decrease in plankton bioproductivity and ultimately, to a lower acritarch diversity and a reduction of the amount of organic matter exported to the sediments. However, the previous authors only measured the organic matter content of 14 samples throughout 1000 m of strata, and that data was determined semi-quantitatively from the amount of organic residue obtained by means of palynological maceration: no total organic content (TOC) analyses were performed. Homogenous micrites or dolomicrites with low organic carbon are, in fact, the preferred material for analyses in isotope stratigraphic studies (Kaufman et al., 1991; Kaufman and Knoll, 1995). The use of organic rich carbonates as those described by Gaucher et al. (2004; 2009) without any treatment for removal of organic material will certainly yield inconsistent results. Furthermore, negative carbon excursions in the middle Polanco carbonates do not fully correlate with a relative decrease of the organic matter (Gaucher et al., 2004, their Figure 6; Gaucher et al., 2009, their Figure 4.4.3). For example, the

nadir of $\delta^{13}C$ coincides with the maximum organic matter contents reported by the authors. In any case, low organic matter content in shallow water facies is a common feature that can be explained by oxidation processes, especially in storm-dominated environments where reworking of the marine sediment increases bottom oxygen in the system facilitating organic matter oxidation. Thus, post-depositional overprinting may alter the original productivity signature and the estimation of the marine carbon flux in the water system can be underestimated (Zonneveld et al., 2010). In terms of the organic-walled microfossils, their rather random distribution (or preservation) could also be facies controlled. Additionally, some of the organic-walled specimens described here have been regarded as possible contaminations and thus, their value as biostratigraphic and bioproductivity indicators would be irrelevant (e.g., Daners et al., 2006; Veroslavsky et al., 2008). Therefore, the model first proposed by Kaufman et al. (1997) and adopted by Gaucher et al. (2004) to explain that enhanced bioproductivity was the cause of CO_2 drawdown through enhanced ^{12}C-burial followed by global cooling and sea-level fall, and that led the authors to propose at least four cold periods during the upper Ediacaran is not supported by the available evidence in the Polanco Limestone Formation.

Intriguingly, however, is the origin of the negative carbon isotopic excursion in the main tempestitic interval and the positive shifts in deeper water facies at the Recalde section. Two alternative hypothesis are put forward: (1) organic carbon supplied from continents and, (2) oxidation of the dissolved organic carbon pool (DOC). Organic carbon enhancement in shallow water facies may be caused by riverine water input, especially during coastline progradation where fresh-water is discharge into what was the open marine environment. Despite the absence of vascular plants, it is widely accepted the existence of microbial communities on land during the late Precambrian, thus it is not unexpected that terrestrial biomass could have entered the oceans which support the hypothesis of carbon depletion in proximal facies due to bacterial activity on land (Horodyski and Knauth, 1994). Indeed, isotopically light inorganic carbon, from CO_2 released by organic respiration in soils (Kaufman et al., 2007), could produce the observed $\delta^{13}C$ negative excursions in the proximal tempestitic levels. Storm activity may also enhance the process by introducing terrestrial material to the marine system by

increasing runoff (Halfar et al., 2006), and consequently, export of terrigenous and dissolved organic carbon from rivers to the open oceanic pool will reduce the marine carbon signature. The presence of siliciclastic strata interbedded with limestones in the upper (Gaucher et al., 2004) and middle Polanco Limestone Formation, concurrent with the main tempestitic level (Pecoits et al., *in press*) support this hypothesis. Because fresh waters are also depleted in $\delta^{18}O$, calcites formed under their influence are lower in ^{18}O relative to sea water; therefore, lowering of ^{18}O ratios would be expected in shallow-water facies. Significantly, $\delta^{18}O$ signatures from the negative anomaly at Recalde section are amongst of the lowest oxygen isotopic vales of the entire profile (~50% are -8‰). Furthermore, if carbonates precipitated from mixing fluids, then their Sr isotopic composition must be higher than that of underlying carbonates. In this regard, the $^{87}Sr/^{86}Sr$ rise occurred at the base of the negative excursion gives support to this hypothesis. Therefore, the negative carbon isotopic shift recorded in the middle Polanco Limestone Formation may result, at least in part, from riverine input due to carbonate weathering with isotopically light carbon and/or introduction of labile organic matter.

On the other hand, the marked ^{13}C enrichment of Neoproterozoic limestones has been argued to reflect the development of a stratified ocean with a lower anoxic layer depleted in ^{13}C (Kaufman et al., 1991; Derry et al., 1992; Grotzinger and Knoll, 1995; Knoll et al., 1996). These authors hypothesized that intense ocean stratification, with a simultaneous buildup of alkalinity via sulphate reduction and $\delta^{13}C$ depletion in anoxic deep waters, might explain the recorded signatures (see also Canfield et al., 2007). This non-steady state process would transfer large volumes of deep water ^{13}C-depleted carbon to the much smaller volume of surface, shallow water, generating large negative $\delta^{13}C_{carb}$ excursions without necessarily shifting $\delta^{13}C_{org}$ since OM would have a much longer residence time in the ocean. By contrast, $\delta^{13}C_{carb}$ would be high at times when the DOC pool was growing (Rothman et al., 2003; Fike et al., 2006; McFadden et al., 2008). The stratified model predicts the enrichment of ^{13}C by biological productivity in shallow environments and the depletion in deep waters by downward flux and remineralisation of organic matter at depth (Knoll et al., 1986; Calver, 2000). In this regard, the $\delta^{13}C$-depth gradient between distal (Los Tapes section), transitional (South Isla Patrulla) and

shallower facies, as those recorded in the Recalde section (Figure 4.11), could be explained by the effect of a stratified ocean characterized by mixing between bottom and surface waters (Kaufman et al., 1991; Grotzinger and Knoll, 1995; Kennedy, 1996; Knoll et al., 1986; Calver, 2000; Shen et al., 2005). The relative contribution of carbon exchange, between surface and deep ocean waters, to the $\delta^{13}C$ signal depends on the water-column structure and depth, as well as on the rates of seawater circulation across the ocean (e.g., Calver, 2000). Under storm dominated conditions, we envisage that the removal of DOC from deep waters and its incorporation into the shallow ocean would provide the characteristic ^{13}C-depleted signature of the main tempestitic interval observed at the Recalde section. Enhanced sulfate reduction would also have provided additional ^{13}C-depleted carbon to the ocean (e.g., Jiang et al., 2007), although no evidence of sulfidic conditions has been recorded. Alternatively, if negative excursions of the carbon isotope profile are linked to short-term sea level falls, then reworking of buried organic matter during sea level fall could be interpreted as being responsible for returning isotopically light carbon to the marine carbon reservoir (e.g., Ruf et al., 2005). However, when more distal facies as those found right bellow the main tempestitic interval are analyzed their $\delta^{13}C$ signature record positive values and thus, this alternative lacks of the necessary support.

In summary, the available evidence suggests that $\delta^{13}C$ variations reflect bathymetric changes in a stratified basin. Whether these bathymetric changes and their associated $\delta^{13}C$ variations were produced by glacially-related conditions or the dynamic of the basin itself remains unresolved. In this regard, $\delta^{13}C_{org}$ data will help to clarify the source of the Polanco Limestone Formation organic matter, although limited by the multiple factors that may contribute to variability in $\delta^{13}C$ (Hayes et al., 1999).

4.6. CONCLUSIONS

Sedimentological, petrographic, geochemical and isotopic data were combined to constrain the depositional environment and age of the Polanco Limestone Formation as

well as to better understand the platform dynamics. By comparing chemostratigraphic profiles across the basin (i.e., shallow vs. deep water) this contribution shows that this type of integrated analysis may help to better interpret Precambrian carbonate system dynamics, especially those associated with major palaeo-climatic and palaeo-environmental events. The following conclusions can be drawn from this study:

Facies analysis indicates that the Polanco Limestone Formation was deposited in a storm-dominated homoclinal ramp, where inner, mid and outer ramp facies associations were recognized and described. Inner ramp facies association is characterized by coarsening- and thickening-upward regressive cycles of clacarenites representing upper, middle and lower shoreface environments deposited above the mean fair weather wave base in well-oxygenated waters. Mid ramp facies association is composed by alternations of calcisiltite rhythmites limestone-dolostone with occasional hummocky cross-stratified calcarenites and thin massive or parallel-stratified calcarenite beds. Outer ramp deposits comprise rhythmites limestone-dolostone and bedded dolostones deposited below the mean storm wave-base and under anoxic conditions.

Petrographic observations have allowed us to recognize two major diagenetic stages and their the relative chronology affecting depositional carbonates of the unit: (1) depositional and/or immediately post-depositional phases (micritic to microspar dolostones and limestones), and (2) burial phases (mechanical compaction-stylolitization, blocky cementation, fracturing, and filling-fracture phases).

Optical, textural and diverse geochemical proxies used here suggest that most of the studied samples do not evidence significant post-depositional alteration of the carbon isotopic composition and thus, these carbonates are regarded as recording near-primary seawater signatures and are of chemostratigraphic significance. Conversely, Sr-isotope compositions are more variable, reflecting the effects of diagenesis and probable leaching of clay detritus. In this regard, carbonates from South Isla Patrulla and Recalde sections are the only suitable for Sr chemostratigraphic considerations excluding those from Los Tapes section from further chemostratigraphic interpretations.

Strontium isotope data from the Polanco Limestone Formation exhibit values compatible with those of the global $^{87}Sr/^{86}Sr$ composite curve between 600 and 575 Ma. Carbon isotope data show values that match the global $\delta^{13}C$ composite curve from numerous Ediacaran sections worldwide where the most negative shift might be tentatively correlated to the ca. 590 Ma negative anomaly. This is supported by new K-Ar ages obtained from diagenetic illite of the underlying Yerbal Formation, which yielded ages ca. 584 Ma.

The age proposed for the Polanco Limestone Formation carries important implications because the deposition of this unit would be concurrent with a major climatic event (Gaskiers glaciation). The association between negative $\delta^{13}C$ excursions and glaciations in the Neoproterozoic is tempting and might account for the C-isotope signature recorded in the middle of the unit. However, the lack of a concurrent negative $\delta^{13}C$ excursion in deep water facies and the good correlation between $\delta^{13}C$ data and facies associations wherein outer ramp facies is characterized by $\delta^{13}C$ values showing a transition towards more positive values associated with mid and inner ramp facies, demands an alternative explanation. Two alternative hypothesis are put forward: (1) organic carbon supplied from continents and, (2) oxidation of the dissolved organic carbon pool. Whether these bathymetric changes and their associated $\delta^{13}C$ variations were produced and in which extent by glacially-related conditions or the dynamic of the basin itself remains unresolved.

4.7. REFERENCES

Azmy, K., Kaufman, A.J. Misi, A., Oliveira, T.F., 2006. Isotope stratigraphy of the Lapa Formation, São Francisco Basin, Brazil: implications for Late Neoproterozoic glacial events in South America. Precambrian Res. 149, 231-248.

Banner, J.L., Hanson, G.N., 1990. Calculation of simultaneous isotopic and trace element variations during water-rock interaction with application to carbonate diagenesis. Geochim. Cosmochim. Acta. 54, 3123-3137.

Blanco, G., Rajesh, H.M., Gaucher, C., Germs, G.J.B., Chemale Jr., F., 2009. Provenance of the Arroyo del Soldado Group (Ediacaran to Cambrian, Uruguay): Implications for the paleogeographic evolution of southwestern Gondwana. Precambrian Res. 171, 57-73.

Bowring, S.A., Myrow, P.M., Landing, E., Ramezani, J., Grotzinger, J.P., 2003. Geochronological constraints on terminal Neoproterozoic events and the rise of metazoans. Geophys. Res. Abstr. 5, 13219.

Brand, U., Veizer, J., 1980. Chemical diagenesis of a multi component carbonate system: 1. Trace elements. J. Sed. Petrol. 50, 1219-1236.

Bristow, T.F., Kennedy, M.J., 2008. Carbon isotope excursions and the oxidant budget of the Ediacaran atmosphere and ocean. Geology. 36, 863–866.

Burchette, T.P., Wright, V.P., 1992. Carbonate ramp depositional systems, Sedimentary Geol. 79, 3-57.

Calver, C., 2000. Isotope stratigraphy of the Ediacaran (Neoproterozoic III) of the Adelaide rift complex, Australia, and the overprint of water column stratification. Precambrian Res. 100, 121-150.

Canfield, D.E., Poulton, S.W., Knoll, A.H., Narbonne, G.M., Ross, G., Goldberg, T., Strauss, H., 2008. Ferruginous Conditions Dominated Later Neoproterozoic Deep-Water Chemistry. Science. 321, 949-952.

Canfield, D.E., Poulton, S.W., Narbonne, G.M., 2007. Late-Neoproterozoic Deep-Ocean Oxygenation and the Rise of Animal Life. Science. 315, 92-95.

Choquette, P.W. and James, N.P. 1988. Introduction, in: Paleokarst, edited by James, N.P. and Choquette, P.W. Springer-Verlag, pp. 1-21.

Condon, D., Zhu, M., Bowring, S., Wang, W., 2005. U-Pb ages from the Neoproterozoic Doushantuo Formation, China. Science. 308, 95-98.

Cozzi, A., Allen, P.A., Grotzinger, J.P., 2004. Understanding carbonate ramp dynamics using d13C profiles: examples from the Neoproterozoic Buah Formation of Oman. Terra Nova. 16, 62–67.

Daners, G., Veroslavsky, G., de Santa Ana, H., 2006. Novedoso registro de microfósiles orgánicos neoproterozoicos en sedimentitas glaciogéncias de Uruguay. In: Actas 9° Congreso de Paleontología, Córdoba (Argentina), pp. 35.

Derry, L.A., Kaufman, A.J., Jacobsen, S.B., 1992. Sedimentary cycling and environmental change in the Late Proterozoic: evidence from stable and radiogenic isotopes. Geochim. Cosmochim. Acta. 56, 1317-1329.

Derry, L.A., Keto, L.S., Jacobsen, S.B., Knoll, A.H., Swett, K., 1989. Strontium isotopic variations in Upper Proterozoic carbonates from Svalbard and East Greenland. Geochim. Cosmochim. Acta. 53, 2331-2339.

Derry, L.A., 2010. A burial diagenesis origin for the Ediacaran Shuram-Wonoka carbon. Earth Planet. Sci. Lett. 294, 152-162.

Fairchild, I.J., Marshall, J.D., Bertrand-Sarfati, J. 1990. Stratigraphic shifts in carbon isotopes from Proterozoic stromatolitic carbonates (Mauritania): influences of primary mineralogy and diagenesis. Amer. J. Sci. 290-A, 46-79.

Faure, G., Mensing, D., 2005. Isotopes—Principles and Applications, 3rd ed. Hoboken, NJ: J. Wiley & Sons.

Fike, D.A., Grotzinger, J.P., Pratt, L.M., Summons, R.E., 2006. Oxidation of the Ediacaran ocean. Nature. 444, 744-747.

Gaucher, C., 2000. Sedimentology, palaeontology and stratigraphy of the Arroyo del Soldado Group (Vendian to Cambrian, Uruguay). Beringeria, 26, 1-120.

Gaucher, C., Boggiani, P. Sprechmann, P., Sial, A.N., Fairchild, T., 2003. Integrated correlation of the Vendian to Cambrian Arroyo del Soldado and Corumba Groups

(Uruguay and Brazil): paleogeographic, paleoclimatic and paleobiologic implications. Precambrian Res. 120, 241–278.

Gaucher, C., Sial, A.N., Blanco, G., Sprechmann, P., 2004. Chemostratigraphy of the lower Arroyo del Soldado Group (Vendian, Uruguay) and paleoclimatic implications. Gond. Res. 7, 715–730.

Gaucher, C., Poiré, D., 2009. Biostratigraphy, in: Gaucher, C., Sial, A.N., Halverson, G.P., Frimmel, H.E. (Eds.), Neoproterozoic-Cambrian tectonics, global change and evolution: a focus on southwestern Gondwana. Dev. Precambrian Geol. Elsevier, Amsterdam, 16, pp. 103-114.

Gaucher, C., Sial, A.N., Poiré, D., Gómez-Peral, L., Ferreira, V.P., Pimentel, M.M., 2009. Chemostratigraphy, in: Gaucher, C., Sial, A.N., Halverson, G.P., Frimmel, H.E. (Eds.), Neoproterozoic-Cambrian tectonics, global change and evolution: a focus on southwestern Gondwana. Dev. Precambrian Geol. Elsevier, Amsterdam, 16, pp. 115-122.

Germs, G.J.B., 1972. New shelly fossils from Nama Group, South West Africa. Am. J. Sci. 272, 752–761.

Goldstein, S.J., Jacobsen, S.B., 1988. Nd and Sr isotopic systematics of river water suspended material: implications for crustal evolution. Earth Planet. Sci. Lett. 87, 249-265.

Grotzinger, J. P., Knoll, A. H., 1995. Anomalous marine carbonate precipitates: Is the Precambrian the key to the Permian? Palaios. 10, 578-596.

Grotzinger, J.P., Bowring, S.A., Saylor, B.Z., Kaufman, A.J., 1995. Biostratigraphic and geochronologic constraints on early animal evolution. Science. 270, 598-604.

Halfar, J., Godinez-Orta, L., Mutti, M., Valdez-Holguin, J.E., Borges, J.M. 2006. Carbonates calibrated against oceanographic parameters along a latitudinal transect in the Gulf of California, Mexico. Sedimentology. 53, 297-320.

Halverson, G.P., Dudas, F.O., Maloof, A.C., Bowring, S.A., 2007. Evolution of the $^{87}Sr/^{86}Sr$ composition of Neoproterozoic seawater. Palaeogeogr. Palaeoclimatol. Palaeoecol. 256, 103-129.

Halverson, G.P., Hoffman, P.F., Schrag, D.P., Maloof, A.C., Rice, A.H.N., 2005. Toward a Neoproterozoic composite carbon-isotope record. Geol. Soc. Am. Bull. 117, 1181-1207.

Halverson, G.P., Hurtgen, M.T., Porter, S.M., Collins, A.C., 2010. Neoproterozoic-Cambrian biogeochemical evolution, in: C. Gaucher, A.N. Sial, G.P. Halverson, and H. Frimmel (Eds.), Neoproterozoic-Cambrian tectonics, global change and evolution: a focus on southwestern Gondwana. Dev. Precambrian Geol., 16, Elsevier, pp. 351-356.

Hartmann, L.A., Santos, J.O., Bossi, J., Campal, N., Schipilov, A., Mac Naughton, N. J., 2002. Zircon and titanite U-Pb SHRIMP geochronology of Neoproterozoic felsic magmatism on the eastern border of the Rio de la Plata Craton, Uruguay. J. South Amer. Earth Sci. 15, 229-236.

Hayes, J.M., Strauss, H., Kaufman, A.J., 1999. The abundance of ^{13}C in marine organic matter and isotopic fractionation in the global biogeochemical cycle of carbon during the past 800 Ma. Chem. Geol. 161, 103-125.

Holmden, C., Creaser, R.A., Muehlenbachs, K., Leslie, S.A., Bergstrom, S.M., 1996. Isotopic and elemental systematics of Sr and Nd in 454 Ma biogenic apatites: implications for paleoseawater studies. Earth Planet. Sci. Lett. 142, 425-437.

Horodyski, R.J., Knauth, L.P., 1994. Life on Land in the Precambrian. Science. 263, 494-498.

Hua, H., Chen, Z., Yuan, X., Zhang, L. and Xiao, S., 2005. Skeletogenesis and asexual reproduction in the earliest biomineralizing animal Cloudina. Geology. 33, 277-280.

Jacobsen, S.B., Kaufman, A.J., 1999. The Sr, C and O isotopic evolution of Neoproterozoic seawater. Chem. Geol. 161, 37-57.

Jiang, G., Kaufman, A. J., Christie-Blick, N., Zhang, S., Wu, H., 2007. Carbon isotope variability across the Ediacaran Yangtzee platform in South China: Implications for a large surface-to-deep ocean gradient. Earth Planet. Sci. Lett. 261, 303-320.

Kaufman, A.J. Knoll, A.H., 1995. Neoproterozoic variations in the carbon isotopic composition of seawater: Stratigraphic and biogeochemical implications. Precambrian Res. 73, 27-49.

Kaufman, A.J., Hayes, J.M., Knoll, A.H., Germs, G.J.B., 1991. Isotopic compositions of carbonates and organic carbon from upper Proterozoic successions in Namibia: stratigraphic variation and the effects of diagenesis and metamorphism. Precambrian Res. 49, 301-327.

Kaufman, A.J., Jacobsen, S.B., Knoll, A.H., 1993. The Vendian record of Sr and C isotopic variations in seawater: Implications for tectonics and paleoclimate. Earth Planet. Sci. Lett. 120, 409-430.

Kaufman, A.J., Knoll, A.H., Narbonne, G.M., 1997. Isotopes, ice ages, and terminal Proterozoic Earth history. Proc. Natl. Acad. Sci. U. S. A. 94, 6600-6605.

Kaufman, A.J., Corsetti, F.A., Varni, M.A. 2007. The effect of rising atmospheric oxygen on carbon and sulfur isotope anomalies in the Neoproterozoic Johnnie Formation, Death Valley, USA. Chem. Geol. 237, 47-63.

Kawashita, K., Gaucher, C., Sprechmann, P., Teixeira, W., Victória, R., 1999. Preliminary chemostratigraphic insights on carbonate rocks from Nico Pérez Terrane (Uruguay), In: Actas II South American Symposium on Isotope Geology. Córdoba (Argentina), pp. 399-402.

Kennedy, M.J., 1996. Stratigraphy, sedimentology, and isotopic geochemistry of Australian Neoproterozoic postglacial cap dolostones: deglaciation, d13C excursions, and carbonate precipitation. J. Sed. Res. 66, 1050-1064.

Knoll, A.H., Hayes, J.M., Kaufman, A.J., Swett, K., Lambert, I.B., 1986. Secular variation in carbon isotope ratios from Upper Proterozoic successions of Svalbard and East Greenland. Nature. 321, 832-838.

Knoll, A.H., Walter, M.R., 1992. Latest Proterozoic stratigraphy and Earth history. Nature. 356, 673-678.

Knoll, A.H. Walter, M.R., Narbonne, G.M., Christie-Blick, N., 2004. A New Period for the geologic time scale. Science. 3005, 621-622.

Kump, L.R., Arthur, M.A., 1999. Interpreting carbon-isotope excursions: carbonates and organic matter. Chem. Geol. 161, 181-198.

Martin, M.W., Grazhdankin, D.V., Bowring, S.A., Evans, D.A.D., Fedonkin, M.A., Kirschvink, J.L., 2000. Age of Neoproterozoic bilatarian body and trace fossils, White Sea, Russia: implications for metazoan evolution. Science. 288, 841-845.

Martin, M.W., Grazhdankin, D.V., Bowring, S.A., Evans, D.A.D., Fedonkin, M.A., Kirschvink, J.L., 2000. Age ofNeoproterozoic bilatarian body and trace fossils, White Sea, Russia: implications for metazoan evolution. Science. 288, 841-845.

McCrea, J.M., 1950. On the isotopic chemistry of carbonates and a paleothermometer scale. J. Chem. Phys. 5, 48-51.

McFadden, K.A., Huang, J., Chu, X., Jiang, G., Kaufman, A.J., Zhou, C., Yuan, X., Xiao, S., 2008. Pulsed oxidation and biological evolution in Ediacaran Doushantuo Formation. Proc. Nat. Acad. Sci. U.S.A. 105, 3197-3202.

Melezhik, V.A., Gorokhov, I.M. Kuznetsov, A.B., Fallick, A.E., 2001. Chemostratigraphy of Neoproterozoic carbonates: implications for 'blind dating'. Terra Nova. 13, 1-11.

Montañez, I.P., Banner, J.L., Osleger, D.A., Borg, L.E., Bosserman, P.J., 1996. Integrated Sr isotope variations and sea-level history of Middle to Upper Cambrian platform

carbonates: Implications for the evolution of Cambrian seawater ^{87}Sr/^{86}Sr. Geology. 24, 917-920.

Oyhantçabal, P., Siegesmund, S., Wemmer, K., Frei, R., Layer, P., 2007. Post-collisional transition from calc-alkaline to alkaline magmatism during transcurrent deformation in the southernmost Dom Feliciano Belt (Braziliano–Pan-African, Uruguay). Lithos, 98, 141-159.

Palmer, M.R., Edmond, J.M., 1989. The strontium isotope budget of the modern ocean. Earth Planet. Sci. Lett. 92, 11-26.

Pecoits. E., Gingras, M., Aubet, N., Konhauser, K., 2008. Ediacaran in Uruguay: palaeoclimatic and palaeobiological implications. Sedimentology. 55, 689-719.

Pelechaty, S.M., 1998. Integrated chronostratigraphy of the Vendian system of Siberia: implications for a global stratigraphy. J. Geol. Soc. London. 155, 957-973.

Peucker-Ehrenbrink, B., Miller, M.W., 2006. Marine ^{87}Sr/^{86}Sr record mirrors the evolving upper continental crust, Geochim. Cosmochim. Acta, 70, A487.

Read, J.F., 1985. Carbonate platform facies models. Am. Assoc. Pet. Geol. Bull. 69, 1-21.

Rothman, D.H., Hayes, J.M., Summons, R.E., 2003. Dynamics of the Neoproterozoic carbon cycle. Proc. Nat. Acad. Sci. U.S.A. 100, 124-129.

Ruf, M., Elmar Link, E., Pross, J., Aigner, T., 2005. A multi-proxy study of deeper-water carbonates (Upper Jurassic, southern Germany): combining sedimentology, chemostratigraphy and palynofacies. Facies. 51, 327-349.

Sawaki, Y., Ohno, T., Fukushi, Y., Komiya, T., Ishikawa, T., Hirata, T., Maruyama, S., 2008. Sr isotope excursion across the Precambrian–Cambrian boundary in the Three Gorges area, South China. Gond. Res. 14, 134-147.

Saylor, B.Z., Kaufman, A.J., Grotzinger, J.P., Urban, F., 1998. A composite reference

section for terminal Proterozoic strata of southern Namibia. J. Sed. Res. 68, 1223-1235.

Shen, Y., Zhang, T., Hoffman, P. F., 2008. On the coevolution of Ediacaran oceans and animals. Proc. Nat. Acad. Sci. U.S.A. 105, 7376-7381.

Shields, G.A., 2007. A normalized seawater strontium isotope curve: possible implications for Neoproterozoic–Cambrian weathering rates and the further oxygenation of the Earth, Earth. 2, 35-42.

Shields, G., Veizer, J., 2002. Precambrian marine carbonate isotope database: version 1.1. Geochem. Geophys. Geosyst. 3.

Thomas, C.W., Graham, C.M., Ellam, R.M., Fallick, A.E., 2004. ^{87}Sr/^{86}Sr chemostratigraphy of Dalradian limestones of Scotland and Ireland: constraints on depositional ages and time scales. J. Geol. Soc. London. 161, 229-242.

Vasconcelos, C., McKenzie, J.A., 1997. Microbial mediation of modern dolomite precipitation and diagenesis under anoxic conditions (Lagoa Vermelha, Rio de Janeiro, Brazil). J. Sed. Res. 67, 378-390.

Veizer, J., 1983. Chemical diagenesis of carbonates: Theory and application of trace element technique, in: Arthur, M.A., Anderson, T.F., Kaplan, I.R., Veizer, J., Land, L.S. (Eds.), Stable Isotopes in Sedimentary Geology. Society of Economic Paleontologists and Mineralogists Short Course No. 10, Dallas, pp. 3-1 to 3-100.

Veroslavsky, G., de Santa Ana, H., Daners, G., 2006. Formación Tacuarí (Nov. Nom.): Litoestratigrafía, facies, ambiente, edad y significado geológico (Cerro Largo-Uruguay). Rev. Soc. Uru. Geol. 13, 23-35.

Walter, M.R., Veevers, J.J., Calver, C.R., Gorjan, P., Hill, A.C., 2000. Dating the 840–544 Ma Neoproterozoic interval by isotopes of strontium, carbon, and sulfur in seawater, and some interpretative models. Precambrian Res. 100, 371-433.

Zonneveld, K.A.F., Versteegh, G. J. M., Kasten, V., Eglinton, T. I., Emeis, K.-C., Huguet, C. , Koch, B. P. , de Lange, G. J. , de Leeuw, J. W., Middelburg, J. J., Mollenhauer, G. , Prahl, F. G. , Rethemeyer, J., Wakeham, S. G., 2010. Selective preservation of organic matter in marine environments; processes and impact on the sedimentary record. Biogeosciences. 7, 483-511.

CHAPTER 5: EDIACARAN IRON FORMATIONS: COMPELLING EVIDENCE FOR FERRUGINOUS LATE NEOPROTEROZOIC SEAWATER

5.1.INTRODUCTION

Having formed throughout much of the Precambrian, iron formations (IF) are widely and globally distributed in all major Archaean and Proterozoic terranes. Their deposition has been linked to outstanding compositional changes in the Earth's atmosphere and hydrosphere, and possibly the diversification of the biosphere. IF reached a maximum abundance between 2.7-2.4 billion years ago (Ga) and their demise, in the Mesoproterozoic (~1.8 Ga), has been related to widespread euxinic (sulfidic anoxic) conditions. After more than a billion years of euxinia, deep ocean waters turned ferruginous (iron rich anoxic) in the late Neoproterozoic in association with globally extensive glaciations, such as the Sturtian (middle-Cryogenian) and Marinoan (end-Cryogenian) (Halverson et al., 2010). Thereafter, IF disappear completely from the rock record. In this light, the recent discovery of Ediacaran IF in Uruguay (Pecoits et al., 2008 and references therein) is fortuitous as they may provide an unparalleled opportunity to elucidate the critical link between the Neoproterozoic chemical evolution of the oceans and atmosphere and the conditions surrounding the emergence of complex life.

Formerly coined by James (1954), the term 'iron formation' was defined as 'a chemical sediment typically thin-bedded or laminated, containing 15 percent or more iron of sedimentary origin, commonly but not necessarily containing layers of chert'. Although preserving the bedding as a distinctive attribute, most recent definitions consider the quantitative lower limit of iron content (≥ 15 wt%) arbitrary and restrictive (Klein, 2005). In this regard, based on purely descriptive grounds, IF have been subdivided in two lithological subtypes (I) banded iron formation or BIF ($\geq$ 2.0 Ga), and (II) granular iron formation or GIF (2.0-1.8 Ga), characterized by regular thin banding and granular components, respectively (Trendall, 2002). The younger Cryogenian IF occurrences (700-750 million years ago (Ma)), however, have been described as a

'special case' and radically different depositional models -to explain their appearance after a billion year hiatus- have been proposed (Beukes and Klein, 1992). Nonetheless, they have also been extensively used to understand the palaeoenvironmental conditions during their deposition. But, what really does make the Cryogenian iron formations so different and 'special' from other iron deposits?

The Cryogenian period (850 to 635 Ma) represents a time in Earth's history when significant environmental changes took place, including a pair of global glaciations ('Snowball Earth' events) that led to ocean stagnation and a build-up of dissolved ferrous iron. Then, as the ice melted and ocean circulation became re-established, the iron became oxidised and formed a suite of IF in the oxic zone of upwelling areas (e.g., Hoffman et al., 2004). Major deposits include the 755-730 Ma old Rapitan Group in northern Canada and the Urucum district in Brazil (Klein and Beukes, 1993; Klein and Ladeira, 2004), the 750-650 Ma Chuos Formation in Namibia (Breitkopf, 1988), and within the 750-700 Ma Adelaide Geosyncline of South Australia (Lottermoser and Ashley, 2000). Simultaneously, a transient, but intense greenhouse climate ensued, caused by enhanced weathering of the glacially eroded landscape, increased alkalinity and carbonate precipitation. This led to the rapid deposition of unusually ^{13}C-depleted, finely-laminated dolomicrites, known as cap carbonates, directly on top of the glacial debris. Following the snowball event, greater primary productivity by phytoplankton facilitated increased environmental oxygenation, and then, once the deep ocean waters no longer remained an immediate sink for oxygen, atmospheric O_2 fugacity finally began to climb towards its present values. Crucially, with bottom waters now oxic, large, metabolically active animals could diversify from shallow waters to pelagic sediments. This initially gave way to an enigmatic group of soft-bodied marine animals (e.g., annelids, coelenterates), the so-called Ediacaran faunas, that were preserved world-wide as impressions, casts, molds and tracks in rocks as old as 575 Ma (e.g., Narbonne, 2005).

Most recently, Canfield et al. (2008) proposed that even during the beginning of the Ediacaran period, and up to the end of the Gaskiers glaciation (635-580 Ma), anoxia remained widespread beneath the mixed layer of the oceans. The deeper waters were sometimes sulfidic, but for the most part, they were Fe(II)-enriched, much like the oceans

before 1.84 Ga (Poulton et al., 2004). Although these conditions would favour the widespread deposition of iron-rich sediments, the evidence supporting this model is based on the speciation of Fe in clastic sedimentary rocks and no iron formations associated with the Ediacaran -despite the plausibility for Fe(II)-enriched ocean waters- have been described. Crucially, IF have shown to retain geochemical and isotopic tracers of conditions and compositions in the ocean and atmosphere that existed at that time (e.g., Derry and Jacobsen, 1990; Bau and Möller, 1993; Bolhar et al., 2004). Their ultimate origin, however, remains highly controversial. Indeed, with few exceptions (Simonson, 1985; Krapež et al., 2003; Pickard et al., 2004) most of the published data on iron formations focuses on their geochemistry and mineralogy, but a poor understanding of the depositional environment.

In this work we describe the sedimentology, stratigraphy and geochemistry of Ediacaran IF -the youngest yet reported- and associated strata deposited after a period of severe glaciations and concurrent with the early evolution of animals. Specifically, we (i) provide detailed sedimentological descriptions and describe the IF within a sequence stratigraphic context, and (ii) analyze the geochemistry of these rocks and associated lithologies with a focus on rare earth elements (REE) and yttrium (Y) and redox sensitive elements. Further, we attempt to show that this methodology leads to a better understanding of how this succession evolved rather than the definition and description of rock units (i.e., the traditional lithostratigraphic approach). Therefore, the resulting palaeoenvironmental and chronostratigraphic framework offers a reliable perspective on the origin and significance of this young IF. Finally, these data are used for testing current models for Ediacaran seawater, and for suggesting a new model that involves suboxic conditions (below mean storm wave base) before and after the Gaskiers glaciation.

5.2. MATERIALS AND ANALYTICAL METHODS

The present study is based on fieldwork carried out at six sections, described in detail along a 250 km long transect. One hundred fifty polished thin sections, including the IF, were prepared and examined using reflected and transmitted light microscopy in order to ascertain the mineralogy and texture. X-Ray Diffraction analyses (n=175) were performed using a Rigaku Geigerflex Power Diffractometer with a Co tube and a graphite monochromator and routine search/match procedures of diffraction patterns using the JCPDS database. Whole-rock major and trace element geochemistry was determined by instrumental neutron activation analysis (INAA) and inductively coupled plasma (ICP) at Actlabs Ltd., Canada. Additional bulk, trace and rare earth elements were analyzed using a PerkinElmer Elan6000 Quad-ICPMS (quadrupole inductively coupled plasma mass spectrometer) following Na_2O_2 sintering digestion. Accuracy and precision of the analytical protocol is verified with the use of well-established international whole-rock standards. Secondary and backscattered electron images as well as elemental distribution maps were acquired using a JEOL Microprobe 8900. Unless specified otherwise, all the detailed analyses were performed at the University of Alberta, Department of Earth and Atmospheric Sciences.

In this study, normalized REY (rare earth elements + yttrium) data refers to Post Archean Average Shale (subscript PAAS, McLennan, 1989), C1 chondrite (subscript CN, Anders and Grevesse, 1989). Normalized REY anomalies will be quantified following the methods of Bau and Dulski (1996) and Bolhar et al. (2004), and are defined as follows: La/La* = La/(3Pr - 2Nd), Ce/Ce* = Ce/(2Pr - Nd), Pr/Pr* = Pr/(0.5Ce + 0.5Nd), Eu/Eu* = Eu/(0.67Sm + 0.33Tb), and Gd/Gd* = Gd/(0.33Sm + 0.67Tb). A value of 1 indicates that there is no anomaly, a value greater than 1 indicates positive anomaly, and a value less than 1 indicates negative anomaly. Relative abundances of Y can be assessed using the Y/Ho ratio and described by deviations of the measured Y/Ho ratio from the shale value (~28). Ratios higher or lower than shale would indicate anomalously high or low Y abundances relative to neighbouring REE.

5.3. GEOLOGICAL SETTING, LITHOSTRATIGRAPHY AND AGE

The Ediacaran successions of Uruguay were deposited prior to the final assembly of the West-Gondwana continent as part of the Neoproterozoic Brasiliano-Pan African orogenic belts developed on the craton's margins. The studied IF is hosted within a mixed carbonate-siliciclastic succession of marine origin (Arroyo del Soldado Group), which is well exposed over 300 km along the eastern border of the Río de la Plata Craton, covering an area of approximately 2400 km^2 (Figure 5.1A-B). The group reaches up to 3 km in thickness, and has been subdivided into four mappable units: Yerbal, Polanco Limestone, Cerro Espuelitas and Barriga Negra formations (Pecoits et al., 2008) that record deep- to shallow-water marine environments developed during a single transgression-regression-transgression cycle with minor superimposed higher-frequency cycles (Figure 5.1C).

The basal Yerbal Formation consists of a fining- and thinning-upward succession with a maximum recorded thickness of 900 m. It contains interbedded mudstones and sandstones with minor contributions of carbonates, cherts and IF. The overlying Polanco Limestone Formation is a coarsening-upward succession, with minor higher-frequency coarsening-upward cycles. Typical lithologies include pure dark grey limestones and dolostones rhythmically interbedded (m to mm-scale) and rare chert layers. Being bracketed between siliciclastic units, the succession thickens from less than 75 m to a maximum of more than 900 m. The Barriga Negra Formation is restricted to the basin margin where it unconformably overlies the Polanco Limestone Formation as a consequence of the development of alluvial fans. The unit is characterized by thick conglomerates, carbonate-breccias, sandstones and mudstones, which gradually pass into the Cerro Espuelitas Formation. The latter consists of an alternation of siltstones, black- and iron-rich shales and cherts with minor occurrences of sandstones and carbonates. In deeper parts of the basin, it overlies the Polanco Limestone Formation and reaches a thickness of more than 550 m.
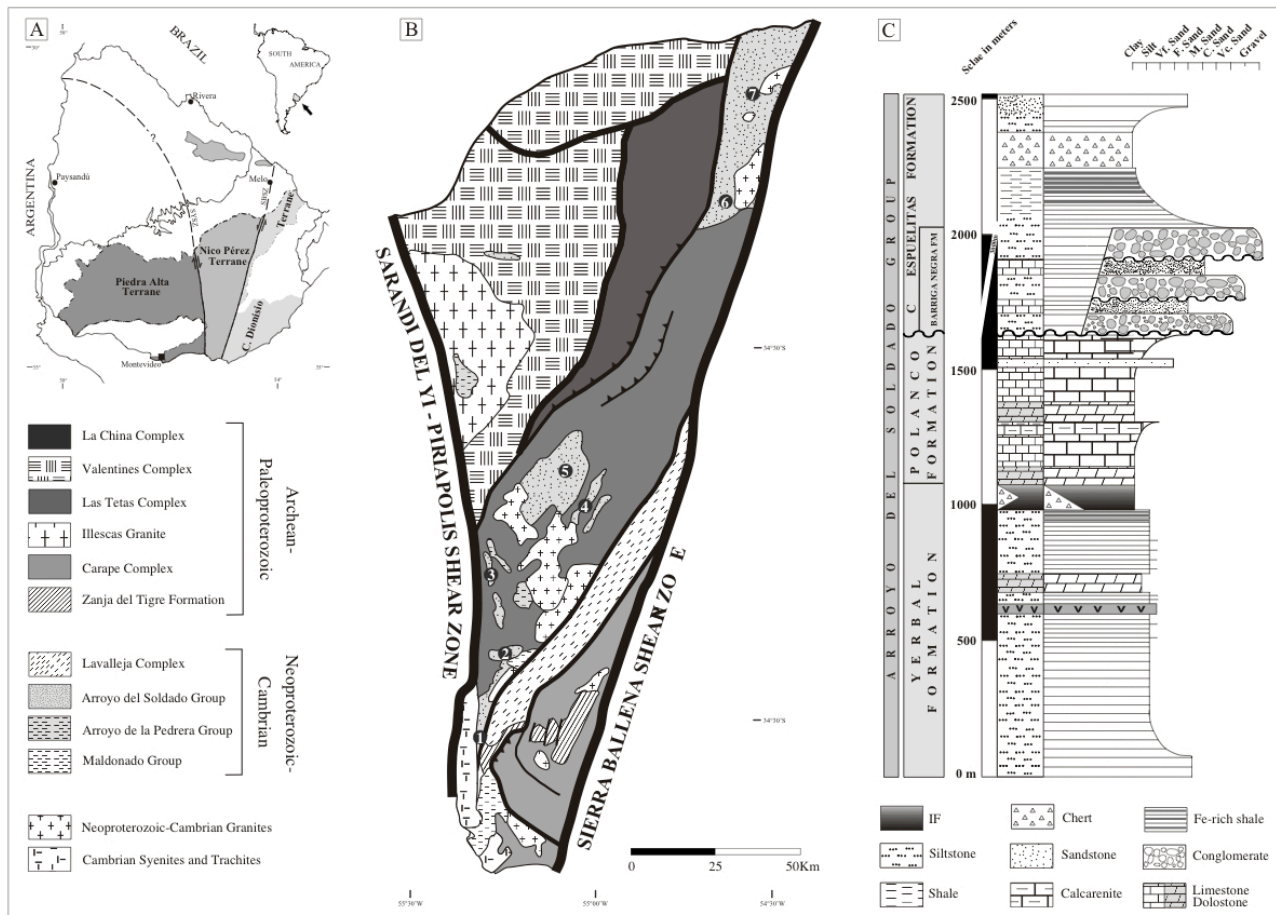
Figure 5.1. (A) Tectonostratigraphic subdivision of the Crystalline Basement of Uruguay according to Bossi (2003). **(B)** Geological-tectonic scheme of the Nico Pérez Terrane and distribution of the Arroyo del Soldado Group showing the localities studied (*1: South Minas; 2: North Minas; 3: Espuelitas; 4: Los Tapes; 5: Barriga Negra; 6: South Isla Patrulla; 7: Southeast Recalde*). **(C)** Simplified stratigraphic column of the Arroyo del Soldado Group (after Pecoits et al., 2008).

The age of the Arroyo del Soldado Group has been radiochronologically constrained by ages obtained from basement rocks and intrusive granites with a maximum U–Pb SHRIMP age of 633±12Ma for the Puntas del Santa Lucía pluton (Hartmann et al., 2002); and (b) a minimum Rb–Sr isochron age of 532±11Ma for the Guazunambí Granite (Rb-Sr, Ro=0.70624) (Kawashita et al., 1999), respectively. Furthermore, K-Ar ages from diagenetic illites of the uppermost Yerbal Formation yielded an age of ca. 584 Ma providing a minimum age for the deposition of the IF. Supporting is data, C- and Sr-isotope chemostratigraphy of the overlying Polanco Limestone Formation indicates a depositional age between 590 and 575 Ma (Pecoits et al., *in press*). Detrital zircon U-Pb age spectra from the Barriga Negra Formation reveals four major peaks: (a) Mesoarchaean (2890-3155 Ma), (b) Palaeoproterozoic (2157-2284 Ma and 1795-1723 Ma), and (c) Neoproterozoic (631-566 Ma). Thus, the youngest detrital zircon ages (566±8 Ma) can be used to constrain the maximum depositional age for the Barriga Negra and the chert-bearing Cerro Espuelitas formations (Blanco et al., 2009).

5.4. LITHOFACIES ANALYSIS

The following section discusses on the main lithofacies found throughout the Arroyo del Soldado Group, especially where these are judged to have important implications on palaeoenvironmental reconstruction and depositional aspects of IF and cherts. Eleven major lithofacies were identified within the Arroyo del Soldado Group; this distinction was made using grain size, stratal surfaces, sedimentary structures and texture. The salient sedimentological attributes of individual lithofacies are summarized in Table 5.1 and discussed bellow.

Lithofacies	Description	Interpretation
Conglomerate	Poorly sorted and polymictic clast-supported conglomerates. Tabular bodies with sharp to erosive bases. Internally massive or crudely zoned. Sub-rounded clasts, from 0.5 to 60 cm diameter.	Fan delta
Carbonate breccia	Sub-facies I: Tabular, massive beds with clasts ranging from 0.5 to 3 cm embedded in a muddy reddish carbonatic matrix. Sub-facies II: Massive, clast-supported and poor-sorted intraformational flat-pebble conglomerates (flakestones) displaying erosive bases.	Sub-aerial to sub-aqueous basin margin
Sandstone	Sub-facies I: Fine to coarse laterally extensive sandstone beds (0.1 to 1.4 m thick). Massive to normal graded with sharp to erosive bases. Amalgamated or interbedded with mudstones. Compositionally correspond to arkoses and sub-arkoses. Usually forming fining-upwards cycles of less than <20 cm thick and show tabular geometry and asymmetrically rippled tops. Sub-facies II: Poorly to well sorted lithic and feldesphatic arenites, often displaying erosive bases and cross-stratification. Occur interbedded with reddish mudstones, calsisiltites and conglomerates.	Shoreface
Couplets siltstone-sandstone	Sub-facies I: Grey-black mudstones interbedded with red or grey sandstones. The latter show slight reverse and normal grading, lamination and ripples. Sub-facies II: Yellowish brown silts interbedded with brownish red sand and occasionally preserving small-scale cross-stratification and rippled tops.	Turbidites (I) Offshore transition (II)
Siltstone	Sub-facies I: Variegated rhythmically bedded siltstones. Laminated and graded intervals are present as well as occasional down-slope oriented current-ripples. The mineralogy is dominated by quartz, muscovite, microcline and kaolinite. Sub-facies II: Laminated green and red siltstones. Mineralogically, they are composed by quartz, microcline, muscovite, clinochlore and rutile, and quartz, muscovite and hematite, respectively.	Offshore
Black- and Fe-rich shales	Tabular bodies, 15 m-thick of highly carbonaceous shales overlying siltstones and passing into carbonates (lower package) or cherts (upper package). The latter is characterized by a cm alternation with iron-rich shales. Mineral assemblage: quartz, orthoclase and muscovite.	Offshore
Calcarenite	Medium- to coarse-grained calcarenite showing a wide variety of sedimentary structures, including: low-angle cross-stratification, asymmetric wave ripples, trough cross-, hummocky and swaley cross-stratification. Occasionally, interbedded with thinner and muddier limestone/dolostone facies.	Inner and mid ramp
Couplets calsisiltite-dolosiltite	It consists of rhythmic alternations (mm to m scale) of medium to coarse calsisiltites and fine dolosiltites layers. The individual rhythmites have tabular geometries and are laterally continuous. This facies thickens seaward and show parallel lamination as well as occasional slumps.	Distal outer ramp
Dolostone	Sub-facies I: Fine- to medium-grained greyish pink dolostones. Although rarely laminated, they are composed of internally structureless dolostone, 50 to 75 m thick and bracketed by silisiclastics. Sub-facies II: Light gray, fine-grained, thin to medium bedded dolostones with chert nodules. Petrographic observations reveal a very fine and uniform texture. These dolostones grade upwards into carbonate mudstones followed by black and iron-rich shales and massive chert.	Mid- to distal outer ramp
Chert	Bedded and laminated cherts, with occasional finely-disseminated impurities of detrital quartz, sericite and minute hematite crystals. Colours vary from white to black, pink and light olive gray. Rarely show soft-sediment deformation.	Offshore
Iron Formation	Approximately 10 m thick, consisting of rhythmic alternations of chert layers, ranging from 0.3 to 15 cm thick, and iron oxides-rich layers of about equal thickness. Compositionally comprise quartz, hematite and magnetite as the main phases.	

5.4.1. Lithofacies 1 (conglomerate-dominated lithofacies)

5.4.1.1. Description

This lithofacies is best developed in the Barriga Negra Formation wherein clast-supported conglomerates reside above an erosional contact to the carbonates of the Polanco Limestone Formation (Figure 5.1C and 5.2A). The conglomerates are poorly sorted and polymictic. Clasts are predominantly composed of intra- and extra basinal carbonates, granitoids, gneisses, sandstones and schists. They range from 0.5 to 60 cm diameter and have irregular but sub-rounded surfaces. Bedding is either massive-appearing or crudely defined and, at the scale of the exposures, appears tabular. The conglomerates show well-organized amalgamated beds with sharp to erosive bases. Although the rudites largely display the above characteristics, other subfacies showing differences in composition, fabric and texture were found (e.g., matrix-supported conglomerate containing poorly sorted clasts, cobble-sized and well-rounded oligomictic beds, normally graded conglomerate-sandstone couplets).

5.4.1.2. Interpretation

The coarsest grained, poorly sorted conglomerates have undergone relatively little transport and were likely deposited close to their source. The lack of evidence for channelization combined with the presence of sheet-like bed geometry, ungraded to well graded beds and clast supported textures indicates deposition from unconfined water flows (Blair and McPherson, 1994). The presence of aligned pebbles on bed tops and wave-generated ripples in interbedded sandy layers further indicate that many rudite beds were emplaced subaqueously, in a nearshore environment, and influenced or reworked by marine processes. The sporadic presence of outsized clasts suggests that the water flow was occasionally highly competent, a feature common on alluvial fans / fan deltas due to comparatively high magnitude of depositional slope. The palaeocurrent analysis suggests a source area northwest of the marine basin where fan deltas prograded southeastward onto the carbonate ramp and the shallow-water carbonate deposition ceased.
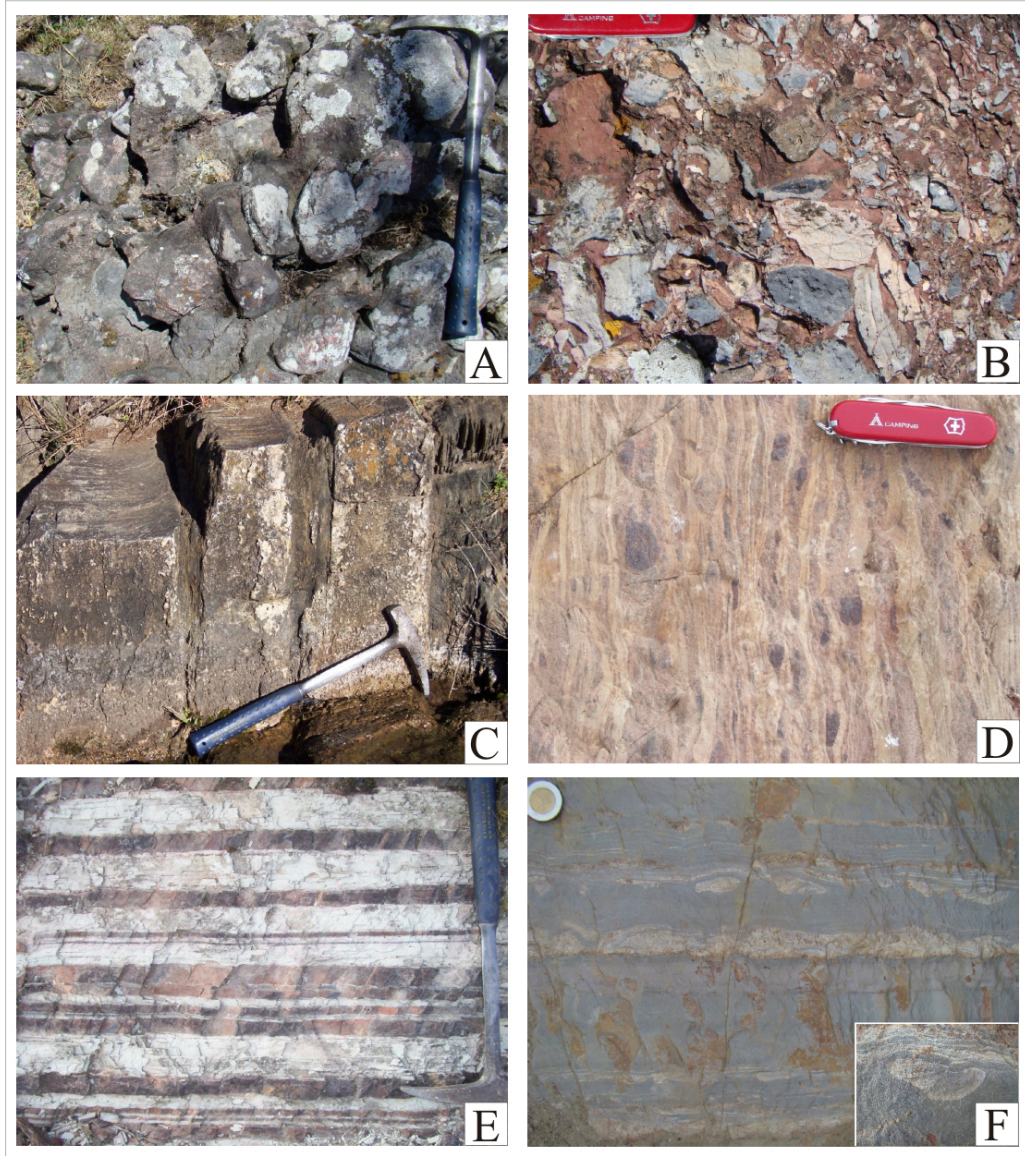
Figure 5.2. (A) Sub-rounded, clast-supported polymictic conglomerates of the Barriga Negra Formation (conglomerate-dominated lithofacies). (B) Calcareous breccias (sub-facies I) of the Barriga Negra Formation with a muddy carbonate matrix and rich in carbonate fragments of the underlying Polanco Limestone Formation (carbonate breccias-dominated lithofacies). (C) Interbedded sandstones and dark mudstones of the Yerbal Formation (couplets siltstone-sandstone-dominated lithofacies: sub-facies I). (D) Thin-bedded couplets of siltstones and sandstone of the Yerbal Formation preserving small-scale ripple-cross stratification (couplets siltstone-sandstone-dominated lithofacies: sub-facies II). (E) Rhythmically banded siltstones of the uppermost Yerbal Formation (siltstone-dominated lithofacies). (F) Alternations of fine and very coarse siltstones of the uppermost Yerbal Formation showing evidence of traction currents. The small-scale ripple crests have sunk down in the underlying soft muddy layer producing load structures (load-casted ripples), (siltstone-dominated lithofacies). Scale: knife: 9 cm; hammer: 40 cm; coin: 2.5 cm.

5.4.2. Lithofacies 2 (carbonate breccia-dominated lithofacies)

5.4.2.1. Description

Breccia is found only at the base of the Barriga Negra Formation (sub-facies I) and in the uppermost Polanco Limestone Formation (sub-facies II). The Barriga Negra breccia consists of a massive appearing, 8 m thick angular to sub-angular carbonate breccia, the clasts typically range from 0.5 to 3 cm (ling axis) embedded in a muddy reddish carbonate matrix (Figure 5.2B). This breccia is made up of massive and laterally extensive tabular beds, a few decimetres to few meters thick, which are intercalated with basal conglomerates and calsisiltites. Breccias present in the uppermost Polanco Limestone Formation comprise massive and poorly-sorted intraformational flat-pebble conglomerates with angular (flakestone) clasts. The sedimentary breccia horizons are clast-supported and almost exclusively contain angular rip-up clasts derived from the underlying carbonate beds. Occasionally, these beds display fining- and thinning-upward trends and the lower contacts are always erosive.

5.4.2.2. Interpretation

In modern and ancient settings the development of well-defined flakestone intervals, intercalated with thin bedded limestones, have been interpreted as fragmentation and subsequent transport and deposition of micrites and cryptalgal laminites from tidal flat areas during high energy events (Davies, 1977; Tucker, 1977). The development of thick siliciclastic alluvial conglomeratic deposits after the cessation of carbonate sedimentation, however, likely indicates that the breccias derived from previously deposited and lithified carbonates as a result of the cannibalization of the ramp. The nearly monogenic nature of the angular carbonate fragments of the Barriga Negra breccia also reflects a proximal origin. Their association with alluvial to fan delta siliciclastic conglomerates and the proximal origin of the clasts suggests that the breccias represent sub-aerial to sub-aqueous basin margin deposits.

5.**4.3. Lithofacies 3 (sandstone-dominated lithofacies)**

5.4.3.1. Description

Lithofacies 3 has been identified at the base and top of the Yerbal Formation, and it is present in the Barriga Negra Formation (Figure 5.1C). The Yerbal sandstones are characterized by laterally extensive, massive to normal graded beds with sharp to erosive lower contacts. The strata are amalgamated or separated by mudstone horizons and occur as units 0.1 to 1.4 m thick (Figure 5.3). Grain size varies from very-fine to coarse sandstone, with occasional beds of pebbly sandstone. Clasts are sub-rounded and the sandstone composition ranges from arkose to sub-arkose. Sedimentary structures present in the sandstones include planar lamination and asymmetric ripples. The Barriga Negra sandstones are best developed at the base and top of the unit. Compositionally the former corresponds to coarse lithic and feldesphatic arenites. They are poorly to well sorted, often displaying erosive bases and cross-stratification, and occur interbedded with reddish mudstones, calsisiltites and conglomerates. The uppermost sandstones are mineralogically more mature than those found at the base. They are usually found in association with mudstones forming fining-upwards cycles of less than < 20 cm thick and show tabular geometry and asymmetrically rippled tops.

5.4.3.2. Interpretation

The basal Barriga Negra sandstones indicate the rapid transition from a shallow water platformal succession to an alluvially dominated deposition. Tabular cross-stratification commonly occurs in this lithofacies indicating traction-dominated subaqueous flow deposits produced by basinward migration of medium-scale bedforms contributing to fan progradation. The small-scale and rippled sandstone-siltstone cycles of the uppermost Barriga Negra Formation are interpreted as wave-generated deposits in shallow water above fair weather wave base. Similarly, an upper shoreface environment is envisaged for the sheet-like strata present within the Yerbal Formation with intercalations of lower shoreface deposits represented by the siltstones. The coarser sand
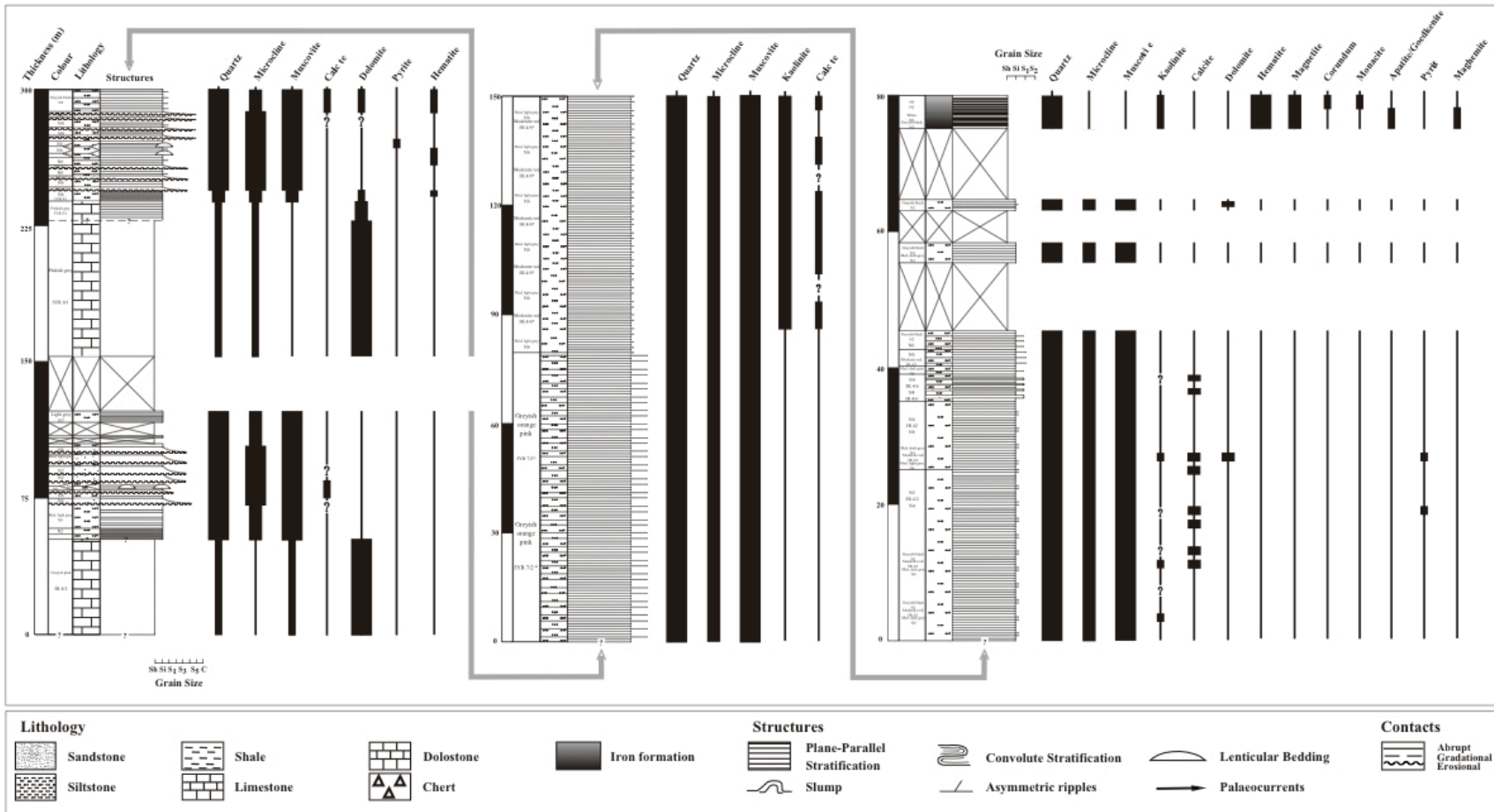
Figure 5.3. Stratigraphic profiles of the Yerbal Formation in the north Minas area showing the occurrence of iron formations (point 2, Figure 5.1B). Bulk mineralogy determined by X-ray diffraction and petrographic analyses (modified from Pecoits et al., 2008).

beds which occur locally near the top of the unit are interpreted as transgressive sandstone that formed as wave-reworked lags of material eroded from coarser shoreface deposits during transgression and transported offshore by storm related processes.

5.4.4. Lithofacies 4 (couplets siltstone-sandstone-dominated lithofacies)

5.4.4.1. Description

This lithofacies is present within both the Yerbal and Cerro Espuelitas formations. In the upper Yerbal Formation, it comprises two 'sub-facies': black mudstones intercalated with grey sandstones and thin-bedded couplets of brownish siltstones and reddish sandstones (Figures. 5.2C-D). The former is characterized by alternating thin beds (5-20 cm) of sandstone and dark mudstones. Internal structures in the sandstones are dominated by slight basal reverse and normal grading, parallel-lamination, and current ripples cross-lamination. Compositionally they are dominated by fine to very coarse grained, although occasionally pebbly, siliciclastics (dominantly quartz and feldspars). The second sub-facies comprises thin-bedded couplets of yellowish brown siltstones separated by brownish red sandstone layers and typically occurs at section 2 (Figures. 5.1B and 5.3), sandwiched between a thick basal package of sandstone and thin-bedded mudstones. The sandstone beds have sharp bases and display grading, load casts, parallel- and ripple cross-stratification. In the south Minas area, and showing an erosional lower contact with the Polanco Limestone Formation, basal deposits of the Cerro Espuelitas Formation also exhibit siltstone-sandstone couplets. These strata are composed of grey mud and red sandy layers (2-5 cm thick) with sharp lower and upper surfaces and attain a maximum thickness of 100 m. The axial plane cleavage accompanying the folding in the area has largely obliterated the primary sedimentary structures, however rare, faint parallel lamination can be observed within these beds.

5.4.4.2. Interpretation

The sedimentary structures present suggest that the uppermost sandstones beds of the Yerbal Formation, and possibly the basal beds from the Cerro Espuelitas Formation, were accumulated from rapid and episodic turbidity currents. The well-defined grading, upward decrease in laminae thickness and presence of current ripples in the thickly bedded massive sets resemble Tacde or Tade Bouma divisions. Ripple migration (turbidity-current flow) was directed primarily to the southeast. The sandstone-siltstones couplets, located down section, preserve current- (towards the northeast) and wave-generated features. These are bracketed by sandstone-dominated lithofacies and banded siltstones. The former is interpreted as a more proximal or landward facies (upper shoreface), the latter a more distal or basinward facies (offshore). Thus, these couplets accumulated to landward of the outer shelf plain setting of the banded siltstones, but basinward of the nearshore sandstone-dominated facies; i.e., in the offshore transition. Some of this thinner graded sandy and silty beds with small-scale cross-stratification and sometimes rippled tops suggest that deposition occurred at greater depths from storm-generated clouds of suspended material, distributed by wind-forced currents or the storm-surge ebb, and locally reworked by waves (distal tempestite of Einsele, 2000).

5.4.5. Lithofacies 5 (siltstone-dominated lithofacies)

5.4.5.1. Description

The siltstone-bearing facies consist of two distinctly different rock types: (1) rhythmically bedded siltstones, and (2) laminated green and red siltstones. Variegated banded siltstones are a common lithotype and invariably occur in the upper part of the Yerbal Formation with thicknesses up to 100 m (Figure 5.1C). The banding is present at two scales, 'microbands' (mm-thick) and 'mesobands (<10 cm-thick) of medium to coarse silt (Figure 5.2E). The rhythmic banding is emphasized by variable amounts of organic matter or, most commonly, due to the mineralogical composition of the cementing mineral phase, mainly iron-oxides and clays. Petrographic examination

revealed a very subtle fining-upward trend and overall reduction in silt-size sediment content in some layers while other layers showed no detectable vertical grain size gradation. Occasionally, centimeter-thick iron-rich and carbonate layers are also present. Down section, a thicker-banded variety of siltstones occur. Although they are essentially preserved as packages of colour-banded siltstones, they also comprise alternations of finer and coarser (fine to very coarse silt) material that display parallel stratification. Evidence of traction currents, in the presence of small scale ripples, is present in some outcrops (Figure 5.2F). Occasional faint scouring is also present at the base of some of the bands, but classic Bouma-style turbidite cycles were not seen. The mineralogy is dominated by quartz, muscovite, microcline and kaolinite. Overlying the banded siltstones, in the Calera de Recalde area, a thick package (80 m) of variably laminated green and red siltstones are exposed. Mineralogically, they are composed by quartz, microcline, muscovite, clinochlore and anatase/rutile, and quartz, muscovite and hematite, respectively.

5.4.5.2. Interpretation

The laminated green and red siltstones included in this facies are interpreted to reflect deposition below storm wave base, in a marine low-energy offshore environment, where sedimentation is primarily from suspension. Similarly, the fine-grained, bedded and evenly laminated siltstones were deposited from suspension under rather tranquil conditions, although the rhythmic banding suggests that the water column received its suspended matter in discrete pulses, possibly due to seasonal flooding of distant rivers. Alternatively, storms moved inland and eroded fine grained material, thus explaining the occasional down-slope oriented current-ripples in coarser layers (coarse silt-very fine sand) interbedded with purely autochthonous shelf muds; i.e., distal mud tempestites. When faintly laminated and graded intervals are present ('graded mud-ungraded mud' couplets) some of these beds resemble hemiturbidites (Stow and Wetzel, 1990; Wetzel and Balson, 1992). As pointed out by Einsele (1991), distal tempestites are thin and fine-grained and show the same sedimentary structures as distal turbidites, but they differ

from turbidites in facies trends. In the uppermost rhythmically bedded siltstones, however, grain-size data of the measured beds indicate that the darker-red horizons are not notably coarser than the light grey sediment portions, as could be expected if they were of (hemi-)turbidity origin. Finally, this lithofacies overlies and represents a finer-grained equivalent of the siltstone-sandstone couplets lithofacies, which suggests similar conditions during sedimentation. However, a slight decrease in the grain size suggests a more distal, lower energy depositional setting. Therefore, the available evidence argue for a deposition in the outer parts of the shelf or ramp, mostly beyond the effect of normal wave activity but intermittently affected by storm-induced offshore return currents.

5.4.6. Lithofacies 6 (black- and iron-rich shales lithofacies)

5.4.6.1. Description

Two black-shale intervals have been identified within the Arroyo del Soldado Group. The oldest package occurs in an isolated exposure in the type area of the Yerbal Formation (Recalde area). Here, the black-shale unit occurs as a 15 m-thick tabular body overlying the banded siltstones of the uppermost Yerbal Formation and abruptly passes into the Polanco Limestone Formation. Petrographic and X-ray diffraction analyses reveal the following mineral assemblage: quartz, orthoclase and muscovite. The next black-shale unit occurs in the middle to upper part of the Cerro Espuelitas Formation, where it forms a 15 m-thick interval of black- and iron-rich shales alternation (Figure 5.4). They are highly carbonaceous but not pyritiferous.

Figure 5.4. Stratigraphic column of the Cerro Espuelitas Formation (point 3, Figure 5.1B). (modified from Pecoits et al., 2008).

5.4.6.2. Interpretation

The organic-rich black shales were deposited during two phases of relative sea-level rise. The apparent lack of sulfides suggests oxygen-deficient bottom waters but not euxinic. In the lowermost black shale interval (Yerbal Formation), the sedimentary features and correlation of lateral facies changes -with IF and cherts- reveals that this black shale records deposition well bellow the storm wave base, most likely hemipelagic sedimentation. Similarly, the upper black shale is composed of a laminated, organic-rich hemipelagic black mudstone and together with the overlying chert form a consistent deepening upward trend during the accumulation of the Cerro Espuelitas Formation. Within this package are dark intervals with extremely high organic content that alternate with brown-colored, laminated iron-rich shale. The Yerbal and Cerro Espuelitas black shales are similar to other varieties of transgressive black shale, in that they are developed upon surfaces of marine starvation and their occurrence is favoured either by high surface-water productivity or favourable conditions for preservation (Stow et al., 2001).

5.4.7. Lithofacies 7 (calcarenite-dominated lithofacies)

5.4.7.1. Description

Medium- to coarse-grained calcarenite showing low-angle cross-stratification and asymmetric (long- and on shore-directed) wave ripples are present in the uppermost Polanco Limestone Formation (Figure 5.1C). Down-section fine calcarenites displaying trough cross-bedding and rare swaley cross-stratification, locally interbedded with thinner and muddier limestones, become common. Tempestitic calcarenites showing hummocky and less commonly swaley cross-stratification are the most prominent facies across the landward margin whereas in deeper sections these facies are interbedded with limestone/dolostone rhythmites (see below).

5.4.7.2. Interpretation

Cross-bedded sandstone facies are interpreted to result from swash and backwash of the waves (inner ramp), where bedding is seaward-dipping. In shallower parts, these facies erosively overlie shoreface deposits with trough cross-bedding generally directed parallel to the shoreline in response to longshore currents; although in deeper depths they are oriented offshore most likely reflecting offshore movement during storms. Hummocky-dominated calcarenites are interpreted as storm-influenced carbonates whose sedimentary structures record storm events in permanent water column above storm-weather wave base. Repetitive alternation of fine-grained rhythmites and coarser calcarenite beds reflects alternating storm- and fair-weather deposition fundamentally in mid ramp areas.

5.4.8. Lithofacies 8 (couplets calcisiltite-dolosiltite-dominated lithofacies)

5.4.8.1. Description

Rhythmites limestone/dolostone, although locally interbedded, underlie the hummocky cross-stratified calcarenites of the Polanco Limestone Formation. They consist of rhythmic alternations (mm to m scale) of dark-grey medium to coarse calsisiltites and fine dolosiltites layers. In most cases, the individual layers have sharp contacts, tabular geometries and are laterally continuous (Figure 5.5A). This facies thickens seaward and shows typically parallel lamination as well as sporadic slumps, mostly (but not exclusively) lacking evidence for storm reworking. Intercalated in these deposits, thin chert layers have been recognized only in one section (Figure 5.6) where pelagic chert-dominated lithofacies were also recorded.
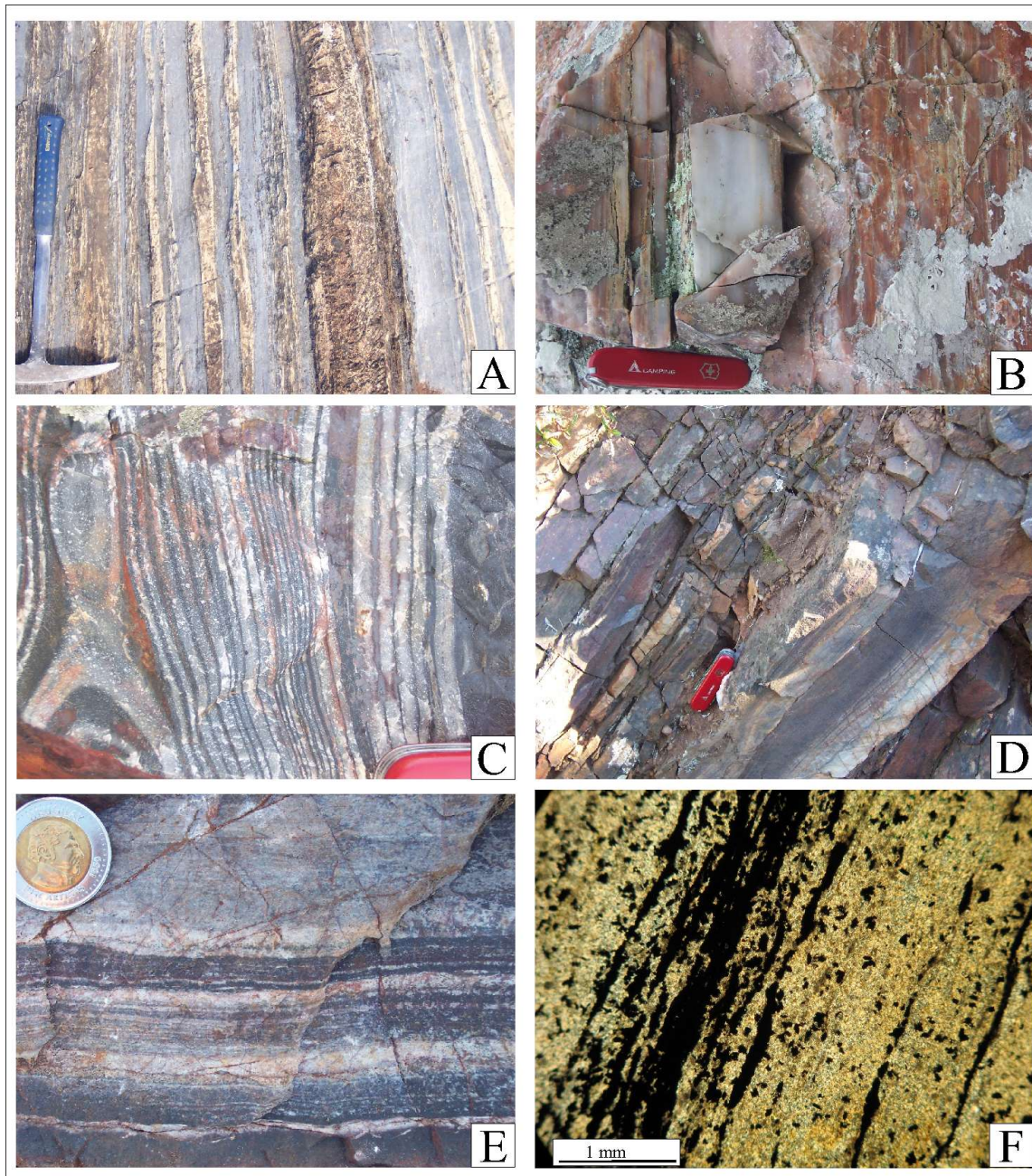
Figure 5.5. (A) Rhythmites limestone/dolostone of the Polanco Limestone Formation (couplets calsisiltite-dolosiltite-dominated lithofacies). (B) Pink-white laminated chert of the Cerro Espuelitas Formation (chert-dominated lithofacies). (C) Finely laminated black and white chert of the Yerbal Formation displaying soft-sediment deformation (chert-dominated lithofacies). (D) Iron formation of the uppermost Yerbal Formation (iron formation-dominated lithofacies). (E) Detail of the iron formation showing the characteristic lamination. (F) Thin section of the Yerbal iron formation with alternating iron-oxides (hematite-magnetite) and quartz microlaminae. Scale: knife: 9 cm; hammer: 40 cm; coin: 2.5 cm.
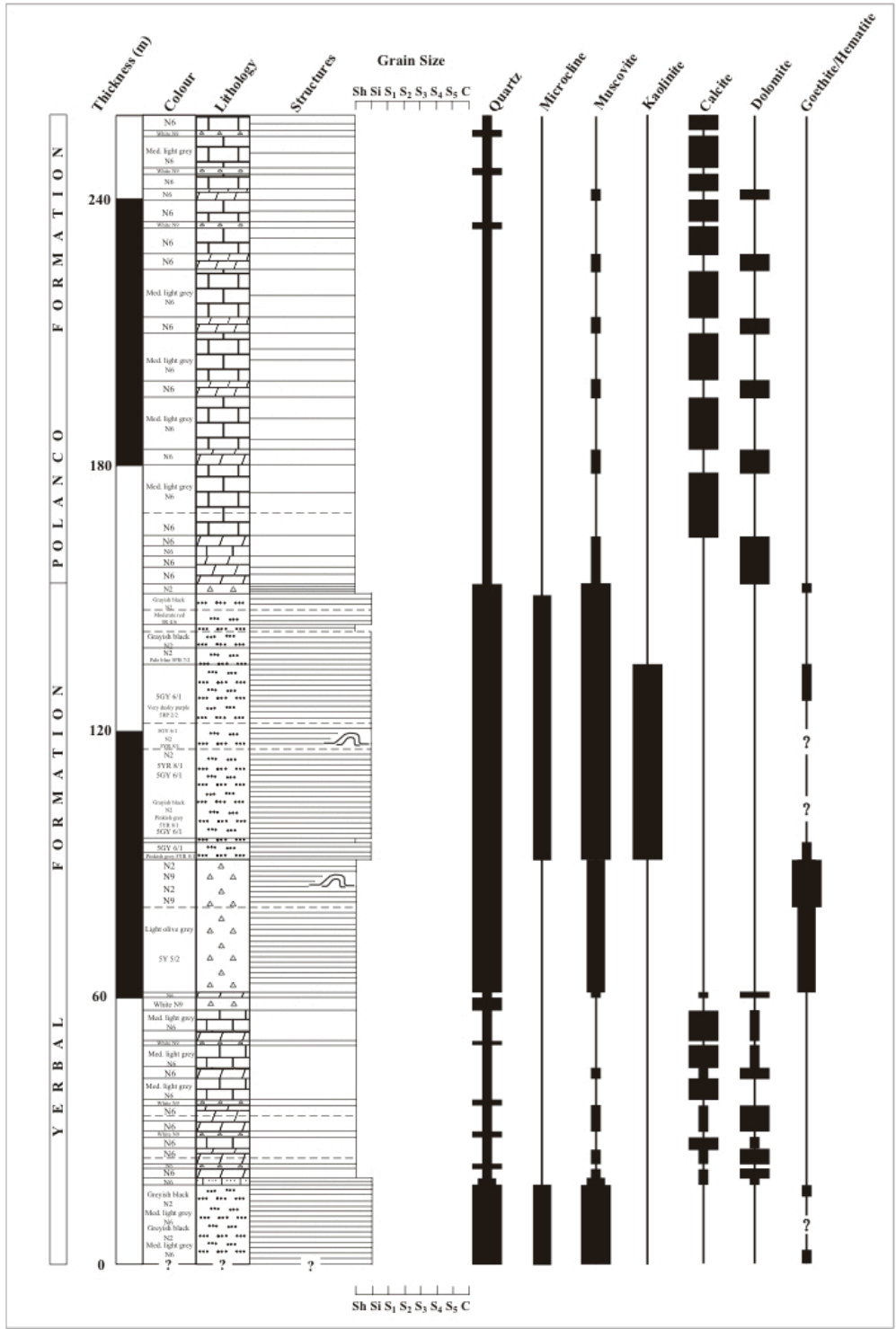
Figure 5.6. Stratigraphic column showing the distribution of cherts within the Yerbal Formation (point 1, Figure 5.1B). Symbols are the same as in Figure 5.3. Bulk mineralogy determined by X-ray diffraction and petrographic analyses (modified from Pecoits et al., 2008).

5.4.8.2. Interpretation

The stratigraphic position of this lithofacies in the individual stratigraphic sections at the different sites and the sedimentary features observed suggest that these high-frequency carbonate rhythmites formed in a distal outer ramp setting. Palaeocurrent trends from interbedded coarser lithologies (calcarenites), lateral change of facies and thickness as well as the few slumps measured indicate that the ramp deepened gradually to the southeast and the coastline was roughly oriented northeast-southwest.

5.4.9. Lithofacies 9 (dolostone-dominated lithofacies)

5.4.9.1. Description

Beds of massive and rarely laminated greyish pink dolostone and light grey bedded dolostone with chert nodules occur near the top of the Yerbal Formation and at the top of the Polanco Limestone Formation (in 'deep water' sections), respectively. In the first case, fine- to medium-grained greyish pink dolostones, occasionally displaying a recrystallized fabric, were documented in two different intervals at section 2 (Figure 5.3) and in the south Minas area (not shown). Bracketed by siliciclastics, this sub-facies is generally composed of internally structureless and laminated dolostone ranging from 50 to 75 m thick. Whereas the first package is overlain abruptly by thin beds of sandstone-siltstone couplets, the uppermost interval grades upwards to marl followed by sandstone, couplets of sandstone-siltstone, and at the top, banded siltstone lithofacies. The uppermost dolostone interval within the Polanco Limestone Formation is found in the Espuelitas area. Here light gray, fine-grained, thin to medium bedded dolostones with chert nodules occur in deep parts of the basin and constitutes the cessation of carbonate sedimentation in this area. Petrographic observations of these beds reveal very fine and uniform texture. These dolostones grade upwards into carbonate mudstones followed by black and iron-rich shales culminating with bedded and massive chert.

5.4.9.2. Interpretation

A low-energy, deep water setting below storm wave base level for the dolostones is indicated by the presence of fine parallel lamination, the lack of wave and current generated sedimentary structures and associated siliciclastic facies. Thus, they likely formed in an mid to distal outer ramp setting. From the analysis of carbonate lithofacies, the transition from proximal to distal facies appears gradual and homoclinal ramp-like (Read, 1985). These types of ramps do not bear major amounts of gravity flow deposits in distal areas and, although slumps and slides may occur, they are relatively scarce (Burchette & Wright, 1992).

5.4.10. Lithofacies 10 (chert-dominated lithofacies)

5.4.10.1. Description

Bracketed by shales, thick deposits of bedded to laminated chert are present in a restricted interval within the Cerro Espuelitas Formation (Figure 5.4). The almost 100 m thick chert succession is remarkably uniform, continuous, and tabular throughout the area. The chert is white to pink and consists of a mosaic of equant quartz crystals with finely-disseminated impurities (Figure 5.5B). The quartz crystals vary in size from 3 μm to 0.4 mm, and in most layers quartz c-axes have a preferred orientation parallel to stratification. X-ray diffraction analyses showed no peaks other than those of quartz, although petrographic observations have revealed sporadic disseminated impurities of detrital quartz, sericite and minute hematite crystals.

The cherts present in the Yerbal Formation, bracketing the banded siltstone facies, display different characteristics depending on their stratigraphic position. These chert strata are much thinner and less continuous in their lateral extent than those described for the Cerro Espuelitas Formation and have been only identified in the southernmost exposures (Figure 5.6). The lowermost interval is composed by approximately 40 m of light olive gray laminated chert passing upwards into 25 m of finely laminated black and

white chert (Figure 5.5C). The latter is characterized by common soft-sediment deformation (bedding distortion and convolution), which indicates an early gel-phase prior to dehydration and consolidation. The uppermost package, which overlies the banded siltstones facies, shows 2 m of black hematite-bearing massive chert.

5.4.10.2 Interpretation

Although rare in Holocene and Phanerozoic sediments, direct inorganic precipitation of chert during the Precambrian was facilitated by the considerably higher oceanic silica concentration (Maliva et al., 1995). At that time, in the absence of silica uptake for skeleton formation, the process of precipitation was localized to the margins of the oceans, as indicated by the prevalence of peritidal chert in Proterozoic carbonate successions (Fischer and Knoll, 2009). On the other hand, late diagenetic carbonate replacement cherts are also common in Proterozoic successions and appear similar to their Phanerozoic counterparts (Fischer and Knoll, 2009). The laminated and massive chert samples examined in this study consist of finely crystalline quartz that does not contain microtextures indicative of replacement. Furthermore, all the chert intervals recorded are closely associated with deep-water siliciclastic facies and, particularly, the uppermost chert interval of the Yerbal Formation constitutes a lateral equivalent of the iron formation. Thus, much if not all of the cherts of the Arroyo del Soldado Group are interpreted as primary precipitates that represent deep-water deposits.

5.4.11. Lithofacies 11 (iron formation-dominated lithofacies)

5.4.11.1.Description

The IF lithofacies, which is approximately 10 m thick (Figure 5.3), consists of rhythmic alternations of 0.3 to 15 cm thick chert and iron oxide-rich layers of about equal thickness (Figures. 5.5D-E). The chert layers are usually light grey and in thin section the

rock is a microcrystalline mosaic of interlocking quartz. Although there is considerable range in particle size, recrystallization of the original silica-rich sediment has produced a remarkably uniform overall texture (Figure 5.5F). Most of the silica is microcrystalline quartz. Iron-rich layers occur as persistent beds and are greyish black in color. Under magnification the iron-rich layers are very fine-grained and fairly uniform in texture, much like the chert. Most of the magnetite crystals have been more or less oxidized to hematite. The 'chert-' and 'iron-rich' layers are compositionally simple, comprising quartz, hematite and magnetite as the main phases. Accessory minerals may include monazite, corundum, maghemite, apatite, goedkenite and kaolinite.

5.4.11.2. Interpretation

Petrographic and field evidence indicate that the IF in the Yerbal Formation is of sedimentary origin. It could have originated by direct precipitation of colloidal silica and iron-oxides to form discrete chert and iron-rich beds, respectively; or silica being disseminated through the iron-rich sediment and syngenetically concentrated into the beds. In the latter case, the original sediment would be an iron-silica gel, from which, the silica became syn- and post-depositionally during and shortly after deposition, the silica became segregated into discrete bands. Alternatively, the cyclic alternation of compositionally dissimilar layers might be interpreted as episodic low-density flows. Certainly, the IF is invariably associated with banded siltstones that are as having been deposited in a deep-water setting but unrelated to turbiditic flows. In fact, the banded siltstones grade basinwards into clastic-free chert and IF suggestive of deep-water deposition (offshore zone) but no evidence of turbidite deposition has been documented. The shut down of the influx of silt and clayey material may reflect the cumulative effect of sea-level rise, disruption of the sediment dispersal system in response to changes in basin configuration, and/or reduction in tectonic activity in the hinterland during IF times (see below). The ultimate source of iron and silica is discussed in section 6.

5.5. SEQUENCE STRATIGRAPHY

The identification of a regional erosional unconformity allows the Arroyo del Soldado Group to be partitioned into two depositional sequences. On the basis of the vertical evolution (i.e., abrupt changes in facies and transition in facies stacking patterns) a more detailed subdivision showing the depositional system tracts has been attempted. The scheme used herein, following the concepts refined by Hunt and Tucker (1992 and references therein), consist of lowstand (LST), transgressive (TST), highstand (HST) and falling stage (FSST) systems tracts (Figure 5.7).

5.5.1. Sequence A

Sequence A, which is the lowest sequence, consists of the Yerbal and Polanco Limestone formations. The overall basal fining- and thinning-upward succession (Yerbal Formation-base not exposed) reaches a maximum thickness of 900 m and documents a progressive upward deepening interpreted to represent a TST. Rhythmic cm- to dm-alternations of fine to very fine sandstone and siltstone, showing internal planar lamination, current ripples and sharp to erosive contacts characterize the lower and medium part of the unit and are interpreted as recording lower shoreface to offshore transition sedimentation. Overlying thin-bedded deposits are indicative of deposition in a more distal, and occasionally storm-influenced offshore area. They consist of bedded mudstones strata grading basinward into thinly bedded and banded siltstones facies. Palaeocurrent measurements from storm-surge-ebb currents indicate flow to the SE, directly away from the basin margin, a view also supported by rare asymmetric slump folds. Although largely dominated by siliciclastics, the Yerbal Formation also hosts a thin layer of volcanic rocks, carbonate, chert and iron-formation. The volcanics occur in the NE area of the basin, near the middle part of the unit, and consist of mafic tuff and lavas interbedded with siltstone and calcisiltite. In the SW, where dolostone and calcisiltite have been documented, pink dolostones overlie thick (dm to m) tabular deposits of coarse to very coarse sandstones, representing lower shoreface deposits, and transitional
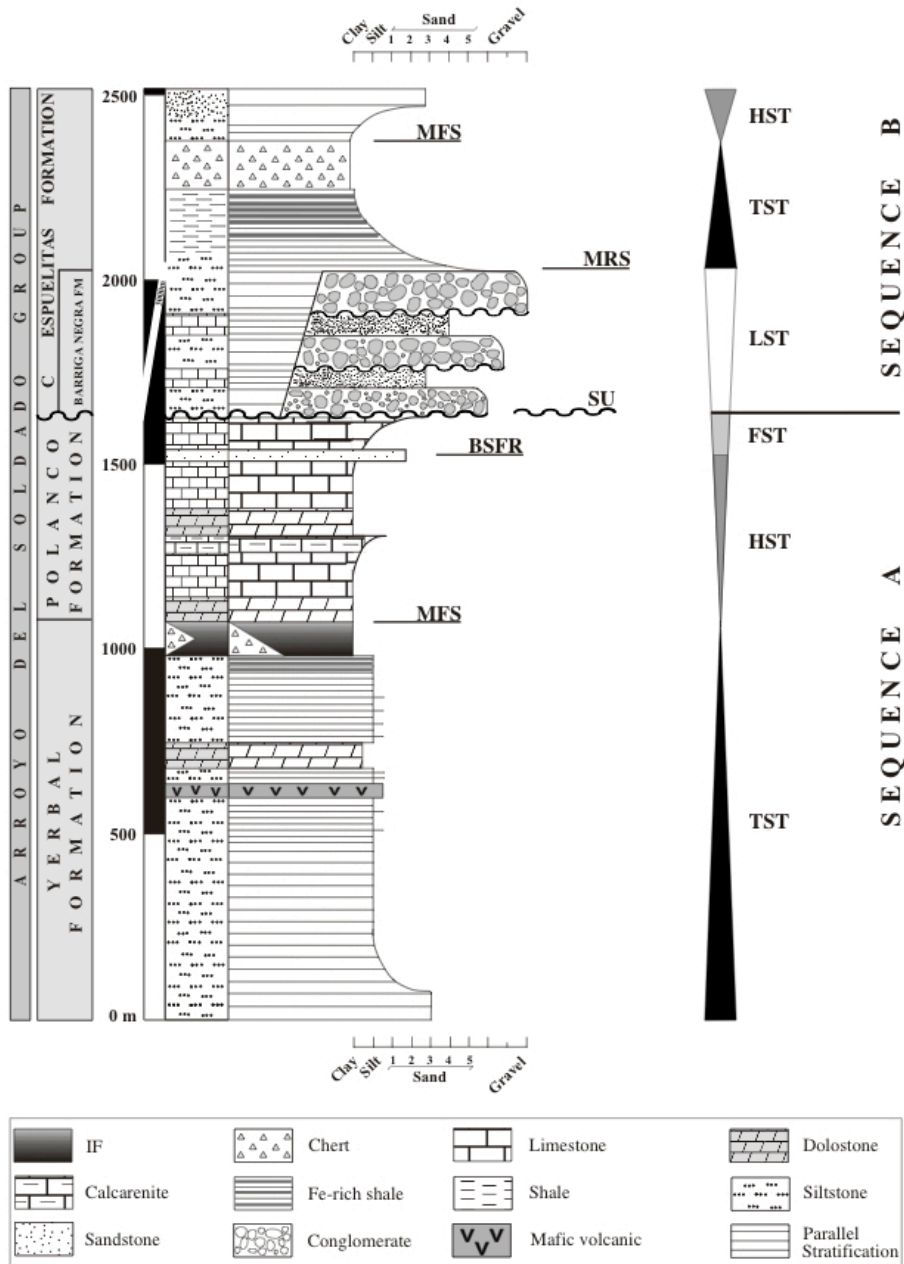
Figure 5.7. Simplified stratigraphic column of the Arroyo del Soldado Group (after Pecoits et al., 2008), and sequence stratigraphic interpretation. Abbreviations: SU = subaerial unconformity; BSFR = basal surface of forced regression; MRS = maximum regressive surface; MFS = maximum flooding surface; LST = lowstand systems tract (*sensu* Hunt and Tucker, 1992); TST = transgressive systems tract; HST = highstand system tract; FSST = falling-stage systems tract.

offshore mudstones. These fining-upward cycles are interpreted to record superimposed relative seal-level fluctuations overprinting the overall TST. Deposition of Yerbal Formation was terminated by widespread transgression with succeeding marine bedded mudstones blanketing the area. These uppermost mudstones represent distal offshore deposits formed below storm wave-base and constitute a basin-wide marker package. The uppermost facies of the Yerbal Formation consist of IF or chert interpreted to represent the maximum flooding surface (MFS).

Grey carbonates, corresponding to the Polanco Limestone Formation, overlie the Yerbal Formation throughout the basin. The sharp contact between both units and the complete cessation of siliciclastic sediment input point to a tectonic control on basin evolution over changes in provenance or climate. The Polanco Limestone Formation as a whole is a shallowing-upward succession with two major thickening- and coarsening-upward cycles interpreted to have accumulated in a homoclinal carbonate ramp setting. The lower and thickest cycle represents the HST (normal regression) and it is characterized by minor stacked coarsening-upward cycles. Cycles commence with dark limestone-dolostone rhythmites (calcisiltites) that are occasionally interbedded with chert layers, which grade upward into interbedded tempestitic calcarenites. The hummocky cross-stratified calcarenites are interpreted as storm deposits that accumulated below fair-weather wave base in the mid-ramp zone (offshore transition). The underlying mudstones represent outer ramp deposits formed below storm wave-base, and the contact between both units indicate alternating storm- and fair-weather deposition in an overall coarsening-upward cycle.

The second cycle of the Polanco Limestone Formation represents the FSST of the sequence wherein minor coarsening-upward cycles are also preserved. These cycles vary from few meters to 100 meters in thickness and, although similar to those present in the lower part of the unit, when fully developed they pass up into siliciclastics. Thus, in contrast to HST, the carbonate factory during FSST was prone to terrigenous poisoning by episodic influx of siliciclastic fines onto the shelf. The sandstone (proximal areas) and mudstone (distal areas) units are therefore interpreted to represent the first forced regressive deposits (i.e., deposits related to the forced regression) overlying outer ramp

mudstones and the basal erosional surface is interpreted as the basal surface of forced regression (= correlative conformity *sensu* Posamentier et al., 1988). Sequence A is truncated from above by a regional erosional unconformity demarcated by overlying conglomeratic rocks that accumulated during sea-level fall when carbonate ramp environments in the study area were subaerially exposed. The scours have northwest-southeast orientations, which parallel both the palaeocurrents in the underlying Polanco Limestone Formation as well as published palaeocurrent readings from the coarse red beds of the overlying strata.

5.5.2. Sequence B

The top of the Polanco Limestone Formation is a surface of subaerial exposure that correlates basinward with the offshore marine expression of the sequence boundary below lowstand deposits. Sequence B consists of a thick wedge of coarse immature siliciclastics (Barriga Negra Formation), which is restricted to the basin margin, that is succeeded up-section and basinwards by finer-grained and comparably mature sediments of the Cerro Espuelitas Formation. As a whole, the lower part of the sequence documents a regressive thickening- and coarsening-upward package that defines the LST. The basal erosive contact and the rapid vertical transition from outer ramp carbonate facies into immature red-bed conglomerates is indicative of a substantial fall in relative sea level. Strong lateral and vertical facies variation of non-marine conglomerate-bearing facies and planar-laminated shoreface sandstone overlie and infill relief along the basal unconformity (sequence boundary) in the central part of the Arroyo del Soldado Basin. The facies associations and stacking pattern point to the development of an alluvial-fan to fan-delta complex onto a relatively high-energy shallow-marine ramp via a high-gradient and narrow system. The facies architecture indicates that the siliciclastic system was to a large degree fed by weakly channelized fluvial systems, and this may explain the scarce evidence of significant fluvial incision and down-cutting into the ramp during sea-level fall. Wave-reworked bed tops indicate deposition above storm wave base. The presence of a variety of facies occurring closely within the same succession suggests that a range

of water depths was present and therefore a steep depositional slope. Further interpretation of the fan-delta physiography is difficult, although the limited geographical extent of the fan-associated lithofacies may indicate a point-sourced fan geometry, or may simply reflect limited preservation. The small bed thickness of fan-delta deposits may be interpreted as being due to local depositional conditions such as a steep local topographic gradient, i.e. a fault scarp.

Although tectonic factors played a prominent role in facies distribution at this time, climatic changes may also have been a contributing factor. Intermittent uplift of fault blocks exposed fresh bedrock to mechanical weathering generated a large amount of detritus. The dominance of fresh metastable clasts in the conglomerate and coarse-grained sandy detritus with a high content of fresh feldspar grains points to mechanical weathering of granites and gneisses of the cratonic basement and a semiarid climate. Non-marine gravel beds grade basinward into marine shaley facies of the Cerro Espuelitas Formation, but the correlative conformity has not yet been traced. Although repeated fault-controlled uplift of the source area, followed by subsidence, generated multiple cycles and finally the retreat of the fan-delta system in proximal areas this is not obvious in distal facies of the Cerro Espuelitas Formation where carbonates of the Polanco Limestone Formation are conformably capped by LST fine-grained deposits. Overlying the maximum regressive surface, which is marked by the upper boundary of the Barriga Negra Formation, a fining- and thinning-upward package marks the onset of the TST, which was deposited during the middle stages of a rise in relative sea-level, when accommodation space due to base-level rise exceed sedimentation rate. The overlying sediments consist of bedded siltstones and mudstones overlain by iron-rich and black-shales. These facies are abruptly overlain by blanketing chert deposits and represent the MFS, which indicate the surface of maximum sediment starvation. In the northern part of the Arroyo del Soldado Basin (Isla Patrulla area) this formation attains its greatest thickness and includes, in its uppermost part, siltstones and sandstones overlying the cherts and represent HST deposition.

5.6. GEOCHEMISTRY

Concentrations of many trace elements in sediments and sedimentary rocks, including rare earth elements and yttrium (REY) as well as redox sensitive trace metals, have been shown to be important proxies in the understanding of processes operating in ancient depositional systems (e.g., Bau and Dulski, 1996; Tribovillard et al., 2006; Schröder and Grotzinger, 2007). The abundance of a given element in sedimentary rocks is typically composed of various independent fractions: detrital, biogenic, hydrothermal and hydrogenous (derived from seawater) which can certainly be altered during diagenesis (Piper, 1994; Piper and Isaacs, 1994; Chester, 2000). Thus, deciphering the influence of each chemical signal is prerequisite for identifying genuine seawater signatures of past oceans. In this work, we focus on the geochemistry of the authigenic sediments of the Yerbal Formation, including the chert and IF. Whole-rock chemical data is presented in Tables 5.2 and 5.3.

5.6.1. Crustal Contamination

Contamination by clastic material may modify the original trace element composition of authigenic sediments. For example, minor amounts of clastic material result in elevated and correlated abundances of incompatible elements, including Th, Hf, Zr, Sc, REE, etc., and anomalous enrichments of redox-sensitive elements such as Ce and U. Accordingly, it is essential to examine the detrital influence that can potentially alter the original chemical signature of the chemical precipitates.

For some of the studied samples, crustal contamination is manifested by somewhat elevated concentrations of Al_2O_3 (0.46-2.7 wt%), Ti_2O (<0.117 wt%) and Zr (1.13-21.9 ppm) but low Th (<1.79 ppm), Sc (<1.9 ppm) and Hf (<0.67 ppm). Additional evidence of contamination is provided by the co-variation of these incompatible elements, for example Hf vs. Zr and Th vs. Zr (Figure 5.8A-B). Low abundances, however, occur in most of the cherts analyzed suggesting that these rocks are less

Table 5.2. Major element concentrations of the Yerbal iron formation (in wt%).

Sample #	Iron-rich layer			Silica-rich layer
	$080108/3_A$	$080108/3_B$	$080108/5_A$	$080105/5_B$
SiO_2	60.94	60.85	56.49	95.33
Al_2O_3	1.21	1.57	2.7	0.46
$Fe_2O_3(T)$	36.82	35.45	40.06	2.32
MnO	0.01	< 0.01	< 0.01	< 0.01
MgO	0.06	0.03	0.03	0.01
CaO	0.06	0.03	0.03	0.02
Na_2O	0.01	< 0.01	0.02	< 0.01
K_2O	0.22	0.1	0.18	0.1
TiO_2	0.08	0.069	0.117	< 0.005
P_2O_5	0.07	0.04	0.03	0.02
LOI	0.49	0.72	0.99	0.26
Total	99.97	98.86	100.7	98.53

Table 5.3. Trace element concentrations of iron formation and cherts in ppm (<DL: bellow detection limit; NM: not measured).

| Lithofacies	Iron Formation								Chert							
	Iron-rich layer					Silica-rich layer			Yerbal Formation			Cerro Espuelitas Formation				
Sample #	080108/3$_A$	080108/3$_B$	080108/5	Fe-layer$_A$	Fe-layer$_B$	080105/5$_B$	050521/1	050521/1$_B$	050628/9	050628/6	050628/17	050522/3	050522/3$_{dup}$	Co.Esp.Fm	050622/6	050523/1
Li	2.70	2.75	2.43	6.55	5.85	0.31	1.17	0.99	13.44	2.27	3.77	1.02	1.11	0.76	1.82	1.29
Be	0.31	0.38	0.43	0.50	0.35	0.13	0.19	0.19	0.81	0.09	0.14	<DL	<DL	<DL	<DL	<DL
Sc	NM	NM	NM	1.22	0.96	NM	0.61	0.34	1.93	0.30	0.41	<DL	<DL	0.18	<DL	0.18
Ti	426.40	437.15	670.88	660.67	539.84	73.24	57.65	77.58	345.47	32.13	73.98	20.25	21.05	18.74	2.24	39.15
V	27.73	29.01	22.83	42.73	34.81	1.40	3.96	3.67	24.63	3.43	3.54	2.38	2.46	8.60	0.19	3.46
Cr	10.17	13.09	16.89	11.69	9.35	4.00	4.23	5.15	7.88	2.26	3.28	2.13	2.19	3.30	1.84	2.67
Mn	37.19	40.23	9.47	116.10	98.07	7.87	35.15	8.65	30.19	6.07	11.13	1.44	1.46	3.29	0.65	2.28
Co	4.11	5.50	3.27	1.64	1.42	2.96	0.59	0.54	0.77	0.59	0.36	0.12	0.12	0.21	0.28	0.89
Ni	NM	NM	NM	6.12	5.20	NM	2.43	1.86	8.93	2.10	1.62	0.46	0.48	0.55	0.50	3.50
Cu	5.68	8.49	5.30	7.84	6.76	1.23	3.03	2.63	10.50	23.52	8.66	2.32	2.33	4.30	6.26	5.86
Zn	14.69	25.76	21.26	20.58	18.13	10.68	6.90	5.46	25.50	6.37	7.15	1.16	1.15	1.16	0.73	4.88
Ga	1.34	1.90	3.42	3.65	3.37	0.54	2.13	1.38	5.45	0.71	1.00	0.48	0.48	0.41	0.33	4.19
Ge	5.01	4.26	5.23	3.68	3.39	4.15	0.06	0.06	0.08	<DL	<DL	<DL	<DL	<DL	<DL	<DL
As	2.80	2.68	2.95	2.06	1.85	0.57	0.53	0.35	14.65	2.43	3.44	0.07	0.08	0.26	0.08	2.63
Se	2.40	3.58	2.93	0.86	0.54	2.86	0.35	0.32	0.58	0.50	0.38	<DL	<DL	0.32	<DL	1.15
Rb	4.01	1.35	2.95	1.95	1.80	2.51	0.67	1.42	34.97	3.83	5.94	0.54	0.55	0.52	0.28	1.34
Sr	67.83	73.07	80.17	16.77	15.55	19.28	5.71	5.15	14.01	3.51	5.93	1.30	1.33	2.68	0.59	3.21
Y	14.95	34.77	24.41	15.06	14.00	0.87	5.60	5.14	2.03	0.68	1.27	0.36	0.36	0.62	0.82	0.45
Zr	9.07	13.64	21.93	21.03	19.29	3.52	6.11	6.15	14.21	1.58	3.51	1.68	1.72	1.13	1.91	3.68
Nb	3.44	1.77	1.74	4.19	3.86	0.27	0.42	0.42	1.45	0.16	0.38	0.10	0.11	0.11	0.09	0.15
Mo	0.42	0.50	0.65	0.71	0.66	0.26	0.17	0.15	3.05	0.46	0.15	0.11	0.11	0.26	0.10	0.37
Cd	<DL	<DL	<DL	<DL	<DL	<DL	<DL	<DL	<DL	<DL	<DL	<DL	<DL	<DL	<DL	<DL
Sn	1.43	1.23	0.70	2.62	2.62	0.19	1.06	0.97	1.40	0.88	2.25	0.95	0.96	1.15	1.95	1.31
Sb	1.84	2.00	1.71	1.34	1.38	0.51	0.44	0.35	0.51	0.11	0.14	0.13	0.13	0.12	0.03	0.14
Cs	1.26	0.27	0.28	0.11	0.10	0.23	0.12	0.31	0.79	0.07	0.13	0.03	0.03	0.16	<DL	0.07
Ba	101.76	69.69	124.80	77.02	76.25	21.93	30.29	180.83	104.03	79.42	31.10	9.63	9.72	43.62	9.92	48.84
La	21.75	31.12	24.01	20.76	20.11	1.23	5.18	8.35	4.08	0.53	1.35	0.58	0.58	0.58	0.08	1.16
Ce	24.86	38.68	29.68	28.25	27.74	1.63	5.66	9.64	6.76	0.87	2.62	1.12	1.13	1.47	0.24	3.47
Pr	4.44	6.56	4.84	4.18	4.16	0.28	1.17	1.77	0.89	0.12	0.34	0.11	0.11	0.12	0.02	0.24
Nd	15.77	25.37	19.95	16.34	16.09	1.02	4.57	6.46	3.38	0.48	1.39	0.39	0.39	0.48	0.11	1.00
Sm	3.06	5.11	4.22	3.11	3.08	0.24	1.06	1.34	0.68	0.14	0.28	0.07	0.07	0.12	0.05	0.21
Eu	0.70	1.20	1.00	0.72	0.72	0.06	0.26	0.35	0.17	0.06	0.07	<DL	<DL	0.04	<DL	0.06
Gd	2.92	5.59	4.72	3.30	3.09	0.23	1.18	1.22	0.52	0.10	0.27	0.06	0.06	0.09	0.05	0.16
Tb	0.42	0.76	0.61	0.41	0.40	0.04	0.15	0.14	0.05	<DL	0.03	<DL	<DL	<DL	<DL	<DL
Dy	2.45	4.56	3.51	2.56	2.48	0.16	0.97	0.91	0.36	0.09	0.19	0.05	0.05	0.09	0.08	0.08
Ho	0.46	0.94	0.69	0.48	0.46	0.03	0.18	0.17	0.07	<DL	0.04	<DL	<DL	0.02	0.02	<DL
Er	1.23	2.57	1.86	1.33	1.28	0.10	0.47	0.45	0.23	0.06	0.11	<DL	<DL	0.06	0.07	0.04
Tm	0.17	0.34	0.25	0.18	0.17	0.01	0.06	0.06	0.04	0.01	0.02	<DL	<DL	0.01	0.01	0.01
Yb	1.03	2.06	1.50	1.02	1.07	0.08	0.36	0.35	0.26	0.05	0.12	<DL	<DL	0.08	0.08	<DL
Lu	0.14	0.29	0.21	0.14	0.15	<DL	0.05	0.05	0.05	<DL	<DL	<DL	<DL	<DL	<DL	<DL
Hf	0.29	0.45	0.67	0.45	0.48	0.16	0.19	0.19	0.41	0.05	0.09	<DL	<DL	0.14	0.06	0.12
Ta	0.23	0.31	0.29	0.18	0.19	0.03	0.02	0.02	0.09	<DL	<DL	<DL	<DL	0.05	0.02	0.03
Tl	<DL	<DL	<DL	<DL	<DL	<DL	<DL	<DL	0.19	<DL	<DL	<DL	<DL	<DL	<DL	<DL
Pb	1.87	2.32	2.27	1.58	1.59	1.47	0.92	0.56	7.46	3.19	0.29	0.66	0.65	0.54	0.37	3.87
Th	0.81	1.37	1.44	1.79	1.78	0.18	0.30	0.30	1.36	0.12	0.27	0.12	0.12	0.19	0.05	0.29
U	0.56	0.58	0.58	0.44	0.43	0.10	0.12	0.12	0.73	0.15	0.13	0.35	0.37	0.14	2.07	0.16
∑REE	94.351	159.914	121.462	97.837	94.996	5.974	26.928	36.385	19.566	3.186	8.100	2.742	2.755	3.758	1.634	6.876
Y/Ho	32.740	36.877	35.462	31.497	30.284	29.050	31.074	30.894	28.624		33.200			30.390	38.960	
Sm/Yb	1.481	1.242	1.405	1.524	1.444	1.434	1.468	1.906	1.296	1.275	1.221			0.766	0.293	
Pr/Sm	0.913	0.807	0.721	0.847	0.849	0.732	0.696	0.834	0.817	0.556	0.751	0.948	0.938	0.658	0.322	0.728
Ce/Ce*	0.614	0.710	0.800	0.822	0.803	0.673	0.585	0.613	0.898	0.848	1.019	1.111	1.106	1.445	1.718	1.846
La/La*	1.117	1.311	1.645	1.403	1.335	1.091	1.237	1.136	1.214	1.199	1.337	1.187	1.173	1.306	2.672	1.553
Eu/Eu*	1.161	1.155	1.182	1.181	1.212	1.268	1.228	1.421	1.431	3.105	1.343			2.313		2.031
Gd/Gd*	1.139	1.237	1.282	1.297	1.241	1.054	1.288	1.267	1.276	2.597	1.346	3.101	2.970	2.692	4.313	2.733
Pr/Pr*	1.243	1.155	1.093	1.089	1.100	1.189	1.235	1.236	1.051	1.075	0.992	0.947	0.949	0.830	0.811	0.734

(A)

(B)
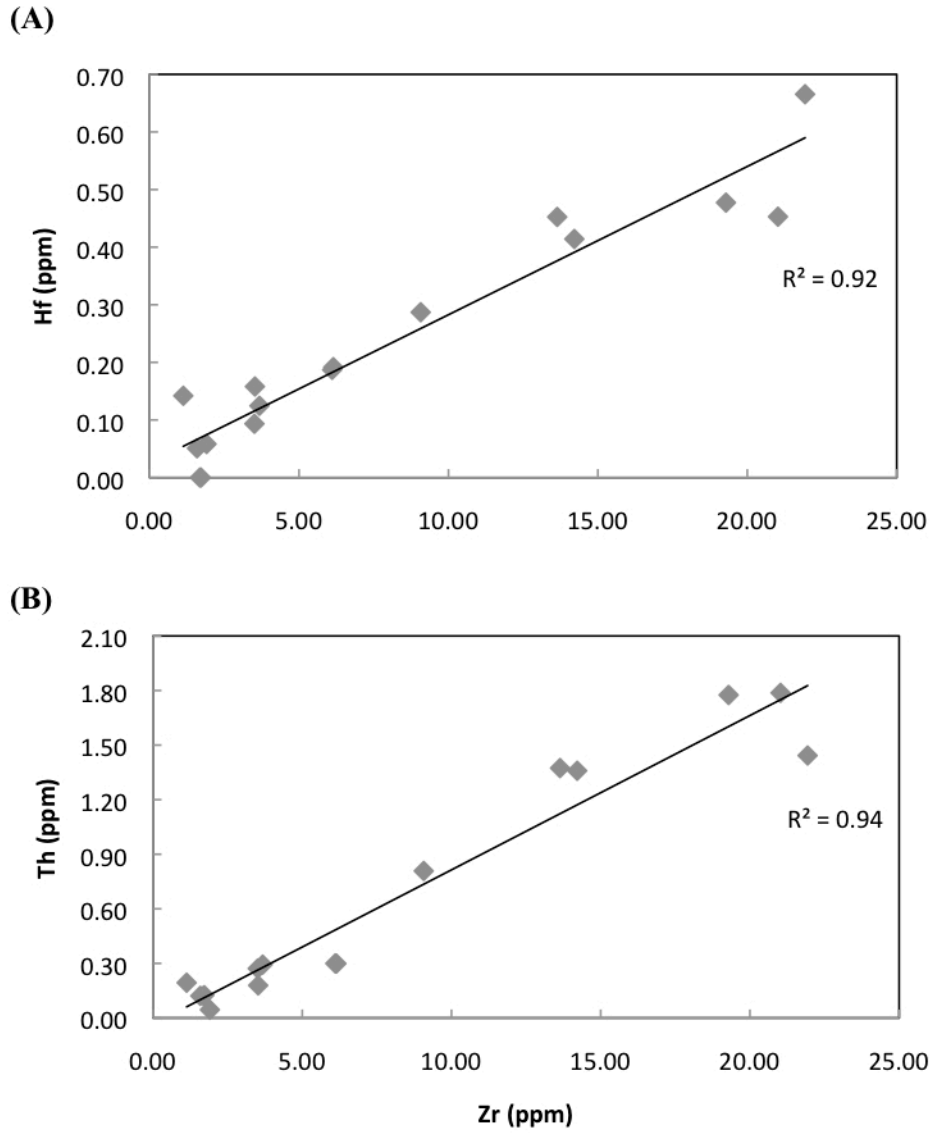
Figure 5.8. Binary plots of Zr vs. Hf (A) and Zr vs. Th (B). Note the positive co-variation in both diagrams.

contaminated and almost devoid of the detrital component. Petrographic and XRD analysis, complemented by cross-plots of various elements, reveal that monazite and occasionally zircon are the contaminant species. This is particularly true for 'Fe-rich' layers from IF of the Yerbal Formation, where the highest concentrations of P and Zr tend to be associated with moderately elevated concentrations of Th, Sc and U and Pb (not shown).

On the other hand, the lack of correlation between lithophile elements and Y/Ho has been used as an argument against crustal contamination (Bolhar et al., 2004). Whereas crustal material possesses a constant Y/Ho value of ca. 26, seawater-like ratios are >44 and thus, any contamination would depress the seawater signature and lead to negative co-variations. The lack of correlation observed for the studied samples suggests that there is no contamination from siliciclastics and that monazite and zircon do not strongly affect the Y/Ho ratios. Although the 'Fe-rich' layers tend to have higher Zr concentrations and relatively low Y/Ho ratios, the associated 'silica-rich' layers -having lower Zr concentrations- display an equivalent Y/Ho range to the Fe-rich layers (Figure 5.9A). Furthermore, the REY patterns of both layers are identical suggesting that the Y/Ho values are a nearly primary feature. Similarly, when Y/Ho is plotted against Ce/Ce* the linear array does not intercept the cross-hair defined by shales (Figure 5.9B) ruling out significant contamination by clays.

In REY shale normalised diagrams, monazite is characterized by light rare earth elements (LREE) and middle rare earth elements (MREE) enrichment relative to heavy rare earth elements (HREE), whereas zircon displays LREE and MREE depletion relative to HREE (Taylor and MacLennan, 1985). Taken in conjunction both mineral species would produce a net enrichment in total REY. However, ΣREY is not only controlled by the relative proportion of monazite and zircon but depends also on the iron content with 'Fe-rich' layers having higher ΣREY than cherts (Table 5.3). In this regard, 'Fe-rich' -and some 'silica-rich'- layers from IF have fairly smooth REE patterns, similar to the average shale (Figure 5.10). However, even in these samples, a noticeable seawater-like signature (e.g., positive La anomaly) is still present. This suggests that the contaminant mineral species buffered the concentration of REY but this was not enough to completely

obliterate the seawater signatures. Indeed, there is a lack of co-variations between P and Zr with La/La*, Ce/Ce*, Eu/Eu*, Gd/Gd* and Y/Ho (not shown).
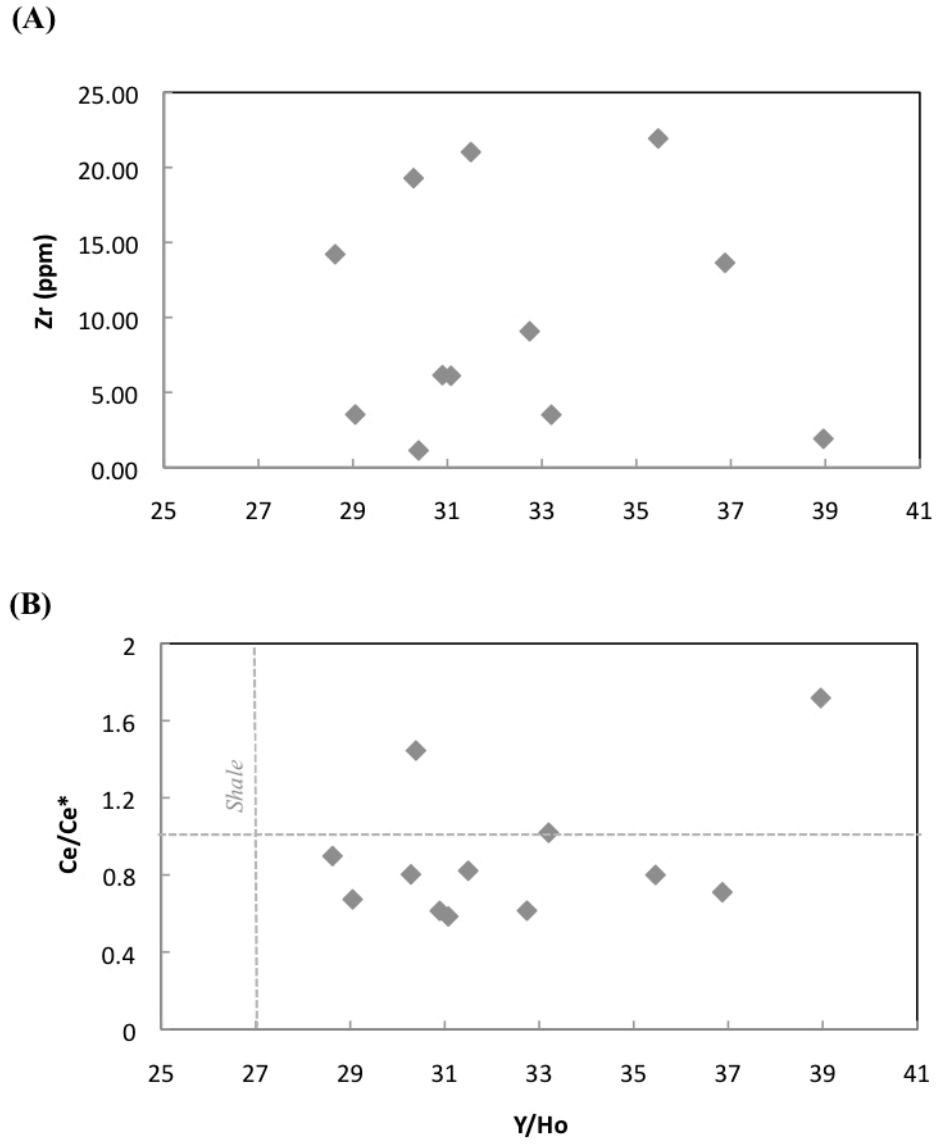
(A)

(B)

Figure 5.9. Binary plots of Zr vs. Y/Ho (A) and Ce/Ce* vs. Y/Ho (B).
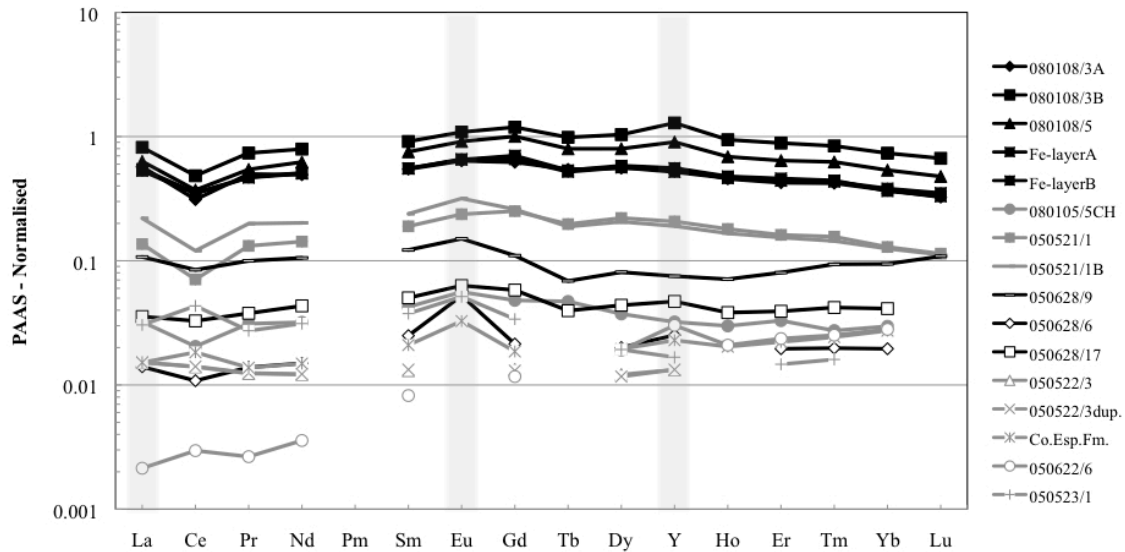
Figure 5.10. PAAS-normalised REY diagram for iron formation and cherts of the Yerbal and Cerro Espuelitas formations.

5.6.2. Hydrogenous and hydrothermal signals

In addition to the terrestrial component, REY abundances in modern ocean waters are controlled by hydrothermal input and particle-solution interaction (Elderfield, 1988). The PAAS-normalized REY diagram, depicted in Figure 5.11, shows representative REY characters of plume derived sediments and plume particles of high and low temperature deep-sea hydrothermal fluids and modern seawater. Except for the Eu signature, sediments and plume particles related to low- and high-temperature hydrothermal fluids share similar features and are characterised by a slight LREE and MREE enrichment respect to HREE. These compositional features contrast strongly with REY patterns displayed by modern seawater. Modern oxic seawater REY patterns are generally similar to those of anoxic basins (German and Elderfield, 1989; German et al., 1991; Bolhar et al., 2004). Both display positive La anomalies, negative Ce anomalies (weaker or even positive in anoxic water), positive Gd anomalies, positive Y anomalies, and depleted

LREE and MREE relative to HREE ($La_{SN}/Yb_{SN} < 1$; $Gd_{SN}/Yb_{SN} < 1$) in PAAS-normalised REY diagrams.

On the basis of their lithofaciology, we subdivided the samples into two groups, (I) iron formation- and (II) chert-dominated lithofacies. In the IF, although 'chert-rich' layers are more depleted in ΣREY (6-36 ppm) relative to 'Fe-rich' layers (94-160 ppm), all the samples are characterized by relatively uniform (subparallel) REY patterns. In shale-normalised REY diagrams, both bands display a slight enrichment of MREE relative to HREE (Sm/Yb_{PAAS}=1.2-1.9) and LREE (Pr/Sm_{PAAS}=0.7-0.9) and are characterised by small, but consistent positive La ($La/La*_{PAAS}$=1.1-1.6), Eu ($Eu/Eu*_{PAAS}$=1.2-1.4) and Gd ($Gd/Gd*_{PAAS}$=1.1-1.3) anomalies (Figure 5.12). Both, 'Fe-rich' and 'chert-rich' layers show relatively low Y/Ho ratios of 29-37 and negative Ce anomalies ($Ce/Ce*_{PAAS}$=0.5-0.8). Chert-dominated lithofacies (group II) is characterized by low ΣREY (1.6-19.6 ppm) and slightly enriched MREE relative to LREE (Pr/Sm_{PAAS}=0.3-0.9) and HREE (Sm/Yb_{PAAS}=1.2-1.3) with the exception of two samples from the Cerro Espuelitas Formation showing Sm/Yb_{PAAS} ratios between 0.3 and 0.8. Lanthanum displays slight positive anomalies ($La/La*_{PAAS}$=1.2-2.7), whilst Ce shows slightly negative to non-existent anomalies ($Ce/Ce*_{PAAS}$=0.8-1.0). The latter is particularly true for Yerbal cherts but those from the Cerro Espuelitas Formation consistently display positive $Ce/Ce*_{PAAS}$ anomalies (1.1-1.8). As for group (I), insignificant positive Eu anomalies ($Eu/Eu*_{PAAS}$=1.3-1.4) and chondritic Y/Ho ratios (29-33) are present, except samples 050628/6, [Co.Esp.Fm.] and 050523/1 where the Eu anomaly is more pronounced (2.0-3.1). All the samples show positive Gd anomalies (>1) particularly those of the Cerro Espuelitas Formation ($Gd/Gd*_{PAAS}$=2.7-4.3). The good correlation between $Eu/Eu*_{PAAS}$ and Ba/Nd ratios (Figure 5.13) suggests that this anomaly may be interpreted as an analytical artefact related to Ba interferences during the ICP-MS analysis (Shields and Stillie, 2001). Therefore, the REY patterns for the IF and chert samples suggest that influence of detrital component was limited and they have largely preserved original signals of palaeo-ocean chemistry.
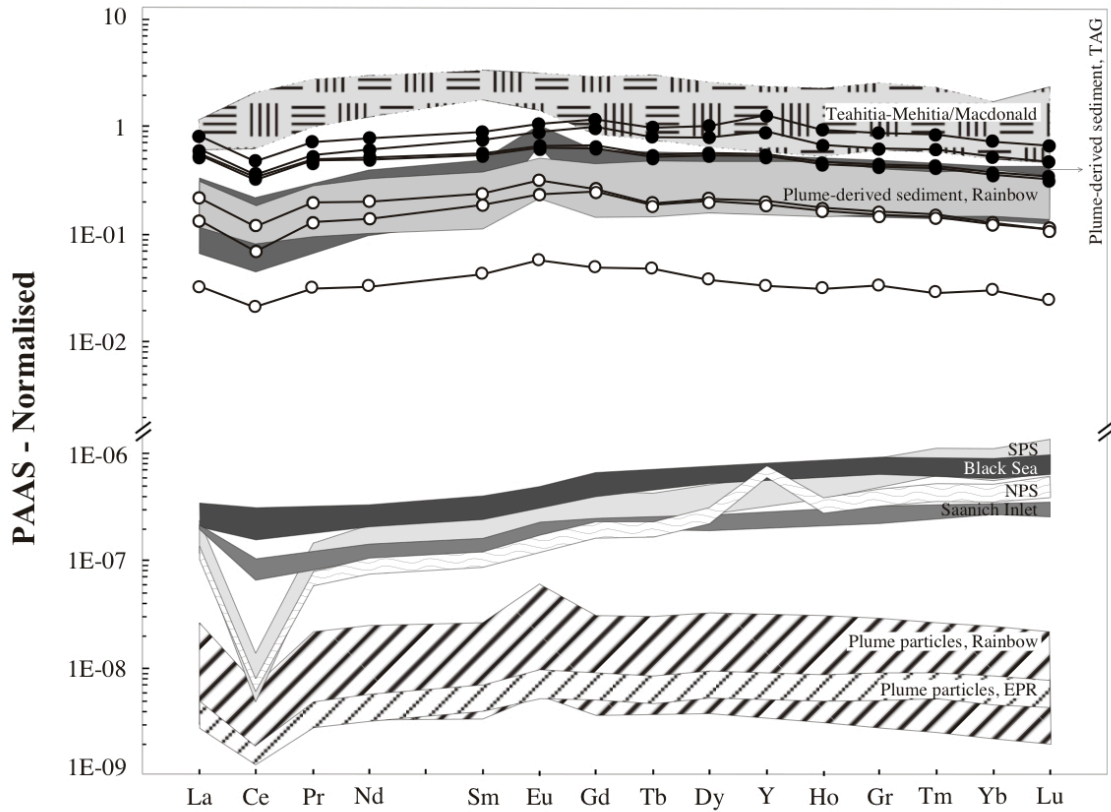
Figure 5.11. PAAS-normalised REY diagram showing compositional range of plume derived sediments and plume particles of high and low temperature deep-sea hydrothermal fluids and modern seawater (see text for explanation). EPR: East Pacific rise; SPS: South Pacific seawater; NPS: North Pacific seawater; TAG: Trans-Atlantic Geotraverse (sources: Michard et al., 1983; De Baar et al., 1985; German and Elderfield, 1989; German et al., 1991; Puteanus et al., 1991; German et al., 1993; Zhang et al., 1994; German et al., 1995; Alibo and Nozaki, 1998; Sherrell et al., 1999; Wheat et al., 2002; Edmonds and German, 2004; Chavagnac et al., 2005). Samples from the Yerbal iron formation (black circles: iron-rich layers; white circles: silica-rich layers) have been plotted for comparison.
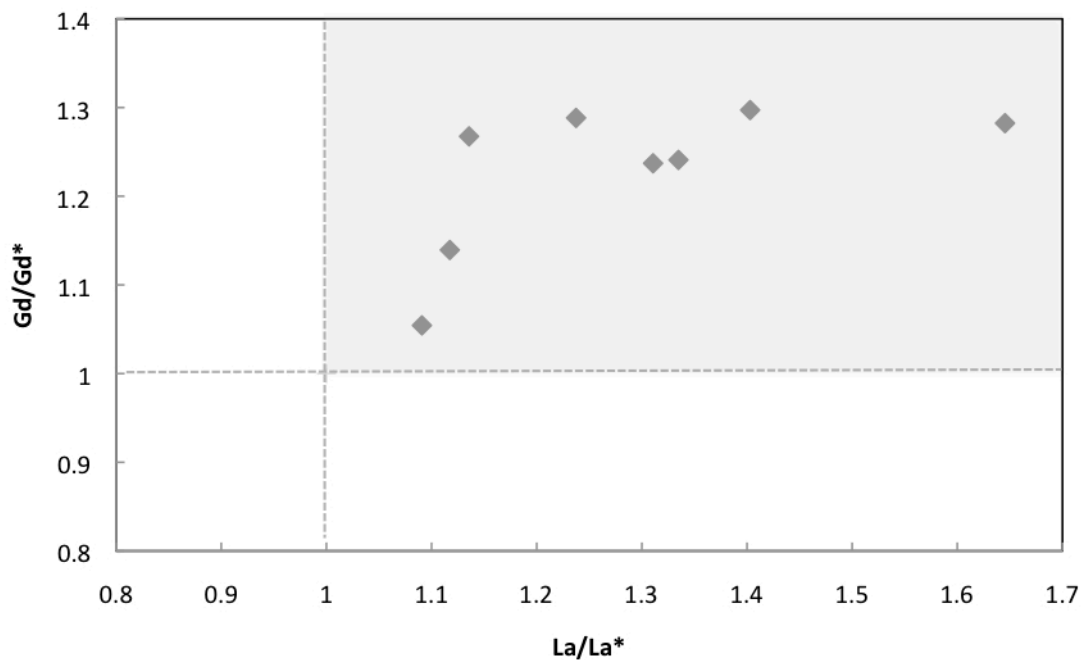
Figure 5.12. La and Gd anomalies of IF and chert samples normalised to PAAS. All samples display La/La* and Gd/Gd* above unit, features characteristic of marine chemical sediments.
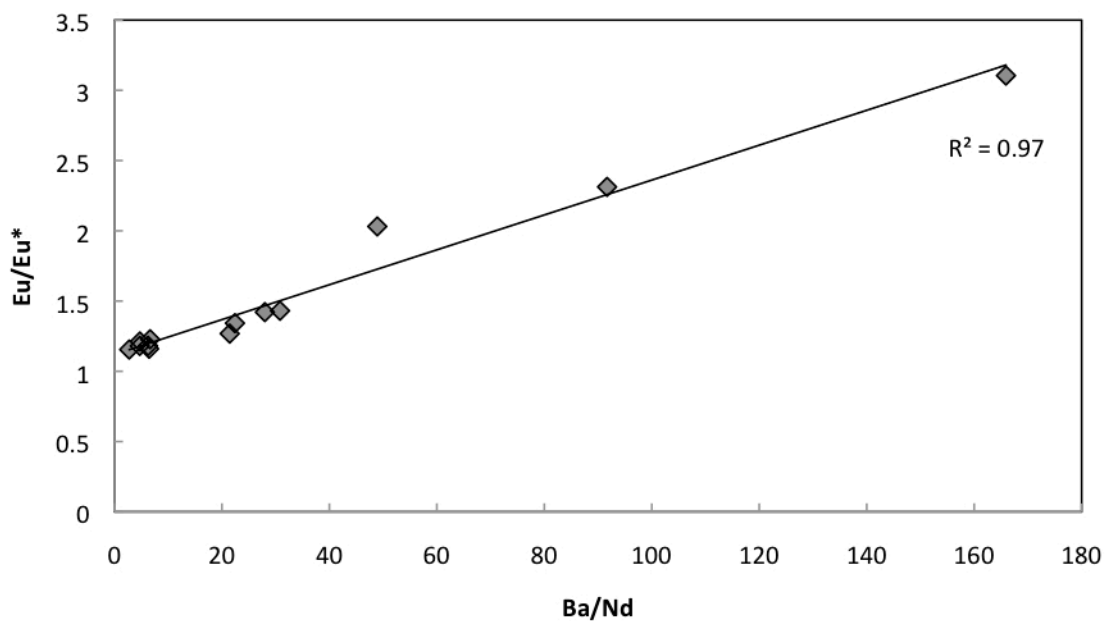
Figure 5.13. Binary plot of Eu/Eu*$_{PAAS}$ vs. Ba/Nd.

Elemental ratios such as $(Sm/Yb)_{CN}$ and $(Eu/Eu)_{CN}$ have also been used to provide constraints on the depositional environment where IF and cherts were deposited (Alexander et al., 2008). The presence of positive Eu anomalies (Eu>1) in modern marine environments is characteristic of high-temperature hydrothermal fluids (>250 °C) and thus, iron oxyhydroxide precipitates on the modern seafloor having such positive Eu anomalies indicate contributions of Eu^{2+} from reduced, high-temperature hydrothermal fluids (German et al, 1993; Bau and Dulski, 1999; Chavagnac, et al., 2005; Slack et al., 2007). The absence of positive Eu anomalies in IF and cherts form the Arroyo del Soldado Group is evidence that the REY from high-temperature hydrothermal input did not influence their chemistry (Figure 5.14A). These samples display different ratios when compared to other BIF, which demonstratively were influenced by high-temperature fluids (Pecoits et al., 2008; 2009), such as those from Isua (3.7-3.8 Ga), Temagami (2.72-2.76 Ga) and Dales Gorge (2.45 Ga). Mixing calculations, using Sm/Yb as a function of Eu/Sm (Alexander et al., 2008), provides further evidence on the negligible contribution of high-temperature solutions (Figure 5.14B). In this regard, the relatively high Sm/Yb of the IF and cherts (2.58) respect to average BIF (0.78) indicates the possible existence of additional REY sources.

Similar HREE depletion in the ca. 2.9 Ga Mozaan IF was interpreted by Alexander et al. (2008) to be possibly related to riverine-derived colloidal particles enriched in the MREE that could exert a strong influence on REY distributions. Whilst modern seawater exhibits a $(Sm/Yb)_{CN}$ ratio of ca. 0.8, estuaries and rivers display ratios up to 5.4 (Elderfield et al., 1990; Kulaskiz and Bau, 2007; Sholkovitz, 1994; Lawrence et al., 2006). Much of the REY load transported by modern rivers is removed in estuaries by the settling of suspended detrital particles and by salinity-induced coagulation and settling of colloidal particles rich in the particle reactive REY (Sholkovitz, 1994). Similarly to our samples, the colloidal fraction carried by rivers –including Fe-rich organic colloids (Sholkovitz, 1994)- would be enriched in the MREE (PAAS-normalised) relative to the light and heavy REY (Elderfield et al., 1990). Although it is presently unclear if the REY fractionation occurring upon mixing of saline and fresh waters implies a change in REY from organic to inorganic speciation and/or corresponding fractionation

upon removal with iron oxyhydroxides, the estuarine fractionation also generates superchondritic Y/Ho ratios (Lawrence et al., 2006). This is in contrast with the low Y/Ho values (29-37) obtained in samples from the Arroyo del Soldado Group and although, an estuarine environment could explain the recorded $(Sm/Yb)_{CN}$ ratios it does not reasonably account for the observed Y/Ho values.

Low Y/Ho ratios are typical of low- and high-temperature hydrothermal solutions and both show, although variable, a significant fractionation of Sm/Yb relative to seawater (Puteanus et al., 1991; Michard et al., 1993; Bau et al., 1996; Pichler et al., 1999; Wheat et al., 2002). Specifically, low-temperature hydrothermal fluids (< 200 °C) are also enriched in the MREE (PAAS-normalised) relative to the LREE and HREE (e.g., Puteanus et al., 1991; Michard et al., 1993) as do our samples. Hence, low-temperature hydrothermal input may reasonably account for the $(Sm/Yb)_{CN}$, $(Eu/Eu)_{CN}$ and Eu/Sm ratios within the Arroyo del Soldado samples. Low Y/Ho ratios have also been recorded in modern hydrogenetic Fe-Mn crusts (Bau et. al., 1996). As stated above, modern seawater is characterized by Y/Ho ratios substantially higher (44-74) than upper crustal rocks and clastic sediments (~28) (Bau et al., 1996). The development of superchondritic Y/Ho values is governed by the fractionation of this pair in the water column, where dissolved Ho absorbs more effectively to particulate matter (Fe and Mn particles) than Y (Bau, 1999). Surprisingly, this fractionation has not been observed in IF and thus, it has been suggested that scavenging Fe-oxyhydroxide particles could not be at or near exchange equilibria with surrounding seawater (Bau and Dulski, 1996). Hence, assuming that the Y/Ho ratios were not modified by crustal contamination (see above), the fact that Yerbal precipitates systematically show chondritic Y/Ho values might reflect either that low-temperature hydrothermal venting input, with a likely Y/Ho ratio of ~28 (Bau and Dulski, 1999), depressed the average Yerbal seawater or that exchange equilibria were reached. Significantly, when 'Fe-' and 'silica-rich' layers from Yerbal IF are plotted in a Y/Ho vs. Eu/Eu* diagram (not shown), the 'Fe-rich layers' display higher Y/Ho and lower Eu/Eu* ratios than 'silica-rich layers'. This might suggest that during the deposition of the silica, hydrothermal activity was more active –as indicated by higher Eu/Eu* ratios- producing the buffering of the Y/Ho seawater-like signature.
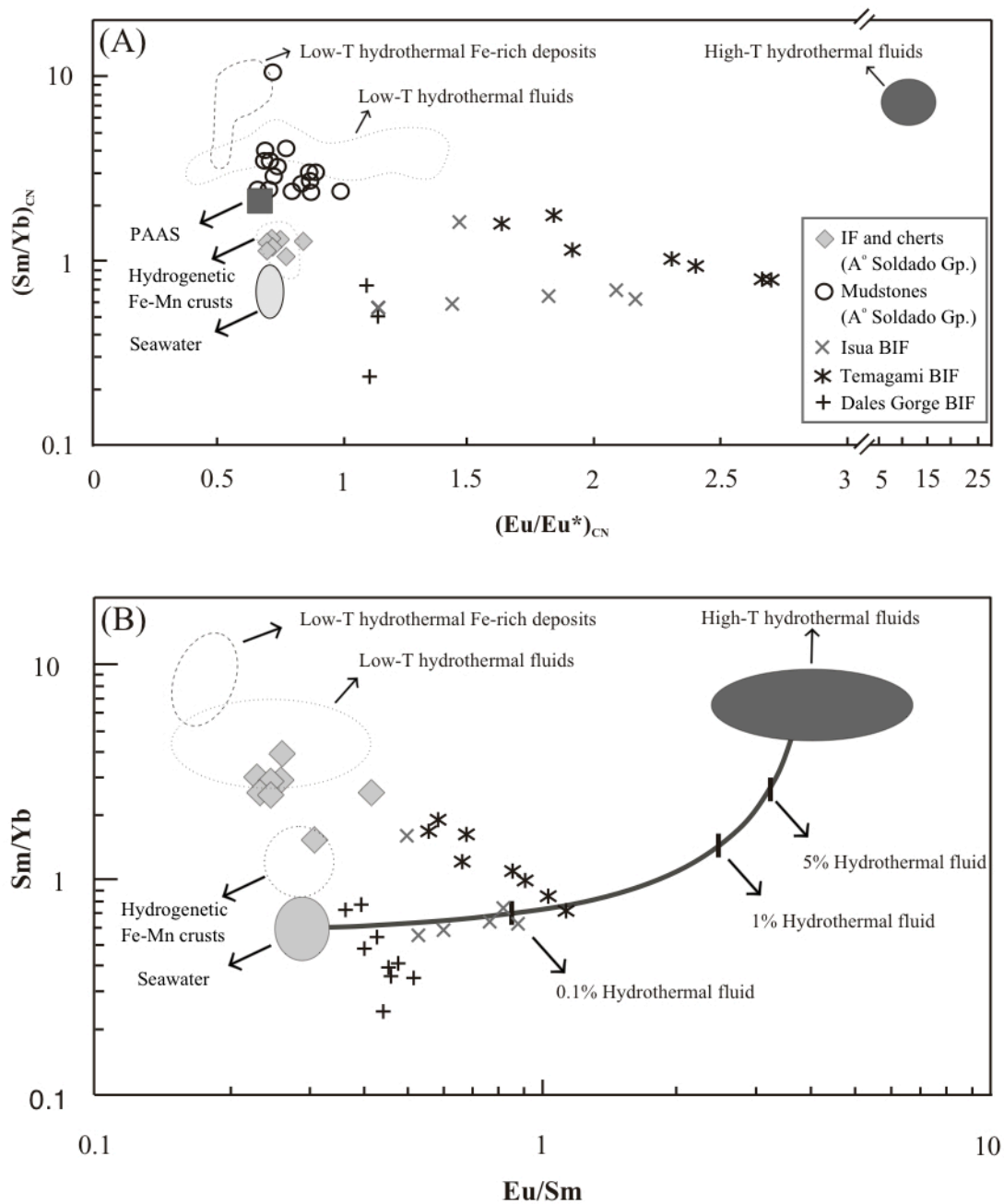
Figure 14. (A) Binary plot of chondrite-normalised Sm/Yb vs. Eu/Eu* for IF and cherts of the Yerbal and Cerro Espuelitas formations. Data from Pacific seawater (Alibo and Nozaki, 1999), low-T hydrothermal fluids (Michard et al., 1993), low-T hydrothermal Fe-rich deposits (Puteanus et al., 1991), high-T hydrothermal fluids (Bau and Dulski, 1999), hydrogenetic Fe-Mn crusts (Bau et al., 1996), Post-Archaean Average Shale (PAAS, McLennan, 1989), Isua (3.7-3.8 Ga), Temagami (2.72-2.76 Ga) and Dales Gorge (2.45 Ga) BIF have been plotted for comparison (Pecoits et al., 2008; 2009) (see also Alexander et al., 2008). (B) Binary plot of Sm/Yb vs. Eu/Sm ratios for data set presented in (A) showing the two-component conservative mixing line (symbols are the same as in A) (modified from Alexander et al., 2008).

5.6.3. Diagenesis and metamorphism

REY and trace metal concentrations in sediments can be affected by mobilization during diagenesis and metamorphism. The effects of diagenesis and metamorphism on REY mobility are a function of water/rock ratios, where LREE depletion and negative Eu anomalies are expected in rocks that host significant amounts of metasomatic fluids during metamorphism (Grauch, 1989; Bau, 1993). Alteration of the REY during post-diagenetic processes in IF and cherts of the Yerbal and Cerro Espuelitas formations is considered unlikely, given the generally accepted low mobility of REE under low water/rock conditions during low-grade regional metamorphism (Bau, 1993). Additionally, the influence of post-depositional processes has been found to be minor in our samples as they display seawater-like anomalies and subparallel patterns in most cases, with no prominent deviation of individual REE.

5.6.4. Redox-sensitive elements

The behaviour of different trace metals is highly variable during diagenesis and depends on the specific pH and Eh conditions during burial (Tribovillard et al., 2006). Redox-sensitive metals, such as U, V, and Mo are insoluble and preferentially concentrated in sediments under anoxic conditions and may be affected by re-oxidation process (Tribovillard et al., 2006; Alibo and Nozaki, 1998; German et al., 1995; Emerson and Huested, 1991; Calvert and Pedersen, 1993).

5.6.4.1. U, V, Mo, and Mn

The concentrations and ratios of redox-sensitive trace elements such as U, V, Mo, and Mn may yield important information about the palaeo-redox conditions during sedimentation (Tribovillard et al., 2006; Morford et al., 2001; Yarincik et al., 2000; Yang et al., 2004; Guo et al., 2007). Diverse trace element ratios and their relative abundances

have been proposed for determining the likely oxygen levels in bottom waters of modern and ancient basins during the formation of a particular facies. Authigenic uranium, U/Th, Th/U, V/Sc, V/Cr, Ni/Co, Ni/V, V/(V+Ni) and (Cu+Mo)/Zn are just some examples of the proxies that have been used to deduce the palaeo-redox conditions of the bottom waters. However, inferences based on a single trace metal distribution are commonly unreliable, because trace metal concentrations are influenced by several factors including clastic contamination, primary productivity rate, organic matter provenance and degree of basin restriction (Tribovillard et al., 2006). Furthermore, trace elements may be mobilized during diagenesis, which can produce elemental distributions that do not reflect "primary" (palaeo-environmental) controls. Based on a case study of Mesozoic mudstones, Jones and Manning (1994) found that only four of the above-mentioned ratios, along with the degree of pyritization (DOP), behaved consistently. Thus, they proposed a tentative correlation chart for the five parameters identified as reliable indices of depositional conditions: DOP, U/Th, authigenic uranium [(authigenic U) = (total U) - (Th/3)], V/Cr and Ni/Co.

The calculated redox indexes for IF, cherts and representative mudstones and shales of the Arroyo del Soldado Group are summarized in Table 5.4. For U/Th, authigenic U and V/Cr the mudstones of the Cerro Espuelitas Formation have the highest average values, and the lowest for Th/U but display relatively low Ni/Co ratios. Comparatively, except for the black siltstones bands which show higher V/Cr ratios, the mudstones of the Yerbal Formation have lower values. Within the Yerbal Formation, the light layers of the banded siltstones -which immediately underlie the IF-, present the highest values for U/Th, authigenic U, V/Cr and Ni/Co, and the lowest Th/U average. With respect to the cherts and IF, there is a slight tendency towards highest ratios (lowest for Th/U) in the Cerro Espuelitas cherts followed, in decreasing order, by the Yerbal cherts, 'Fe-rich' and 'silica-rich' layers from the IF. The last two, however, are quite similar except for V/Cr ratios which are higher in 'Fe-rich' layers whilst the average Ni/Co ratio is higher in the Yerbal cherts. Therefore, the interpretation of these ratios is somewhat difficult because there is not a strong consistency in all the ratios considered for the same lithology or unit. This makes it difficult to decide which ratios are directly

related to palaeo-oxygenation, although they still convey some important information. For example, average ratios of the shales and cherts from the Cerro Espuelitas tend to indicate less oxygenated conditions than those from the Yerbal Formation. Within the latter the picture is more complicated because the oxygen levels seem rather variable, even from band to band and any lithology shows constant oxygen levels in all the ratios used, except for one sample from light bands which invariably shows dysoxic conditions through all the ratios.

On the other hand, the use of trace element concentrations to reconstruct palaeo-environmental conditions also depends on whether they are relatively enriched or depleted relative to shale averages, such as the Post Archaean Australian Sedimentary Rocks (PAAS) (Taylor and McLennan, 1985; Wedepohl, 1991; McLennan, 2001). In this regard, when compared with shales, 'Fe-rich' layers from the Yerbal IF are enriched (in U,V, Mo, Mn) with respect to 'silica-rich' layers and cherts from Yerbal and Cerro Espuelitas formations but all of them are depleted in all the trace metals respect to PAAS (Figure 5.15). With the exception of one sample, siltstones and shales show similar patterns between them with Mn and Co strikingly depleted. Significantly, the patterns of redox-sensitive trace elements, although variable, is quite similar in chemical precipitates and siliciclastics. This is the case of U, V, Mo and less notably Cr all of which are associated with poorly oxygenated conditions (see below). Nonetheless, it is also necessary to consider the possibility that some anomalies may arise from inappropriate normalization as used standard shales are not necessarily representative of the sedimentary rocks in the study area. Thus, one approach to minimize normalization biases is to analyze the stratigraphic variation in enrichment factors or Al-normalized elemental concentrations rather than on absolute values (Tribovillard et al., 2006). Furthermore, if a good correlation exists between certain trace elements and aluminum or titanium (for other normalizing elements see Francois, 1988), which are dominantly of detrital origin and usually immobile during diagenesis, it can be inferred that the trace elements are mainly of detrital provenance and cannot be used for palaeo-environmental analysis (Tribovillard et al., 2006).

Sample	U/Th Oxic (<0.75)	U/Th Dysoxic (0.75-1.25)	U/Th Suboxic & anoxic (>1.25)	Th/U Oxic (2-8.0)	Th/U Anoxic (<2)	Auth. U Oxic (<5.00)	Auth. U Dysoxic (5.00-12.0)	Auth. U Suboxic & anoxic (>12.0)	V/Cr Oxic (<2.00)	V/Cr Dysoxic (2.00-4.25)	V/Cr Suboxic & anoxic (>4.25)	Ni/Co Oxic (<5.00)	Ni/Co Dysoxic (5.00-7.00)	Ni/Co Suboxic & anoxic (>7.00)
Iron Formation / Yerbal Fm. / Fe-rich layers	0.69				1.45	0.29				2.73				
	0.42			2.38		0.12				2.22				
	0.40			2.50		0.10			1.35					
	0.25			4.06		-0.16				3.66		3.73		
	0.24			4.10		-0.16				3.72		3.66		
Yerbal SiO$_2$-RL	0.54				1.86	0.04			0.35					
	0.39			2.59		0.02			0.94			4.09		
	0.39			2.53		0.02			0.71			3.44		
Chert / Yerbal SiO$_2$-RL	0.54				1.87	0.27				3.13			11.61	
		1.22			0.82	0.11			1.52			3.58		
	0.47			2.11		0.04			1.08			4.54		
Co Esp. Fm.			2.92		0.34	0.31			1.12			3.88		
			2.93		0.34	0.32			1.12			3.90		
	0.72				1.40	0.07				2.61		2.65		
			45.88		0.02	2.06			0.10			1.76		
	0.55				1.82	0.06			1.29			3.94		
Mudstones / Yerbal Fm. / Light bands	0.30			3.39		-0.45			1.70					
	0.62				1.61	1.79				3.05				
	0.11			9.19		-2.46			0.78				6.65	
		0.88			1.14		8.29			2.84			5.42	
	0.23			4.36		-1.66			1.64			3.65		
			0.18	5.55		-3.14				2.41				22.14
Red bands	0.16			6.26		-3.11			1.07				5.22	
	0.26			3.86		-1.49				2.00			6.24	
	0.26			3.80		-0.48			1.51					
	0.24			4.22		-1.05			1.14					
Black b.	0.41			2.43		0.96					5.29			10.03
	0.41			2.44		0.95					5.28			10.02
	0.61				1.64	1.92				2.99				
	0.38			2.61		0.42					4.51			
CEFm / GGSt	0.15			6.83		-2.78			0.57				5.28	
	0.20			5.07		-1.32			0.74					
	0.17			6.02		-2.99					4.88			11.36
IBSh	0.48			2.07		2.73				2.64			5.81	
	0.35			2.90		0.13				2.12				
	0.54				1.85	1.68				2.49				

This is often the case for Cr and Co, for example, but only occasionally so for U and rarely for V and Mo (Jones and Manning, 1994; Caplan and Bustin, 1999). When averages values of U, V and Mo -normalised respect to Al- from the different lithologies are compared, some differences arise (Figure 5.16). For example, U/Al in cherts from the Cerro Espuelitas Formation is almost one order of magnitude higher than in other sedimentary rock considered here. In the case of V/Al, the highest ratios are found associated with black shales from the Cerro Espuelitas Formation followed by black siltstones bands of the Yerbal Formation. Conversely, Mo/Al tends to be low in siltstones, with the exception of black shales, and it is higher in cherts and IF.
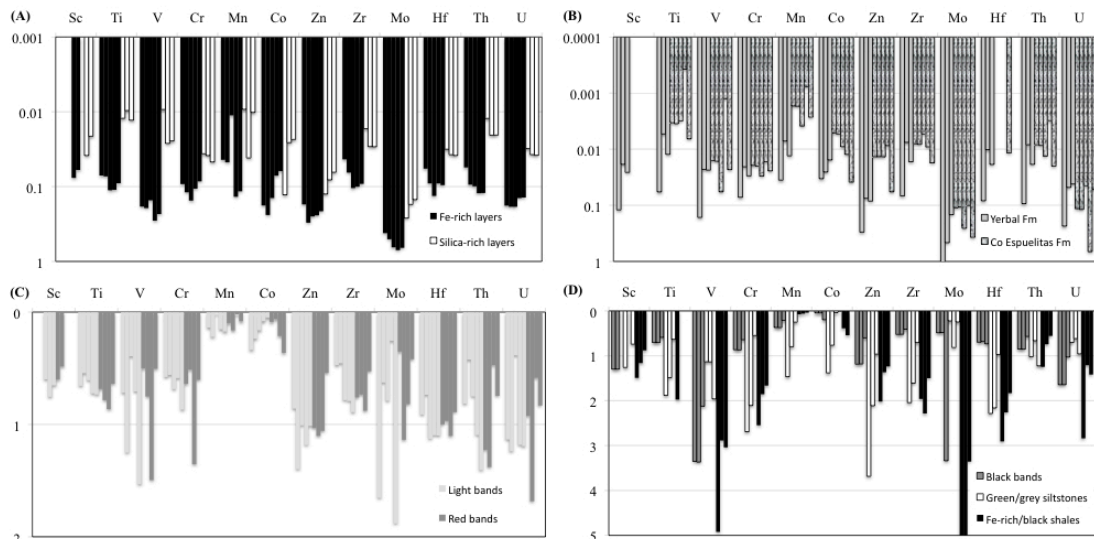
Figure 5.15. Depletion-enrichment diagram for iron formations (iron-rich and silica rich layers) **(A)**, cherts **(B)**, banded siltstones of the uppermost Yerbal Formation **(C)**, and other siltstones of the Yerbal Formation and iron-rich and black shales of the Cerro Espuelitas Formation **(D)**, as compared to Post-Archaean Average Shale (PAAS, McLennan, 1989).
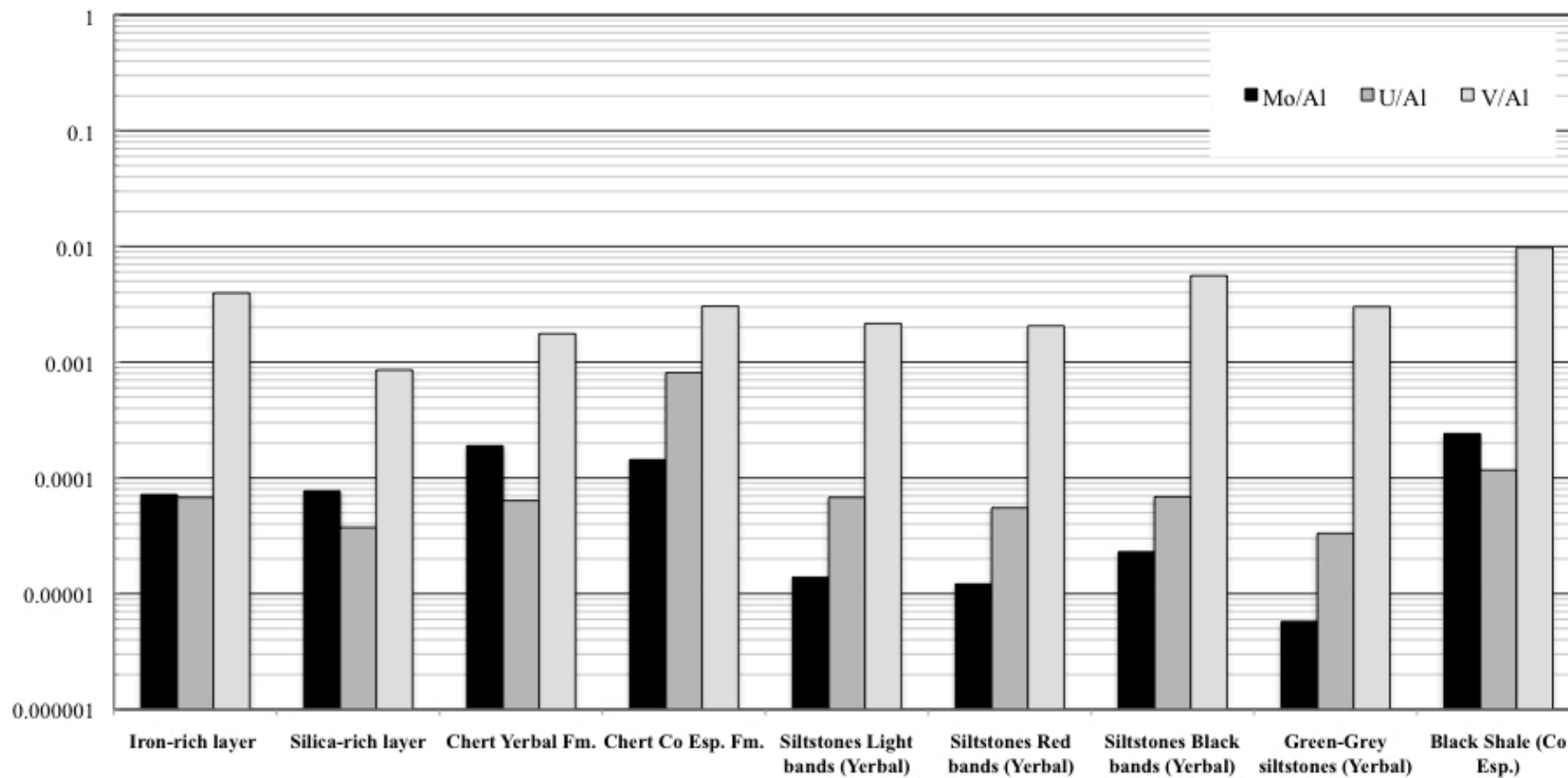
Figure 5.16. Al-normalised average concentrations of selected redox-sensitive trace metals.

As stated above, single elemental ratios do not yield conclusive evidence about the palaeo-redox conditions during the sedimentation of the IF, cherts and mudstones of the Arroyo del Soldado Group. Notwithstanding, when taken in conjunction and normalised with PAAS, chemical precipitates and fine-grained siliciclastics display similar patterns wherein U, V and most importantly Mo show higher ratios in comparison to other elements, whilst Mn and Co show strikingly low values. Both, enrichment and depletions of the above mentioned elements relative to PAAS, along with sedimentological features (e.g., absence of pyrite) suggests sedimentation under oxygen-poor and non-sulfidic (suboxic) conditions. The first scenario is preferred herein for IF and cherts of the Yerbal Formation due to the absence of marked enrichment in redox-proxying elements and the presence of iron-rich deposits (IF: Fe_2O_{3T}=37-40 wt%) lacking of pyrite. Additionally, the presence of abundant hematite in cherts and IF requires somewhat oxygenated seawater during the precipitation of primary iron oxyhydroxides but fully oxic conditions are inconsistent with the uniformly and consistently low Mn concentrations in both lithofacies. Cherts from Cerro Espuelitas Formation, in turn, tend to show a higher enrichment in redox-sensitive elements, than those from the overlying Yerbal Formation, and are associated with pyrite-free 'Fe-rich' and black shales which show the highest calculated redox index average values arguing for more widespread suboxic conditions.

5.6.4.2. Ce anomaly

Of the rare earth elements only Ce and Eu have multiple redox states, occuring in the tetravalent-trivalent and trivalent-divalent states, respectively (McLennan, 1989). Since Ce fractionates from the other REE in oxidizing environments, anomalies of Ce are of particular interest, because they can record redox conditions in the overlying water column and during early diagenesis (German and Elderfield, 1989; Holser, 1997). Modern ventilated deep-ocean waters have large negative Ce anomalies due to oxidation of Ce and removal in hydrogenous deep-sea Mn-Fe nodules and crusts wherein such fractionation produces positive Ce anomalies (Bau and Dulski, 1996). This scenario is

different from the suboxic and anoxic waters (Figure 5.11) in which Ce anomalies are smaller or absent due to reductive dissolution of settling Fe and Mn-oxide particles (e.g., German et al., 1991).

Chert samples from the Cerro Espuelitas Formation display positive Ce anomalies indicating anoxic conditions during precipitation as evidenced by other redox-sensitive elements (see above). Anoxic conditions in the upper Cerro Espuelitas Formation are also supported by redox-sensitive elements documented in 'Fe-rich' and black shales, stratigrpahically below the cherts. Such positive anomalies are absent in older chert and IF of the Yerbal Formation, which in turn, have negative Ce anomalies, with the exception of one sample (050628/17) that shows no anomaly (Figure 5.17). These observations indicate that oxygen concentrations in the water column were sufficient to oxidize Ce during the deposition of the uppermost Yerbal Formation. Comparatively, well-known Palaeoproterozoic and Archaean BIF (Dales Gorge, Temagami and Isua) have positive or non negative Ce anomalies indicating that the oxygen content of seawater was not high enough for the oxidation of Ce (Figure 5.17). Notwithstanding negative Ce depletion in samples from the Arroyo del Soldado Group is accompanied with progressively higher U/Th ratios for each lithology (i.e., negative correlation), which suggests that silica and iron-oxides originated within oxic surface water, and then were deposited under reducing (dominantly suboxic) bottom waters (Figure 5.18).
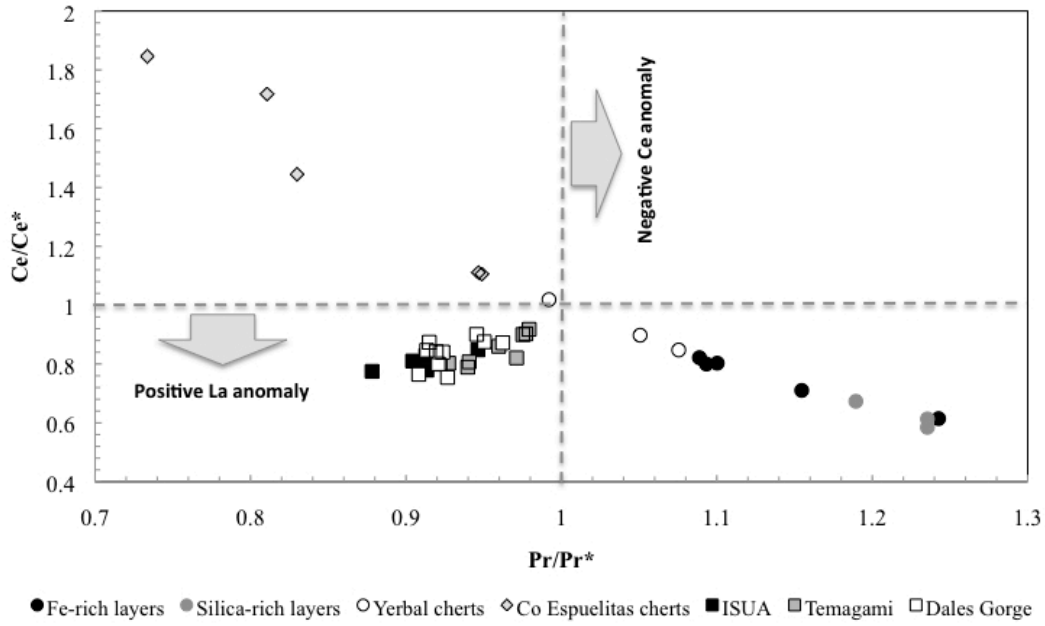
Figure 5.17. Binary plot of Ce/Ce* vs. Pr/Pr* used to identify La and Ce anomalies in seawater derived sediments (see Bau and Dulski, 1996).
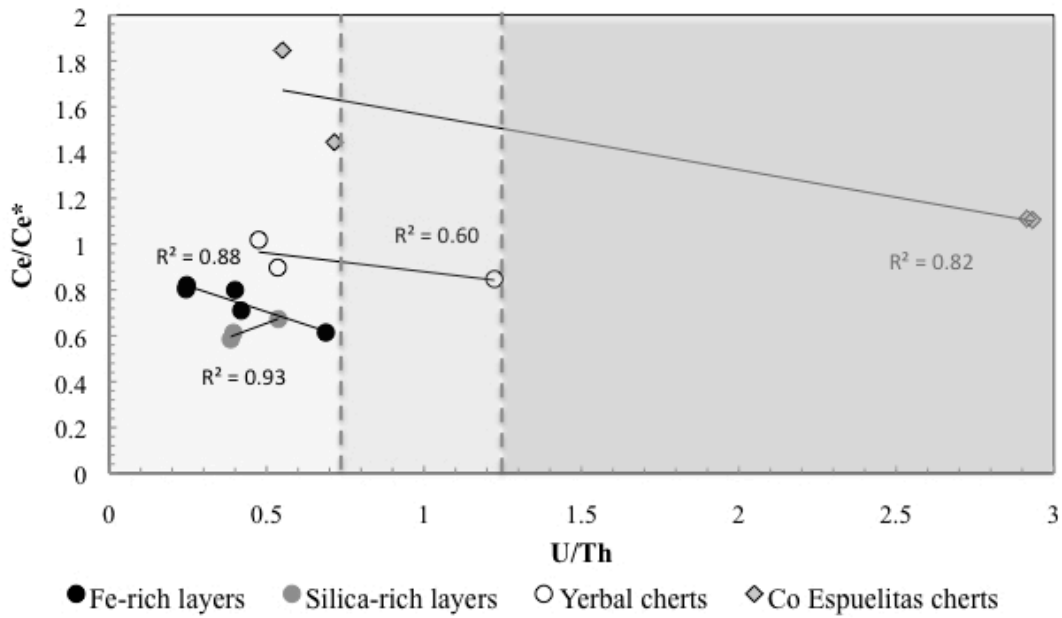

Figure 5.18. Binary plot Ce/Ce* vs. U/Th.

5.7. IMPLICATIONS FOR THE REDOX CHEMISTRY OF THE EDIACARAN OCEAN

Previous studies have suggested that the ocean became increasingly oxygenated after the end of the Marinoan glaciation, which led to the oxidation of deep ocean and eventually the rise of animal life after the Gaskiers glaciation (Fike et al., 2006; Canfield et al., 2007; McFadden et al., 2008; Scott et al., 2008). Alternatively, it has also been proposed that anoxic ferruginous [Fe(II)-enriched] (Canfield et al., 2008) and euxinic conditions [H_2S-containing water column] (Shen et al., 2008) were common below the mean storm wave base by the end of the Neoproterozoic and probably up to the Early Cambrian. In an attempt to reconcile this seemingly conflicting evidence, a recent model invoked the existence of a stratified ocean with coeval oxic, sulfidic and ferruginous zones during that time (Li et al., 2010). Although ferruginous conditions would favour the widespread deposition of 'Fe-rich' sediments, the only evidence supporting Fe(II)-enriched seawater to date is based on the speciation of iron in clastic sedimentary rocks and stable isotopes (C and S) - no IF associated with the Ediacaran has yet been described. Based on the sedimentological, stratigraphical and geochemical features of cherts, IF and associated shales and siltstones from the Yerbal (pre-Gaskiers) and Cerro Espuelitas (post-Gaskiers) formations we propose a simple two-layer stratified system involving suboxic deep seawaters and an oxygenated surface layer.

The anoxic (non-euxinic) to suboxic redox state proposed here for the low- and mid-Ediacaran deep waters (below the mean storm wave base) of the Arroyo del Soldado basin does not concur with previously suggested models that infer either sulfidic (Shen et al., 2008) and oxic (Fike et al., 2006; McFadden et al., 2008; Scott et al., 2008; Canfield, 2007) seawater before and after the Gaskiers glaciations, respectively. The iron speciation study, carried out by Shen et al. (2008), on pyrites from the Sheepbed Formation in Canada and Doshantuo Formation in China, suggested a global deep-water euxinia for ca. 55 Ma after the end-Cryogenian glacial termination at 635 Ma. According to the same authors, the S-isotopic records indicate a rise in sulfate and therefore atmospheric oxygen concentrations; however, early Ediacaran oxygen levels were insufficient to oxidize the deep oceans. Conversely, the deepest water facies from the Yerbal Formation,

represented by pelagic to hemipelagic black mudstones interbedded with turbiditic sandstones, contain no pyrite and present redox parameters indicating anoxic (non-euxinic) bottom waters (Pecoits et al., 2010). Similarly, IF and cherts deposited in a shallower outer shelf setting, always below the mean storm wave base, shows features of being precipitated under a vertically stratified water column conditions characterized by a probably well oxygenated surface layer (ca. 0-75m) and an underlying suboxic zone (>75m) characterized by very low oxygen and sulfide (if any) concentrations (Figure 5.19). In this regard, our results reinforce previous work arguing for a ferruginous ocean before the Gaskiers glaciation (see below).

Deep-sea ventilation would have occurred later, ca. 580 Ma, as recorded by the shift in the ratio of highly reactive iron to total iron (Fe_{HR}/Fe_T) ratios in the Avalon region of Newfoundland (Canfield et al., 2007). The Neoproterozoic sediments of Newfoundland were deposited in deep-water environments well below the photic zone in a basinal, deep-water slope to delta front environments (Canfield et al., 2007 and references therein). The iron content of these sedimentary rocks would imply that the deep ocean was anoxic and ferruginous before and during the Gaskiers glaciation 580 million years ago and that it became oxic afterward (Canfield et al., 2007). Similar data for the Huqf Supergroup in the Sultanate of Oman also indicate that the ocean became increasingly oxygenated after the end of the Marinoan glaciation (Fike et al., 2006), as do results from the Doshantuo Formation (McFadden et al., 2008; Scott et al. 2008) and the Datangpo Formation in south China (Scott et al., 2008). All these studies indicate that the Ediacaran oceans were pervasively oxidized by ca. 551 Ma but differences arise on the initiation of this oxygenation. The study carried out by Fike et al. (2006) in the Huqf Supergroup suggests a three-stage oxidation of the Ediacaran ocean. The first stage occurred immediately after the Marinoan glaciation and corresponds to an increase in sulphate concentrations. Although it is difficult to estimate the magnitude of this increase it would have been appreciably lower than modern values (28 mM). The second stage corresponds with the Shuram (Wonoka/Johnie equivalent) excursion in the carbon isotope record and seems to have involved the oxidation of a large reservoir of organic carbon suspended in the deep ocean, probably the last major redox barrier to ocean
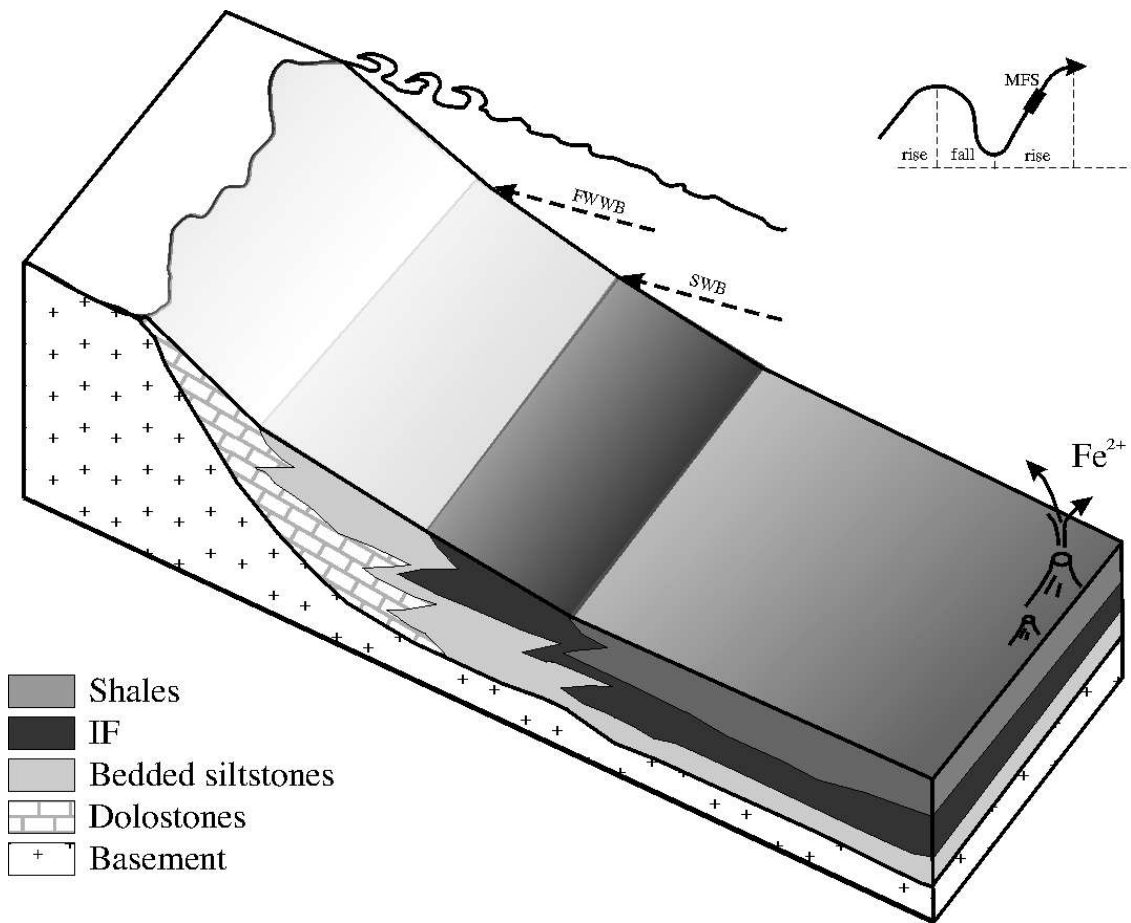
Figure 5.19. Simplified model for the deposition of the Yerbal iron-formation during *late* transgressive system tract (TST). FWWB: fair weather wave base; SWB: storm wave base.

oxygenation. The third and final stage of oxidation of the Ediacaran Ocean is immediately after the Shuram recovery oxidation and is characterized by strong signals of bacterial sulphur disproportionation and covariation in $\delta^{13}C_{carb}$ and $\delta^{13}C_{org}$, coincident with an increase in the diversity of acanthomorph acritarchs and the first appearance of the calcifying metazoa *Namacalthus* and *Cloudina* (see Fike et al., 2006).

The first oxygenation event identified by Fike et al. (2006), which coincides with the Yerbal Formation (i.e., >580 Ma), is recorded in shallow shelf environments (Khufai and Masirah Bay formations) and as a result may not record the redox state of deep seawater. Significantly for our model, iron is oxidized at the oxic-suboxic interface thus supporting oxygenated shallow-marine settings, as proposed by Fike et al. (2006). Similarly, although suboxic environments of the modern ocean are generally restricted to narrow transitional layers between oxic and anoxic waters, they were probably much more extensive when atmospheric and ocean oxygen levels were lower (e.g., Slack et al., 2007). Due to the lack of other Ediacaran IF in the geological literature, comparison with other successions is limited. Nonetheless, this occurrence –together with the geochemical features described here- imply that the deep Ediacaran ocean, around 590-610 Ma, was not uniformly oxygenated. Preliminary $\delta^{13}C_{org}$ have shown a general absence of covariation between $\delta^{13}C_{org}$ and $\delta^{13}C_{carb}$ in the overlying shallow-marine carbonates of the Polanco Limestone Formation (Figure 5.1C). Furthermore, in the absence of glacial deposits in this unit and in light of apparent decoupling of DOC and DIC reservoirs, the negative excursion in $\delta^{13}C_{carb}$ might be interpreted as evidence for episodic oxidation of the large DOC reservoir in the suboxic deep ocean (Pecoits et al., *in press*). This suggests that the bulk of the DOC pool lay below an oxygen chemocline and supports the idea of a redox stratification of the Arroyo del Soldado seawater. Subsequent positive $\delta^{13}C_{carb}$ isotopic excursion in the upper Polanco Limestone Formation and contemporaneous increase of $\Delta\delta^{34}S$ along with BSR -under sulphate-replete conditions- coupled with bacterial sulphur disproportionation (BSD) are consistent with the transition to a more oxidized deep ocean (Fike et al., 2006; McFadden et al., 2008). However, suboxic conditions are also recorded in the post-Gaskiers Cerro Espuelitas Formation where outer shelf non-pyritiferous 'Fe-rich' and black shales along with cherts, showing clear Ce

anomalies, provide evidence for ferruginous seawater below the mean storm wave base. Therefore, full oxygenation of the deep ocean was probably not attained until the uppermost Ediacaran or even lower Cambrian, as previously suggested by Canfield et al. (2008). While anoxic and suboxic conditions apparently dominated the slope and distal shelf settings of the Arroyo del Soldado basin, respectively, the bottom waters of some basins may have been, at least, partially sulfidic but conditioned by overall low oceanic sulfate concentrations (e.g., Li et al., 2010). This would help to explain the seemingly conflicting evidence gathered from other Ediacaran basins.

In summary, the palaeo-environmental trends and geochemical data suggest a co-occurrence of ferruginous deep anoxic waters (>75m) with an oxygenated surface layer. Most likely at the interface between these two layers IF and cherts precipitated. Our new results reinforce previous work showing ostensible ferruginous conditions before the Gaskiers glaciation (ca. 580 Ma), as evidenced by the deposition of oxide-facies IF and the geochemical features of associated rocks. Notwithstanding this conditions were sustained after the Gaskiers glaciation, which caused the deposition of pyrite-free 'Fe-rich' and black shales overlaid by thick cherts hosting positive Ce anomalies.

5.8. CONCLUSIONS

Through the application of sequence stratigrpahic concepts, the ~2500m thick sedimentary succession of the Arroyo del Soldado Group, ranging in age from ca. 610 to 560 Ma, has been divided into two stratigraphic sequences. Based on facies stacking patterns a more detailed subdivision showing the depositional system tracts has been possible. Sequence A includes the Yerbal and Polanco Limestone formations whilst sequence B, separated from the former by a regional erosional unconformity, consists of the Barriga Negra and Cerro Espuelitas formations. The basal and mainly siliciclastic Yerbal Formation records transgressive system tracts (TST) passing upward to high stand (HST) and falling stage system tracts (FSST) infilling the carbonate ramp system represented by the Polanco Limestone Formation. The succeeding alluvial Barriga Negra

and marine Cerro Espuelitas formations, capping the erosional unconformity that divides both stratigraphic sequences, were deposited during low stand system tracts (LST) followed by TST and culminating in HST. Significantly, the top of the TST in both sequences, which marks the maximum flooding surface (MFS) and a period of extreme sediment starvation, are represented by iron formations (IF) and cherts as well as associated 'Fe-rich' and black shales, and banded siltstones, which encompass pre- (Yerbal Formation) and post-Gaskiers scenarios (Cerro Espuelitas Formation).

The analysis of rare earth elements plus yttrium (REY) patterns of these IF and cherts has allowed us to identify genuine seawater signatures typical of marine chemical sediments, consistent with a marine depositional setting. The negative Eu anomalies in all the IF and chert samples suggests that high-T hydrothermal fluids did not exert any influence over the seawater from which they precipitated. This constitutes a substantial difference when compared with other well-studied Archaean-Palaeoproterozoic BIF, which display positive –although variable- Eu anomalies. Furthermore, Arroyo del Soldado samples show significantly higher Sm/Yb ratios than older BIF. Taken in conjunction, the lack of Eu anomalies and the higher Sm/Yb ratios, account for a low-T hydrothermal fluid component during IF and chert precipitation. The presence of Ce anomalies in all of the IF and chert samples from the Yerbal Formation indicates the presence of oxygen in shallow waters. Redox-sensitive element concentrations from the same samples, in turn, suggest rather suboxic conditions and define negative-correlations with Ce/Ce*. This contrasted redox-sensitive element concentrations and Ce anomalies suggest that the upper seawater layer had enough oxygen to oxidizes Ce(III) to Ce(IV) and a lower suboxic zone from were IF and chert precipitated and acquired suboxic redox signatures. Cherts from the Cerro Espuelitas Formation, however, show positive Ce anomalies and larger enrichments in redox-sensitive elements indicating even more widespread anoxic (non-sulfidic) conditions.

Therefore, based on sedimentological and geochemical evidence, we envisage IF and cherts being deposited in an outer shelf setting (ca. 50-100m) at the oxic/suboxic interface, which separated a lower anoxic (non-sulfidic) deep-water layer (>100m) and a superficial and well-oxygenated seawater layer (<50m). This scenario is supported by:

the absence of marked enrichment in redox-proxying elements and the presence of iron-rich deposits (IF and hematite-bearing cherts) with very low Mn concentrations, Ce anomalies and no pyrite (suboxic zone); positive Ce anomalies and larger enrichment in redox-sensitive elements in Cerro Espuelitas cherts and associated pyrite-free 'Fe-rich' and black shales (anoxic zone). Hence, our data suggest that neither sulfidic nor fully oxic conditions were widespread in the deep ocean between 610-560 Ma. Anoxic (non-sulfidic) deep seawater is consistent with low sulfate levels. In a low sulfate anoxic-suboxic ocean, a larger portion of the hydrothermal Fe flux would extend farther from submarine vents facilitating the precipitation of Ediacaran IF and cherts. Crucially, our results not only confirm previous work arguing for a rather ferruginous ocean before the Gaskiers glaciation but also demonstrates that similar conditions were sustained even after the Gaskiers glaciation.

5.9. REFERENCES

Alexander, B.W., Bau M., Anderson, P., Dulski, P., 2008. Continentally-derived solutes in shallow Archean seawater: Rare earth element and Nd isotope evidence in iron formation from the 2.9 Ga Pongola Supergroup, South Africa. Geochim. Cosmochim. Acta. 72, 378-394.

Alibo, D.S., Nozaki Y., 1999. Rare earth elements in seawater: particle association, shale-normalization, and Ce oxidation. Geochim. Cosmochim. Acta. 63, 363-372.

Anders, E., Grevesse, N., 1989. Abudances of the elements: meteoric and solar. Geochim. Cosmochim. Acta. 53, 197-214.

Bau, M., 1991. Rare earth element mobility during hydrothermal and metamorphic fluid–rock interaction and the significance of the oxidation state of europium. Chem. Geol. 93, 219-230.

Bau, M., 1993. Effects of syn- and post-depositional processes on the rare-earth element distribution in Precambrian iron-formations. Eur. J. Mineral. 5, 257-267.

Bau, M., 1999. Scavenging of dissolved yttrium and rare earths by precipitating iron oxyhydroxide: experimental evidence for Ce oxidation, Y–Ho fractionation, and lanthanide tetrad effect. Geochim. Cosmochim. Acta. 63, 67-77.

Bau, M., Dulski, P., 1992. Small-scale variations of the rareearth element distribution in Precambrian iron formations. Eur. J. Mineral. 4, 1429–1433.

Bau, M., Dulski, P., 1996. Distribution of yttrium and rare-earth elements in the Penge and Kuruman iron-formations, Transvaal Supergroup, South Africa. Precamb. Res. 79, 37-55.

Bau, M., Dulski, P., 1999. Comparing yttrium and rare earths in hydrothermal fluids from the Mid-Atlantic Ridge: implications for Y and REE behaviour during near-vent mixing and for the Y/Ho ratio of Proterozoic seawater. Chem. Geol. 155, 77-90.

Bau, M., Möller, P., 1993. Rare earth element systematics of the chemically precipitated component in Early Precambrian iron formations and the evolution of the terrestrial atmosphere–hydrosphere–lithosphere system. Geochim. Cosmochim. Acta. 57, 2239-2249.

Bau, M., Koschinsky, A., Dulski, P., Hein J.R., 1996. Comparison of the partitioning behaviours of yttrium, rare earth elements, and titanium between hydrogenetic marine ferromanganese crusts and seawater. Geochim. Cosmochim. Acta. 60, 1709-1725.

Beukes, N, J., Klein, C .1992, Models for iron-formation deposition. In, Schopf J.W. and Klein, C., eds., The Proterozoic biosphere A: multidisciplinary study. Cambridge Cambridge Univ. Press, pp. 147-151.

Blair, T.C., McPherson, J.G., 1994. Alluvial fan processes and forms. In: (Eds. A.D., Abrahams, A., Parsons), Geomorphology of Desert Environments, Chapman & Hall, London, pp. 354-402.

Blanco, G., Rajesh, H.M., Gaucher, C., Germs, G.J.B., Chemale Jr., F., 2009. Provenance of the Arroyo del Soldado Group (Ediacaran to Cambrian, Uruguay): Implications for the paleogeographic evolution of southwestern Gondwana. Precambrian Res. 171, 57-73.

Bolhar R., Kamber B.S., Moorbath S., Fedo C.M., Whitehouse M.J., 2004. Characterisation of early Archaean chemical sediments by trace element signatures. Earth Planet. Sci. Lett. 222, 43-60.

Breitkopf, J.H., 1988. Iron formations related to mafic volcanism and ensialic rifting in the southern margin zone of the damara orogen, Namibia. Precambrian Res. 38, 111-130.

Burchette, T.P., Wright, V.P., 1992. Carbonate ramp depositional systems. Sediment. Geol. 79, 3-57.

Calvert, S.E., Pedersen, T.F., 1993. Geochemistry of Recent oxic and anoxic marine sediments: Implications for the geological record. Mar. Geol. 113, 67-88.

Canfield, D.E., Poulton, S.W., Knoll, A.H., Narbonne, G.M., Ross, G., Goldberg, T.,Strauss, H., 2008. Ferruginous conditions dominated later Neoproterozoic deep-water chemistry. Science. 321, 949-952.

Canfield, D.E., Poulton, S.W., Narbonne, G.M., 2007. Late Neoproterozoic deep-ocean oxygenation and the rise of animal life. Science. 315, 92-95.

Caplan, M.L., Bustin, R.M., 1999. Devonian-Carboniferous Hangenberg mass extinction event, widespread organic-rich mudrock and anoxia: causes and consequences. Palaeogeo. Palaeoclim. Palaeoecol. 148, 187-207.

Chavagnac, V. German, C.R. Milton, J.A. Palmer M.R., 2005. Sources of REE in sediment cores from the Rainbow vent site (36°14′N, MAR). Chem. Geol. 216, 329-352.

Chester, R., 2000. Marine Geochemistry, 2nd ed. Blackwell Science, Oxford, pp. 506.

Davies, G.R., 1977. Carbonate-Anhydrite Facies Relations in Otto Fiord Formation (Mississippian-Pennsylvanian), Canadian Arctic Archipelago Graham. AAPG Bulletin 61, 1929-1949.

De Baar, H.J.W., Bacon, M.P., Brewer, P.G., 1985. Rare earth elements in the Pacific and Atlantic Oceans. Geochim. Cosmochim. Acta. 49, 1943-1959.

Derry, L.A., Jacobsen, S.B., 1990. The chemical evolution of Precambrian seawater: evidence from rare earth elements in banded iron formations. Geochim. Cosmochim. Acta. 54, 2965-2977.

Einsele, G., 1991. Submarine mass flow deposits and turbidites. In: (Eds. G., Einsele, W., Ricken, A., Seilacher), Cycles and events in stratigraphy. Springer- Verlag, New York, pp. 313-339.

Einsele, G., 2000. Sedimentary Basins. Evolution, Facies, and Sediment Budget, 2nd ed. Berlin, Springer-Verlag, New York, pp. 792.

Elderfield, H., 1988. The oceanic chemistry of the rare-earth elements. Phil. Trans. R. Soc. London Ser. A 325, 105-126.

Elderfield, H., Upstill-Goddard, R., Sholkovitz, E. R., 1990. The rare earth elements in rivers, estuaries, and coastal seas and their significance to the composition of ocean waters. Geochim. Cosmochim. Acta. 54, 971-991.

Edmonds, H.N., German, C.R., 2004. Particle geochemistry in the Rainbow hydrothermal plume, Mid-Atlantic Ridge. Geochim. Cosmochim. Acta. 68, 759-772.

Emerson, S.R., Husted, S.S., 1991. Ocean anoxia and the concentrations of molybdenum and vanadium in sea-water. Mar. Chem. 34, 174-196.

Fike, D.A., Grotzinger, J.P., Pratt, L.M., Summons, R.E., 2006. Oxidation of the Ediacaran ocean. Nature. 444, 744-747.

Fischer, W.W., Knoll, A.H., 2009. An iron shuttle for deepwater silica in Late Archean and early Paleoproterozoic iron formation. Geol. Soc. Am. Bull. 121, 222-235.

François, R., 1988. A study on the regulation of the concentrations of some trace metals (Rb, Sr, Zn, Pb, Cu, V, Cr, Ni, Mn and Mo) in Saanich Inlet sediments, British Columbia. Mar. Geol. 83, 285-308.

German, C.R., Klinkhammer, G.P., Edmond, J.M., Mitra, A., Elderfield, H., 1990. Hydrothermal scavenging of rare earth elements in the ocean. Nature. 345, 516-518.

German, C.R., Fleer, A.P., Bacon, M.P., Edmond, J.M., 1991. Hydrothermal scavenging at the Mid-Atlantic Ridge: Radionuclide distributions. Earth Planet. Sci. Lett. 105, 170-181.

German, C.R., Higgs, N.C., Thomson, J., Mills, R., Elderfield, H., Blusztajn, J., Fleer, A.P., Bacon, M.P., 1993. A geochemical study of metalliferous sediment from the TAG hydrothermal mound, 26º08' N, Mid-Atlantic Ridge. J. Geophys. Res. 98, 9683-9692.

German, C.R., Barreiro, B.A., Higgs, N.C., Nelsen, T.A., Ludford, E.M., Palmer, M.R., 1995. Seawater metasomatism in hydrothermal sediments - Escanaba Trough, northeast Pacific. Chem. Geol. 119, 175-190.

German, C.R., Elderfield, H., 1989. Rare earth elements in Saanich Inlet, British Columbia, a seasonally anoxic basin. Geochim. Cosmochim. Acta. 53, 2561-2571.

German, C.R. Holliday, B.P. Elderfield, H., 1991. Redox cycling of rare earth elements in the suboxic zone of the Black Sea, Geochim. Cosmochim. Acta. 55, 3553-3558.

Grauch, R., 1989. Rare earth elements in metamorphic rocks. In: (Eds. B.R., Lipin, G.A., McKay), Geochemistry and Mineralogy of Rare Earth Elements. Rev. Mineral. 21, 147-167.

Guo, L.D., Ping, C. L., MacDonald, R.W., 2007. Mobilization pathways of organic carbon from permafrost to arctic rivers in a changing climate. Geophys. Res. Lett. 34,

L13603, doi10.1029/2007GL030689.

Halverson, G.P., Wade, B.P., Hurtgen, M.T., Barovich., K.M., 2010. Neoproterozoic Chemostratigraphy. Precambrian Research doi:10.1016/j. Precambrian Res. 2010.04.007.

Hartmann, L., Santos, O., Bossi, J., Campal, N., Schipilov A., Mc Naughton, N.J., 2002. Zircon and Titanite U-Pb SHRIMP geochronology of Neoproterozoic felsic magmatism on the eastern border of the Rio de la Plata Craton, Uruguay. J. S. Am. Earth Sci. 15, 229-236.

Hoffmann, K.H., Condon, D.J., Bowring, S.A., Crowley, J.L., 2004. U–Pb zircon date from the Neoproterozoic Ghaub Formation, Namibia: Constrains on Marinoan glaciation. Geology. 32, 817–820.

Holser, W.T., 1997. Geochemical events documented in inorganic carbon isotopes. Palaeogeo. Palaeoclim. Palaeoecol. 132, 173-182.

Hunt, D., Tucker, M.E., 1992. Stranded parasequences and the forced regressive wedge systems tract: deposition during base-level fall. Sed. Geol. 81, 1-9.

James, H. L., 1954. Sedimentary facies of iron-formation. Econ. Geol. 49, 235-293.

Jones, B., Manning, D.A.C., 1994. Comparison of geochemical indices used for the interpretation of paleoredox conditions in ancient mudstones. Chem. Geol. 114, 111-129.

Kawashita, K., Gaucher, C., Sprechmann, P., Teixeira, W., Victória, R., 1999. Preliminary chemostratigraphic insights on carbonate rocks from Nico Perez Terrane (Uruguay). In: Actas, II South Amer. Symp. on Isotope Geology. Córdoba (Argentina), pp. 399-402.

Klein, C., 2005. Some Precambrian banded iron-formations (BIFs) from around the world: their age, geologic setting, mineralogy, metamorphism, geochemistry, and origin. Am. Miner. 90, 1473-1499.

Klein, C., Beukes, N.J., 1993. Sedimentology and geochemistry of the glaciogenic late Proterozoic Rapitan ironformation, in Canada. Econ. Geol. 80, 542-565.

Klein, C., Ladeira, E.A., 2004. Geochemistry and Mineralogy of Neoproterozoic Iron-formations and some selected Siliceous Manganese Formations from the Urucum District, Mato Gross do Sul, Brazil. Econ. Geol. 99, 1233-1244.

Krapêz, B., Barley, M.E., Pickard, A.L., 2003. Hydrothermal and resedimented origins of the precursor sediments to banded iron-formation: sedimentological evidence from the Early Palaeoproterozoic Brockman Supersequence of Western Australia. Sedimentology. 50, 979-1011.

Kulaksiz S., Bau M., 2007. Contrasting behaviour of anthropogenic gadolinium and natural rare earth elements in estuaries and the gadolinium input into the North Sea. Earth Planet. Sci. Lett. 260, 361-371.

Lawrence, M.G., Kamber, B.S., 2006. The behaviour of the rare earth elements during estuarine mixing-revisited. Mar. Chem. 100, 147-161.

Li, Ch., Love, G.D. Lyons, T.W., Fike, D.A., Sessions, A.L Chu, X., 2010. A Stratified Redox Model for the Ediacaran Ocean. Science. 328, 80-83.

Lottermoser, B.G, Ashley, P.M., 2000. Geochemistry, petrology and origin of Neoproterozoic ironstones in the eastern part of the Adelaide Geosyncline South Australia. Precambrian Res.101, 49-67.

Maliva, R.G, Knoll, A.H., Simonson, B.M., 2005. Secular change in the Precambrian silica cycle: Insights from chert petrology. Geol. Soc. Am. Bull. 117, 835-845.

McFadden, K.A., Huang, J., Chu, X., Jiang, G., Kaufman, A.J., Zhou, Ch., Yuan., X., Xiao, S., 2008. Pulsed oxidation and biological evolution in the Ediacaran Doushantuo Formation. Proc. Natl. Acad. Sci. U.S.A. 105, 3197-3202.

McLennan, S.M., 1989. Rare earth elements in sedimentary rocks: influence of

provenance and sedimentary processes. In: (Eds. B.R., Lipin, G.A., McKay), Geochemistry and Mineralogy of Rare Earth Elements. Rev. Mineral. 21, 169-200.

McLennan, S.M., 2001. Relationships between the trace element composition of sedimentary rocks and upper continental crust. Geochem. Geophy. Geosy. 4, 1021-1025.

Michard, A., 1989. Rare earth element systematics in hydrothermal fluids. Geochim. Cosmochim. Acta. 53, 745-750.

Michard, A., Michard, G., Stoben, D., Stoffers, P., Cheminée, J-L., Binard, N., 1993. Submarine thermal springs associated with young volcanoes: The Teahitia vents, Society Islands, Pacific Ocean Geoch. Cosmochim. Acta. 57, 4977-4986

Morford, J.L., Russell, A.D., Emerson, S., 2001. Trace metal evidence for changes in the redox environment associated with the transition from terrigenous clay to diatomaceous sediment, Saanich Inlet, B.C. Mar. Geol. 174, 355-369.

Narbonne, G.M., 2005. The Ediacaran biota: Neoproterozoic origin of animals and their ecosystems. Ann. Rev. Earth Planet. Sci. 33, 421-442.

Pecoits, E, Aubet N.R, Gingras, M.K., Muehlenbachs, K., Konhauser, K.O., 2010b. Chemostratigraphy and trace elements of the Ediacaran Polanco Limestone Formation (Uruguay). Chemical Geology (in review).

Pecoits, E., Gingras, M.K., Barley, M., Kappler, A., Posth, N., Konhauser, K.O., 2009. Petrography and Trace Element Geochemistry of Dales Gorge Banded Iron Formation: Paragenetic Sequence, Source and Implications for the Palaeo-ocean Chemistry. Precambrian Res. 172, 163-187.

Pecoits, E., Gingras, M.K., Aubet, N.R., Konhauser, K.O., 2008. Ediacaran in Uruguay: palaeoclimatic and palaeobiologic implications. Sedimentology. 55, 689-719.

Pecoits, E., Lalonde, S.V., Kamber, B., Konhauser, K.O., 2008. REE and Y compositions of Archean and Paleoproterozoic Banded Iron-Formations. Goldschmidt Conference. Geochim. Cosmochim. Acta.

Pecoits, E., Konhauser, K.O., Aubet, N.R., Heaman, L.M., Veroslavsky, G., Gingras, M.K., 2010. Evidence of early Ediacaran bilaterians. Science (in 2nd review).

Pichler, T., Veizer, J., Hall, G.E.M., 1999. The chemical composition of shallow-water hydrothermal fluids in Tutum Bay, Ambitle Island, Papua New Guinea and their effect on ambient seawater. Mar. Chem. 64, 229-252.

Pickard, A.L., Barley, M.E., Krapez, B., 2004. Deep-marine depositional setting of Banded iron formation: sedimentological evidence from interbedded clastic sedimentary rocks in the early Paleoproterozoic Dales Gorge Member of Western Australia. Sed. Geol. 170, 37–62.

Piper, D.Z., 1994. Seawater as the source of minor elements in black shales, phosphorites and other sedimentary rocks. Chem. Geol. 114, 95-114.

Piper, D.Z., Isaacs, C.M., 1994. Seawater as a source of minor elements in black shales, phosphorites, and other sedimentary deposits. Canadian Society of Petroleum Geologists Annual Meeting, Calgary.

Posamentier, H.W., Jervey, M.T., Vail, P.R., 1988. Eustatic controls on clastic deposition. I. Conceptual framework. In: (Eds. Wilgus, C.K., Hastings, B.S., Kendall, C.G.St.C., Posamentier, H.W., Ross, C.A., Van Wagoner, J.C.), Sea Level Changes-An Integrated Approach, Vol. 42. SEPM Spec. Pub., pp. 110-124.

Poulton, S.W., Fralick, P.W., Canfield, D.E., 2004. The transition to a sulphidic ocean ~1.84 billion years ago. Nature, 431, 173-177.

Puteanus, D., Glasby G.P., Stoffers P., Kunzendorff H., 1991. Hydrothermal iron-rich deposits from the Teahitia-Mehitia and Macdonald hot spot areas, Southwest Pacific Mar. Geol. 98, 389-409.

Read, J.F., 1985. Carbonate platform facies models. AAPG Bull. 69, 1-21.

Schröder, S., Grotzinger, J.P., 2007. Evidence for anoxia at the Ediacaran-Cambrian boundary: the record of redox-sensitive trace elements and rare earth elements in Oman. J. Geol. Soc., London. 164, 175-187.

Scott, C., Lyons, T.W., Bekker, A., Shen, Y., Poulton, S. W., Chu, X., Anbar, A.D., 2008. Tracing the stepwise oxygenation of the Proterozoic ocean. Nature. 452, 456-459.

Shen, Y., Zhang, T., Hoffman, P. F., 2008. On the coevolution of Ediacaran oceans andanimals. Proc. Nat. Acad. Sci. U.S.A.105, 7376–7381.

Shields, G., Stille P., 2001. Diagenetic constraints on the use of cerium anomalies as palaeoseawater redox proxies: an isotopic and REE study of Cambrian phosphorites. Chem. Geol. 175, 29-48.

Sholkovitz E. R., 1994. The aquatic chemistry of rare earth elements in rivers and estuaries. Aqua. Geochem. 1, 3-34.

Simonson, B.M., 1985. Sedimentology of cherts in the Early Proterozoic Wishart Formation, Quebec-Newfoundland, Canada. Sedimentology. 32, 23-40.

Slack, J.F., Grenne, T., Bekker, A., Rouxel, O.J., Lindberg, P.A., 2007. Suboxic deep seawater in the late Paleoproterozoic: Evidence from hematitic chert and iron formation related to seafloor-hydrothermal sulfide deposits, central Arizona, USA. Earth Plan. Sci. Lett. 255, 243-256.

Stow, D.A.V., A. Wetzel., 1990. Hemiturbidite: a new type of deep water sediment. J.R. Cochran and D.A.V. Stow. Proceedings ODP Scientific Results. 116: 25-34.

Stow, D.A.V., Huc, A.Y., Bertrand, P., 2001. Depostional processes of black shales in deep water. Mar. Pet. Geol. 18, 491-498.

Taylor S.R., McLennan, S.M., 1985. The continental crust: its composition and evolution.

Blackwell Scientific, Oxford, pp. 312.

Trendall, A.F., 2002. The significance of iron-formation in the Precambrian stratigraphic record. In: (Eds. W., Altermann, P.L., Corcorane), Precambrian Sedimentary Environments: A Modern Approach to Depositional Systems. IAS Special Publication 44. Blackwell Science, Oxford.

Tribovillard, N., Algeo, T., Lyons, T.W., Riboulleau, A., 2006. Trace metals as paleoredox and paleoproductivity proxies: an update. Chem. Geol. 232, 12-32.

Tucker, M.E., 1977. Stromatolite biostromes and associated facies in the late precambrian porsanger dolomite formation of Finnmark, Arctic Norway. Palaeogeog. Palaeocl. Palaeoec. 21, 55-83

Wedepohl, K.H., 1991, Chemical composition and fractionation of the continental crust: Geologische Rundsch. 80, 207-223.

Wetzel, A., Balson, P., 1992. Sedimentology of fine-grained turbidites inferred from continuously recorded physical properties data. Mar. Geol. 104, 165-178.

Wheat, C.G., Mottl, M.J., Rudnicki, M., 2002. Trace element and REE composition of a low-temperature ridge-flank hydrothermal spring. Geochim. Cosmochim. Acta. 66, 3693-3705.

Yang, S.Y., Lim, D.I., Jung, H.S., Oh, B.C., 2004. Geochemical composition and provenance discrimination of coastal sediments around Cheju Island in the southeastern Yellow Sea. Mar. Geol. 206, 41-53.

Yarincik, K.M., Murray, R.W., Peterson, L.C., 2000. Climatically sensitive eolian and hemipelagic deposition in the Cariaco Basin, Venezuela, over the past 578,000 years: results from Al/Ti and K/Al. Paleoceanography 15, 210-228.

Zhang, J., Amakawa, H., Nozaki, Y., 1994. The comparative behaviors of Yttrium and Lanthanides in the seawater of the North Pacific. Geophys. Res. Lett. 21, 2677-2680.

CHAPTER 6: EVIDENCE OF EARLY EDIACARAN BILATERIANS

6.1. INTRODUCTION

Animals with bilateral symmetry, segmentation, and musculature most probably emerged in the Neoproterozoic and were a major part of the subsequent Cambrian "explosion", but it has proven difficult to date the appearance of the first bilaterians. Recent molecular clock analyses give dates ranging from 1153-1443 Ma (Hedges, et al., 2004) to 580-635 Ma (Peterson and Butterfield, 2005; Peterson et al., 2008) for the emergence of stem-group bilaterians, but no definite bilaterian fossils had previously been found within this broad time interval. Putative microscopic bilaterian fossils from the Doushantou Formation in China (Chen et al., 2004) are probably about 580 Ma in age (Condon et al., 2005), but their attribution to bilaterians remains controversial (Bengston and Budd, 2004; Conway-Morris, 2006). Similarly, putative burrow systems back to 2.1 Ga have been described, but only those younger than about 555 Ma satisfy the strict criteria for bilaterian burrows (Jensen et al., 2005). The oldest reasonably accepted evidence for bilaterians had come from fossil burrows - also known as trace fossils - and probable body fossils such as *Kimberella* in shallow-water deposits from Russia that are approximately 555 Ma (Fedonkin and Waggoner, 1997). In the present study we report indisputable bilaterian burrows from shallow-water Ediacaran sediments in Uruguay that are as much as 25 million years older than the putatively reported trace fossils mentioned above.

6.2. EDIACARAN TRACE FOSSILS

One of the profound evolutionary changes that took place during the Ediacaran is associated primarily with the rise of animal life. Significantly, and although it is rarely possible to determine the trace-making organism, one of the most important sources of

fossil evidence for the early evolution of animals consists of trace fossils. The first trace fossils are, by a large extent, two-dimensional surface-movement structures (*Repichnia* of Seilacher, 1964). They are parallel to sea floor surfaces and were preserved in sediments deposited in relatively shallow water – examples being *Planolites, Nenoxites, Aulichnites, Bulinichnus and Helminthoidichnites* (Fedonkin et al., 2007). True grazing ichnofossils (*Pascichnia*), however, do not occur until 555 million years ago, when the likely metazoan *Kimberella* -a mollusk-like, bilaterally symmetrical, benthic animal with a soft and unmineralized shell- appeared (Fedonkin and Waggoner, 1997).

Ediacaran metazoans were not capable of burrowing bottom sediments. The change from two-dimensional biomat-related life styles to three-dimensional plowing and deep burrowing, called the "Agronomic Revolution" by Seilacher and Pfluger (1994), did not occur until the Ediacaran-Cambrian transition. This change was most likely favored as a way to escape from predators (Dzik, 2007) and/or the advent of mining for food (Seilacher and Pfluger, 1994). As pointed out by Seilacher (2007), neither the radiation of metazoans (Cambrian "explosion") nor the ecological revolution ("Agronomic Revolution") were globally instantaneous and both started in shallow marine environments and subsequently spread into deep-sea bottoms. Even though shallow marine Ediacaran deposits are characterized by a relatively low ichnofossil diversity dominated by horizontal simple traces and shallow burrows, there is some variety that reflects a number of different feeding strategies related to the exploitation of microbial matgrounds (Hagadorn and Bottjer, 1999; Jensen, 2003; Porada et al., 2008). These matgrounds also appear to have played a fundamental role in the nature of fossil preservation wherein Ediacaran animals moving over the mats might not leave trails that would be preserved unless they could break through, furrow into them or dissolve away these mats (Fedonkin et al., 2007).

In South America, Ediacaran trace fossils have been documented in a number of localities, such as the Itajaí and Camaquã basins in Brazil, and the Puncoviscana Formation located in Argentina. In the Itajaí and Camaquã basins, preliminary studies recorded several ichnotaxa including, *Helminthoidichnites sp., Oldhamia, Bifungites,*

Gordia, Didymaulichnus, Intrites, Planolites, Cochlichnus, Cruziana, Didymaulichnus, Gyrolithes, Rusophycus and *Skolithos* (Netto et al., 1992, Da Rosa, 2005; Netto and Da Rosa, 1997). The trace fossils of the better studied Puncoviscana Formation are represented by the *Nereites* (shallower sedimentary facies) and *Oldhamia* (deeper sedimentary facies) ichnoassociations, and include: *Archaeonassa fossulata, Asaphoidichnus sp., Cochlichnus anguineus, Didymaulichnus lyelli, Dimorphichnus obliquus, Diplichnites sp., Glockerichnus sp., Helminthoraphe sp., Helminthopsis abeli, H. tenuis, Helminthoidichnites tenuis, Monomorphichnus lineatus, M. isp., cf. Multipodichnus, Nereites saltensis, Neonereites uniserialis, N. biserialis, Oldhamia alata, O. antiqua, O. curvata, O. flabellata, O. geniculata, O. radiata, cf. Thalassinoides isp., Palaeophycus tubularis, Palaeophycus isp., Protichnites isp., Protovirgularia isp., Tasmanadia cachii, Treptichnus isp., Treptichnus cf. aequalternus* and *T. pollardi*, and a variety of undetermined arthropod-related scratch marks and isolated imprints (Aceñolaza and Aceñolaza, 2007 and references therein). No trace fossils have been recorded by previous studies in Ediacaran successions of Uruguay.

6.3. STRATIGRAPHY AND AGE

The fossil burrows documented here come from the Tacuarí Formation in east-central Uruguay (Figure 6.1). The Tacuarí Fm. comprises basal diamictites, sandstones and minor pelites that grade upwards into finegrained rhythmites containing abundant out-sized clasts. The latter, interpreted as dropstones, along with diamictites hosting faceted and striated clasts and associated varved sediments, provide definitive evidence for the glacial origin of these deposits. Trace fossils in the Tacuarí Fm. occur within the uppermost fine-grained rhythmites that mark the last waning stages of glaciation.

A U-Pb zircon age (TIMS) obtained from an intrusive (granitic) complex that crosscuts and deforms the Tacuarí Fm. places a minimum age of the unit to 561±9 Ma (see Figure S.1 and Table S.1-Apendix I). A heat affected zone is observed locally in the Tacuarí

strata at the Tacuarí/pluton contact: the granite shows a well developed chill-margin at the discontinuity. This intrusive contact occurs approximately 5 m below - in continuous section - one of the three trace-fossil quarries and is 150 m along strike from a second quarry. The age of the Tacuarí Fm. is also regionally constrained by numerous radiometric ages of intrusive syenites and granites (ca 520-530 Ma), overlying rhyolitic flows (ca 575 Ma), cross-cutting strike-slip and thrust faults (ca 570-580 Ma) and the occurrence of the upper Ediacaran index fossil *Cloudina* (~550-540 Ma) in overlying strata (Figure 6.1) (Pecoits et al., 2008). ^{40}Ar/^{39}Ar data for intrusives and basalts of the lowermost Maldonado Group (correlative of the Tacuarí Fm.) also constrain the age of deposition between 579.0±1.5 and 615±30 Ma (Pecoits et al., 2008, Oyhantçabal et al., 2006). Recent analysis of detrital zircons (SHRIMP U-Pb) from the basement of the Maldonado Group show ages between 3,400 and 600 Ma and provides a new maximum depositional age for the unit (Basei et al., 2008). The acritarch assemblage previously described in the Tacuarí Fm (Veroslavsky et al., 2006) is consistent with the Ediacaran Leiosphere Palynoflora, deposited between ca. 635 and 582 Ma (Grey, 2005). This combination of radiometric and paleontological dates indicates that the age of the Tacuarí Fm. is early Ediacaran, most likely Gaskiers in age (ca. 580 Ma).

Figure 6.1. Sample location and generalized cross-section of Neoproterozoic-Cambrian units of Uruguay detailing the stratigraphic section of the Tacuarí Formation and the location of trace fossils.

6.4. TRACE FOSSILS OF THE TACUARÍ FORMATION

Trace fossils from the Tacuarí Fm. are preserved on bedding planes in two ways (Figure 6.2, S.2-Appendix I). The first preservational mode is as bilobate grooves, locally containing a beaded backfill (inset Figure 6.2A, 6.2G). Where present, the beaded backfill comprises very small, ovate sediment piles, the long axis of which are oriented transverse to the burrow length. The second mode of preservation is as irregular to massively filled burrows that generally exhibit minor positive relief from the lamination surfaces and commonly show collapse features on their tops (Figure 6.2B). Both types of burrows are 2-3 mm in width, and some of the collected specimens pass laterally from one form to the other along the length of the burrow. The trace fossils commonly possess raised lateral ridges adjacent to the burrow margins. Rarely, small circular indentations are preserved near the edges of bilobate furrows (inset Figures 6.2D, 6.2H). The dents are approximately 0.5 mm in diameter and serially emplaced along the trail. Plan-view morphology ranges from sinuous to sinusoidal (Figures 6.2B-6.2C). Abrupt adjustments in curve radius accompanied by slight lateral jumps are also observed. Three of the specimens show the burrow abruptly leaving the plane of preservation and reappearing 4-10 mm away. The small amplitude of the sinusoidal burrows likely inhibits single burrows from crossing. Several instances of one burrow crossing another with no evidence of avoidance are observed (Figure 6.2A). In three examples a later burrow intersects a pre-existing burrow, turns and follows the earlier structure, then resumes its initial trajectory (Figure 6.2F).
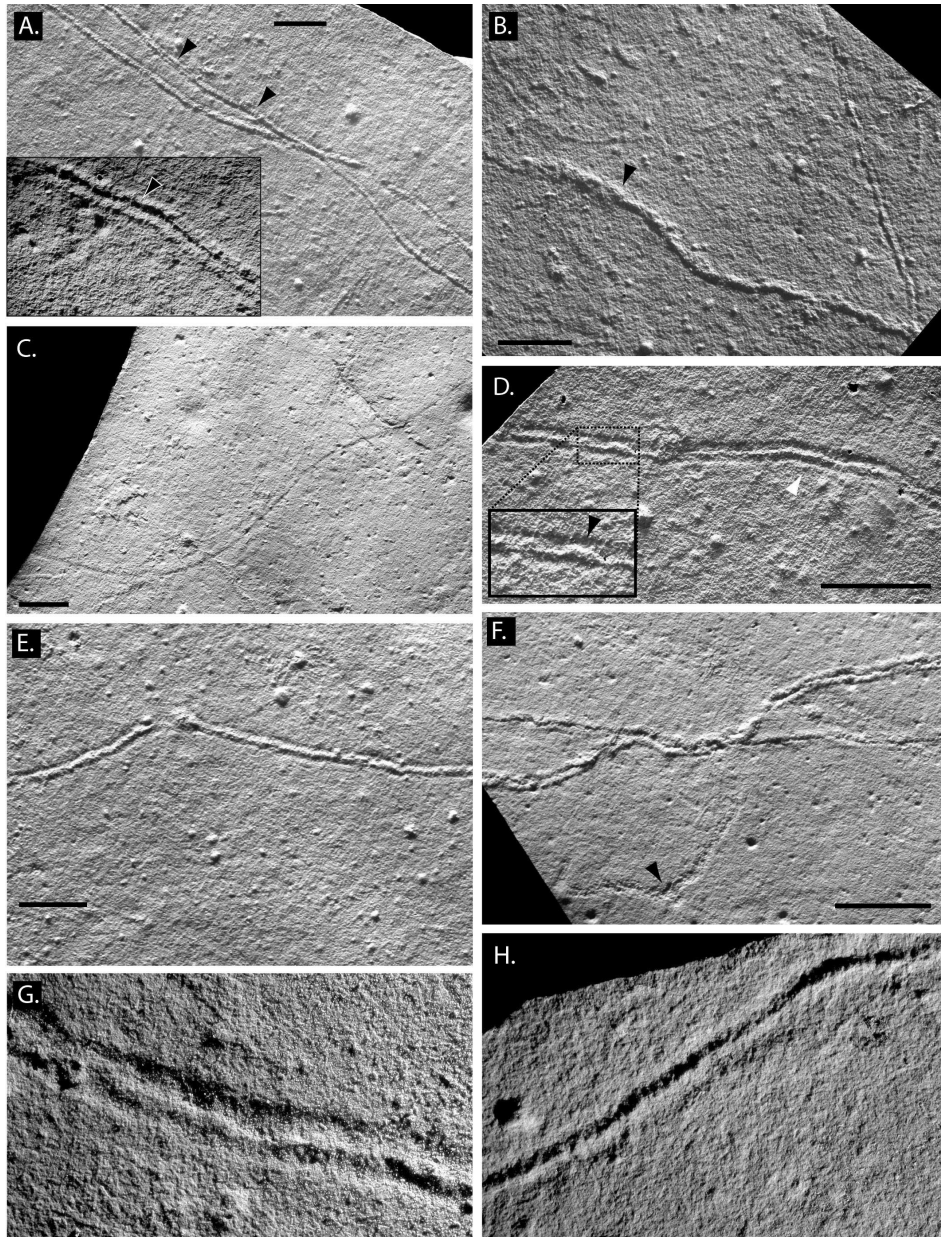
Figure 6.2. Various digital images of the Tacuarí trace fossils. (A) Typical bilobate furrow with beaded backfill / meniscae visible (black arrows). (B) Irregular trace fossil showing the "collapsed" top part of the burrow. (C) Sinuous trail illustrating the typical amplitude and wavelength of sinusoidal trails in the Tacuarí Formation. (D) Well developed bilobate furrow with circular indentations (black arrow, inset) and raised burrow margins (white arrow). E. Bilobate furrow showing departure from and return to the plane of preservation. (F) Later burrow intersecting and following a pre-existing burrow. (G) Close up of bedding-plane (view top) clearly showing the bilobate furrow that is preserved in many of the burrows. (H) Close up of the Ediacaran burrow-maker's trail, showing serial indentations along the furrow margin.

6.5. DISCUSSION

The reported trace fossils reveal many aspects of the trace-making animal's behavior and morphology. Well-preserved bilateral furrows represent the bottom of the burrow. Irregularly and massively filled trace fossils suggest that the burrow was emplaced within sediment, remained partially open as a tunnel, and then collapsed: these examples approximately represent the top of the burrow. Given the shallow intrastratal occurrence of this trace fossil, it is likely that the animal grazed on organic material—possibly relict biomat material—situated between sedimentary laminae. Rare but clear departures of some burrows from the plane of grazing may represent movement of the tracemaker to the sediment-water interface to access dissolved oxygen: reappearance of the burrow nearby and in the same plane show the animal's subsequent return to the food source. Regularly sinusoidal trails suggest that the tracemakers were engaged in rudimentary spatial optimization of patchy food resources or used a search pattern that improved the likelihood of intersecting optimal food resources. Notably, the lack of mutual burrow avoidance suggests that phobotaxis had not yet evolved. The specimens that show later burrows coincident with pre-existing burrows may imply primitive chemotaxis, or may simply reflect the greater ease of burrowing through previously burrowed sediment.

The presence of raised lateral ridges and the preservation of a beaded backfill show that the animal moved by expanding and extending it's body and pushing against the sediment. The spacing of the backfilled beads reveals ponderous forward movement of less than 0.5 mm (per peristaltic push): serial indentations along the burrow margin have a similar spacing. The indents further show that the tracemaker had prehensile 'feet' of sorts, and could extend those parts into the sediment to assist motility. Abrupt changes in the meander radius with abrupt lateral jogs further suggest that the animal, although possibly elongate, did not exceed 1 cm in length. The bilateral furrow is indicative of bilateral symmetry of the tracemaker, and when coupled with the mode of locomotion, strongly point to an early bilaterian tracemaker.

A variety of inorganic sedimentary processes can superficially mimic the shape of simple burrows (Jensen et al., 2005; Jensen et al., 2006), but none of these seem applicable to the Uruguay trace fossils. All of the specimens exhibit remarkably consistent size and morphology. There is no evidence of alignment such as might be produced by depositional currents, nor are there abrupt changes in orientation, diameter, or relief along the length of the structures that might reflect tool markings or shrinkage cracks. The bilobate lower surface of the structures is typical of many modern and Phanerozoic bilaterian burrows, especially but not exclusively molluscan and annelid burrows, and would be difficult to produce consistently in numerous specimens by any known inorganic sedimentary process. Poorly preserved algal filaments or tubular animals can also mimic simple trace fossils (Jensen et al., 2006; Jensen et al., 2007), but there are no carbonaceous or calcareous films, and angular (i.e. broken) edges that might mark a body fossil, are not observed (Figure 6.2E).

Importantly, the Uruguay structures exhibit abundant evidence for sediment displacement and processing in the formation of these structures. These include lateral ridges of displaced sediment flanking a bilobate furrow at the base, the beaded-meniscate internal fill of the structures, and the collapse features that followed abandonment of partly open structures – the latter very strongly suggests that they represent the burrows of muscular organisms. Some prokaryotes and protists are capable of moving on or through sediment and can leave traces of their activity (Bengtson et al., 2007), but are too small and lack evidence for the strong musculature used in the construction of eumetazoan burrows. Among the simple Eumetazoa, flatworms and anemones can produce lateral ridges of displaced sediment as they move across the surface using mucociliary creeping (Collins et al., 2000), but no modern Platyhelmininthes or Cnidaria are known to construct horizontal burrows that are either infaunal or backfilled. The combination of features seen in the Uruguay trace fossils makes it difficult to regard them as representing the activity of anything below the biological grade of the Eumetazoa, and in modern seas these fossils are consistent only with those produced by bilaterian eumetazoans.

Although the internal structure of the Uruguay burrows is strikingly similar to that of Phanerozoic and modern bilaterian burrows, their ethology is considerably less complex, even in comparison with later Ediacaran burrows from NW Canada (Narbonne and Aitken, 1990) and Australia (Droser et al., 2005). Conspicuously absent are parallel meanders and 3-D avoidance that appeared later in the Ediacaran (Narbonne and Aitken, 1990). Nevertheless, sinusoidal grazing likely hallmarks the advent of more sophisticated grazing behaviors and is in of itself evidence of early burrowing adaptation.

6.6. CONCLUSIONS

These findings extend the fossil record of bilaterian eumetazoans 25 million years backward to the early Ediacaran, a time coincident with the youngest ages for the appearance of bilaterians predicted by molecular clock analyses (Peterson et al., 2005; Peterson et al., 2008). Based on our trace fossils, it seems likely that bilaterians evolved in shallow-water settings, perhaps reflecting greater food availability in this environment and because their mobility and burrowing habit required higher oxygen levels than those of the sessile Ediacarans. Deep-sea bilaterian burrows do not appear until ca. 550 Ma (Narbonne, 2005), and it is likely that the invasion of deep-sea environments occurred in concert with the stepwise oxygenation of the Ediacaran seas (Canfield et al., *2007;* Narbonne and Gehling, 2003; McFadden et al., 2008; Shen et al., 2008).

These early Ediacaran burrows demonstrate very early grazing activity by eumetazoans, and they show that the burrowing behaviors used, although primitive, are very likely derived. In other words, older trace fossils almost certainly wait to be discovered.

6.7. REFERENCES

Aceñolaza, G., F. Aceñolaza F. 2007. Insights in the Neoproterozoic–Early Cambrian transition of NW Argentina: facies, environments and fossils in the proto-margin of western Gondwana. Geol. Soc. Sp. Pub. London. 286, 1-13.

Basei, M. A. S., Frimmel, H. E., Nutman, A. P., Preciozzi, F., 2006. West Gondwana amalgamation based on detrital zircon ages from Neoproterozoic Ribeira and Dom Feliciano belts of South America and comparison with coeval sequences from SW Africa, Geol. Soc. Sp. Pub. London. 294, 239-256.

Bengston, S., Budd, G., 2004. Comment on "Small Bilaterian Fossils from 40 to 55 Million Years Before the Cambrian". Science. 306, 1291a.

Bengtson, S., Rasmussen, B., Krape, B., 2007. The Paleoproterozoic megascopic Stirling biota. Paleobiology. 33, 351-381.

Canfield, D.E., Poulton, S.W., Narbonne, G.M., 2007. Late Neoproterozoic deep ocean oxygenation and the rise of animal life. Science. 315, 92-95.

Chen, J.-Y., Bottjer, D.J., Oliveri, P., Dornbos, S.Q., Gao, F., Ruffins, S., Chi, H., Li, C.-W., Davidson, E.H., 2004. Small Bilaterian Fossils from 40 to 55 Million Years Before the Cambrian. Science. 305, 218-222.

Collins, A.G., Lipps, J.H., Valentine, J.W., 2000. Modern mucociliary gliding trails and the body plans of Neoproterozoic trace-makers. Paleobiology. 26, 47-55.

Condon, D., Zhu, M., Bowring, S., Wang, W., Yang, A., Jin, Y., 2005. U-Pb Ages from the Neoproterozoic Doushantuo Formation, China. Science. 308, 95-98.

Conway-Morris, S., 2000. The Cambrian "explosion": slow-fuse or megatonnage?. Proc. Natl Acad. Sci. USA, 99, 4426-4429.

Da Rosa, A. L. Z., 2005. Evidências de vida no Ediacarano Inferior da Bacia do Itajaí, SC. MSc thesis, Universidade do Vale do Rio dos Sinos, São Leopoldo, pp. 56.

Droser, M. L., Gehling, J. G., Jensen, S. R., 2005. Ediacaran trace fossils: true and fals, in : Briggs, D.E.G. (Eds), Evolving Form and Function: Fossils and Development: Proceedings of a symposium honoring Adolf Seilacher for his contributions to paleontology, in celebration of his 80th birthday. New Haven, Peabody Museum of Natural History, Yale University, pp. 125-138.

Dzik, J., 2007. "The Verdun Syndrome: simultaneous origin of protective armour and infaunal shelters at the Precambrian–Cambrian transition", in: Vickers-Rich, P.,Komarower, P. (Eds), The Rise and Fall of the Ediacaran Biota, Geol. Soc. Sp. Pub. London, 286, 405-414.

Fedonkin, M. A., Waggoner, B. M., 1997. The Late Precambrian fossil Kimberella is a mollusc-like bilaterian organism. Nature. 388, 868-871.

Fedonkin, M.A., Gehling, J.G., Grey, K., Narbonne, G.M. and Vickers-Rich, P. 2008. The Rise of Animals: Evolution and Diversification of the Kingdom Animalia. Mikhail Johns Hopkins University Press, pp. 344.

Grey, K., 2005. Ediacaran Palynology of Australia. Memoir of the Association of Australasian Palaeontologists, Canberra, Vol 31, pp. 439.

Hedges, S. B., Blair, J. E., Venturi, M. L., Shoe, J.L., 2004. A molecular timescale of eukaryote evolution and the rise of complex multicellular life. BMC Evol. Biol. 4:2.

Jensen, S., Droser, M. L., Gehling, J. G., 2005. Trace fossil preservation and the early evolution of animals. Palaeogeo. Palaeoclim. Palaeoecol. 220, 19-29.

Jensen, S., Droser, M. L., Gehling, J. G., 2006. A critical look at the Ediacaran trace fossil record. In: (Eds. S. Xiao, A.J. Kaufman), Neoproterozoic Geobiology and Paleobiology, Springer, Dordrecht, pp. 115-157.

Jensen, S., Palacios, T., Martí Mus, M., 2007. A brief review of the fossil record of the Ediacaran–Cambrian transition in the area of Montes de Toledo–Guadalupe, Spain. In: (Eds. P. Vickers-Rich, P. Komarower), The Rise and Fall of the Ediacaran Biota. Geol. Soc. Sp. Pub., Lond. 286, 223-235.

McFadden, K.A., Huang, J., Chu, X., Jiang, G., Kaufman, A.J., Zhou, C., Yuan, X., Xiao, S., 2008. Pulsed oxidation and biological evolution in the Ediacaran Doushantuo Formation, Proc. Natl. Acad. Sci. U.S.A. 105, 3197-3202.

Narbonne, G. M., Aitken, J. D., 1990. Ediacaran fossils from the Sekwi Brook area, Mackenzie Mountains, northwestern Canada. Palaeontology. 33, 945-980.

Narbonne, G.M., 2005. The Ediacara biota: Neoproterozoic origin of animals and their ecosystems. Ann. Rev. Earth Planet. Sci. 33, 421-442.

Narbonne, G.M., Gehling, J.G., 2003. Life after snowball: the oldest complex Ediacaran fossils. Geology. 31, 27-30.

Netto, R. G., Paim, P. S. G., Da Rosa, C. L. M., 1992. Informe preliminar sobre a ocorrência de traces fósseis nos sedimentitos das Bacias do Camaquâ e Santa Bárbara. In: I Workshop Bacias Molássicas Brasilianas, Sao Leopoldo, Resumos Expandidos, pp. 90–96. Universidade do Vale do Rio dos Sinos.

Oyhantçabal, P., Siegesmund, S., Wemmer, K., Naumann, R., 2006. Age and Geochemical Signature of post-Collisional Plutons of the Southern Extreme of the Dom Feliciano Belt (Uruguay), 5th South American Symposium on Isotope Geology, Punta del Este, Maldonado, pp. 148.

Pecoits, E., Gingras, M., Aubet, N., Konhauser, K., 2008. Ediacaran in Uruguay: palaeoclimatic and palaeobiologic implications. Sedimentology. 55, 689-719.

Peterson, K.J., Butterfield, N.J., 2005. Origin of the Eumetazoa: Testing ecological predictions of molecular clocks against the Proterozoic fossil record. Proc. Nat. Acad. Sci. USA. 102, 9547-9552.

Peterson, K.J., Cotton, J.A., Gehling, J.G., Pisani, D., 2008. The Ediacaran emergence of bilaterians: congruence between the genetic and the geological fossil records. Phil. Trans. R. Soc. B. 363, 1435-1443.

Seilacher, A., 2007. Trace Fossil Analysis. Berlin, Heidelberg, New York: Springer-Verlag. pp. 226.

Seilacher, A. 1964. Sedimentological classification and nomenclature of trace fossils. Sedimentology. 3, 253-256.

Seilacher, A., Pflüger, F., 1994. From biomats to benthic agriculture: a biohistoric revolution. p. 97-105. In Krumbein, W.E. (ed.), *Biostabilization of Sediments*. Oldenburg, Bibliotheks and Informationsystem del Carl von Ossietzky Universitat.

Shen, Y., Zhang, T., Hoffman, P. F., 2008. On the coevolution of Ediacaran oceans and animals, Proc. Natl. Acad. Sci. U.S.A. 105, 7376-7381.

Veroslavsky, G., de Santa Ana, H., Daners, G., 2006. Tacuarí Formation (Nov. Nom.): Lithostratigraphy, facies, environment, age and geological significance (Cerro Largo-Uruguay). Rev. Soc. Uru. Geol. 13, 23-35.

CHAPTER 7: CONCLUSIONS

7.1. SUMMARY

Field-based research coupled with sedimentological, stratigraphical and geochemical data, and are-assessment of previous research, was carried out on Ediacaran (volcano) sedimentary units from Uruguay. The studied units comprise the Tacuarí Formation and the Maldonado, Arroyo del Soldado and Arroyo de la Pedrera Groups. The estimated time of deposition for these successions ranges from ca. 630 to 535 Ma, thereby indicating an Ediacaran–lowermost Cambrian age. This study shows a temporal correlation between sedimentation and significant changes in global climate, palaeoceanography and palaeobiology.

7.1.1. Sedimentology and stratigraphy of Ediacaran units of Uruguay

The Maldonado Group is largely interpreted as a thick glacially-influenced marine (Playa Hermosa Formation) and fan-delta sedimentary system (Las Ventanas and San Carlos formations) deposited in a strike-slip basin. Based on stratigraphic and sedimentological characteristics it was suggested that this succession, containing glacially-influenced diamictite and dropstones, records the Gaskiers Glaciation (ca. 580 Ma). Compelling evidence suggests that the Gaskiers event would be also contained within the Arroyo del Soldado basin and thus, the Maldonado Group might be correlative with the Polanco Limestone and Barriga Negra formations. The total thickness of the gorup reaches *ca*. 2000 m comprising mafic and acidic volcanic rocks, pyroclastic rocks, diamictite, sandstone, conglomerate and pelite. Structurally, the Maldonado Group is extensively deformed, although variably, throughout the region. Strike-slip faults, westward verging detachment faults, and folds with axis sub-parallel to the strike-slip planes are common features. The presence of pumpellyite, prehnite, chlorite and epidote in mafic rocks indicate very low to low-grade metamorphic conditions. Reliable palaeomagnetic data

indicate that the Maldonado Group accumulated at high palaeolatitudes, however, the palaeogeographic evolution of the Río de la Plata Craton during the Neoproterozoic remains conjectural. Radiometric data from intrusive bodies and cross-cutting strike-slip faults place the minimum age of the group at *ca.* 565 Ma, whereas basement volcanic rocks dated at 590 ±2 Ma interbedded with meta-sandstones hosting detrital zircons ~600 million years old provide the best constraint on the maximum age of deposition. Given the absence of carbonate rocks, no chemostratigraphic studies (e.g. C, O, Sr) are available. The recently defined Tacuarí Formation comprises basal diamictites, sandstones and minor pelites that grade upwards into fine-grained rhythmites containing abundant out-sized clasts. The latter, interpreted as dropstones, along with diamictites hosting faceted and striated clasts and associated varved sediments, provide definitive evidence for the glacial origin of these deposits. Trace fossils in the Tacuarí Formation occur within the uppermost fine-grained rhythmites that mark the last waning stages of glaciation. A U-Pb zircon age (TIMS) obtained from an intrusive (granitic) complex that crosscuts and deforms the Tacuarí Formation places a minimum age of the unit to 561±9 Ma.

Through the application of sequence stratigrpahic concepts, the ~2500m thick sedimentary succession of the Arroyo del Soldado Group, ranging in age from ca. 610 to 560 Ma, has been divided into two stratigraphic sequences. Based on facies stacking patterns a more detailed subdivision showing the depositional system tracts has been possible. Sequence A includes the Yerbal and Polanco Limestone formations whilst sequence B, separated from the former by a regional erosional unconformity, consists of the Barriga Negra and Cerro Espuelitas formations. The basal and mainly siliciclastic Yerbal Formation records transgressive system tracts (TST) passing upward to high stand (HST) and falling stage system tracts (FSST) infilling the carbonate ramp system represented by the Polanco Limestone Formation. The succeeding alluvial Barriga Negra and marine Cerro Espuelitas formations, capping the erosional unconformity that divides both stratigraphic sequences, were deposited during low stand system tracts (LST) followed by TST and culminating in HST. Significantly, the top of the TST in both sequences, which marks the maximum flooding surface (MFS) and a period of extreme

sediment starvation, are represented by iron formations (IF) and cherts as well as associated 'Fe-rich' and black shales, and banded siltstones, which encompass pre- (Yerbal Formation) and post-Gaskiers scenarios (Cerro Espuelitas Formation).

The Arroyo de la Pedrera Group is erected as a new lithostratigraphic unit, which consists -from base to top- of the Piedras de Afilar Formation and the Cerro Victoria Formation. Although the Cerro Espuelitas Formation (uppermost Arroyo del Soldado Group) and the Piedras de Afilar Formation were originally interpreted as conformable this has not been corroborated in this study. Instead, the latter unit rests directly on an angular unconformity to the pre-Ediacaran basement supporting its exclusion from the Arroyo del Soldado Group. The Piedras de Afilar Formation includes sandstones and siltstones, showing well-preserved sedimentary structures, and represents a fining- and thinning-upward cycle. Although it contains abundant organic-walled microfossils they have no stratigraphic significance and the age of the unit remains controversial. The overlying Cerro Victoria Formation was originally characterized as having stromatolites and micritic limestones at the base, oolitic calcarenites and micritic limestones in the middle part of the succession and stromatolitic limestones interbedded with micritic limestones and organic-rich chert layers at the top. Even though dolomite has not been recognized previously, almost the whole unit is composed of dolostones ('post-depositional' dolomites). Based on the trace fossil association (Thalassinoides–Gyrolithes–Palaeophycus assemblage), the Cerro Victoria Formation was placed in the lowermost Cambrian (542 to 535 Ma). However, the illustrated structures resemble diagenetic concretions of inorganic origin and thus, the age is regarded as equivocal.

7.1.2. Carbonates

Well preserved C- and Sr-isotope data obtained from marine carbonates can provide a detailed record of isotopic variation in seawater through time and have proven to be a valuable tool for correlating these isotopic changes worldwide. Negative carbon isotope excursions (up to -4.5‰) in the Ediacaran-aged Polanco Limestone Formation, Uruguay,

have been interpreted as recording post-Gaskiers glacial events in the Río de la Plata craton. The new available evidence, however, do not support this model and alternative hypotheses have not been considered to account for the isotopic patterns. The record of both deep- and shallow-water settings in the Polanco Limestone Formation provides a unique opportunity to examine $\delta^{13}C$ variability across the platform and to evaluate whether the carbon isotope signatures are the result of local (intrinsic) or global (extrinsic) processes.

Sedimentological, petrographic, geochemical and isotopic data were combined to constrain the depositional environment and age of the Polanco Limestone Formation as well as to better understand the platform dynamics. By comparing chemostratigraphic profiles across the basin (i.e., shallow vs. deep water) this contribution shows that this type of integrated analysis may help to better interpret Precambrian carbonate system dynamics, especially those associated with major palaeo-climatic and palaeo-environmental events.

Facies analysis indicates that the Polanco Limestone Formation was deposited in a storm-dominated homoclinal ramp, where inner, mid and outer ramp facies associations were recognized and described. Inner ramp facies association is characterized by coarsening- and thickening-upward regressive cycles of clacarenites representing upper, middle and lower shoreface environments deposited above the mean fair weather wave base in well-oxygenated waters. Mid ramp facies association is composed by alternations of calcisiltite rhythmites limestone-dolostone with occasional hummocky cross-stratified calcarenites and thin massive or parallel-stratified calcarenite beds. Outer ramp deposits comprise rhythmites limestone-dolostone and bedded dolostones deposited below the mean storm wave-base and under anoxic conditions.

Optical, textural and diverse geochemical proxies used here suggest that most of the studied samples do not evidence significant post-depositional alteration of the carbon isotopic composition and thus, these carbonates are regarded as recording near-primary seawater signatures and are of chemostratigraphic significance. Conversely, Sr-isotope compositions are more variable, reflecting the effects of diagenesis and probable leaching

of clay detritus. In this regard, carbonates from South Isla Patrulla and Recalde sections are the only suitable for Sr chemostratigraphic considerations excluding those from Los Tapes section from further chemostratigraphic interpretations.

Strontium isotope data from the Polanco Limestone Formation exhibit values compatible with those of the global $^{87}Sr/^{86}Sr$ composite curve between 600 and 575 Ma. Carbon isotope data show values that match the global $\delta^{13}C$ composite curve from numerous Ediacaran sections worldwide where the most negative shift might be tentatively correlated to the ca. 590 Ma negative anomaly. This is supported by new K-Ar ages obtained from diagenetic illite of the underlying Yerbal Formation, which yielded ages ca. 584 Ma.

The age proposed for the Polanco Limestone Formation carries important implications because the deposition of this unit would be concurrent with a major climatic event (Gaskiers glaciation). The association between negative $\delta^{13}C$ excursions and glaciations in the Neoproterozoic is tempting and might account for the C-isotope signature recorded in the middle of the unit. However, the lack of a concurrent negative $\delta^{13}C$ excursion in deep water facies and the good correlation between $\delta^{13}C$ data and facies associations wherein outer ramp facies is characterized by $\delta^{13}C$ values showing a transition towards more positive values associated with mid and inner ramp facies, demands an alternative explanation. Two alternative hypothesis are put forward: (1) organic carbon supplied from continents and, (2) oxidation of the dissolved organic carbon pool. Whether these bathymetric changes and their associated $\delta^{13}C$ variations were produced and in which extent by glacially-related conditions or the dynamic of the basin itself remains unresolved.

7.1.3. Iron Formations

It was widely believed that the Earth's oceans became fully oxygenated after the end of the Marinoan glaciation approximately 635 million years ago. This process then facilitated the rise of animal life. However, recent geochemical analyses from various

Ediacaran sediments suggests that the deep oceans instead remained anoxic and highly ferruginous [Fe(II)-enriched] throughout the Ediacaran and possibly into the Cambrian. Unfortunately, acceptance of this idea has been hindered by the virtual absence of iron formations (IF), which were relatively common under such Fe-rich conditions in earlier Archean-Palaeoproterozoic oceans. Crucially, the Yerbal IF represent pre-Gaskiers deposits (ca. 600-590 Ma) whilst the Cerro Espuelitas cherts and iron-rich shales is post-Gaskiers (ca. 570-560 Ma) in age, which allow us to analyze the palaeoceanographic conditions before and after the last major Precambrian glacial event.

The analysis of rare earth elements plus yttrium (REY) patterns of these IF and cherts has allowed us to identify genuine seawater signatures typical of marine chemical sediments, consistent with a marine depositional setting. The negative Eu anomalies in all the IF and chert samples suggests that high-T hydrothermal fluids did not exert any influence over the seawater from which they precipitated. This constitutes a substantial difference when compared with other well-studied Archaean-Palaeoproterozoic BIF, which display positive –although variable- Eu anomalies. Furthermore, Arroyo del Soldado samples show significantly higher Sm/Yb ratios than older BIF. Taken in conjunction, the lack of Eu anomalies and the higher Sm/Yb ratios, account for a low-T hydrothermal fluid component during IF and chert precipitation. The presence of Ce anomalies in all of the IF and chert samples from the Yerbal Formation indicates the presence of oxygen in shallow waters. Redox-sensitive element concentrations from the same samples, in turn, suggest rather suboxic conditions and define negative-correlations with Ce/Ce*. This contrasted redox-sensitive element concentrations and Ce anomalies suggest that the upper seawater layer had enough oxygen to oxidizes Ce(III) to Ce(IV) and a lower suboxic zone from were IF and chert precipitated and acquired suboxic redox signatures. Cherts from the Cerro Espuelitas Formation, however, show positive Ce anomalies and larger enrichments in redox-sensitive elements indicating even more widespread anoxic (non-sulfidic) conditions.

Therefore, based on sedimentological and geochemical evidence, we envisage IF and cherts being deposited in an outer shelf setting (ca. 50-100m) at the oxic/suboxic interface, which separated a lower anoxic (non-sulfidic) deep-water layer (>100m) and a

superficial and well-oxygenated seawater layer (<50m). This scenario is supported by: the absence of marked enrichment in redox-proxying elements and the presence of iron-rich deposits (IF and hematite-bearing cherts) with very low Mn concentrations, Ce anomalies and no pyrite (suboxic zone); positive Ce anomalies and larger enrichment in redox-sensitive elements in Cerro Espuelitas cherts and associated pyrite-free 'Fe-rich' and black shales (anoxic zone). Hence, our data suggest that neither sulfidic nor fully oxic conditions were widespread in the deep ocean between 610-560 Ma. Anoxic (non-sulfidic) deep seawater is consistent with low sulfate levels. In a low sulfate anoxic-suboxic ocean, a larger portion of the hydrothermal Fe flux would extend farther from submarine vents facilitating the precipitation of Ediacaran IF and cherts. Crucially, our results not only confirm previous work arguing for a rather ferruginous ocean before the Gaskiers glaciation but also demonstrates that similar conditions were sustained even after the Gaskiers glaciation.

7.1.4. Trace Fossils

Bilaterian burrows occur in shallow-water glaciomarine sedimentary rocks in Uruguay. These sediments are demonstrably Gaskiers in age (ca. 580 Ma), implying that these are the oldest definite animal tracks yet reported. Their features, including lateral ridges of displaced sediment flanking a bilobate furrow at the base, beaded-meniscate internal fill of the structures, and collapse features that followed abandonment of partly open structures, indicate infaunal grazing activity by early eumetazoans. Crucially, our new discovery unites the palaeontological and molecular data pertaining to the origin of bilaterians, and brings the origin of animals firmly into the interval of the Neoproterozoic glaciations. It also implies that ancestral bilaterians likely evolved first in relatively shallow seas, and only colonized the deep-sea floor once sufficient bottom water oxygenation had taken place.

These findings extend the fossil record of bilaterian eumetazoans 25 million years backward to the early Ediacaran, a time coincident with the youngest ages for the

appearance of bilaterians predicted by molecular clock analyses. Based on our trace fossils, it seems likely that bilaterians evolved in shallow-water settings, perhaps reflecting greater food availability in this environment and because their mobility and burrowing habit required higher oxygen levels than those of the sessile Ediacarans. Deep-sea bilaterian burrows do not appear until ca 550 Ma, and it is likely that the invasion of deep-sea environments occurred in concert with the stepwise oxygenation of the Ediacaran seas. These early Ediacaran burrows demonstrate very early grazing activity by eumetazoans, and they show that the burrowing behaviors used, although primitive, are very likely derived. In other words, older trace fossils almost certainly wait to be discovered.

7.2. FUTURE WORK

Future efforts should focus on four primary areas of research:

7.2.1. Geomicrobiology

Understanding the climatic and oceanic chemical conditions that ultimately led to the origin of Earth's earliest animals will help resolve major outstanding questions regarding the origins of animal life and the so-called 'Cambrian explosion' in general; these include:

(1) the role of deep-sea oxygenation;

(2) bioessential major and trace element availability;

(3) trophic relationships between microorganisms and first animals;

(4) effects on the biosphere imposed by severe climatic fluctuations;

(5) timing of the events and conciliation between molecular clock dates and fossil evidence.

7.2.2. Organic carbon isotopes

The evidence gathered from carbonates of the Polanco Limestone Formation suggests that $\delta^{13}C$ variations reflect bathymetric changes in a stratified basin. Whether these bathymetric changes and their associated $\delta^{13}C$ variations were produced by glacially-related conditions or the dynamic of the basin itself remains unresolved. In this regard, $\delta^{13}C_{org}$ data will help to clarify the source of the Polanco Limestone Formation organic matter and thus, to improve our understanding about the carbon isotopic record and ultimately, the carbon cycle during the Ediacaran.

7.2.3. Palaeomagnetism

Further palaeomagnetic studies will be especially useful for determining the palaeogeography of the Río de la Plata Craton during the Ediacaran and establish its relationships to neighbouring strata hosting similar successions. For example, focused sampling in the glacially-related units will be useful to determine the extent of the alleged non-global Gaskiers glaciation.

7.2.4. Geochronology

The integration of data gathered from rocks, carbon isotopes, trace-element geochemistry, paleomagnetism and palaeontology along with a robust geochronological framework will produce consistent results and consequently improve understanding of the sequence of the events, both biotic and environmental during the Ediacaran.
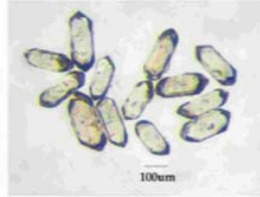
APPENDIX I
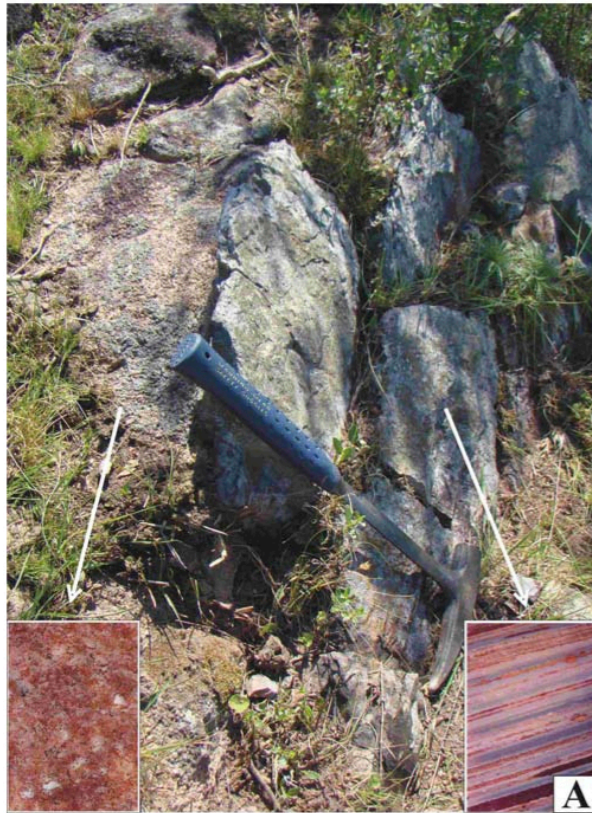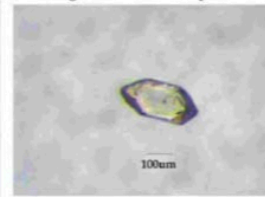
080105/3-1 FOV 1.0mm
1 large colorless zircon prism

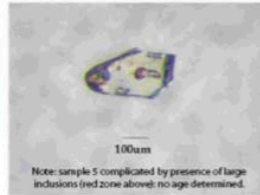080105/3-2 FOV 1.3mm
9 prismatic colorless zircons
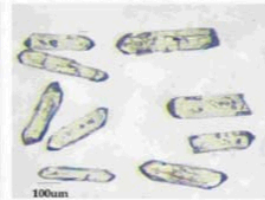
080105/3-3 FOV 1.3mm
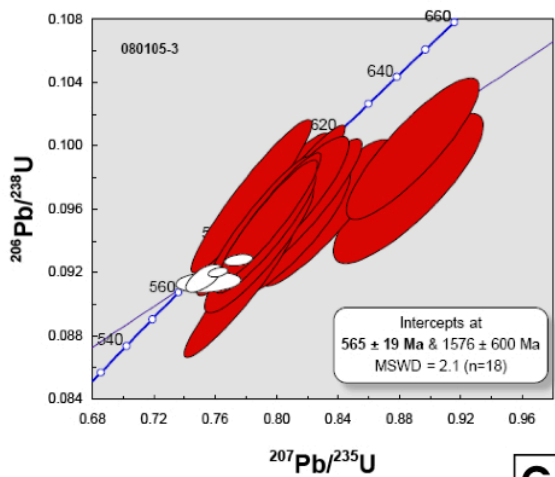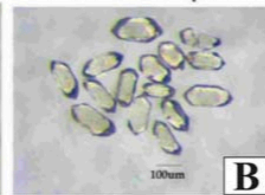13 best 3:1 colorless zircon prisms

080105/3-4 FOV 1.0mm
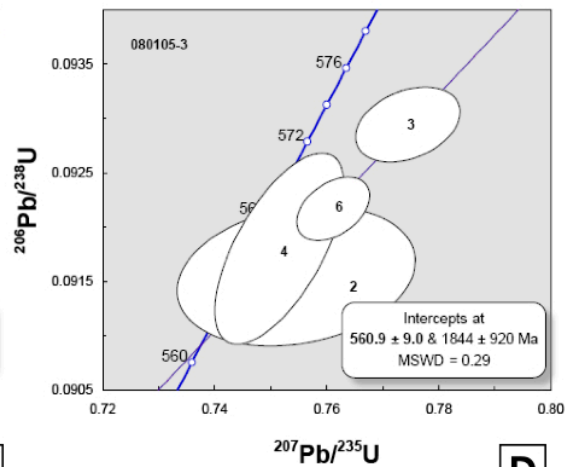1 large colorless zircon prism

080105/3-5 FOV 1.0mm
1 large broken zircon prism

080105/3-6 FOV 1.0mm
15 colorless 2:1 zircon prisms

Note: sample 5 complicated by presence of large inclusions (red zone above): no age determined.

Intercepts at
565 ± 19 Ma & 1576 ± 600 Ma
MSWD = 2.1 (n=18)

Intercepts at
560.9 ± 9.0 & 1844 ± 920 Ma
MSWD = 0.29

230

Figure S1. Lithologies and geochronological data from the study area. (A) Medium-grained leucocratic granite intruding the rhythmites of the Tacuarí Formation, which host the trace fossils reported herein. The insets show a polished slab of the granite on the left and the rhythmically bedded Tacuarí Formation on the right. See Figure S2 for magnified views of the chilled margins. (B) Microphotographs of the zircon populations used for TIMS analyses. (C) Concordia diagram showing LA-ICP-MS (red) and TIMS (white) U-Pb zircon analyses. A regression line yields a lower intercept date of 565±19 Ma. (D) An expanded view of the Concordia diagram in (C) showing only TIMS U-Pb analyses (excluding single grain fraction #1). The TIMS results yield a similar but more precise lower intercept date of 561±9 Ma and is the best estimate for the emplacement age of the crosscutting granite intrusion. This interpretation is supported by the zircon geochemistry; the high Th/U (0.93-1.24) is typical for magmatic zircons. A number of zircon analyses by both techniques are discordant and indicate slightly older 207Pb/206Pb ages (Table S1). These older ages are interpreted to indicate the presence of an inherited zircon component. Based on the Proterozoic upper intercept dates, some of the inherited zircon component could result from incorporation of Paleoproterozoic to Mesoproterozoic basement zircon in the granite magma during emplacement.
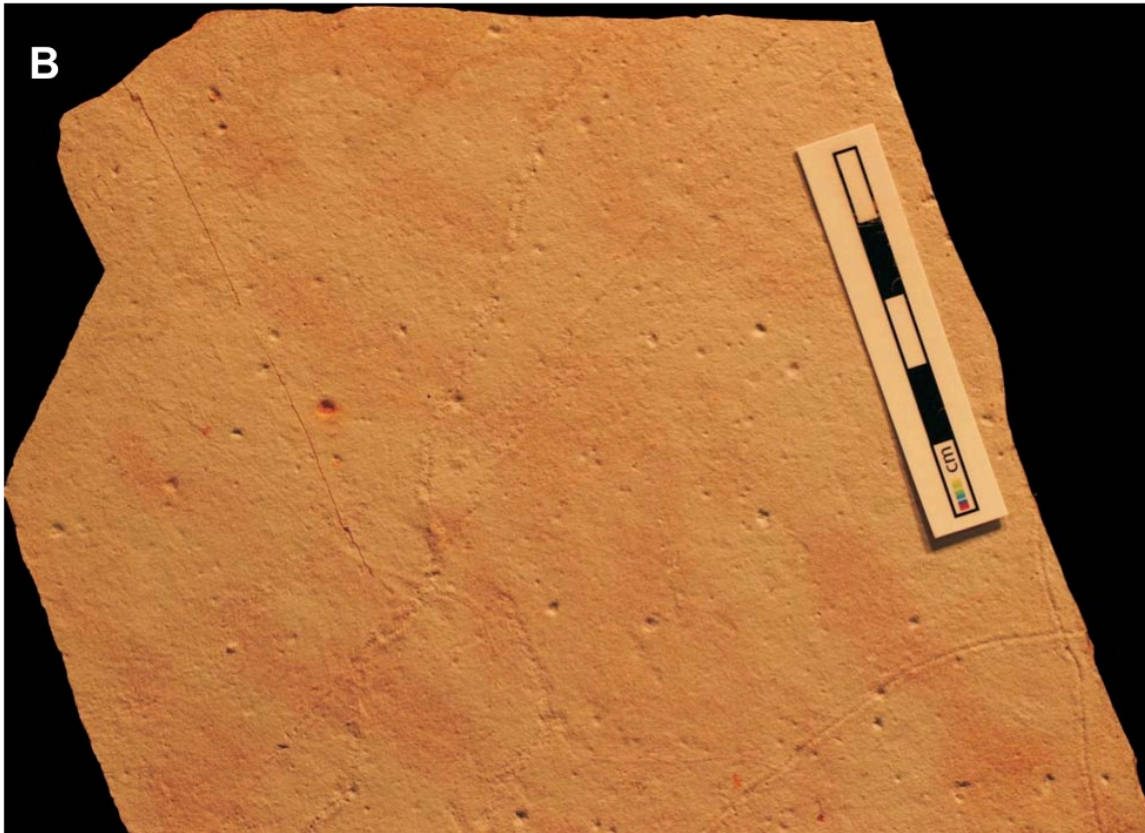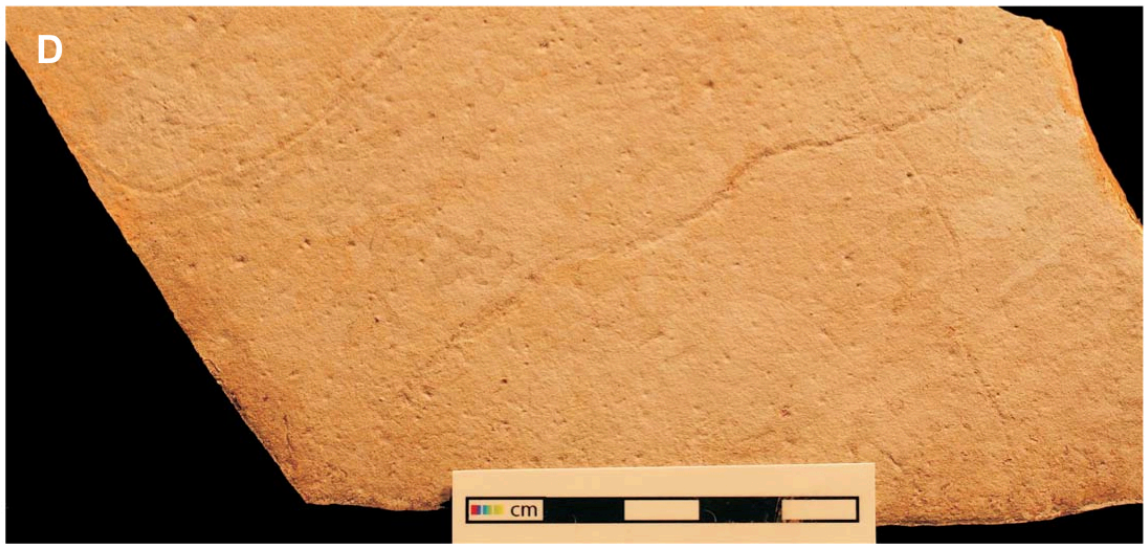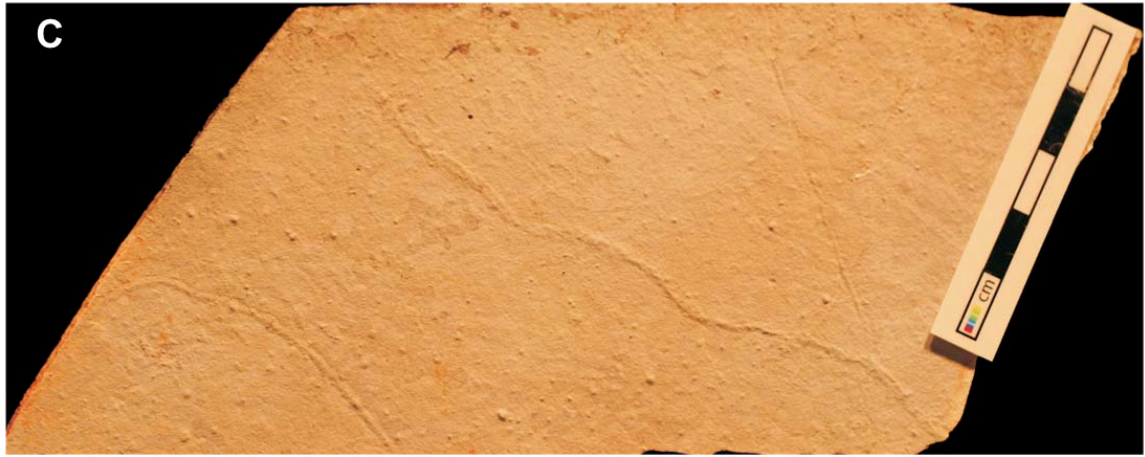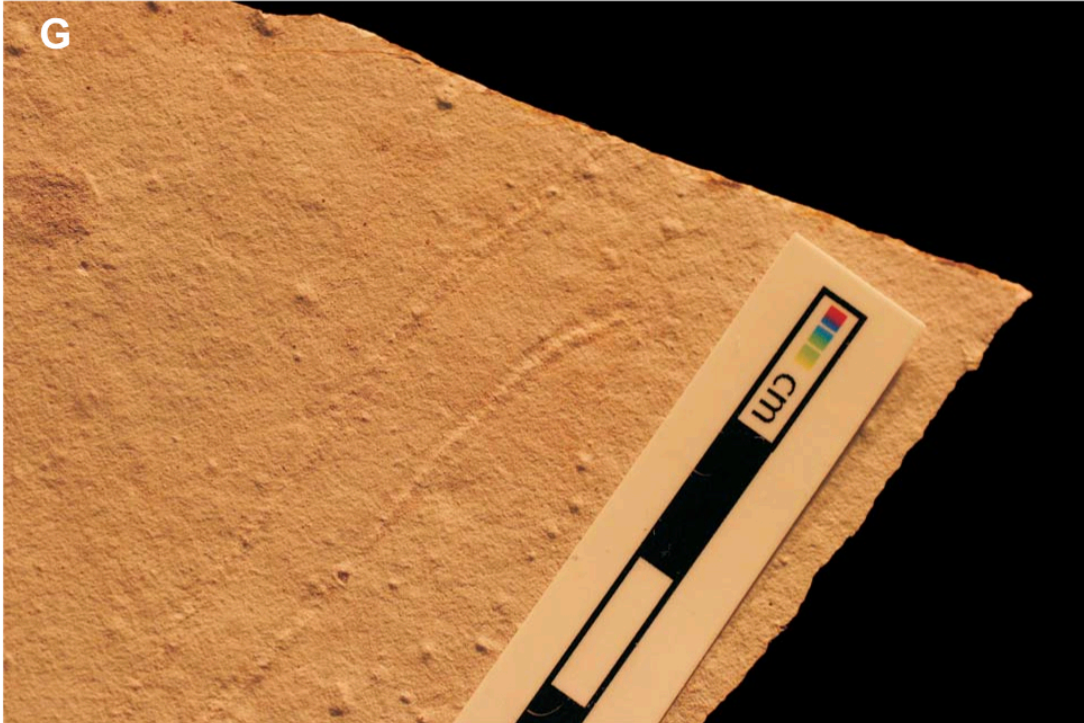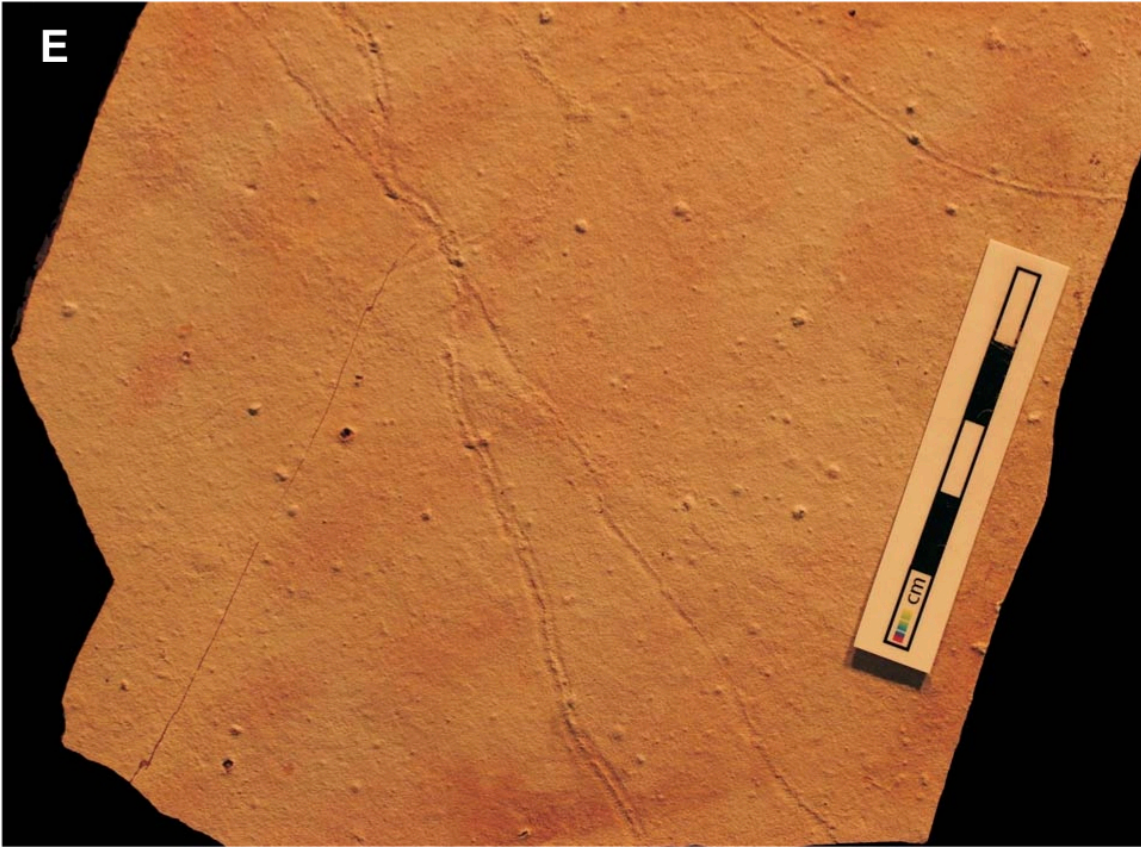
Figure S2. (A) Epirelief preservation corresponding to the hyporelief in Figure 6.2A. Circular pits, in this slab and the others that follow, represent impressions of small glacial dropstones on the bedding surface. Two sinuous crossing burrows (top) and one curved burrow (bottom left) exhibit prominent flanking levees and local preservation of beaded backfill (see especially Figure 6.2A inset). These views are interpreted as the bottoms of infaunal burrows. Note burrow in the upper left leaving the bedding plane and then returning to it along the same path (arrow), with ovate burrow cross-sections at the points of exit and entry. (B) Epirelief preservation. Two slightly sinuous crossing burrows with prominent levees (bottom right) are interpreted as representing the bottom-view of infaunal burrows. Crossing the middle of the sample are two cross-cutting burrows showing collapse features interpreted as representing the top-view of infaunal burrows. Burrow sinuosity and diameter are similar in both preservational modes. (C, D) Hyporelief (C) and epirelief (D) preservation corresponding to Figure 6.2F. Central burrow showing irregular collapse features on top (most easily seen in the hyporelief) are interpreted as representing the top-view of infaunal burrows. Burrows on the left and right exhibit beaded backfill and flanking levees and are interpreted as representing cross-sections near the bottoms of infaunal burrows and are, therefore, more evident in the basal slab (D). Burrow sinuosity and diameter are similar in both preservational modes. (E) Hyporelief preservation of the complete slab containing Figure 6.2F. The prominent, bilobate burrow shows beaded backfill and locally distinct levees (interpreted as representing a cross-section near the bottom of an infaunal burrow) intersecting, following, then diverging from an older burrow that exhibits poorly developed lateral levees along its length (interpreted as representing a slightly undulose burrow moving up and down with respect to the plane of preservation shown). Also present is a poorly preserved burrow with irregular collapse features on top (upper center) and a burrow represented by a ridge with flanking levees (top right). Note that all three preservational grades of burrows on this slab show similar sinuosity and burrow diameter. (F) Epirelief preservation.. Several curved burrows show bilobate lower surfaces. Note that the burrows continue undisturbed beneath unburrowed lamination, indicating that they are not later penetrative surface features imposed on the bed. (G) Hyporelief preservation. Two burrows, with right-hand burrow passing from unilobate with beaded backfill to bilobate with prominent levees reflecting preservation of progressively deeper levels in the burrow from the lower left to upper right of the image. (H) Epirelief preservation with poorly preserved sinuous burrow preserved between two glacial dropstones.

Table S1: Zircon U-Pb geochronological results from the granite dyke. **(A)** LA-ICP-MS (for analytical protocol see Simonetti et al., 2006). **(B)** TIMS.

(A)

Anal. #	^{206}Pb (cps)	^{206}Pb/^{204}Pb	^{207}Pb/^{206}Pb	±2σ	^{207}Pb/^{235}U	±2σ	^{206}Pb/^{238}U	±2σ	Rho value	^{207}Pb/^{206}Pb (Ma)	±2σ	^{206}Pb/^{238}U (Ma)	±2σ	% discord.
6_1	56711	infinite	0.0600	0.0010	0.8093	0.0303	0.0965	0.0033	0.887	603	±38	594	±21	1.5
3_15	94815	infinite	0.0598	0.0007	0.7937	0.0262	0.0954	0.0031	0.930	597	±27	587	±19	1.6
4_18	51916	infinite	0.0594	0.0007	0.7945	0.0277	0.0956	0.0033	0.945	583	±25	589	±20	-0.9
4_20	104989	infinite	0.0595	0.0007	0.7883	0.0276	0.0954	0.0033	0.942	584	±26	587	±20	-0.5
7_4b	39402	infinite	0.0590	0.0010	0.7905	0.0355	0.0958	0.0041	0.934	566	±35	590	±25	-4.1
8_5a	64654	infinite	0.0602	0.0008	0.8036	0.0301	0.0950	0.0035	0.941	611	±28	585	±21	4.3
1_9a	63614	infinite	0.0591	0.0007	0.8052	0.0314	0.0967	0.0037	0.956	573	±25	595	±23	-4.0
2_10	54590	104223	0.0600	0.0010	0.7877	0.0289	0.0936	0.0032	0.902	605	±34	577	±20	4.6
2_12	50602	infinite	0.0605	0.0009	0.8174	0.0303	0.0963	0.0034	0.912	621	±33	593	±21	4.6
3_16	54541	infinite	0.0599	0.0008	0.7916	0.0268	0.0947	0.0031	0.910	600	±31	583	±19	2.9
7_3	57653	28827	0.0610	0.0009	0.8052	0.0303	0.0957	0.0034	0.918	639	±32	589	±21	7.8
7_4a	55279	infinite	0.0611	0.0013	0.8075	0.0325	0.0948	0.0034	0.848	642	±46	584	±21	9.1
1_7a	74846	infinite	0.0604	0.0007	0.7746	0.0290	0.0910	0.0033	0.945	617	±27	561	±21	9.0
1_8a	52059	infinite	0.0620	0.0012	0.8308	0.0349	0.0959	0.0037	0.895	675	±40	590	±23	12.6
1_8b	48857	infinite	0.0639	0.0012	0.8877	0.0352	0.0999	0.0036	0.871	739	±41	614	±22	16.9
1_9b	58396	infinite	0.0586	0.0008	0.7829	0.0322	0.0969	0.0039	0.947	553	±29	596	±24	-7.8
4_19	66744	infinite	0.0647	0.0016	0.8850	0.0400	0.0974	0.0038	0.835	764	±52	599	±23	21.6

Spot size: 40 μm

(B)

Analyses	Weight (μg)	U (ppm)	Th (ppm)	Pb (ppm)	Th/U	TCPb (pg)	^{206}Pb/^{204}Pb	^{206}Pb/^{238}U	±1s	^{207}Pb/^{235}U	±1s	^{207}Pb/^{206}Pb	±1s	^{206}Pb/^{238}U (Ma)	±1s	^{207}Pb/^{235}U (Ma)	±1s	^{207}Pb/^{206}Pb	±1s	% discord.
080105/3																				
1 (1)	18.9	87	85	13	0.97	57	188	0.09461	0.00028	0.7679	0.0155	0.05887	0.00112	582.7	1.6	578.6	8.8	562.1	41.0	-3.8
2 (9)	61.8	94	117	11	1.24	41	831	0.09182	0.00035	0.7517	0.0047	0.05938	0.00028	566.3	2.1	569.2	2.7	581.0	10.3	2.6
3 (13)	65.8	80	92	10	1.14	66	484	0.09295	0.00014	0.7746	0.0038	0.06044	0.00028	572.9	0.8	582.4	2.2	619.4	10.0	7.8
4 (1)	9.8	44	41	6	0.93	16	172	0.09158	0.00026	0.7547	0.0087	0.05977	0.00067	564.8	1.5	570.9	5.0	595.3	24.2	5.3
6 (15)	29.0	69	74	8	1.06	13	882	0.09218	0.00012	0.7613	0.0026	0.05989	0.00019	568.4	0.7	574.7	1.5	599.7	6.8	5.4

Numbers in parentheses correspond to the number of crystals analysed
Atomic ratios corrected for blank (5pg Pb; 1pg U), fractionation and initial common Pb (Stacey and Kramers, 1975)
TCPb refers to the total amount of common lead present in the analyses in picograms
Th concentration estimated from the amount of ^{208}Pb present in the analysis and the ^{207}Pb/^{206}Pb age
%Disc refers to the amount of discordance along a reference line to zero age